# Conformational change in the C-terminal domain of *B. subtilis* GyrA and in the ATPase-gate of *M. mazei* topoisomerase VI

Genehmigt von der Philosophisch-Naturwissenschaftlichen Fakultät

auf Antrag von

Prof. Dr. Dagmar Klostermeier

Prof. Dr. Joachim Seelig

Basel, den 21. Juni 2011

Dekan Prof. Dr. Martin Spiess

# Summary

Type II DNA topoisomerases catalyze the ATP-dependent passage of a double-stranded DNA through a gap in a second duplex by coordinating the sequential opening and closing of three dimerization interfaces (gates). Gyrase is a specialized type II topoisomerase possessing a spiral domain (GyrA CTD) that wraps DNA for intramolecular strand passage of a Transfer-segment (T-segment) and thus confers negative supercoiling activity.

The exact position of the GyrA CTD relative to the catalytic core is not known as no full-length high-resolution structure of GyrA or gyrase has been solved. To monitor potential dynamics of a single GyrA CTD and localize the domain with respect to the core of the enzyme, single-molecule FRET (smFRET) experiments were performed. Stable dimeric constructs with one wt and one mutant subunit (carrying solvent-accessible cysteine residues for fluorescent labeling on the GyrA core and on the CTD) were produced in a hetero-dimeric expression system. FRET efficiencies from GyrA constructs labeled at different positions were converted to inter-dye distances, allowing the triangulation of the position of the N-terminal region of the CTD. In absence of DNA and GyrB, the FRET model placed the CTD close to the catalytic core domain, indicating a position suitable to contact a DNA bound to the DNA-gate. Upon addition of GyrB and supercoiled plasmid, the N-terminal region of the CTD is displaced from the core by 2.5 to 2.6 nm (depending on the labeling position of the CTD monitored), indicating an extended conformation of the CTD.

Fluorescence anisotropy titrations suggest that the extended CTD conformation is characterized by simultaneous binding of the DNA to the DNA-gate and the CTDs. However, in the absence of GyrB the CTDs are the main DNA interaction sites of GyrA. Binding of plasmid DNA induces conformational flexibility in the CTDs, which indicates transient bridging interaction of the DNA to both the CTDs and the DNA-gate. Binding of GyrB to GyrA induces only a small movement of the CTDs, probably by spatial interference, indicating that GyrB itself is not responsible for the extended CTD conformation, but rather for the stabilization of the enzyme-DNA complex.

Addition of neg. supercoiled or relaxed plasmid or linear DNAs of 48 to 110 bp to gyrase results in an extended CTD conformation; anisotropy measurements clearly showed that the linear DNAs bind to both the DNA-gate and the CTDs in presence of GyrB. However, a 37bp DNA showed similar $K_D$ values for GyrA and GyrA-core in the presence of GyrB. Moreover, binding to gyrase did not result in an extended CTD conformation. These findings indicate that a small interaction between DNA and CTDs (not more than approx. 5 bp) is sufficient to induce the conformational change. Meanwhile, the extended position of the CTD does neither

depend on the topology of the substrate nor extensive wrapping or the presence or absence of a T-segment.

In contrast to previous speculations, binding of ADPNP (a non-hydrolysable ATP-analog) to the gyrase-DNA complex did not result in the release of the GyrA CTDs, and no conformational change connected to strand passage could be detected. A cleavage-deficient GyrA mutant exhibits a 1.5-fold higher DNA affinity but retains wild-type like CTD conformations; suggesting that the latter are independent of DNA distortion and cleavage. Deletion of a conserved heptapeptide on the CTD (GyrA-box) abolished the supercoiling activity, but did not alter the DNA affinity or the conformational behavior of the enzyme. Taken together, the present data suggests that the conformational change of the CTDs is mediated by simultaneous binding of DNA to the CTDs and the DNA-gate (a complex which is stabilized by GyrB) and represents an early event in the supercoiling cycle of gyrase.


Topoisomerase VI possesses only two dimerization interfaces compared to the three in conventional type II enzymes, thereby exhibiting less complexity than e.g. gyrase. It catalyzes DNA relaxation and decatenation in an ATP-dependent manner. In smFRET experiments, a fluorescently labeled 50bp DNA was used as a FRET probe for potential DNA-gate dynamics in TopoVI. A reduction in the DNA affinity upon deletion of the active site tyrosine residue inducing DNA cleavage indicated the formation of a covalent protein-DNA intermediate in wild-type TopoVI, although DNA cleavage could not be demonstrated directly; the conformation of the DNA was similar in complexes with wild-type and active-site mutant enzyme. No distortion of the DNA or gate opening could be detected upon addition of ATP and ADPNP.

Conformational changes in the ATPase-gate of TopoVI were monitored in smFRET measurements, using fluorescently labeled enzyme with one dye attached to each nucleotide-binding domain. We have observed four different conformational states in the ATPase-gate: In absence of nucleotide or DNA substrates the ATPase-gate exhibits conformational flexibility, indicating gate opening and closing. Binding of supercoiled plasmid to TopoVI forces the ATPase-gate to open up even wider, although considerable flexibility of the domains is retained; both these states have been proposed on the basis of two crystal structures of intact TopoVI holoenzymes, showing a closed and an open gate conformation. Addition of ADPNP to TopoVI induces a well-defined conformation of the ATPase domains close to each other, indicating dimerization; this is in agreement with crystal structures from isolated TopoVI-B domains which show tight association when bound to ADPNP. Addition of both nucleotide and plasmid immobilizes the domains in a conformation different from the

one observed for the closed gate, indicating that the presence of a T-DNA segment in the central cavity induces physical strain to the TopoVI complex; this state has not been proposed so far. During all these conformational changes of the ATPase-gate, the transducer domain linking the two gates barely moves, suggesting that the ATPase domains exhibit a rotational flexibility in absence of nucleotide. TopoVI shows a different conformational behavior than type II topoisomerases (e.g. gyrase) in that it exhibits dynamic opening and closing of the ATPase-gate in absence of ligands. Furthermore it does not show DNA-induced pre-closure, but rather opening of the gate in presence of a supercoiled DNA.

# Table of contents

# 1. Introduction

## 1.1 Topoisomerases: An essential enzyme class to solve topological problems in DNA

Stable storage of genetic information is vital for all organisms, and is achieved in a universal manner via the nucleotide sequence in DNA. Its double-helical structure protects the nucleobases from the chemistry of the environment, while the complementary nature of the two strands enable organisms to repair DNA mismatches and damaged nucleobases, thus minimizing the risk of losing information. To fit the long DNA molecules into the restricted space of a cell or a sub-cellular compartment, organisms keep the DNA in a compact configuration. For example, in case of mesophilic prokaryotes, the DNA is slightly underwound, resulting in a compact configuration, while in eukaryotes the DNA is organized in a plectonemic structure mediated by scaffolding proteins [1]. While formation of the double helix and the packing of the DNA successfully protect the genetic information, it counteracts processes, which require access to the genetic information stored in the base-pairs and their need to induce strand separation, such as replication and transcription. Besides not being favored energetically, the local melting of base-pairs creates strain in the adjacent region of the DNA duplex: Progression of a transcription complexes along the DNA induces overwinding of the double-helix in the direction of movement, while the DNA behind the transcription bubble is underwound [2]. These effects are normally compensated by the formation of so-called supercoils, i.e. the coiling of the DNA duplex around itself. DNA replication also induces positive supercoiling in front of the replication fork, leaving behind intertwined DNA duplexes consisting of mother and daughter strands; in case of a bacterial chromosome, the ligation of the two circular daughter chromosomes results in interlocked DNA circles, known as catenanes [3, 4]. Negative or positive supercoiles or superstructures like catenanes or knots disturb the normal DNA topology of a cell, impairing DNA packing, maintenance, and read-out. In order to solve topological problems in DNA cells express a very diverse class of enzymes known as topoisomerases.

The only common property of topoisomerases is the ability to induce topological change into DNA: They transiently cleave one or two DNA strands by nucleophilic attack of one or two active site tyrosines on the phosphate backbone, respectively, forming a covalent phosphotyrosyl intermediate. They allow a second DNA segment (also a single or a double strand, respectively) to rearrange, and religate the cleaved phosphate backbone [5-7]. Topoisomerases are divided in two structurally and functionally very different families: Type

I topoisomerases induce a single-strand DNA break, while the complementary strand is either actively transported through the gap, changing the linking number in steps of 1 (type IA) [8, 9], or allow one double-strand next to the cleavage site to swivel around the non-cleaved phosphate backbone (type IB, C) [8, 10-12]. Type I enzymes generally consist of monomeric enzymes, with the only known exception being the type IB topoisomerase from *L. donovani* which consists of two subunits [13]. They relax negatively or positively supercoiled DNA or disentangle catenated DNAs in a nucleotide-independent manner, using the free energy stored in DNA supercoils [14]. The only type I topoisomerase not following this principle is reverse gyrase, an enzyme found exclusively in hyperthermophilic bacteria and archaea, which combines a topo IA domain with a nucleotide-binding helicase-like domain and catalyzes positive supercoiling coupled to ATP-hydrolysis [15, 16].

In contrast to type I topoisomerases, the type II topoisomerases are oligomeric protein complexes of $A_2$ or $A_2B_2$ arrangements normally, and exhibit a two-fold structural symmetry. This property enables this class of enzymes to introduce double-strand breaks, forming a covalent intermediate between the two DNA phosphate backbones and the active-site tyrosines. Through the gap a second DNA duplex is transported, a process which, in case of a relaxation reaction, removes two supercoils at a time [17]. Strand passage has been shown to require ATP hydrolysis and the presence of $Mg^{2+}$ cations [18]. Type II topoisomerases are divided in two very different sub-families: Type IIA enzymes were found in different variants in all three kingdoms of life as well as in viruses and bacteriophages, while type IIB proteins have been mainly identified in archaea as well as in plants, some bacteria and algae [19-22]. Type IIA topoisomerases are specialized in relaxation of supercoiled DNA (eukaryotic topoisomerases II and bacterial topoisomerase IV), decatenation of daughter chromosomes in bacteria prior to cell division (bacterial topoisomerase IV), and introduction of negative supercoiles into bacterial circular chromosomes (bacterial gyrase), while type IIB (topoisomerase VI) enzymes are involved in the removal of supercoils, cantenanes, and DNA knots. Structure and function of both the type II topoisomerase subfamilies will be introduced in the following paragraphs.

To manage the topological state of the DNA every organism expresses at least one type I and type II topoisomerase each [23]. The thermophilic archaeum *S. shibatae* for example expresses reverse gyrase and topoisomerase VI: The first is required for maintaining the characteristic positively supercoiled state of the genomic DNA, while the second relaxes negative supercoiles occurring in transcription and decatenates daughter chromosomes prior to cell division [24, 25]. *E. coli* employs four topoisomerases: gyrase and topoisomerase IV are resolve supercoils resulting from replication and transcription; the negatively supercoiled

state of the genome is regulated in competition between gyrase and topoisomerases IV, I and III [23].
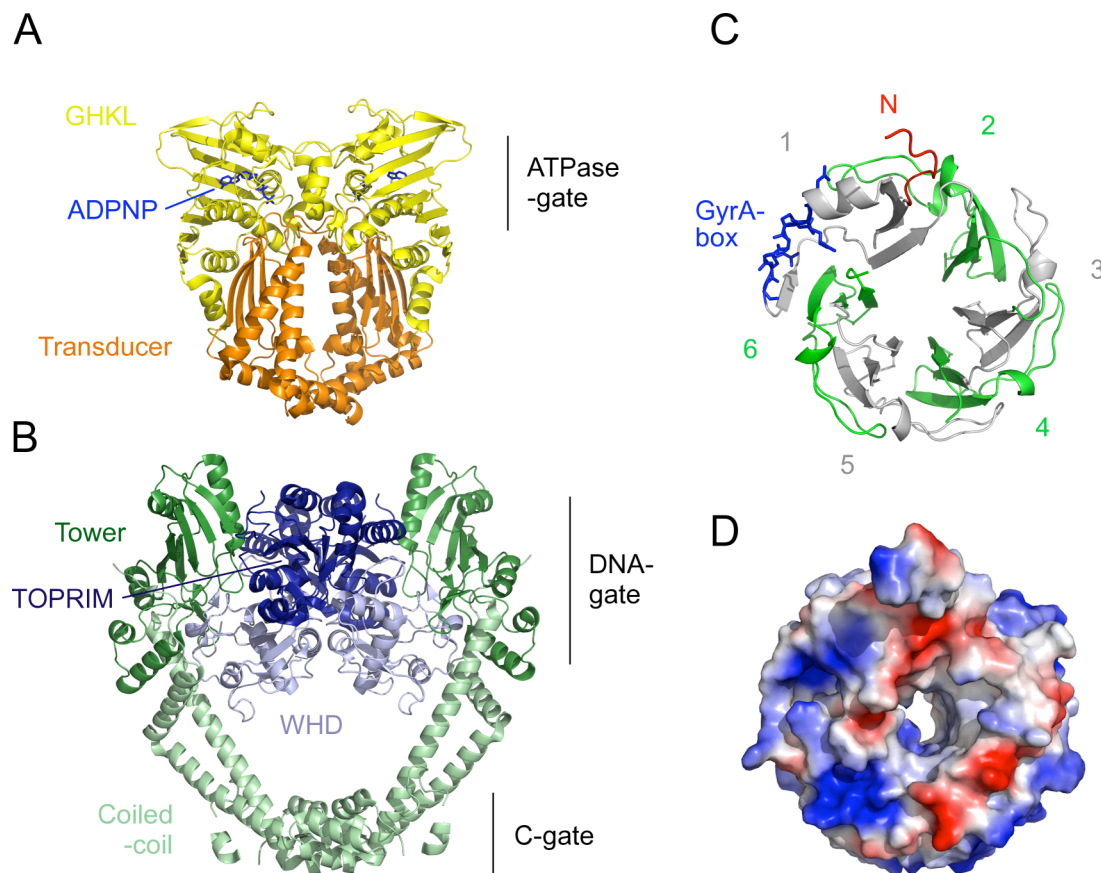


**Fig. 1.1:** Structural organization of gyrase.
**A:** Dimer of an *E. coli GyrB* fragment, encompassing the GHKL and transducer domains, indicated in yellow and orange. These two domains form the ATPase-gate, which is closed in this structure due to ADPNP (blue) bound to the nucleotide-binding pockets (PDB-entry: 1EI1 [37]).
**B:** High-resolution structure of an *E. coli* GyrBA fusion construct, encompassing the TOPRIM-domain of GyrB (dark blue) and the GyrA core domain consisting of winged-helix (WHD), tower and coiled-coil domains (light blue, dark green and light green, respectively). A domain specific for gram-negative bacteria (an insert to the TOPRIM fold of 170 amino-acids length) is present in the published structure, but was omitted here for clarity (PDB-entry: 3NUH [28]). The DNA-gate is formed by the WHD and the TOPRIM fold which contain the active site tyrosines and a $Mg^{2+}$-binding motif assisting in DNA binding, respectively. The C-gate (also termed Exit-gate) is formed by a highly conserved region of the coiled-coil structure.
**C:** Structure of the GyrA C-terminal domain from *X. campestris*, the only strucuture showing the highly conserved GyrA-box motif (stick representation, blue) (PDB-entry: 3L6V [38]). The domain consists of 6 blade-like β-sheets (numbered 1 − 6) assembled in a slightly spiral ring; extended loops at the periphery of the domain connect two neighboring blades. The N-terminus of the CTD shown in red is the anker for a linker peptide connecting the GyrA tower domain with the CTD.
**D:** The CTD as shown in C, but in electrostatic surface representation. Positively and negatively charged regions are shown in blue and red, respectively. The rim of the CTD is highly negatively charged and supposed to mediate DNA wrapping.

## 1.2 The catalytic core of gyrase is homologous to conventional type IIA proteins

Bacterial gyrase is the only known enzyme catalyzing the negative supercoiling of circular DNA. It is responsible to balance the topological state of the DNA of its host in an underwound state, rendering the genetic material more compact [18]. Introduction of neg. supercoils is the main activity of gyrase and depends on ATP-hydrolysis, while it can also relax supercoils in a nucleotide-independent manner [26]. Despite this very unusual activity profile – all other type IIA topoisomerases catalyze the relaxation and decatenation of DNA – gyrase shares structural and mechanistic similarities with the core domains of the other type IIA topoisomerases (with the exception of a 170 amino-acid insert in GyrB of some gram-negative bacteria involved in DNA binding [27, 28]).

Eukaryotic topoisomerase II consists of a homo-dimer, while all bacterial type IIA topoisomerases (topoisomerase IV, gyrase) form a hetero-tetrameric complex ($ParE_2ParC_2$, $GyrB_2GyrA_2$, respectively). The catalytic core forms three dimerization interfaces encompassing two cavities. The main subunit interactions are found at the so-called DNA- and C-(or Exit-)gates (Fig. 1.1B), while the latter seems to mediate a stronger interaction [29]. The DNA-gate is responsible for binding and cleaving the scissile DNA double-strand (termed gate DNA segment or G-segment) and consists of the winged helix (WHD) and the TOPRIM domains, which harbor the catalytic tyrosine residue and an essential $Mg^{2+}$-binding motif involved in DNA cleavage/religation, respectively [30, 31]. DNA cleavage results in phosphotyrosyl bonds to the 5'-ends of the DNA, creating 4bp-overhangs [6]. In bacterial topoisomerase IV and gyrase, the WHD and the TOPRIM domain are located on separate subunits. Binding and cleavage of a DNA substrate at the DNA-gate induces strand distortion, as shown by crystal structures and in single molecule experiments [31-34]. The DNA binding site of the DNA-gate extends to the tower domains located at the sides of the DNA-gate (Fig. 1.1A).

The N-terminal part of topoisomerase II and the topoisomerase IV and gyrase subunits ParE and GyrB, respectively, consist of a GHKL domain, an ATP-binding and hydrolysis fold found in all type II enzymes, and the transducer domain [30, 35]. The name GHKL originates from the presence of the domain in gyrase, the molecular chaperone Hsp90, in CheA-type histidine kinases, and in the DNA-mismatch repair enzyme MutL. The transducer domain is thought to structurally couple ATP hydrolysis to strand passage, involving an invariant lysine residue acting as a sensor and for the γ-phosphate of a bound ATP [30]. The ATPase domains dimerize upon nucleotide binding, forming an extensive subunit interface comprising an N-

terminal extension (strap), which interacts with the neighboring subunit and the bound nucleotide (Fig. 1.1A). This dimerization interface is also known as ATPase- or N-gate [36].

The catalytic cycle of the strand passage was proposed to function according to a 2- or 3-gate mechanism (depending on counting the dimerization interface of the ATPase domains as a gate or not), in which subsequent opening and closing of dimerization interfaces guide a DNA double-strand through the gap of a cleaved double helix, initiated by binding of one DNA segment (known as gate-DNA or G-DNA segment) to the DNA-gate and formation of the complex of the WHDs and TOPRIM domains [39]. A second DNA duplex, known as the transfer- or T-DNA segment, inserts into the cavity between DNA- and ATPase-gate; the latter dimerizes upon nucleotide binding, resulting in physical strain on the DNA-gate due to the restricted space in the cavity, probably inducing cleavage of the G-DNA and opening of the DNA-gate, thereby forcing the T-DNA to pass through the second cavity and the C-gate [40, 41]. Dynamics of the ATPase-gate of gyrase as well of the DNA-gate of topoisomerase II have been observed, while DNA-gate opening could not be detected in the case of gyrase [33, 42, 43]. On the basis of crystal structures DNA-gate opening is proposed to involve major structural rearrangement of the DNA-binding domains [29, 32]. Cross-linking of the C-gate was shown to abolish strand passage in gyrase, indicating a transient opening during strand passage [44]. A slightly open conformation has been observed in a crystal structure of a topoisomerase II fragment bound to DNA [32].

The role of ATP hydrolysis has not been fully elucidated. Hydrolysis of the first ATP molecule is suggested to induce strand passage, while hydrolysis of the second nucleotide and product release would reset the enzyme for another strand passage cycle [45-47]. Somewhat contradictory has been the finding that binding of the non-hydrolysable ATP-analog ADPNP supports one supercoiling cycle in gyrase, resulting in a stalled enzyme with closed a ATPase-gate [48].

## 1.3    The GyrA CTD is indispensable for the supercoiling activity of gyrase

While the catalytic core of type IIA topoisomerases is structurally and functionally fairly invariant, a carboxy-terminal domain in topoisomerase II, ParC and GyrA exhibits differences in amino-acid sequences and the three-dimensional structure, which apparantly account for the specialized activities. In GyrA, the CTD adopts a β-pinwheel fold with 6 blades exhibiting a cylindrical or spiral shape [49, 50] (Fig. 1.1C). The ParC CTDs also consists of blades of β-structure, but the number of blades is less conserved between different organisms [51]. The

CTD of eukaryotic topoisomerase II seems to be unstructured [52], indicating that the CTDs from bacterial organisms play a distinct role in the regulation of the enzymatic activity of the core.

Indeed, deletion of the CTD in gyrase abolishes the ATP-dependent supercoiling activity. Instead the truncated enzyme behaves similar to a topoisomerase II, relaxing supercoiled DNA and decatenating interlocked circular DNA in an ATP-dependent manner [53]. The CTD has been known for a long time to bind DNA. It was shown to bend a linear DNA in an angle of 180°, thus wrapping the substrate around itself [49]. The DNA is supposed to bind around the outer rim of the CTD, judged by the highly positive charge on loops located at the periphery of the domain, connecting blades 1, 4, 5, and 6 [49, 50] (Fig. 1.1D). Probably due to the spiral arrangment of the DNA-binding site, the isolated CTD stabilizes positive supercoiled DNA (an exception being the CTD of GyrA from *B. burgdorferi*, which adopts a cylindrical shape). All these data suggest that the GyrA CTD binds the DNA segment extending from the DNA-gate, wraps it around itself and delivers the double-strand back to the enzymatic core where it is supposed to function as the T-DNA segment. This hypothesis is supported by eletron microscopy and single-molecule FRET data [42, 54]. A highly conserved hepta-peptide located on the loop connecting blades 1 and 6, termed the GyrA-box, is indispensable for the supercoiling activity of gyrase and is absent in ParC CTDs (Fig. 1.1C). Deletion or substitution of the consensus amino-acid sequence QRRGGKG (*E. coli*) almost abolishes the supercoiling activity, but does not influence the nucleotide-independent DNA relaxation activity [55]. The molecular mechanism for this finding is unclear, but the inability of GyrA-box mutants to induce positive supercoiles into DNA suggests that wrapping and delivery of the T-segment is impeded. Sequence alignments indicate the presence of GyrA-box like motifs in every blade, suggesting a role in DNA binding. Mutations of a single arginine in blade 5 abolishes DNA binding, supercoiling, and relaxation, indicating a role of the CTD in both the supercoiling and the relaxation reactions of gyrase [56].

While the importance of the CTDs in the supercoiling reaction has been elucidated, the arrangement of the domains with respect to the enzymatic core is not known, as a high-resolution structure of the full-length gyrase complex is lacking. A SAXS study determined the position of the CTDs in the non-complexed GyrA *ab initio*, placing them close to the C-gate. The domain is thought to complex the DNA bound to the DNA gate, suggesting a conformational change of the CTDs with respect to the catalytic core during the catalytic cycle [57]. Surprisingly, a recent SAXS model of gyrase in presence of a 140bp DNA placed the CTDs even further away from the DNA-gate, almost on the opposite side of the C-gate,

not supporting a CTD position close to the catalytic center [58]. DNA footprinting experiments with gyrase and an electron microscopy study of DNA bound to gyrase suggest a loss of DNA wrapping upon binding of ADPNP, indicating a movement of the CTDs during strand transfer [48, 54]. Taken together, available information about the location and potential dynamics of the CTD is scarce and somewhat contradictory.

## 1.4   Gate dynamics in topoisomerase VI

The only family member of the type IIB topoisomerases, the topoisomerase VI [19], is in many ways similar to the type IIA superfamily. It cleaves a double stranded DNA by active site tyrosines, forming 5'-phosphotyrosyl bridges and 2-bp overhangs [59]. In a reaction dependent on ATP and $Mg^{2+}$, the enzyme catalyzes the passage of a second duplex through the gap, exhibiting activities similar to the eukaryotic topoisomerase II or bacterial topoisomerase IV, namely the relaxation of negative or positive supercoiles and decatenation of circular DNAs [25, 58, 60].

Topoisomerase VI consists of a two-fold symmetric, heterotetrameric $A_2B_2$ complex [61] (Fig. 1.2A, B). Namely the B subunit is very similar to the one found in type IIA topoisomerase (e.g. GyrB and ParE): It consists of a GHKL fold, responsible for ATP binding and hydrolysis; a transducer domain that links the ATPase domain and the part of the enzyme which is involved in DNA binding, cleavage and religation; and a small helix-2-turn-helix domain (H2TH) which is inserted between the two classical domains, probably involved in stabilization of the ATPase-domain interface [62] (Fig. 1.2A – C). The H2TH domain is not present in type IIA topoisomerases. The TopoVI-A subunit dimer forms the DNA-gate, indicated by its ability to bind a DNA double-strand [63]. The TopoVI-A subunits consist of two domains, sharing similarities with the domains forming the DNA-gate in type IIA topoisomerases: A WHD and a TOPRIM domain, harboring the catalytic tyrosine residue and an acidic cluster binding $Mg^{2+}$, which assists in DNA binding. A and B subunits interact via a four-helix bundle, forming a hydrophobic interface [61]. In some archaea (e.g. *M. mazei*), the TopoVI-B subunit exhibits a small C-terminal domain of unknown function. Structural similarity with the immunoglobulin fold suggests a protein-protein interaction site.
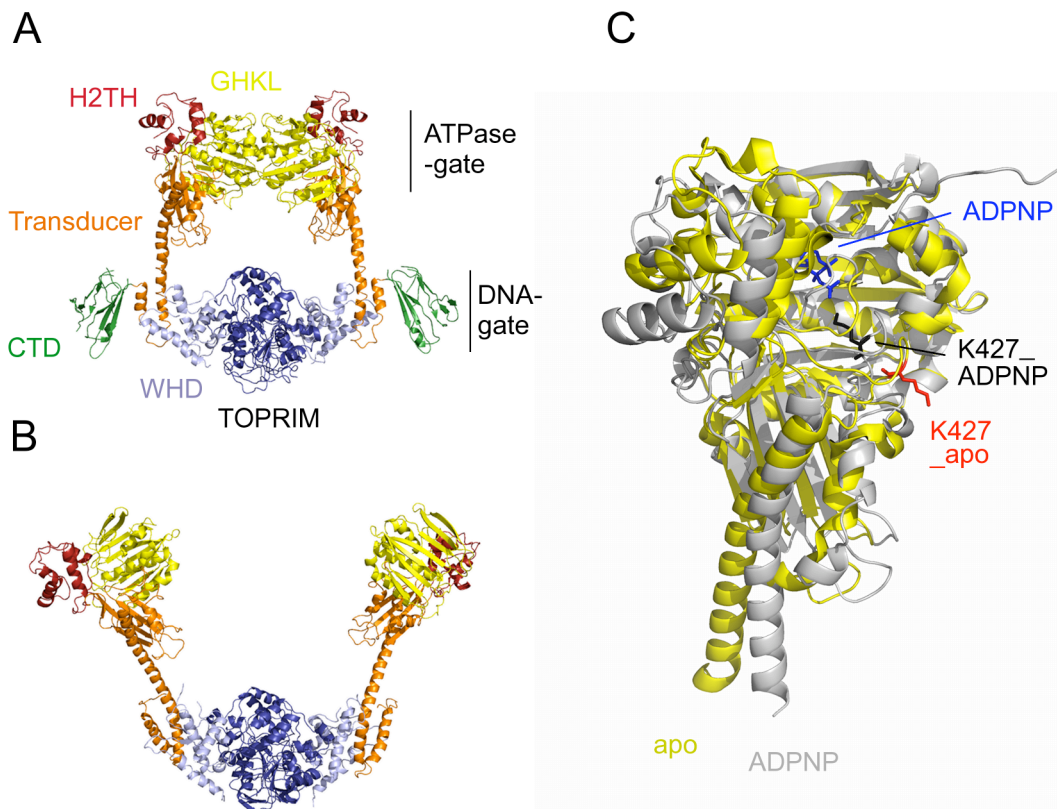
**Fig. 1.2:** Structural organization of topoisomerase VI and different conformations of the ATPase domain.

**A:** X-ray structure of the hetero-tetrameric topoisomerase VI holoenzyme from *M. mazei* (PDB-entry: 2Q2E [61]). It consists of 2 TopoVI-A and 2 TopoVI-B subunits, forming the DNA- and the ATPase-gate, respectively. The A subunits encompass the winged-helix domains (WHD, light blue) and the TOPRIM-domains (dark blue), containing the active site tyrosines and a $Mg^{2+}$-binding motif. The B subunits consist of the ATP-binding fold (GHKL), the Helix-2-Turns-Helix and the transducer domain (in yellow, dark red and orange, respectively); the ATPase-gate adopts a half-closed conformation in this structure. The latter links the ATPase- and the DNA-gates, forming a 4-helix bundle with the WHD. A small C-terminal domain (CTD, green) is present in *M. mazei* TopoVI-B.

**B:** X-ray structure of the hetero-tetrameric topoisomerase VI holoenzyme from *S. shibatae* (PDB-entry: 2ZBK [64]). The domain organization corresponds to the one in topoisomerase VI from *M. mazei* as depicted in A; the same color code is used in A and B. In contrast to A, the ATPase-gate adopts a wide-open conformation, indicating significant conformational flexibility of the ATPase-domains.

**C:** Alignment of TopoVI-B domains from *S. shibatae*, in the apo form (yellow) and bound to ADPNP (grey) (PDB-entries: 1MU5 and 1MX0, respectively [62]. The TopoVI-B domains are aligned by the GHKL domain, showing conformational differences in the transducer domains. Binding of ADPNP (blue) induces the rotation of the conserved lysine-427 from an outward orientation (red; apo) to complex the nucleotide (black; ADPNP-bound form), resulting in the rotation of the transducer domain relative to the ATPase-domain.

Two crystal structures of the full-length enzyme from *S. shibatae* and *M. mazei* show a two-gate complex with a wide-open and a half closed ATPase-gate, respectively, indicating conformational dynamics of the ATPase-domains [61, 64] (Fig. 1.2A, B). Several high-resolution structures of the isolated ATPase- and transducer domains in absence and presence of different nucleotides suggest dimerization of the domains upon ADPNP binding [62] (Fig. 1.2C). Very similar to type IIA topoisomerases, an invariant lysine residue, located on a loop in the transducer domains, acts as a phosphate sensor and mediates rotation of the transducer relative to the ATPase-domain. Upon binding of ATP to TopoVI-B, the lysine residue rotates towards the nucleotide binding site, inducing the conformational change of the transducer domains, and switches back in an outward conformation hydrolysis [65] (Fig. 1.2C). Eventually, as shown by SAXS studies, dimerization of the ATPase-domains and signal transduction by the transducer domain seems to alter the conformation of the DNA-gate [61]. Together, this information suggests that DNA relaxation is mediated by a two-gate mechanism: One DNA duplex binds to the DNA-gate, and a second one (the T-DNA segment), is accommodated in the central cavity; this arrangement should be the case in strand crossings in supercoiled or catenated DNA. ATP-binding induces dimerization of the ATPase domains, and rotation of the transducer might induce physical strain on the enzyme-DNA complex, forcing the G-DNA segment to be cleaved, the DNA-gate to open and the T-segment to be released. Due to the structural similarities of the ATPase-domains in type IIA and IIB topoisomerases, the role of ATP hydrolysis has been suggested to be the same; the first ATP is supposed to drive strand passage, while hydrolysis of the second could reset the enzyme [65].

## 1.5 Aim of this work

The goal of this work was to characterize potential conformational changes in the C-terminal domain of *B. subtilis* GyrA and in the dimerization interfaces of *M. mazei* topoisomerase VI. The conformational change should be monitored using single-molecule fluorescence resonance energy transfer (FRET), requiring the coupling of fluorescent dyes to appropriate locations on the surface of the proteins. This can be achieved for example by labeling solvent-exposed cysteine residues introduced by site-specific mutagenesis, using dyes with a maleimide linker. In DNA supercoiling and relaxation assays, the enzymatic activities after the modification procedures needs to be quantified in order to validate the link between smFRET data and the enzymatic activities.

The first project addressed the potential conformational change in the GyrA CTD. For the lack of a full-length structure of the gyrase complex, the GyrA CTDs should be localized relative to the enzymatic core, using combinations of dye pairs coupled to multiple sites on the GyrA subunit. It has been shown that inter-dye distances can be extracted from smFRET data and used to triangulate reference points [66], as planned for the localization of the GyrA CTD. To quantify a potential conformational change of the CTDs upon formation of the $GyrA_2B_2$-DNA complex, the localization procedure should be applied to the situation of the ligand-free GyrA and the gyrase-DNA complex.

A further goal was to link conformational changes of the CTDs to the presence of the individual binding partners of GyrA. SmFRET experiments and complementary binding studies can provide evidence on the influence of complex formation with DNA and GyrB on the position of the CTDs. The conformational change should be linked to the supercoiling cycle by characterizing the influence of DNA substrates of different topology and length and by the introduction of functional mutations to the enzymatic core. In order to establish the relation of conformational changes to individual steps in the supercoiling cycle, we aimed on characterizing the influence of functional mutations (e.g. cleavage-deficiency) on the conformational behavior of the CTD. Ultimately, the mechanistics of strand passage and its manifestation in a potential switch of the CTD conformation should be addressed in smFRET experiments in the presence of nucleotide.

A second project aimed on characterizing gate dynamics in topoisomerase VI. To observe conformational change in the DNA-gate, a fluorescently labeled DNA should be devised as a FRET probe. The binding and cleavage properties of the substrate DNA to topoisomerase VI can be addressed in anisotropy titrations and DNA cleavage assays, while the a potential distortion of the DNA upon complex formation, cleavage and opening of the DNA-gate might be monitored in smFRET experiments. To achieve site-specific fluorescent labeling of the protein, native cysteines need to be removed and topoisomerase VI mutants tested for remaining DNA relaxation and ATPase hydrolysis activity. Coupling of fluorescent dyes to the cysteine residues introduced at the ATPase-gate should yield a system appropriate for smFRET studies. To complement structural data, the gate dynamics might be determined in the presence of DNA ligands and nucleotides.

SmFRET studies of the conformational dynamics in GyrA CTD and of the gates in topoisomerase VI should give valuable insight to the enzymatic behavior of the proteins, linking structural changes to complex formation and the supercoiling and relaxation activities observed for gyrase and topoisomerase VI, respectively.

# 2. Materials and Methods

## 2.1 Chemicals

**Applichem** (Darmstadt, D) glycerol, anhydrous, p.A.

**Carl Roth** (Karlsruhe, D) chloramphenicol, $\geq$ 98 %; kanamycin sulfate, $\geq$ 750 I.E. / mg; peptone; yeast extract, pouder

**Fermentas** (St. Leon-Rot, D) PageRuler Plus protein ladder

**Fluka** (Buchs, CH) activated charcoal, purum; ciprofloxacine, $\geq$ 98 % (HPLC); L-glutamic acid monopotassium salt monohydrate, p.A.; methanol, p.A.; oxolinic acid, $\geq$ 97 %

**GERBU Biochemicals** (Gaiberg, D) ampicillin sodium salt

**Invitrogen** (Eugene, USA) Alexa Fluor 488 C5-maleimide; Alexa Fluor 546 C5-maleimide; TMR C5-maleimide

**Merck** (Darmstadt, D) Calf thymus DNA, sodium salt (Calbiochem); ethanol, absolute; 2-propanol, p.A.

**New England BioLabs** (Ipswich, USA) DNA ladder, 1 kb, 100 bp

**Pharma Waldhof** (Düsseldorf, D) ATP disodium salt; ADP disodium salt

**Radiant Dyes Laser Acc.** (Wermelskirchen, D) fluorescein (Uranin)

**Reuss-Chemie** (Tägerig, CH) 2-propanol, tech.

**Roche Diagnostics** (Mannheim, D) Complete EDTA-free Protease Inhibitor Cocktail Tablets; NADH disodium salt; PEP

**Sigma Aldrich** (St. Louis, USA) ADPNP tetralithium salt hydrate, ~ 95 % (HPLC); Bis-Tris propane, $\geq$ 99.0 %; deoxynucleotide set (dATP, dCTP, dGTP, dTTP; as sodium salts); DMSO, $\geq$ 99.9 %; ethanol, purum; etoposide, $\geq$ 98 %

Chemicals not listed above were purchased from Carl Roth (Karlsruhe, D), in either p.A. or puriss. quality.

Stock solutions were prepared using ultrapure water purified with Barnstead Nanopure Diamond Lab Water System (by Thermo Fisher Scientific, Rockford, USA) and sterilized using membrane filters (Durapore 0.22 µm Millipore, Billerica, USA).

## 2.2 Enzymes

GoTaq DNA Polymerase (Promega, Madison, Wisconsin): 5 U/µl

GyrB wt from *B. subtilis* (home purified as described [46]): approx. 200 µM        .

L-Lactate Dehydrogenase (LDH) (Roche Diagnostics GmbH, Mannheim, Germany): 5 mg/ml, from rabbit muscle, suspension in 3.2 M ammonium sulfate solution

Pfu DNA Polymerase (Promega, Madison, Wisconsin): 2 - 3 U/µl, 10 x Pfu DNA Polymerase reaction buffer

Phusion High Fidelity DNA Polymerase (Fynnzymes Oy, Espoo, Finland): 2 U/µl, 5 x Phusion HF Buffer

Proteinase K, recombinant, PCR Grade (Roche Diagnostics GmbH, Mannheim, Germany): lyophilized

Pyruvate Kinase (Roche Diagnostics GmbH, Mannheim, Germany): 10 mg/ml, from rabbit muscle, suspension in 3.2 M ammonium sulfate solution

Ristriction Endonucleases (New England BioLabs, Ipswich, Massachusetts): BamHI, DpnI, HindIII, XhoI: 20000 U/ml; NcoI: 10000 U/ml; 10 x NEB buffers 2; supplied with 100 x BSA

Shrimp Alkaline Phosphatase (SAP) (Promega, Madison, Wisconsin): 1 U/µl, 10 x SAP reaction buffer

T4 DNA Ligase (New England BioLabs, Ipswich, Massachusetts): 400'000 cohesive end units/ml, 10 x T4 DNA Ligase reaction buffer

T4 Polynucleotide kinase (PNK) (New England BioLabs, Ipswich, Massachusetts): 10000 U/ml, 10 x T4 PNK reaction buffer

Tobacco Edge Virus protease (TEV) (home purified after [67]): 30 µM

## 2.3   DNA oligonucleotides

Primers for PCR, mutagenesis and sequencing reactions were order from Microsynth AG (Balgach, Switzerland) or Sigma-Aldrich Co. (St. Louis, Missouri). Non-modified and fluorescently labeled DNA substrates for *B. subtilis* gyrase or *M. mazei* topoisomerase VI were synthesized by Purimex (Grebenstein, Germany).

### 2.3.1   PCR primers

gyrA_Bs_DuetBamHI_for: CCA AGG ATC CGA TGA GTG AAC AAA ACA CAC CAC

gyrA_Bs_DuetHindIII_rev: CCT TAA GCT TTC ACA CTT CTT CTT GTT CTT CTT C

gyrA_Bs_XhoI_rev:          GCG CTC GAG TCA CAC TTC TTC TTG TTC TTC TTC

pUC18_110_for:            GGG TTT TCC CAG TCA CGA CGT TG

pUC18_110_rev:           ACA TGA TTA CGA ATT CGA GCT CGG

T7 promotor:              TAA TAC GAC TCA CTA TAG GG

### 2.3.2   Mutagenesis primers

Mutagenesis primers for the substitution and deletion of the GyrA-box (AboxA, delAbox), the removal of an internal NcoI binding and cleavage site (NcoI_remove; silent mutation), and the introduction of a sequence coding for a TEV-protease cleavage site (NHis-TEV) (all for *B. subtilis* GyrA).

| | |
|---|---|
| gyrA_Bs_AboxA_5: | GCA TCA ACT TAC CGC AGT GCA GCA GCG GCC GCA GCA GCT GTA CAA GGT ATG GG |
| gyrA_Bs_AboxA_3: | CCC ATA CCT TGT ACA GCT GCT GCG GCC GCT GCT GCA CTG CGG TAA GTT GAT GC |
| gyrA_Bs_delAbox_5: | CGT CTT CCT GCA TCA ACT TAC CGC AGT GTA CAA GGT ATG GGA ACA AAC G |
| gyrA_Bs_delAbox_3: | CGT TTG TTC CCA TAC CTT GTA CAC TGC GGT AAG TTG ATG CAG GAA GAC G |
| gyrA_Bs_NcoI_remove_5: | CGG TAT ATG AAT CTA TGG TCA GAA TGG |
| gyrA_Bs_NcoI_remove_3: | CCA TTC TGA CCA TAG ATT CAT ATA CCG |
| gyrA_Bs_NHis_TEV_5: | CCA CAG CCA GGA TCC GGA AAA CCT GTA CTT CCA AAG TGA ACA AAA CAC ACC |
| gyrA_Bs_NHis_TEV_3: | GGT GTG TTT TGT TCA CTT TGG AAG TAC AGG TTT TCC GGA TCC TGG CTG TGG |

The following mutagenesis primers were used for single amino acid substitution in GyrA (single letter amino acid code) as well as for screening purposes (analytical PCR reactions)

gyrA_Bs_Y123F_5:        GCG GCG GCC ATG CGT TTT ACA GAA GCA CGA ATG

gyrA_Bs_Y123F_3:        CAT TCG TGC TTC TGT AAA ACG CAT GGC CGC CGC

gyrA_Bs_T140C_5:        GGA GAT TCT TCG CGA CAT CTG CAA AGA CAC AAT CGA TTA CCA GG

17

| | |
|---|---|
| gyrA_Bs_T140C_3: | CCT GGT AAT CGA TTG TGT CTT TGC AGA TGT CGC GAA GAA TCT CC |
| gyrA_Bs_E211C_5: | CCA GAG CTT ATG TGT GTC ATT CCA GGG C |
| gyrA_Bs_E211C_3: | GCC CTG GAA TGA CAC ACA TAA GCT CTG G |
| gyrA_Bs_E250C_5: | GCA AAA GCT GAG ATC TGC CAA ACA TCT TCG |
| gyrA_Bs_E250C_3: | CGA AGA TGT TTG GCA GAT CTC AGC TTT TGC |
| gyrA_Bs_N314C_5: | CGA TGC CAA TGC GTG CGT TAT CTT AAA CAA TC |
| gyrA_Bs_N314C_3: | GATTGTTTAAGATAACGCACGCATTGGCATCG |
| gyrA_Bs_C350L_5: | CGA AAG TTT TAA CTC TTA AGC AAC TGC TGG AGC ATT ACC |
| gyrA_Bs_C350L_3: | GGT AAT AGCT CCA GCA GTT GCT TAA GAG TTA AAA CTT TCG |
| gyrA_Bs_N399C_5: | GCA GTT ATC TCC CTT ATC CGT TGT TCT CAA ACG GCT GAA ATT GCG |
| gyrA_Bs_N399C_3: | CGC AAT TTC AGC CGT TTG AGA ACG GAT AAG GGA GAT AAC TGC |
| gyrA_Bs_T408C_5: | CGG CTG AAA TTG CGA GAT GTG GTT AAT TGA ACA ATT CT C |
| gyrA_Bs_T408C_3: | GAG AAT TGT TCA ATT AAA CCA CAT CTC GCA ATT TCA GCC G |
| gyrA_Bs_S490stop_5: | GAG ATC GTC ACT TAA GGA CTG GAG AC |
| gyrA_Bs_S490stop_3: | GTC TCC AGT CCT TAA GTG ACG ATC TC |
| gyrA_Bs_K570C_5: | GTG TAT CGT GCA TGC GGG TAT GAA ATC |
| gyrA_Bs_K570C_3: | GAT TTC ATA CCC GCA TGC ACG ATA CAC |
| gyrA_Bs_D695C_5: | CAC CCT GAC GTG TGA CGA CGT TG |
| gyrA_Bs_D695C_3: | CAA CGT CGT CAC ACG TCA GGG TG |
| gyrA_Bs_E726C_5: | CGA ACT CCT GCT TGT GAG TAC AGA ACC |
| gyrA_Bs_E726C_3: | GGT TCT GTA CTC ACA AGC AGG AGT TCG |
| gyrA_Bs_K594C_5: | GCT GGA GGT AGA ATG TGG TGA GTG GAT CAA CG |
| gyrA_Bs_K594C_3: | CGT TGA TCC ACT CAC CAC ATT CTA CCT CCA GC |

The following mutagenesis primers were used for single amino acid substitution in *M. mazei* topoisomerase VI A or B (single letter amino acid code) as well as for screening purposes (analytical PCR reactions).

| | |
|---|---|
| TopoVIA_Y106F_for: | CGA GAA CTT TAT TTC ATT TCC GAA GGC |
| TopoVIA_Y106F_rev: | GCC TTC GGA AAT GAA ATA AAG TTC TCG |
| TopoVIB_R87C_for: | CCG GGA ATT GTA TGC GAG CAG ATC CCC |
| TopoVIB_R87C_rev: | GGG GAT CTG CTC GCA TAC AAT TCC CGG |
| TopoVIB_D159C_for: | GCA CAA ATG AAC CTT GCA TCC TTG TAG ACG AGG |
| TopoVIB_D159C_rev: | CCT CGT CTA CAA GGA TGC AAG GTT CAT TTG TGC |
| TopoVIB_E164C_for: | GAT ATC CTT GTA GAC TGC GTC AGG GAC TGG |
| TopoVIB_E164C_rev: | GTC CCT GAC GCA GTC TAC AAG GAT ATC AGG |
| TopoVIB_C267S_for: | GCG TTA CTC TTT TTC TAA AAT AGG GC |
| TopoVIB_C267S_rev: | GCC CTA TTT TAG AAA AAG AGT AAC GC |
| TopoVIB_C278A_for: | GGA GGA AAT CGC TAA AGC CGC AG |
| TopoVIB_C278A_rev: | CTG CGG CTT TAG CGA TTT CCT CC |
| TopoVIB_C316A_for: | GAC GGA CGC GCT TTC TCC TAT CGG |

| | |
|---|---|
| TopoVIB_C316G_for: | CGA CGG ACG GTC TTT CTC C |
| TopoVIB_C316S_for: | CGA CGG ACT CTC TTT CTC C |
| TopoVIB_C316A_rev: | GGA GAA AGC GCG TCC GTC GGA G |
| TopoVIB_C316G_rev: | GGA GAA AGA CCG TCC GTC G |
| TopoVIB_C316S_rev: | GGA GAA AGA GAG TCC GTC G |
| TopoVIB_P408C_for: | GGC TTA AAC CAG TGC GGA GGG GGA ATT C |
| TopoVIB_P408C_rev: | GAA TTC CCC CTC CGC ACT GGT TTA AGC C |
| TopoVIB_C550A_for: | CGA AAT GCT CCC CGC TAA AGT TAG CGG |
| TopoVIB_C550A_rev: | CCG CTA ACT TTA GCG GGG AGC ATT CG |

## 2.3.3 DNA substrate for *B. subtilis* gyrase or *M. mazei* topoisomerase VI

Positions indicated by X stand for fluorescently labeled thymine nucleotides. The dye is covalently attached to an amino linker on C6 of the base.

| | |
|---|---|
| Gyr_37bp_1bs_for: | GTG CCA AGC TAT GCA TGA TCA TAC GTC GAC TCT AGA G |
| Gyr_37bp_1bs_rev: | CTC TAG AGT CGA CGT ATG ATC ATG CAT AGC TTG GCA C |
| Gyr_37bp_1bs_rev_A546: | CTC TAG AGT CGA CGT ATG ATC ATG CAX AGC TTG GCA C (X = T labeled with Alexa546) |
| Gyr_48bp_1bs_for: | CTC GCA GTG CCA AGC TAT GCA TGA TCA TAC GTC GAC TCT AGA GTC TCG |
| Gyr_48bp_1bs_rev: | CGA GAC TCT AGA GTC GAC GTA TGA TCA TGC ATA GCT TGG CAC TGC GAG |
| Gyr_48bp_1bs_rev_A546: | CGA GAC TCT AGA GTC GAC GTA TGA TCA TGC AXA GCT TGG CAC TGC GAG (X = T labeled with A546) |
| Gyr_60bp_1bs_for: | GTC TCG CAG TGC CAA GCT ATG CAT GAT CAT ACG TCG ACT CTA GAG TCT CGC AGT GTA CCG |
| Gyr_60bp_1bs_rev: | CGG TAC ACT GCG AGA CTC TAG AGT CGA CGT ATG ATC ATG CAT AGC TTG GCA CTG CGA GAC |
| Gyr_60bp_1bs_rev_A546: | CGG TAC ACT GCG AGA CTC TAG AGT CGA CGT ATG ATC ATG CAX AGC TTG GCA CTG CGA GAC (X = T labeled with Alexa546) |
| Gyr_90bp_2bs_for: | AGT CAC GAC GTT GTA AAA CGA CGG CCA GTG CCA AGC TAT GCA TGA TCA TAC GTC GAC TCT AGA GGA TCC CCG GGT ACC GAG CTC GAA TTC |
| Gyr_90bp_2bs_rev: | GAA TTC GAG CTC GGT ACC CGG GGA TCC TCT AGA GTC GAC GTA TGA TCA TGC ATA GCT TGG CAC TGG CCG TCG TTT TAC AAC GTC GTG ACT |
| TopoVI_51_f: | TCA ATA ATA TTG AAA AAG GAA GAG TAT GAG TAT TCA ACA TTT CCG TGT CGC |
| TopoVI_51_f_fl: | XCA ATA ATA TTG AAA AAG GAA GAG TAT GAG TAT TCA ACA TTT CCG TGT CGC (X = T labeled with fluorescein) |
| TopoVI_50_f_546: | CAA TAA TAT TGA AAA GGA AGA GTA TGA GTA TCA ACA TTT CGT GTC GC (X = T labeled with A546) |
| TopoVI_51_r: | GCG ACA CGG AAA TGT TGA ATA CTC ATA CTC TTC CTT TTT CAA TAT TAT TGA |
| TopoVI_50_r_488: | GCG ACA CGG AAA TGT TGA ATA CTC ATA CTC TXC CTT TTT CAA TAT TAT TG (X = T labeled with Alexa488) |

19

### 2.3.4 Sequencing primers

| | |
|---|---|
| gyrA_Bs_mid1: | CCA GGA TAA CTA TGA CGG G |
| gyrA_Bs_mid2: | CGA TGC CAA TGC GAA TGT TAT C |
| pETDuet_DuetDOWN1: | GAT TAT GCG GCC GTG TAC AAT AC |
| pETDuet_DuetUP1: | ATG CGT CCG GCG TAG A |
| T7 promotor: | TAA TAC GAC TCA CTA TAG GG |
| T7 terminator: | TGC TAG TTA TTG CTC AGC GG |
| TopoVI_mid1: | CCC TTG GTC TTA CAG GAT CTA TGC |
| TopoVI_mid2: | CCG TAC TGC TTC CAC TTA ATG TCC |

## 2.4 Consumables

**BD** (Franklin Lakes, USA) 50 ml conical tubes, PP; Microlance-3 needles, 0.90 x 40 mm

**Bio-Rad Laboratories** (Hercules, USA) Econo-Pac Columns, Micro Bio-Spin 30 columns, RNase-free

**Brand** (Wertheim, D) UV-cuvettes PLASTIBRAND micro, z = 8.5 mm, 2 x 3.5 mm

**CODAN Medical** (Rødby, DK) ONCE inject syringes, 2, 10, 20 ml

**GE Healthcare** (Chalfont, St. Giles, UK) illustra Microspin G-25 column

**Eppendorf** (Hamburg, D) Safe-lock tubes amber, 1.5 ml; Safe-lock tubes 2.0 ml

**G. Kisker** (Steinfurt, D) Quali-‚Low Retention' tubes, 1.7 ml

**Promega** (Madison, USA) PureYield Plasmid Midiprep System; Wizard SV Gel and PCR Clean-Up system

**Qiagen** (Hilden, D) QIAGEN Plasmid Midi Kit; QIAprep Spin Miniprep Kit; QIAquick Nucleotide Removal Kit; QIAquick PCR purification kit

**Sarstedt** (Nürnbrecht, D) 15 ml conical tubes, PP; cuvettes 10 x 4 x 45 mm; Filtropur S 0.20 µm; Micro Tube 1.5 ml, PP; Multiply-Pro cup, 0.2 ml, PP

**Sartorius Stedim Biotech** (Aubagne, F) Midisart 2000 filter; Vivaspin 20 concentrator 10,000 MWCO PES; Vivaspin 6 concentrator 10,000 MWCO PES

**Spectrum Laboratories** (Rancho Dominguez, USA) Spectra/Por dialysis membranes, 12 – 14,000 MWCO

**Starlab** (Ahrensburg, D) TipOne Tips 10, 200, 1000 µl

**Thermo Fisher Scientific** (Rockford, USA) Lab-Tek chamber slides, 8 chambers, glass slide

**Treff AG** (Degersheim, CH) Microtubes ClickFit, 1.5 ml

## 2.5 Instrumentation

**Centrifugation** Beckmann Coulter Allegra 21R Centrifuge, rotor S4180 (Brea, USA); Heraeus Biofuge pico, rotor 33258; Sorvall RC 5C plus, rotors SS34 and SLA3000 (Kendro Laboratory Products, Langenselbold, D); Eppendorf centrifuge 5402, rotor F-45-18-11 (Hamburg, D)

**Electrophoresis** Home-built agarose gel caster and gel-electrophoresis unit; Hoefer multiple gel caster; gel electrophoresis unit Mighty Small II (8 x 7 cm); power supply EPS 300, 301, 1001 (Amersham Biosciences Europe, Freiburg, D); gel documentation system EDAS 290 (Kodak, Stuttgart, D); transilluminator FT-20/254/365 (Herolab, Wiesloch, D)

**Thermocycler** GeneAmp PCR System 9600 (Perkin Elmer Inc., MA, USA); Mastercycler gradient (Eppendorf, Hamburg, D); Techne TC-3000 Thermal Cycler (Bibby Scientific Limited, Staffordshire, UK)

**Incubator** Minitron (Infors, Bottmingen, CH)

**Microfluidizer** M-110L (Microfluidics, Newton, USA)

**Preparative HPLC** ÄKTAprime plus (GE Healthcare, Chalfont, St. Giles, UK); HiLoadTM 16/60 Superdex 200 pg SEC column; resins: chelating sepharose, SP sepharose, Q sepharose, Heparin sepharose (all Fast Flow); LC column XK 16; Superloop 50 ml (all Amersham Biosciences, Freiburg, D)

**Absorption measurements** Ultrospec 2100 pro (Amersham Biosciences Europe, Freiburg, D); precision cuvettes from Quartz SUPRASIL for absorption measurements, no. 105.202, path 10 mm (Hellma, Müllheim, D); UV/Vis Biophotometer (Eppendorf, Hamburg, D)

**Fluorescence measurements** FluoroMax-3 (HORIBA JOBIN YVON, Stanmore, UK); precision cuvettes from Quartz SUPRASIL for absorption measurements, no. 105.250, path 10 x 2 mm (Hellma, Müllheim, D)

**Thermostat** ThermoStat plus (Eppendorf, Hamburg, D)

**Confocal fluorescence microscope for single-molecule FRET experiments**

Fluorescence from freely diffusing single molecules was detected on a home-built confocal microscope. The excitation light was generated by a modelocked solid-state Ti:sapphire laser (Tsunami, Spectra-Physics, Mountain View, USA), which was pumped by a countinuous-wave Nd:$VO_4$ diode laser (Millenia pro, Spectra-Physics), emitting light of 951 nm pulsed at an interval of 40 ns and a pulse-width of 2.5 ps. The beam was frequency-doubled (to 475 nm; Model GWU, Spectra-Physics), directed into an inverted microscope (IX71, Olympus, Tokyo, J) and focused into the sample volume by a water-immersion objective with a high numerical

aperture (NA = 1.2; UPlanApo, Olympus). Fluorescence from single molecules was collected by the same objective and directed to the detection part by a dichroic beam splitter (DM505, Olympus). Detection of light emitted exclusively from molecules in the excitation volume was achieved by focusing the photons on a 100 µm pinhole. Donor and acceptor fluorescence was split by a second dichroic mirror and separately detected by avalanche photo diodes (APD). The signal transmitted to a single photon counting card (SPC-630, Becker & Hickl, Berlin, D) and processed *in silico*.

## 2.6 DNA plasmids

pET-27b(+)_*gyrA*: Ahead of this work wild-type *B. subtilis gyrA* has been ligated into pET-27b(+) vector (Novagen by Merck, Darmstadt, Germany) using NdeI and XhoI restriction sites. The vector confers kanamycin resistance.

pETDuet-1 (Novagen by Merck, Darmstadt, Germany) contains two multiple cloning sites (MCS) and encodes beta-lactamase (mediating ampicillin resistence). It was used for sub-cloning of *B. subtilis gyrA* from pET-27b(+). The *gyrA* ORF was fused in frame to a $His_6$-tag sequence using BamHI and HindIII restriction sites.

pACYCDuet-1 (Novagen by Merck, Darmstadt, Germany) contains the same MCS as pETDuet-1 but comes with a different origin of replication and confers kanamycin resistance. *his$_6$_gyrA* was sub-cloned from pETDuet-1 using NcoI and XhoI restriction sites. The construct was co-transformed with pET-27b(+)_*gyrA* for co-production of two GyrA protein versions.

pDEST_topoVIA_B was a gift by Prof. J. M. Berger (University of California, Berkeley, California). The ORFs of the topoisomerase VI subunits from *M. mazei* are cloned in a bi-cistronic operon with one T7 promotor sequence. *topoVIB* is positioned 5' to *topoVIA* and fused to a N-terminal $His_6$-tag cleavable by TEV protease.

pUC18 (Fermentas by Thermo Fisher Scientific, Waltham, Massachusetts) is a small expression vector (2686 bp). It was used as a substrate in DNA supercoiling and relaxation assays. pUC18 confers ampicillin resistance. A modified pUC18 vector containing a preferred binding/cleavage site for gyrase is used as a template for the PCR based production of the gyr_110bp DNA substrate as described [42].

22

## 2.7 Bacterial strains

All strains used in this work were derived from *E . coli* B which is deficient for Lon protease.

*E. coli* XL1-Blue (Stratagene, La Jolla, California): *recA1 endA1 gyrA96 thi-1 hsdR17 supE44 relA1 lac* [F′ *proAB lacI*$_q$*ZΔM15* Tn*10* (Tet$^r$)]

Xl1-Blue was used as host strain for routine cloning (transformation of ligation and mutagenesis products) and plasmid DNA propagation. Plasmid DNA extracted from *E. coli* is methylated on N6 positions of adenine bases in the palindromic nucleotide sequence GATC due to the presence of DNA adenine methyltransferase [68].

*E. coli* BL21(DE3) (Stratagene, La Jolla, California): F$^−$ *dcm ompT hsdS*(r$_B$$^−$ m$_B$$^−$) *gal* λ(DE3)

The strain was used for the expression of *B. subtilis* GyrA from pACYCDuet-1 vector alone or in combination with pET-27b(+) vector.

*E. coli* BL21-CodonPlus(DE3)-RP (Stratagene, La Jolla, California): F$^−$ *ompT hsdS*(r$_B$$^−$ m$_B$$^−$) *dcm*$^+$ Tet$^r$ *gal* λ(DE3) *endA* Hte [*argU proL;* Cam$^r$]

In this strain we expressed His$_6$-tagged or non-tagged *B. subtilis* GyrA from pETDuet-1 or pET-27b(+) vectors.

*E. coli* Rosetta(DE3) (Merck, Darmstadt, Germany): F$^−$ *ompT hsdS*$_B$(r$_B$$^−$ m$_B$$^−$) *gal dcm* (DE3) pRARE (*argU, argW, argX, glyT, ileX, leuW, metT, proL, thrT, thrU, tyrU;* Cam$^r$)

Rosetta(DE3) was used as an expression host for the co-production of *M. mazei* TopoVIA and TopoVIB proteins.

<u>Culturing Media for *E. coli*</u>

Luria Broth (LB) (after [69], containing 10g/l tryptone, 5 g/l yeast extract, and 10 g/l NaCl was used to culture *E. coli* for plasmid DNA production or expression (inoculation culture). Single clone propagation was performed on LB agar plates (containing 19 g/l agar).

Autoinducing medium (AIM) (after [70]) was used for large-scale recombinant expression in *E. coli*.

Appropriate antibiotics (ampicillin: 100 μg/ml; kanamycin: 20 μg/ml; chloramphenicol: 10 μg/ml) were added to media and agar plates to select for bacterial strains and vectors.

## 2.8 General Methods

### 2.8.1 Transformation of *E. coli* cells

50 – 100 µl of chemically competent *E. coli* cells suspended in 100 mM $CaCl_2$ were mixed with 20 – 50 ng purified plasmid DNA or 10 µl ligation or mutagenesis product and incubated on ice for 5 min before being subjected to heat treatment (42°C, 90 s). The cells were cooled on ice for a 2 – 3 minutes, then mixed with 1 ml of LB medium and incubated at 37°C for 1 h. Cells were pelleted gently (Eppendorf table-top centrifuge, 3000 rpm, 2 min), resuspended in 200 µl supernatant and plated on LB agar containing appropriate antibiotics for strain and plasmid selection.

### 2.8.2 Agarose gel electrophoresis

- 0.5 x TBE buffer: 5.5 g/l Tris, 2.75 g/l boric acid, 2 g/l EDTA sodium salt
- 6 x loading buffer: 10 mM Tris/HCl pH 7.6, 60 mM EDTA, 60 % glycerol, 0.03 % (w/v) bromphenol blue, 0.03 % (w/v) xylene cyanol
- Staining solution: approx. 1 µg/ml ethidium bromide in MQ-$H_2O$

Agarose gel electrophoresis is a simple method to analyze and separate DNA fragments (PCR products, plasmid DNA, restriction fragments, etc.). 0.8 to 2.0 % (w/v) agarose were suspended in 0.5 x TBE buffer, boiled, volume adjusted and poured in a gel caster for solidification. DNA samples were mixed with 6 x loading buffer and applied to the gel. DNAs were separated in an electric field of 11 – 16 V/cm. After electrophoresis gels were incubated in staining solution for 15 – 30 min and visualized by a UV transilluminator.

### 2.8.3 Discontinuous polyacrylamide gel electrophoresis (SDS-PAGE)

- Stacking gel: 125 mM Tris/HCl pH 6.8 (25°C), 0.06 % (w/v) SDS, 4.5 % (v/v) acrylamide, 0.1 % (v/v) bisacrylamide, 0.1 % (w/v) APS, 0.1 % (v/v) TEMED
- Separating gels: A: 375 mM Tris/HCl pH 8.8 (25°C), 0.1 % (w/v) SDS, 10 % (v/v) acrylamide, 0.26 (v/v) bisacrylamide, 0.086 % (w/v) APS, 0.057 % (v/v) TEMED
  B: 375 mM Tris/HCl pH 8.8 (25°C), 0.1 % (w/v) SDS, 15 % (v/v) acrylamide, 0.39 % (v/v) bisacrylamide, 0.086 % (w/v) APS, 0.057 % (v/v) TEMED
- Running buffer: 24 mM Tris, 200 mM glycine, 0.1 (w/v) SDS
- 4 x loading buffer: 130 mM Tris/HCl pH 6.8 (25°C), 200 mM DTT, 20 % (v/v) glycerol, 4 (w/v) SDS, approx. 0.01 % (w/v) bromophenol blue
- Staining solution: 50 % (v/v) methanol, 10 % (v/v) acetic acid, 0.1 % (w/v) Coomassie Brilliant Blue R-250
- Destaining solution: 20 % (v/v) ethanol, 10 % (v/v) acetic acid

Proteins were analyzed under denaturing conditions by SDS-PAGE introduced by Laemmli [71]. Protein samples (expression cultures, purified or chemically modified protein) were mixed with loading buffer, heated to 95°C for approx. 5 min, and applied to a gel consisting of 2 cm of stacking and 5 cm of separating gel approx. Electrophoresis was performed at an

electric current of 30 mA for 25 – 40 min using bromphenol blue as a tracking dye. Fluorescently labeled samples were made visible by UV illumination. Non-labeled protein was stained with Brilliant Blue by incubating the gel in staining and destaining solution for at least 15 and 30 min respectively; over-night incubation in Millipore water was performed for increased contrast.

Non-labeled GyrA and GyrB proteins from *B. subtilis* were generally analyzed on gels containing 10% acrylamide (A) *M. mazei* topoisomerase VI and fluorescently labeled protein on 15% acrylamide (B) gels.

### 2.8.4   Concentration determination

The concentration of proteins, DNAs, nucleotides and fluorescent labels in solution were determined spectrophotometrically. Absorption spectra were recorded on Ultrospec 2100 pro photometer using quartz cuvettes and single wave-length absorption on an Eppendorf Biophotometer. According to the Beer-Lambert law (eq. 2.1) the absorption scales with the concentration of the absorbing species:

$$A_\lambda = \varepsilon_\lambda \cdot c \cdot d \qquad\qquad (2.1)$$

$A_\lambda$ denominates the absorption, $\varepsilon_\lambda$ the molar extinction coefficient at a given wavelength, c the concentration of the solute, and d the path length (given by the cuvette: 1 cm).

Extinction coefficients $\varepsilon$ of proteins at 280 nm were calculated with Protparam [72]:

*B. subtilis* GyrA wild-type and mutants: 42750 $M^{-1}cm^{-1}$

*B. subtilis* GyrA Y123F: 41260 $M^{-1}cm^{-1}$

*B. subtilis* GyrA $\Delta$CTD: 25330 $M^{-1}cm^{-1}$

*B. subtilis* GyrB wild-type: 52720 $M^{-1}cm^{-1}$

*M. mazei* TopoVIA wild-type: 47330 $M^{-1}cm^{-1}$

*M. mazei* TopoVIA Y106F: 45840 $M^{-1}cm^{-1}$

*M. mazei* TopoVIB wild-type and mutants: 46300  $M^{-1}cm^{-1}$

According to the only available crystal structure for *M. mazei* topoisomerase VI [61], no cysteine residue formed disulfide bonds: For the calculation of extinction coefficients the number of disulfide bonds (cystines) was assumed to be 0.

The concentration of co-expressed and co-purified TopoVIAB proteins was estimated by assuming equimolarity. As extinction coefficient for TopoVIAB the sum of the individual coefficients was used:

*M. mazei* TopoVIA (wild-type) B (wild-type and mutants): 93630 $M^{-1}cm^{-1}$

*M. mazei* TopoVIA (Y123F) B (wild-type): 92140 $M^{-1}cm^{-1}$

Extinction coefficients for single-stranded DNAs were estimated with the nearest-neighbor model [73]:

Gyr_90bp_for: 871700 $M^{-1}cm^{-1}$

Gyr_90bp_rev: 851300 $M^{-1}cm^{-1}$

Gyr_60bp_for: 569000 $M^{-1}cm^{-1}$

Gyr_60bp_rev: 580000 $M^{-1}cm^{-1}$

Gyr_48bp_for: 453800 $M^{-1}cm^{-1}$

Gyr_48bp_rev: 467000 $M^{-1}cm^{-1}$

Gyr_37bp_for: 360600 $M^{-1}cm^{-1}$

Gyr_37bp_rev: 355500 $M^{-1}cm^{-1}$

TopoVI_51bp_for: 520200 $M^{-1}cm^{-1}$

TopoVI_51bp_rev: 492100 $M^{-1}cm^{-1}$

The concentration of double stranded DNAs (Gyr_110bp, plasmid DNA) was estimated by:

1 $A_{260}$ = 50 ng/ml

Extinction coefficients for nucleotides and analogs:

ATP, ADPNP, ADP: $\varepsilon_{260}$ = 15400 $M^{-1}cm^{-1}$

NADH: $\varepsilon_{340}$ = 6300 $M^{-1}cm^{-1}$ [74]

Extinction coefficients of fluorescent dyes (provided by the manufacturer and in [75]):

Alexa Fluor488 C5 maleimide (A488): $\varepsilon_{493}$ = 72000 $M^{-1}cm^{-1}$ ($\varepsilon_{280}$ = 72000 $M^{-1}cm^{-1}$)

Alexa Fluor546 C5 maleimide (A546): $\varepsilon_{554}$ = 93000 $M^{-1}cm^{-1}$ ($\varepsilon_{280}$ = 10538 $M^{-1}cm^{-1}$, $\varepsilon_{493}$ = 7025 $M^{-1}cm^{-1}$)

TMR maleimide (TMR): $\varepsilon_{550}$ = 95000 $M^{-1}cm^{-1}$ ($\varepsilon_{280}$ = 18531 $M^{-1}cm^{-1}$, $\varepsilon_{493}$ = 11259 $M^{-1}cm^{-1}$)

Uranine (fluorescein): $\varepsilon_{490}$ = 93000 $M^{-1}cm^{-1}$

## 2.9 DNA manipulation methods

### 2.9.1 Cloning: PCR amplification of linear DNA, restriction enzyme digestion and ligation into target vector DNA

The polymerase chain reaction (PCR) [76] was used to preparatively amplify target gene open reading frames (ORF) on an Eppendorf Mastercycler gradient. A DNA primer pair complementary to the 3' ends of sense and antisense strands of the gene was used for the amplification of a target gene contained in plasmid DNA serving as a template. PCR reactions generally contained 1 ng/μl template DNA, 0.5 μM forward and reverse primer each, 0.2 mM deoxynucleotide triphosphates (dATP, dGTP, dCTP, dTTP) each, 0.02 U/ μl Phusion Polymerase in 1x Phusion HF Buffer. The PCR was performed according to the manufacturers instructions, typically applying annealing temperatures between 58 and 70°C and elongation times of 20 – 30 s / kb.

PCR products were purified with PCR clean-up kit (Sigma) and cut with appropriate restriction endonucleases in the appropriate buffers alongside with target cloning vectors. Cut vectors were dephosphorylated with Shrimp Alkaline Phosphatase (SAP) according to instructions by the manufacturer. Restriction fragments were purified with QIAquick nucleotide removal kit (Qiagen) and ligated over-night at 16°C using T4 ligase with the appropriate buffer and insert:vector ratios varying between 3:1 and 6:1; the concentration vector DNA was set to approx. 2.5 ng/μl. For transformation of the ligation product, 50 μl of *E. coli* XL1-Blue cells were mixed with 10 μl of ligation reaction and grown on agar plates containing antibiotics to select for the plasmid to yield single clone colonies.

### 2.9.2 Site-directed mutagenesis

Mutagenesis was performed according to the QuikChange site-directed mutagenesis protocol (Stratagene, La Jolla, USA) [77] and used for nucleotide base substitution, insertion or deletion on a given template (usually a vector containing an ORF of a gene of interest). The latter is amplified in a PCR reaction using a pair of complementary DNA primers containing the mutant nucleotide sequence. Mutagenesis reactions generally contained 1 ng/μl template DNA, 0.25 μM primers each, 0.2 mM deoxynucleotide triphosphates (dATP, dGTP, dCTP, dTTP) each, 0.02 U/ μl Phusion Polymerase in 1x μM Phusion HF Buffer. The reaction mix was split in 5 aliquots for parallel annealing temperature screening. The mutagenesis was performed like usual PCR reactions (section 2.9.1)

10 µl of reaction mix containing PCR product was cut with DpnI (1.8 U/µl, 37°C, 2 h) for template DNA degradation and transformed into *E. coli* XL1-Blue cells. Transformed cells were grown on agar plates containing antibiotics to select for the plasmid to yield single clone colonies.

### 2.9.3  Analytical DNA amplification by PCR: Selection of correct DNA constructs

- Buffer Y: 20 mM Tris/HCl (pH 8.6), 16 mM $(NH_4)_2SO_4$, 0.01 % Tween20, 2 mM $MgCl_2$

*E. coli* XL1-Blue cells transformed with ligation or mutagenesis constructs were screened for correct insert orientation (ligation) and insertions (mutagenesis) by PCR-amplification of 200 – 600 nucleotides encompassing the sequence of interest. Primers used were often not fully complementary to the template (mutagenesis primers), but annealing conditions were not stringent to compensate.

PCR reactions contained 1 µM forward and reverse primers, 0.2 µM dNTPs each, 0.025 U/µl GoTaq polymerase, and 1x buffer Y. A minimal amount of cell material containing the test plasmid was added to 8.5 µl reaction mix. The PCR was performed using a standard annealing temperature of 52°C and elongation times of approx. 60 s / kb.

Plasmid DNA of positive clones was propagated in *E. coli*, purified with Miniprep Kit (Qiagen), and sequenced (Microsynth AG, Balgach, CH).

### 2.9.4  Cloning and mutagenesis of *B. subtilis gyrA* constructs

pET-27b(+)_*gyrA* and mutants

Ahead of this work the *gyrA* ORF had been amplified by PCR and cloned into pET-27b (+) vector using restriction endonuclease cleavage sites NdeI and XhoI, yielding a non-tagged GyrA when expressed [46]. Moreover, several cysteine mutants (all in combination with C350L: T140C, E211C, N399C, T408C, K594C, and E726C) as well as the active site mutant Y123F were constructed previously. Further single cysteine mutants were produced by quick-change mutagenesis [77] using respective mutagenesis primers: E250C, N314C, K570C, D695C (all mutations in combination with C350L). Double cysteine mutants with one mutant residue in the GyrA body and one in the CTD were constructed from single cysteine mutants. Functional mutants were produced on the basis of the wild-type or C350L_T140C_K594C double cysteine mutant templates, using corresponding primers. GyrA-box mutants with residues deleted (ΔAbox) and exchanged to alanines (AboxA) were both constructed using

the wt template, while a cleavage-deficient Y123F and a ΔAbox were constructed on the basis of the double-cysteine mutant template.

A C-terminal domain deletion mutant was constructed from the wild-type template by mutation of the S490 codon to a translation stop codon (TAA).

## pETDuet-1_His$_6$_gyrA

gyrA C350L was amplified by PCR from pET-27b(+)_gyrA with primers gyrA_Bs_DuetBamHI_for and gyrA_Bs_DuetHindIII_rev, cut with BamHI and HindIII endonucleases (using NEB buffer 2) and ligated by T4 DNA ligase (in T4 DNA ligase buffer) into multiple cloning site 1 (MCS1) of pETDuet-1 vector, in frame with a sequence coding for an N-terminal His$_6$-tag.

## pETDuet-1_His$_6$_TEV_gyrA and _gyrA_ΔCTD

The nucleotide sequence for a TEV protease (TEVp) cleavage site was introduced to the pETDuet-1_His$_6$_gyrA construct by mutagenesis (section 2.9.2). Primers used were gyrA_Bs_NHis_TEV_5 and _3 comprising an insertion of 18 nucleotides. Expression of the construct yielded a protein with the amino acid sequence H$_6$-P-E-N-L-Y-F-Q|-S-GyrA, underlined letters denoting the recognition sequence of TEVp with the cleavage site indicated by the vertical line.

A construct lacking the nucleotide sequence for the CTD was produced by introducing the S490stop mutation.

## pACYCDuet-1_His$_6$_TEV_gyrA and mutants Y123F and ΔAbox

For these constructs pETDuet-1_His$_6$TEV_gyrA served as a template: An internal sequence for the restriction endonuclease NcoI was mutated with primers gyrA_Bs_NcoI_remove_5 and _3 and the construct encompassing the fused ORF His$_6$_TEV_gyrA was amplified by PCR (section 2.9.1) with the primers T7 promotor and gyra_rev (containing the gyrA stop codon and an XhoI restriction site). Enzymatic cleavage and subsequent ligation of the PCR product using NcoI and XhoI restriction sites of pACYCDuet-1 vector resulted in a sequence encoding the same expression product as the pETDuet-1 construct.

Functional mutants Y123F and ΔAbox were produced following the same protocol as for gyrA constructs in pET-27b(+).

### 2.9.5 Mutagenesis of pDEST_*topoisomerase VI* construct

The plasmid encoding *M. mazei* topoisomerase VI subunits A and B was a gift from Prof. James Berger (University of California, Berkeley, California, USA). The vector was derived from a common pET vector (Prof. Berger: personal communication) confering kanamycin resistance. The ORFs coding for topoisomerase VI were cloned in a bi-cistronic operon with the ORF of *topoVIA* arranged 5' to the one of *topoVIB*. TopoVIB was fused to an N-terminal His$_6$-tag cleavable with TEV protease.

All mutagenesis reactions were performed on the pDEST construct as a template (section 2.9.2) using appropriate primers.

### 2.9.6 DNA sequence verification

Plasmid DNA was sequenced at Microsynth AG (Balgach, Switzerland) applying the chain termination method [78], using primers listed in section 2.3.4. Correct sequences were confirmed for all DNA constructs and corresponding proteins described in this work.

## 2.10 Protein preparation and purification

Proteins purified ahead of this work were wild-type *B. subtilis* GyrA and GyrB and the GyrA mutants Y123F, T140C, E211C, T408C, K594C, and E726C. All mutants with the exception of Y123F contained the mutation C350L.

Ines Hertel (Group Klostermeier, Biozentrum, University of Basel) assisted in the production and purification of hetero-dimeric GyrA proteins (section 2.10.2).

### 2.10.1 Fermentation

All proteins purified in course of this work were recombinantly over-produced using *E. coli* (individual fermentation protocols below). A single colony of expression strains transformed with the appropriate vector(s) (section 2.8.1) were pre-cultured in LB medium (section 2.7) at 37°C over night and used to inoculate auto-induction medium in a 1:100 (v/v) ratio. If not indicated otherwise expression cultures were shaken at 37°C for approx. 24 h. Cells were pelleted by centrifugation (SLA3000 rotor, 5000 rpm, 10 min, 4°C) and stored at -20°C.

Non-tagged GyrA mutant proteins with corresponding open reading frames inserted into pET-27b(+) were produced in *E. coli* BL21(DE3)RP cells as described before [46].

Full-length and CTD deletion mutant GyrA His$_6$-tag fusion constructs cloned into pETDuet-1 vector were expressed in *E. coli* BL21(DE3)RP. GyrA expressed from pACYCDuet-1 vector were produced in *E. coli* BL21(DE3).

Hetero-dimeric GyrA were expressed in *E. coli* BL21(DE3) strain transformed with pET27b and pACYCDuet-1, each containing a copy of *gyrA* open reading frame. Selection was done for both plasmids by using kanamycin and chloramphenicol. For enhanced protein production and solubility co-transformed cells were cultured at 30°C for 24 h.

Wild-type and mutant *M. mazei* Topoisomerase VI A and B were co-expressed in *E. coli* Rosetta(DE3) cells as described before [61] at 37°C for 24 h.

## 2.10.2 Purification of GyrA constructs

All protein purification steps involving chromatography were performed on the liquid chromatography system ÄKTAprime plus. The flow rate was generally set to 1 ml/min. Dialysis of protein solutions was performed in tubular cellulose membranes (Dialysis Membrane Spectra/Por 4) with a molecular cut-off of 12 to 14 kDa. Protein was concentrated by ultrafiltration using Vivaspin concentrators on a Beckmann Allegra 21R Centrifuge (S4180 rotor, 4800 rpm, 4°C).

Purification of full-length GyrA mutants and GyrA ΔCTD

- GyrA purification buffer: 50 mM Tris/HCl pH 7.5 (4°C), 10 mM MgCl$_2$, 2 mM β-mercaptoethanol; concentrations of NaCl and imidazole as indicated.
- GyrA storage buffer: 50 mM Tris/HCl pH 7.5 (4°C), 300 mM NaCl, 10 mM MgCl$_2$, 2 mM β-mercaptoethanol

Cells from 1.5 – 2.0 l culture were thawed, resuspended in approx. 25 ml purification buffer containing 1 M NaCl and protease inhibitor cocktail (Complete EDTA-free), and disrupted in a micro-fluidic cell. Cell debris was removed by centrifugation (SS-34 rotor, 14'000 rpm, 60 min, 4°C), and the supernatant was dialyzed over night against 2 x 1l purification buffer containing 200 mM NaCl. The protein solution was cleared by centrifugation and loaded onto a heparin sepharose column (1 ml/min). GyrA was eluted in a gradient of 0.2 – 1 M NaCl. Fractions containing GyrA with UV absorption ratio $A_{280}/A_{260}$ higher than 1.4 were pooled, concentrated by ultrafiltration and further purified on a Superdex S200 size exclusion column equilibrated in GyrA storage buffer. Protein eluted after approx. 55 ml were concentrated, shock-frozen, and stored at -80°C.

<u>Purification of GyrA His$_6$-tag fusion protein (His$_6$-GyrA)</u>

Cells were disrupted and the protein purified on a heparin Sepharose column as described above. It was further purified by IMAC using a Ni$^{2+}$-NTA column equilibrated in purification buffer containing 200 mM NaCl and 20 mM imidazole. The protein was eluted with 500 mM imidazole and dialyzed over night against 2 x 1l purification buffer containing 200 mM NaCl. Precipitate was removed by centrifugation, the supernatant adjusted to 300 mM NaCl and concentrated by ultrafiltration. The protein was further purified by SEC using a Superdex S200 column equilibrated in storage buffer containing 400 mM NaCl, concentrated and stored at -80°C.

<u>Purification of homo- and hetero-dimeric GyrA His$_6$-tag fusion proteins with TEV cleavage site (His$_6$-TEV-GyrA)</u>

Cell containing recombinant proteins were disrupted and the debris removed as described above. The purification buffer containing 1 M NaCl was adjusted to 20 mM imidazole and the protein was loaded onto a Ni$^{2+}$-NTA column. Adsorbed protein was eluted with 500 mM imidazole, mixed with 0.5 – 1 ml TEV protease (self-purified; 30 µM) to cleave the His$_6$-tag, and dialyzed over night against buffer containing 500 mM NaCl. Dialyzed GyrA was adjusted to 20 mM imidazole and loaded onto a Ni$^{2+}$-NTA column for separation from non-cleaved protein and the tag peptide. The flow-through was dialyzed for 2 h against 0.5 l of GyrA storage buffer, concentrated by ultrafiltration and passed over a Superdex S200 size exclusion column equilibrated in the same buffer. Fractions containing GyrA were concentrated by ultrafiltration, shock-frozen and stored at -80°C.

### 2.10.3 Co-purification of *M. mazei* Topoisomerase VI A and B subunits

- T6 purification buffer: 20 mM Tris/HCl pH 7.5 (4°C), 10% (v/v) glycerol, 2 mM β-mercaptoethanol; concentrations of NaCl and imidazole as indicated.
- T6 storage buffer: 20 mM Tris/HCl pH 7.5 (4°C), 150 mM NaCl, 10% (v/v) glycerol, 2 mM β-mercaptoethanol

The purification protocol for TopoVI was derived from [61]. Cell containing recombinant protein were disrupted and the debris removed as described for GyrA (section 2.10.2); the buffer used was T6 purification buffer containing 800 mM NaCl. The protein solution was adjusted to 20 mM imidazole and applied to a Ni$^{2+}$-NTA column equilibrated with the same buffer (flow rate: 0.5 – 1 ml/min). TopoVI A + B bound to the resin, the non-tagged A subunits being pulled down by His$_6$-TopoVIB subunits, and was eluted with 500 mM imidazole. The eluate was mixed with 0.5 – 1 ml of TEV protease (self-purified; 30 µM) and

dialyzed over night against 2 x 1l of buffer containing 150 mM NaCl. Precipitate was removed by centrifugation and cleaved protein separated from non-cleaved, tag peptide and TEV protease in a second IMAC run. The protein found in the flow-through was dialyzed again (0.5 l, 2 h, 150 mM NaCl) and passed over a SP sepharose cation exchange column equilibrated with the same buffer thus separating the TopoVI complex from proteolyzed TopoVIB proteins [61]. The flow-through was applied to a Q sepharose anion exchange column equilibrated with the same buffer and eluted in gradient of 150 – 1000 mM NaCl and a length of 50 ml, separating the protein from co-purified nucleic acids. Fractions containing TopoVI were concentrated by ultrafiltration and purified on a Superdex S200 size exclusion column equilibrated with T6 storage buffer. Proteins were concentrated by ultrafiltration, flash-frozen, and stored at -80°C.

## 2.11 DNA substrate preparation and purification

### 2.11.1  Plasmid DNA production and purification

*E. coli* XL1-Blue cells transformed with a target plasmid were cultured in LB medium (37°C, over night). Plasmid DNA was extracted and purified with Plasmid Miniprep Kit or Plasmid Midiprep Kit (both Qiagen N. V., Netherlands) for small (5 – 10 ml) and large culture volume (50 – 100 ml), respectively. Purified DNA were stored in sterile $H_2O$ at -20°C.

pUC18 (negatively supercoiled as extracted from *E. coli*) used as a substrate for *B. subtilis* gyrase or *M. mazei* topoisomerase VI was further purified by ethanol precipitation (section 2.11.3).

### 2.11.2  Preparative relaxation of pUC18 plasmid DNA

• Gyrase activity buffer: 50 mM Tris/HCl (pH 7.5 at 25°C), 100 mM KCl, 10 mM $MgCl_2$

Negatively supercoiled pUC18 plasmid was mixed with *B. subtilis* gyrase in absence of nucleotide. The relaxation reaction containing 200 nM wild-type GyrA , 800 nM wild-type GyrB and 100 nM pUC18 in gyrase activity buffer was incubated at 37°C for 2 to 3 h. The DNA was sequentially purified with Enzyme Removal Kit (Qiagen N. V., Netherlands) and ethanol precipitation (described below).

### 2.11.3 Ethanol precipitation

To remove residual salt and fluorescent background from DNA substrates used for smFRET measurements they were precipitated by sequentially mixing with 0.1 volume of 3 M KOAc (used instead of NaOAc due to a preference for $K^+$ ions of both gyrase and topoisomerase VI) and 2.5 volumes of ethanol p.a. Precipitated nucleic acids were pelleted by centrifugation (Eppendorf Centrifuge 5402, F 45-18-11 rotor, 13'000 rpm, 30 min, 4°C). The supernatant was decanted and the pellet carefully washed twice with ice-cold 70% ethanol, dried under vacuum (Eppendorf Concentrator 5301, 45°C, approx. 30 min) and re-dissolved in charcoal treated $H_2O$ or appropriate buffer.

### 2.11.4 Linear double-stranded DNA substrates

Non-modified or fluorescently labeled linear DNA substrates for *B. subtilis* gyrase (A; 37bp, 48bp, 60bp, 90bp) and for topoisomerase VI (B; 50bp, 51bp) were assembled from complementary single-stranded DNA oligomers (section 2.3.3). DNAs were denatured (95°C, 5 min) and annealed (A: 95 – 4°C gradient, 36 min; B: 95 – 20°C gradient, 60 min) on a thermocycler (GeneAmp PCR System 9600, Perkin Elmer Inc., MA, USA) and stored at -20°C.

The 110bp DNA substrate for gyrase was produced by PCR (section 2.9.1) using primers pUC18_110bp_for pUC18_110bp_rev and pUC18 containing a preferred binding / cleavage site for gyrase as a template. The PCR product was separated from enzymes and residual nucleotides and primer DNA by using the PCR clean-up kit (Promega). The theoretical nucleotide sequence of the 110bp DNA forward strand is:

5'-GGGTTTTCCCAGTCACGACGTTGTAAAACGTCTCGCAGTGCCAAGCTATGCATGATCATACGT
CGACTCTAGAGTCTCGCAGTGTACCGAGCTCGAATTCGTAATCATGT-3'

## 2.12 Topoisomerase assays

### 2.12.1 DNA supercoiling and relaxation assays with *B. subtilis* gyrase

- Gyrase activity buffer: 50 mM Tris/HCl (pH 7.5 at 25°C), 100 mM KCl, 10 mM MgCl$_2$
- 5x quenching solution: 50 mM EDTA, 5% (v/v) SDS, 50% glycerol, 0.05% (w/v) bromphenol blue

The DNA supercoiling and relaxation assays are used to report on the overall activity of mutant and / or chemically modified enzyme compared to the wt. Proteins were generally diluted from storage or labeling buffer.

DNA relaxation experiments were typically performed using 200 nM GyrA, 800 nM wt GyrB, and 15 nM neg. supercoiled pUC18 plasmid, in gyrase activity buffer, with a reaction volume was 10 - 16 µl. The reaction mix was incubated at 37°C for 30 min (Eppendorf ThermoStat plus).

The DNA supercoiling assays typically used 50 or 200 nM GyrA, 800 nM wt GyrB, 50 nM relaxed pUC18 plasmid, and 2 mM ATP, in gyrase activity buffer, with a reaction volume of 10 µl. The reaction being very fast, it was kept on ice before incubation at 37°C for 2 min.

Both relaxation and supercoiling reactions were quenched by adding 5x quenching solution (0.25 x the reaction volume) and flash-frozen in liquid N$_2$. The reaction mix containing 300 ng of plasmid DNA was applied to a 1.2% agarose gel and topoisomers were separated by electrophoresis and visualized by ethidium bromide staining and UV illumination (section 2.8.2).

### 2.12.2 DNA relaxation assay with *M. mazei* topoisomerase VI

- T6 activity buffer: 40 mM Bis-Tris propane/HCl (pH 6.5 at 25°C), 150 mM potassium glutamate, 20 mM MgCl$_2$, 1 mM DTT
- 5x quenching solution: 50 mM EDTA, 5% (v/v) SDS, 50% glycerol, 0.05% (w/v) bromphenol blue

DNA relaxation reactions typically contained approx. equimolar concentrations of TopoVIA and B proteins, 15 nM of neg. supercoiled pUC18 plasmid, and 2 mM ATP in T6 activity buffer. 16 µl reaction mix were incubated at 30°C for 30 min (Eppendorf ThermoStat plus) and subsequently stopped by the addition of quenching solution and flash-freezing in liquid N$_2$. The stopped reactions containing 400 ng plasmid DNA were analyzed by agarose gel electrophoresis as described above (section 2.8.2).

## 2.13 TopoisomeraseVI DNA cleavage assay

1 μM single stand DNA TopVI_51_f was radioactively labeled on the 5' end using 10 μCy [γ-$^{32}$P]ATP (corresponding to approx. 0.3 m) and Polynucleotide kinase (PNK) (1 U/μl) in PNK buffer (supplied by the manufacturer). The reaction mix was incubated at 37°C for 60 min and the enzyme was inactivated by incubating the reaction at 65°C for 20 min. The DNA was separated from nucleotides and proteins by size exclusion chromatography (illustra Microspin G-25 column) according to the manufacturer's protocol. Approx. 25 nM labeled oligonucleotide was annealed with 25 nM of its complementary DNA TopVI_51_r by heating to 95°C for 5 min and cooling to room temperature in 90 min.

The DNA cleavage reaction was performed with approx. 12.5 nM [$^{32}$P]DNA and 5 μM topoisomerase VI in T6 activtiy buffer (see above). Nucleotides (ATP, ADPNP) were added at concentrations of 2 mM. The reaction mix was incubated at 37°C for 2 h, the enzyme degraded for 20 min by the addition of 0.1 μg/μl proteinase K, and the reactions stopped with quenching solution (see 2.12.2) and heating to 95°C for 5 min.

The DNA products were applied to a 15 % polyacrylamide gel and separated by electrophoresis using 1 x TBE as buffer (150V, 2.5 h). The gel was exposed to a storage phosphor screen over night and the bands were visualized by a Storm 820 phosphor imager (GE Healthcare).

## 2.14 Steady-state ATP hydrolysis assay for *M. mazei* topoisomerase VI

- T6 ATPase buffer: T6 activity buffer (see above), containing 1 mM PEP, 0.2 mM NADH, 13 μg/ml pyruvate kinase, 23 μg/ml lactate dehydrogenase.

The steady-state ATP hydrolysis rate of topoisomerase VI was monitored in a coupled enzymatic assay [79]: ATP hydrolysed by the enzyme is regenerated from ADP by pyruvate kinase in a phosphotransfer reaction driven by the dephosphorylation of PEP. The product pyruvate is reduced to lactate by lactate dehydrogenase in a reaction coupled to the oxidation of NADH to NAD$^+$, which can be monitored spectrophotometrically by the decrease in absorption by NADH at 340 nm. The method was used to assay the basic (i. e. non-stimulated) topoisomerase VI ATP hydrolysis activity.

8 hydrolysis reactions were performed in parallel on a Ultrospec 2100 photometer. Quartz cuvettes containing ATPase buffer and varying concentrations of ATP were incubated at 37°C until reaching equilibrium (after approx. 30 min). Then 4 μM topoisomerase VI was added (by direct dilution from storage buffer conditions) with incubation continuing for at least 30

min. The absorption at 340 nm was monitored for both part of the experiment as a function of time at an interval of 16 s.

The concentration of NADH can be calculated from the NADH absorption at 340 nm by using the Beer-Lambert law (Eq. 2.1) and the extinction coefficient of NADH (6300 $M^{-1}cm^{-1}$ at 340 nm) [74]. ATP hydrolysis is correlated in a 1 : 1 stoichiometry to the decrease in NADH concentration over time; thus the velocity of ATP hydrolysis can be expressed as the absolute value of the time derivative of NADH concentration (Eq. 2.2):

$$v = \frac{d[ATP]}{dt} = \left\langle \frac{d}{dt}\left( \frac{A_{340nm}}{\varepsilon_{340nm} \cdot d} \right) \right\rangle \tag{2.2}$$

v being the velocity of ATP consumption, [ATP] the nucleotide concentration, $A_{340nm}$ the absorption at 340 nm, and d the pathlength given by the cuvette (1 cm). The velocity was corrected with the apparent ATP consumption in absence of topoisomerase VI.

The velocity of ATP consumption was plotted against the ATP concentration and analyzed according to the Michaelis-Menten formalism, calculating the maximal velocity of ATP consumption $v_{max}$, the Michaelis-Menten constant $K_M$, and the ATP turnover number $k_{cat}$ (Eqns. 2.3 and 2.4):

$$v = \frac{v_{max}[ATP]}{K_M + [ATP]} \tag{2.3}$$

$$k_{cat} = \frac{v_{max}}{[TopoVI]} \tag{2.4}$$

[TopoVI] denominates the concentration of topoisomerase VI.


## 2.15 Fluorescence anisotropy titrations

Fluorescence from dyes excited with linearly polarized light can be split in parallel and perpendicular contributions relative to the polarization of the incoming beam; in case these contributions differ the fluorescence is called anisotropic. Fluorescence anisotropy r is defined as (Eq. 2.5):

$$r = \frac{I_{\parallel} - I_{\perp}}{I_{\parallel} + 2I_{\perp}} \tag{2.5}$$

where $I_{\parallel}$ and $I_{\perp}$ are the measured fluorescence intensities parallel and perpendicular to the excitation polarization. The fluorescence anisotropy reports on the rotational mobility of a

fluorescently labeled molecule and can therefore be used to describe association of fluorescently labeled species with other molecules. Affinities of *B. subtilis* gyrase and *M. mazei* topoisomerase VI for DNA substrates were determined on a fluorimeter (Jobin Yvon FluoroMax 3) by titration of fluorescently labeled DNAs.

### 2.15.1 Titrations with GyrA and GyrB

- Gyrase activity buffer: 50 mM Tris/HCl (pH 7.5 at 25°C), 100 mM KCl, 10 mM MgCl$_2$, 2 mM β-mercaptoethanol

10 nM linear double-stranded DNA substrates internally labeled with Alexa546 were titrated with GyrA or GyrB proteins in absence of the other and with GyrA in presence of 4 μM wt GyrB, using gyrase activity buffer containing 2 mM β-mercaptoethanol. Proteins were diluted from stock solutions (section 2.10). Displacement titrations with negatively supercoiled pUC18 were performed with 100 nM fluorescently labeled DNA and 1 μM GyrA in the absence, or with 10 nM labeled DNA and 250 μM GyrA in the presence of 4 μM GyrB.

Measurements were performed at 37°C with equilibration time of 1 min. Alexa546 was excited at 555 nm (slit: 3 nm) and fluorescence detected at 571 nm (slit: 6 nm).

### 2.15.2 Titrations with topoisomerase VI

- T6 activity buffer: 40 mM Bis-Tris propane/HCl (pH 6.5 at 25°C), 150 mM potassium glutamate, 20 mM MgCl$_2$, 1 mM DTT

50 nM linear double-stranded DNA substrates single labeled with fluorescein (end), Alexa488 (A488; internal), or Alexa546 (A546; internal) or double-labeled with Alexa488 and 546 were titrated with topoisomerase VI complex in T6 activity buffer. Proteins were diluted from respective stock solutions (section 2.10).

Measurements were performed at 37°C with equilibration time of 1 min. Excitation and emission detection wavelengths were 496, 493, 554 nm and 520, 515, 569 nm for substrates labeled with fluorescein, A488 and A546, respectively. Slit widths for the excitation and emission were 4 and 10 nm for fluorescein and 3 and 6 nm for A488 and A546. For titrations of a double-labeled DNA (A488, A546) the same parameters were used as for a substrate labeled with A546 only.

### 2.15.3 Data evaluation

Titrations with GyrA and topoisomerase VI were analyzed under the assumption of a 1:1 complex formation with DNA. The dissociation constant for the enzyme-DNA complex can be expressed as in equation 2.6:

$$K_d = \frac{[E][DNA]}{[E \cdot DNA]} \tag{2.6}$$

$K_d$ is the dissociation constant, [E] the free enzyme concentration, [DNA] the free DNA concentration, and [EDNA] the concentration of the enzyme-DNA complex.

The detected fluorescence anisotropy r is a function of the initial anisotropy and the maximal anisotropy amplitude scaled with the saturation degree of the labeled DNA (Eq. 2.7):

$$r = r_0 + \Delta r \frac{[E \cdot DNA]}{[DNA]_{tot}} \tag{2.7}$$

$r_0$ is the anisotropy of the free DNA, $[DNA]_{tot}$ the total DNA concentration, and $\Delta r$ the maximal anisotropy difference at saturation enzyme concentration. [E·DNA] can be substituted by a quadratic equation applying the principle of mass conservation; r can be rewritten as follows (Eq. 3.8):

$$r = r_0 + \frac{\Delta r}{[DNA]_{ot}} \left( \frac{[E]_{ot} + [DNA]_{ot} + K_d}{2} - \sqrt{\frac{([E]_{ot} + [DNA]_{ot} + K_d)^2}{4} - [E]_{ot}[DNA]_{ot}} \right) \tag{2.8}$$

Equilibrium titrations of DNA with GyrA in presence of 4 µM GyrB were evaluated as in eq. 2.8. We assume, that the affinity of one species for another is much lower than for the complex of the two others [46], leading to a preferred population of the tripartite complex. The binding of GyrB to GyrA or DNA alone is neglected.

Anisotropy data from titration of a DNA substrate with GyrB was analyzed with the Hill equation, assuming high co-operativity of binding (eq. 2.9).

$$v = \frac{[GyrB]_{ot}^{n}}{K_d + [GyrB]_{ot}^{n}} \tag{2.9}$$

v is the degree of occupancy of DNA, n is the Hill coefficient, $[GyrB]_{tot}$ is the total concentration of GyrB, and $K_d$ is the dissociation constant for the DNA-GyrB$_n$ complex. Following eq. 3.8, the anisotropy can be expressed as in eq. 2.10:

$$r = r_0 + \Delta r \frac{[GyrB]_{ot}^{n}}{K_d + [GyrB]_{ot}^{n}}$$

<div align="right">(2.10)</div>

To determine binding of non-labeled plasmid DNA to GyrA or gyrase we performed displacement titrations on the enzyme bound to linear labeled DNA were performed. 1 μM GyrA and 100 nM fluorescently labeled DNA were titrated with negatively supercoiled pUC18 in the absence, 10 nM labeled DNA and 250 μM GyrA in the presence of 4 μM GyrB. As no binding model was found that could describe the data sufficiently well, no dissociation constants for supercoiled plasmid were obtained.

## 2.16 Fluorescent labeling of proteins

Mutant proteins constructed for FRET experiments were fluorescently labeled using maleimide-linked dyes for the coupling to free thiol groups. Purified protein was transferred to labeling buffer by size-exclusion chromatography (Micro Bio-Spin 30 columns) according to the manufacturer's protocol, mixed with fluorescent dyes, and incubated at 25°C. Fluorescent dyes (Alexa Fluor 488 C5-maleimide, Alexa Fluor 546 C5-maleimide, TMR C5-maleimide) were directly diluted into labeling reactions from stock solutions (20 mM in DMSO). Non-reacted dye molecules were efficiently removed by SEC in two steps reusing the same micro-spin columns.
Labeled proteins were stored at 4°C and reused for experiments up to 3 days.

### 2.16.1 Fluorescent labeling of *B. subtilis* GyrA

- GyrA labeling buffer: 50 mM Tris/HCl (pH 7.5 at 25°C), 200 mM NaCl, 10 mM MgCl$_2$, 1 mM TCEP

GyrA mutants for single molecule (sm) and ensemble FRET experiments or activity assays were diluted to 50 - 80 μM and the buffer exchanged to buffer A. Proteins were diluted to 30 μM and simultaneously (i.e. statistically) labeled with 90 – 120 μM Alexa488 and / or 120 μM Alexa546 for smFRET and 120 μM Alexa488 and 150 μM TMR for denaturation experiments. Fluorescent dyes were premixed before addition to protein solutions for fully statistical labeling. Chemical modification was done at 25°C for 1 h.
Proteins used for correction parameter determination were labeled with one dye only.

### 2.16.2 Fluorescent labeling of TopoVIB

- T6 labeling buffer: 20 mM Tris/HCl (pH 8.0 at 25°C), 300 mM NaCl, 10 % glycerol, 1 mM TCEP

Co-purified TopoVIA and B proteins were subject to labeling as a complex. Initial labeling experiments to identify accessible native cysteines were performed with 30 µM proteins and 150 – 300 µM A546 in T6 labeling buffer, with incubation at 25°C for 2 h.

Mutant proteins for FRET experiments were labeled at a concentration of 30 µM using 24 µM A488 and 36 µM A546 with dyes being premixed prior to addition. The labeling reaction mix was incubated at 25°C for 10 min. Non-reacted dyes were removed as described above.

### 2.16.3 Determination of labeling degrees

Fluorescently labeled proteins were probed for free dye by SDS-PAGE, and protein and dye concentrations were determined with absorption measurements, employing the Beer-Lambert law (eq. 2.1) and correcting for dye absorption at 280 nm and (in case of simultaneous labeling with donor and acceptor dye) acceptor contribution at 493 nm as well as buffer contributions (eqns. 2.11 – 2.13).

$$c_{acc} = \frac{A_{\lambda \max, acc}}{\varepsilon_{\lambda \max, acc} \cdot d} \tag{2.11}$$

$$c_{A488} = \frac{A_{493} - c_{acc} \cdot \varepsilon_{493, acc} \cdot d}{\varepsilon_{493, A488} \cdot d} \tag{2.12}$$

$$c_{prot} = \frac{A_{280} - c_{A488} \cdot \varepsilon_{280, A488} \cdot d - c_{acc} \cdot \varepsilon_{280, acc} \cdot d}{\varepsilon_{280, prot} \cdot d} \tag{2.13}$$

$A_{\lambda}$ is the absorption at wavelength $\lambda$, $\varepsilon_{\lambda,x}$ the molar extinction coefficient of species x at wavelength $\lambda$, $c_x$ the concentration of species x, and d the path-length (1 cm). Values are listed in section 2.8.4. If the concentration of free dye could be neglected the degree of labeling is given by the ratio $c_{dye}/c_{prot}$.

## 2.17 Guanidinium chloride induced GyrA dimer dissociation monitored by ensemble FRET

- Buffer G: 50 mM Tris/HCl (pH 7.5 at 25°C), 200 mM NaCl, 10 mM MgCl$_2$

Guanidinium chloride is a powerful denaturant inducing protein unfolding and complex dissociation [80]. We tried to separate GyrA dimer by addition of GuHCl. Ensemble FRET between GyrA monomers labeled with donor and acceptor dyes at the dimerization interfaces was measured to monitor intramolecular proximity [81].

GyrA mutants T140C or T408C were labeled with A488 as donor and TMR as acceptor and labeling efficiencies determined as described above (sections 2.16.1 / 2.16.3). The protein was diluted into buffer G to a final donor label concentration of 10 nm. Fluorescence measurements of individually mixed samples containing varying concentrations (0 – 5 M) of GuHCl were recorded on a fluorimeter (Jobin Yvon FluoroMax 3) with a low excitation wavelength of 460 nm (slit: 5 nm) to avoid direct excitation of the acceptor. Fluorescence emission spectra were recorded in a range from 500 – 650 nm (slit: 10 nm) and corrected for buffer contributions. Incubation temperature was 37°C; samples were equilibrated for 1 min prior to spectra recording. From individual fluorescence spectra an apparent FRET efficiency ($E_{FRET,app}$) was calculated (Eq. 2.14):

$$E_{FRET,app} = \frac{I_{574nm}}{I_{574nm} + I_{519nm}} \qquad (2.14)$$

$I_{519nm}$ and $I_{574nm}$ denominate single-wavelength fluorescence intensities.

## 2.18 Single molecule experiments

- Gyrase FRET buffer: 50 mM Tris/HCl (pH 7.5 at 25°C), 100 mM KCl, 10 mM MgCl$_2$; treated with active charcoal
- T6 FRET buffer: 40 mM Bis-Tris propane/HCl (pH 6.5 at 25°C), 150 mM potassium glutamate, 20 mM MgCl$_2$; treated with active charcoal.

Single molecule experiments were performed on a home-built confocal microscope. Chambered coverglass cuvettes were passivated with 0.1 mg/ml BSA in the appropriate buffer for at least 1 h. Measurements were performed in gyrase or T6 buffer (depending on the enzyme involved) at 37°C, with fluorescently labeled protein (section 2.16) or DNA at 50 – 75 pM concentration with respect to donor label. If not indicated otherwise, substrate concentrations used were 8 μM, 25 nM, and 2 mM for GyrB, plasmid DNA, and nucleotides.

Fluorescence was excited with monochromatic pulsed light of 475 nm from a mode-locked, wavelength doubled Ti:sapphire laser. The intensity of the excitation beam was set to 75 µW, the pulse width to 2.5 ps at an interval of 40 ns. Fluorescence from freely diffusing molecules passing the confocal volume was collected by an objective with high numerical aperture and split onto two avalanche photo diodes to be detected as donor or acceptor signals. Fluorescence was recorded for 20 to 30 min.

### 2.18.1 Data processing

Labeled molecules passing through the confocal volume emit a large number of photons yielding a fluorescence burst. Background fluorescence (from impurities) is removed by an algorithm described by [82]. Bursts with more than 100 photons above background were considered significant and the transfer efficiency calculated from fluorescence intensities (eq. 2.15):

$$E_{FRET} = \frac{I_A}{I_A + I_D}$$

(2.15)

$E_{FRET}$ is the transfer efficiency, $I_A$ and $I_D$ are the fluorescence intensities of the acceptor and the donor fluorophors respectively.

Autocorrelation of the donor fluorescence signal can be used to calculate a diffusion time of the detected fluorescent species [83]. Visual inspection of the curvature of the autocorrelation curve in the range between $10^{-4}$ and $10^{-2}$ s was used to follow complex formation of GyrA or gyrase with plasmid DNA: an inflection point at $< 10^{-3}$ s was indicative of a MW complex corresponding to GyrA or gyrase, while one at $\geq 10^{-2}$ s was characteristic for complexes containing plasmid DNA.

### 2.18.2 Correction of single molecule fluorescence intensities

Fluorescence intensities are affected by spectral over-lap of donor and acceptor absorption and fluorescence and non-ideal physical properties of the fluorescence detection set-up [82]. These effects have to be corrected for when calculating FRET efficiencies [84]. Correction parameters are presented in the following paragraphs.

<u>Measurements for the determination of correction parameters for GyrA mutants</u>

- Gyrase FRET buffer: 50 mM Tris/HCl (pH 7.5 at 25°C), 100 mM KCl, 10 mM MgCl$_2$; treated with active charcoal

GyrA mutants were labeled with A488 or A546 as described above (section 2.16). A fraction of labeled protein was digested with proteinase K (0.2 mg/ml, 37°C, 30 min), and complete proteolytic degradation of GyrA was confirmed by SDS-PAGE. The fluorophore concentration was determined from absorption spectra using extinction coefficients listed in section 2.8.4. Absorption spectra of approximately 5 µM labeled GyrA protein were recorded in absence and presence of 6 µM wt GyrB and 0.3 µg/µl calf thymus DNA (assuming saturation of GyrA) in gyrase FRET buffer containing 1 mM TCEP. Absorption spectra were corrected for buffer contributions.

Fluorescence excitation spectra of labeled protein were recorded in absence and presence of 20 nM supercoiled pUC18 plasmid and 8 µM GyrB in gyrase FRET buffer at 37°C, with label concentration of 10 nM. Fluorescence was excited in a range between 350 and 520 nm in case of A488 and between 400 and 580 nm in case of A546; emission was detected at 530 and 590 nm (slits: 5 nm). Fluorescence emission spectra of protein labeled with A488 were recorded between 470 and 700 nm with excitation set at 460 nm (slits: 5 nm). Fluorescence spectra were corrected for buffer contributions.

Fluorophore extinction coefficients at 475 nm were not calculated directly from absorption spectra, but from fluorescence excitation spectra fitted to the corresponding absorption spectra, assuming that the spectral shapes were the same. This was done due to the higher sensitivity of the fluorescence measurement.

For the correction of detection-related problems counting rates of single dye labeled proteins were recorded on the single-molecule confocal microscope with the dye concentration set to 50 nM. Measurements were performed in gyrase FRET buffer, in absence and presence 20 nM supercoiled pUC18 plasmid (section 2.11) and 8 µM GyrB. A neutral filter (OD = 0.5) was used to decrease fluorescence intensity.

<u>Measurements for the determination of correction parameters for a 50bp DNA</u>

- T6 FRET buffer: 40 mM Bis-Tris propane/HCl (pH 6.5 at 25°C), 150 mM potassium glutamate, 20 mM MgCl$_2$; treated with active charcoal.

50bp DNAs labeled with A488 or 546 were annealed from complementary single-stranded DNA pairs TopoVI_51_f / TopoVI_50_r_488 and TopoVI_50_f_546 / TopoVI_51_r, respectively. Absorption spectra were recorded at 25°C in the absence and presence of 12 µM

TopoVI A+B, using T6 FRET buffer. The concentration of the fluorescent labels was set to 4 μM (using extinction coefficients given by the manufacturer: $\varepsilon_{A488,\,493\,nm}$ = 78'000 $M^{-1} \cdot cm^{-1}$ and $\varepsilon_{A546,\,554\,nm}$ = 112'000 $M^{-1} \cdot cm^{-1}$ for A488 and A546, respectively). The direct excitation δ was calculated from absorption values at 475 nm.

Counting rates of single-dye labeled 50bp DNAs were recorded on the single-molecule confocal microscope with the dye concentration set to 100 nM. Measurements were performed at room temperature in T6 FRET buffer in absence and presence of 12 μM TopoVI A+B. Counting rates were corrected for buffer contributions.

Correction for direct excitation of the acceptor: δ

Significant over-lap in the absorption spectra of donor and acceptor fluorophores impedes exclusive excitation of the donor. The acceptor dye is directly excited by light of the excitation wavelength of 475 nm following a non-zero extinction coefficient $\varepsilon_{475\,nm}$. The correction for direct excitation is given by the ratio of the extinction coefficients of acceptor and donor dyes (eq. 2.16):

$$\delta = \frac{\varepsilon_{Acc,475nm}}{\varepsilon_{Do,475nm}}$$

(2.16)

$\varepsilon_{Acc,475nm}$ and $\varepsilon_{Do,475nm}$ are the extinction coefficients of the fluorophores calculated from absorption and fluorescence excitation spectra.

Correction for fluorescence cross detection:  α and β

Photons emitted from fluorophores and collected by the objective are separated by a beam splitter (dichroic) onto two detection units (APDs), thus being detected either as donor or acceptor fluorescence. The discrimination is not perfect due to overlap in the emission spectra of the two dyes and non-ideal separation of emitted photons into the detection channels by the beam splitter, leading to photons emitted by the donor to be detected in the acceptor channel and *vice versa*. Parameters correcting for cross detection are α and β, describing leakage of donor photons into acceptor channel and *vice versa*, respectively (eqns. 2.17, 18).

$$\alpha = \frac{I_A^{donor} - I_A^{buffer}}{I_D^{donor} - I_D^{buffer}}$$

(2.17)

$$\beta = \frac{I_D^{acceptor} - I_D^{buffer}}{I_A^{acceptor} - I_A^{buffer}}$$

(2.18)

$I_D$ and $I_A$ are fluorescence intensities detected in donor and acceptor channels, exponents indicate measurements of protein labeled with the denominated fluorophore or of the background (buffer).

Correction for unequal detection efficiency: γ

The parameter γ corrects for different quantum efficiencies of donor and acceptor fluorophores and different detection efficiencies of emitted fluorescence (eq. 2.19):

$$\gamma = \frac{I_A^{acceptor} - I_A^{buffer}}{I_D^{donor} - I_D^{buffer}} \cdot \delta^{-1}$$

(2.19)

$I_D$ and $I_A$ are fluorescence intensities detected in donor and acceptor channels, exponents indicate measurements of protein labeled with the denominated fluorophore or of the background (buffer).

Corrected FRET efficiencies

The corrected FRET efficiency is described by eq. 2.15 with incorporated correction parameters α, β, γ, and δ. Correction parameters with direct excitation taken into account write as (eqns. 2.20 – 2.22):

$$\alpha' = \frac{\alpha + \gamma\delta}{1 + \beta\gamma\delta}$$

(2.20)

$$\beta' = \beta$$

(2.21)

$$\gamma' = \frac{\gamma + \gamma\delta}{1 + \beta\gamma\delta}$$

(2.22)

Using modified correction parameters α', β', and γ', eq. 2.15 transforms to (eq. 2.23):

$$E_{FRET} = \left(1 + \gamma' \frac{I_D - \beta' I_A}{I_A - \alpha' I_D}\right)^{-1}$$

(2.23)

### 2.18.3 Determination of Förster distance ($R_0$)

The Förster distance for a given pair of fluorescent dyes is the distance at which the transfer efficiency ($E_{FRET}$) is 0.5 [85]. It is an essential factor for the conversion of a given FRET efficiency to the corresponding distance (eq. 2.24):

$$E_{FRET} = \frac{R_0^{\,6}}{R_0^{\,6} + r^6}$$

(2.24)

$R_0$ is the Förster distance of two fluorophores, r the distance between them. The Förster distance is described by eq. 2.25:

$$R_0 = \sqrt[6]{\frac{9000 \cdot \ln 10}{128\pi^5 \cdot N_A} \cdot \phi_D \cdot \kappa^2 \cdot n^{-4} \cdot J}$$

(2.25)

$N_A$ is the Avogadro number, $\varphi_D$ the donor quantum yield, $\kappa^2$ the dipole orientation factor, n the refractive index of the medium between the fluorophores, and J the overlap integral of the fluorescence and absorption spectra of donor and acceptor dyes respectively. The dipole orientation factor was assumed to be 2/3, equivalent to freely rotating fluorophores [86]. The refractive index was set to 1.33, the one of water at 25°C [87].

The overlap integral and the donor quantum yield were determined individually for each FRET pair (cysteine positions, donor and acceptor dyes) as described below.

The overlap integral: J

The overlap integral is the degree of overlap between the normalized donor fluorescence and acceptor absorption spectra according to equation 2.26 [86]:

$$J = \frac{\int_0^\infty F_D(\lambda) \cdot \varepsilon_A(\lambda) \cdot \lambda^4 d\lambda}{\int_0^\infty F_D(\lambda) d\lambda} \cong \frac{\sum_{i=470}^{700} F_D(\lambda_i) \cdot \varepsilon_A(\lambda_i) \cdot \lambda_i^4}{\sum_{i=470}^{700} F_D(\lambda_i)}$$

(2.26)

J is the overlap integral, $F_D$ the donor fluorescence and $\varepsilon_A$ the absorption coefficient for the acceptor at a certain wavelength $\lambda$. The spectra were recorded as described above. The fluorescence emission spectrum of the donor was normalized by its integral, the absorption spectrum by the dye concentration (equaling the extinction coefficients for each wavelength). For practical reasons the integrals are substituted by sums of overlap values at a given wavelength with a $\lambda$ step size of 1 nm.

<u>The fluorescence quantum yield $\varphi_D$</u>

The fluorescence quantum yield of A488 bound to protein was determined relative to the one of uranine (fluorescein) in solution [88] using corresponding absorption and fluorescence emission spectra (eq. 2.27):

$$\varphi_D = \frac{\sum\limits_{i=470}^{700} F_D(\lambda_i) \cdot \varepsilon_{U,460nm} \cdot \varphi_U}{\sum\limits_{i=470}^{700} F_U(\lambda_i) \cdot \varepsilon_{D,460nm}}$$

(2.27)

$\varphi_D$ is the quantum yield of A488, $\varphi_U$ the one of uranine, $\varepsilon_D$ and $\varepsilon_D$ are the extinction coefficients at 460 nm as determined from absorption spectra (A488) or given in section 2.8.4 (uranine). The quantum yield of uranine in aqueous solutions is 0.93 [89]. Absorption and fluorescence emission spectra of uranine were recorded in 0.1 NaOH and corrected for buffer contributions. Fluorescence measurements of uranine and A488 were performed using 10 nM fluorophore with identical parameters ($\lambda_{ex}$ of 460 nm, $\lambda_{em}$ from 470 to 700 nm, slits: 5 nm).

# 3. Results

## 3.1 Part I: CTD from *B. subtilis* GyrA

Gyrase is a heterotetrameric complex consisting of two GyrA and two GyrB subunits. Both proteins were produced individually and purified in their wild-type forms by ion-exchange (IEX) and size-exclusion chromatography (SEC). Protein yields were high, but overlapping elution profiles of protein and nucleic acids on the IEX column lead to selecting of only a restricted elution fraction, resulting in a significant loss of protein. This work reports purification protocols for *B. subtilis* GyrA $His_6$-fusion proteins, using immobilized metal affinity chromatography (IMAC).

### 3.1.1 Production and purification of $His_6$-tagged GyrA

*B. subtilis gyrA*_C350L (cysteine-free mutant: hereafter abbreviated *gyrA*\*) open reading frame was subcloned from pET-27b(+) into a pETDuet-1 vector (section 2.9.4), resulting in a DNA sequence coding for an N-terminal $His_6$-tagged fusion protein ($His_6$-GyrA\*) with a length of 835 amino acids and a calculated molecular weight (MW) of 93.7 kDa [72]. $His_6$-GyrA\* was recombinantly expressed in *E. coli* BL21 CodonPlus(DE3)RP cells, yielding a high amount of protein visible as the main band with the expected MW on a denaturing acrylamide gel (Fig. 3.1 E).

$His_6$-GyrA\* was purified as described in section 2.10.2. Dialysis of the crude extract against 200 mM NaCl resulted in protein precipitation; this effect was known from the purification of non-tagged GyrA, albeit to a lower degree [36]. $His_6$-GyrA\* was adsorbed to a heparin column and eluted in a NaCl gradient with an elution maximum at approx. 400 mM NaCl, similar to the non-tagged protein. Judged from absorption spectra (ratio of the absorption at wavelengths of 280 nm versus 260 nm) the tagged protein co-eluted with a similar amount of nucleic acids as the wild-type protein. Several protein impurities were visible on SDS polyacrylamide gel (Fig. 3.1 E).

To test $His_6$-GyrA\* for accessibility of the $His_6$-tag, the protein was applied to $Ni^{2+}$-NTA column. $His_6$-GyrA\* was eluted with 500 mM imidazol, but not by washing with 20 mM imidazole, indicating specific binding of the N-terminal $His_6$-tag to the immobilized metal ions as shown by the UV chromatogram and SDS-PAGE (Fig. 3.1 A and E).

Protein precipitation was high during a second dialysis against a buffer containing 200 mM NaCl, but could be avoided by increasing the salt concentration to 300 mM. In the subsequent

49

size-exclusion chromatography step most of the protein eluted in the exclusion volume as a high-MW species, probably due to aggregation (Fig. 3.1 B and E). A small fraction of $His_6$-GyrA* eluted at a retention volume of 55 ml corresponding to an apparent MW of 270 kDa, which was the same for the non-tagged protein [36]. This fraction was pure as judged by SDS-PAGE (coommassie staining) (Fig. 3.1 G) and UV absorption. It was pooled and stored in 400 mM NaCl. The protein yield was 1.7 mg per liter culture, which is very low compared to the one of non-tagged protein (10 – 15 mg/l) [36].

### 3.1.2 Introduction of a TEV protease cleavage site to the GyrA $His_6$ fusion protein

Due to the low solubility of the $His_6$-tagged GyrA protein, a version with a cleavable $His_6$-tag was devised: The nucleotide sequence encoding a TEV-protease cleavage site was inserted between the tag and the GyrA ORF by site-specific mutagenesis on the template vector pETDuet-1_ $His_6$-*gyrA*\* (section 2.9.4), allowing for the selection of the tagged proteins from the crude extract and subsequent removal of the tag. The tagged protein has a length of 840 amino acids and an MW of 94.4 kDa. Removal of the tag should yield a wild-type like protein GyrA* lacking the N-terminal Met residue with a reduced length of 820 amino acids and a MW of 92.0 kDa.

Like $His_6$-GyrA*, the cleavable GyrA $His_6$-tag fusion protein ($His_6$-TEV-GyrA*) was produced in *E. coli* BL21 CodonPlus(DE3)RP cells (section 2.10.1) exhibiting a comparable expression level (Fig. 3.1 F). Most of the protein was found in the soluble fraction after cell disruption. The protein was efficiently adsorbed to a $Ni^{2+}$-NTA column in a 1 M NaCl buffer containing 20 mM imidazole and eluted with 500 mM imidazole (Fig. 3.1 F). The protein was incubated with TEV protease at 4°C during dialysis against a buffer only 300 mM NaCl to facilitate protease cleavage. Subsequently the protein was passed over a $Ni^{2+}$-NTA column where it could be found in the flow-through indicating a successful separation of GyrA from the $His_6$-tag (Fig. 3.1 C and F).

The cleaved protein was further purified by size-exclusion chromatography where most of it eluted as a dimer at a retention volume of 55 ml approx. (Fig. 3.1 D), similar to the non-tagged protein and $His_6$-GyrA* (section 3.1.1). Contamination by other proteins or nucleic acids was very low as judged by SDS-PAGE (Fig. 3.1 G) and UV absorption (the ratio $A_{280}/A_{260}$ being 2.0, which was similar to the value observed for GyrA purified by IEX [46]). 21 mg of protein were obtained per liter of culture, which marks a 2-fold increase compared to the yields of non-tagged GyrA [36].
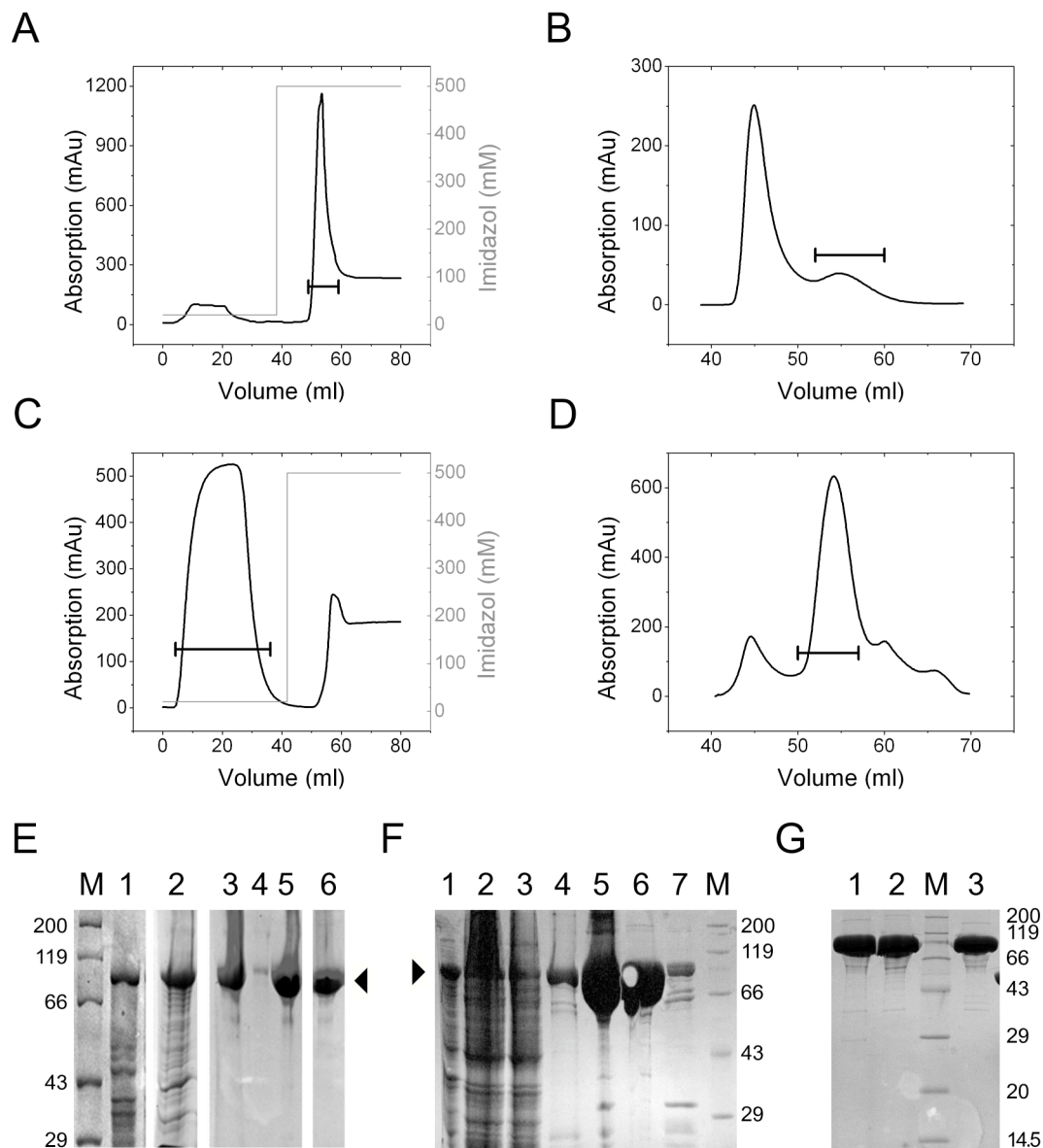
**Fig. 3.1:** Production and purification of N-terminal His$_6$-tagged full-length GyrA* (C, D).

**A – D:** Chromatograms of selected purification steps for His$_6$-GyrA* (A, B) and His$_6$-TEV-GyrA*, monitored by absorption at 280 nm. Horizontal bars denominate protein fractions used for subsequent steps.

**A:** Ni$^{2+}$-IMAC of His$_6$-GyrA* pre-purified by IEX; the protein bound to the resin at 20 mM imidazol and eluted with 500 mM.

**B:** SEC of His$_6$-GyrA* using a Superdex S200 column: GyrA predominantly eluted in the exclusion volume as a high MW species (45 ml). Only a small fraction of GyrA eluted as an apparent dimer (55 ml).

**C:** Second Ni$^{2+}$-IMAC of His$_6$-TEV-GyrA* cleaved with TEV protease (GyrA*): The protein does not bind to the resin and is found in the flow-through.

**D:** SEC of cleaved His$_6$-TEV-GyrA* using an Superdex S200: Most of the protein is eluted as a dimer at 55 ml retention volume.

**E – G:** SDS polyacrylamide gels of different purification stages with protein marker (M) and corresponding MW indicated in kDa.

**E:** Purification of His$_6$-GyrA* (◄). 1: Expression from BL21(DE3). 2: Crude extract. 3: GyrA purified by IEX chromatography (Heparin). 4 and 5: Flow-through and elution from Ni$^{2+}$-NTA column (see A). 6 His$_6$-GyrA* eluted in the exclusion volume (46 ml; see B).

Continued on following page.

51

**F:** Purification of His$_6$-TEV-GyrA* (►). 1: Expression from BL21(DE3). 2: Crude extract. 3 and 4: Flow-through and elution from the first Ni$^{2+}$-NTA column. 5: His$_6$-TEV-GyrA* cleaved with TEV protease. 6 and 7: Flow-through and elution from the second Ni$^{2+}$-NTA column (see C). TEV protease is visible as a faint band with an apparent MW of 30 kDa approx. (lanes 5 and 7); the cleaved His$_6$-tag is missing due to its low MW of 2.4 kDa.

**G:** Purified proteins as eluted from the Superdex S200 column (see B and C: collected fractions assigned with horizontal bars) in comparison with non-tagged GyrA wt purified by IEX chromatography and SEC. 1: His$_6$-GyrA*. 2: GyrA* (NHT) (cleaved His$_6$-TEV-GyrA*). 3: GyrA wt. All preparations are of similar purity.

### 3.1.3 Affinity-purified GyrA proteins exhibit wild-type like activity

His$_6$-GyrA* and cleaved His$_6$-TEV-GyrA* (hereafter abbreviated GyrA* NHT) were assayed for their relaxation and supercoiling activities in topoisomerase assays (section 2.12.1).

DNA relaxation by His$_6$-GyrA* was performed with 200 nM GyrA, 800 nM GyrB and 15 nM supercoiled pUC18 plasmid substrate. After 120 min incubation time at 37°C, half of the relaxation reaction was supplied with 2 mM ATP to induce supercoiling activity and incubated for further 2 min. Tagged GyrA and the wild-type control showed comparable relaxation and supercoiling activities under these experimental conditions (Fig. 3.2 A) indicating that neither the introduction of an N-terminal His$_6$-tag nor the modification of the purification protocol significantly influenced the overall enzymatic activity of GyrA.

The DNA relaxation and supercoiling activity tests of GyrA* NHT were performed in separate reactions. Both experiments were done under conditions described above. GyrA* NHT showed the same topoisomer distributions as wild-type GyrA in both relaxation and supercoiling tests (Fig. 3.2 B).
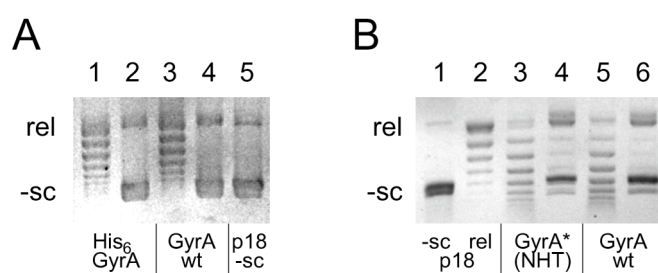


**Fig. 3.2:** Plasmid DNA relaxation and ATP-dependent supercoiling activities of GyrA proteins purified as His$_6$-tag fusions using 200 nM GyrA, 800 nM GyrB and 15 nM pUC18 in gyrase activity buffer (section 2.12.1). Incubation times were 30 and 2 min for DNA relaxation and ATP-dependent supercoiling reactions, respectively.

**A:** 1 and 2: Relaxation and supercoiling reaction products for His$_6$-GyrA*. 3 and 4: Relaxation and supercoiling reaction products for GyrA wt. 5: Control DNA (neg. supercoiled pUC18).

**B:** 1 and 2: Control DNAs (neg. supercoiled and relaxed pUC18). 3 and 4: Relaxation and supercoiling reaction products for GyrA* NHT. 5 and 6: Relaxation and supercoiling reaction products for GyrA wt.

### 3.1.4 Purification of GyrA lacking the C-terminal domain

A simple approach towards understanding the role of the C-terminal domain (CTD) in GyrA is the characterization of a CTD deletion mutant ($\Delta$CTD). We produced two versions of GyrA_$\Delta$CTD, both truncated after Thr489: A translational stop codon was introduced to the constructs pET-27b(+)_gyrA* and pETDuet-1_ His$_6$-TEV-gyrA* by site-specific mutagenesis yielding a truncated wild-type GyrA body (MW: 55.3 kDa) and an N-terminal His$_6$-tag fusion protein (MW: 57.6 kDa), respectively. Both constructs were expressed in *E. coli* BL21 CodonPlus(DE3)RP cells, showing high expression levels of the respective proteins.

The clarified crude extract containing non-tagged GyrA*_$\Delta$CTD was applied to a heparin column in 200 mM NaCl. Under these conditions most of the protein was adsorbed and subsequently eluted in an NaCl gradient, achieving separation from the majority of *E. coli* proteins. However, the fractions containing the target protein still contained undesirable protein and nucleic acid. GyrA*_$\Delta$CTD was further purified by size-exclusion chromatography using a Superdex S200 column: The protein eluted at a retention volume of 64 ml (Fig. 3.3 A). Nucleic acid contaminations were efficiently removed as judged from the absorption ratio $A_{280}/A_{260}$ of 2.2, but the purified protein still contained minor protein impurities (Fig. 3.3 B and C). The yield was exceptionally high compared to full-length GyrA (45 mg compared to 10 – 20 mg per liter of bacterial culture).

The tagged protein His$_6$-TEV-GyrA*_$\Delta$CTD was purified on a Ni$^{2+}$-NTA column as described for the full-length enzyme His$_6$-TEV-GyrA* (section 3.1.2): Most of the protein was adsorbed to the resin and eluted with 500 mM imidazole in a pure form. During over-night dialysis against a buffer containing 500 mM NaCl the protein was cleaved from the N-terminal His$_6$-tag by TEV protease (GyrA*_$\Delta$CTD NHT). After a second IMAC step most of the protein was found in the flow-through indicating efficient proteolytic removal of the tag. Further purification on a Superdex S200 size-exclusion column showed the same elution profile peaks observed for GyrA*_$\Delta$CTD at retention volumes of 64 ml with a minor shoulder at approx. 67.5 ml (Fig. 3.3 A) corresponding to apparent MW of 120 and 88 kDa respectively, both containing pure truncated GyrA (Fig. 3.3 C). Fractions from the first peak reflecting the expected size of the dimeric protein were pooled and concentrated. GyrA*_$\Delta$CTD was free from protein or nucleic acid contamination (absorption ratio $A_{280}/A_{260}$ of 2.45; Fig. 3.3 B). The protein yield was similar as the one for the non-tagged construct (42 mg per liter of bacterial culture).

Both proteins could be concentrated to 1.1 mM without showing precipitation.
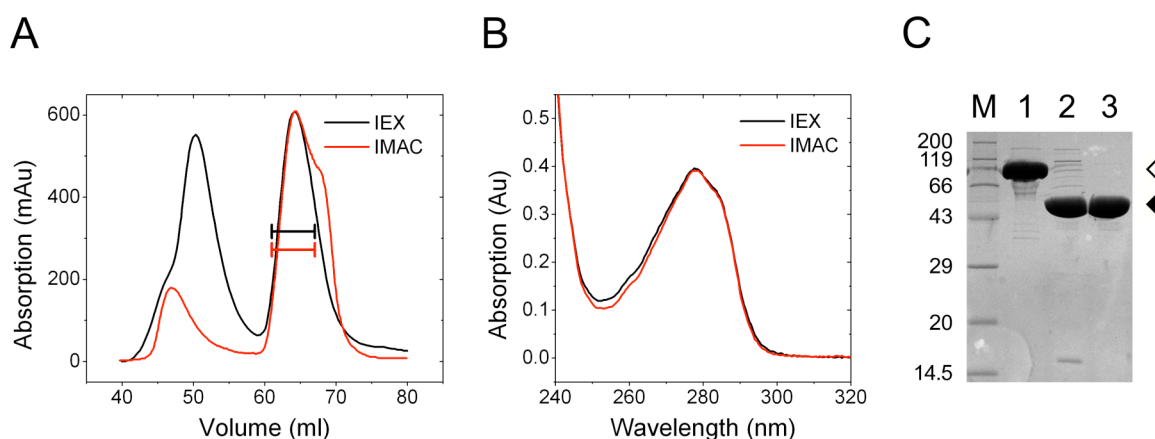
**Fig. 3.3:** Purification by SEC of GyrA*_ΔCTD pre-purified by IEX chromatography (non-tagged, I) and IMAC (N-terminal His$_6$-tag, cleaved with TEV protease, II).
**A:** Chromatograms of SEC purification of GyrA*_ΔCTD I (black line) and II (red line) with elution volumes of 64 ml. Horizontal bars denominate protein fractions pooled and concentrated for further use. Different contaminations could be eliminated successfully (I: nucleic acids eluting at 50 ml; II: GyrA*_ΔCTD with anomalous behavior eluting at 67.5 ml).
**B:** UV absorption spectra for GyrA*_ΔCTD preparations I (black) and II (red) in storage buffer. Protein concentrations were 15 µM. Absorption maxima are found at 278 nm, the A280/A260 ratio is 2.2 and 2.45 for preparations I and II, respectively.
**C:** SDS polyacrylamide gels of purified GyrA*_ΔCTD (◄, 55 kDa) compared to wild-type GyrA (△, 92 kDa). 1: GyrA wt. 2: Preparation I. 3: Preparation II. M: Protein marker with corresponding MW indicated in kDa. GyrA*_ΔCTD purified as a His$_6$-tag fusion protein (preparation II) is of superior purity compared to protein from preparation I.

### 3.1.5 GyrA_ΔCTD is supercoiling deficient

The truncated GyrA proteins were tested for their remaining DNA relaxation and supercoiling activity. 200 nM GyrA proteins (ΔCTD and wild-type control) were incubated with 800 nM GyrB and 15 nM neg. supercoiled or relaxed pUC18, in the absence or presence of ATP at 37°C. Both GyrA*_ΔCTD proteins showed a significantly decreased ATP-independent DNA relaxation activity compared to the wt control. In the presence of 2 mM ATP the relaxation of supercoiled plasmid DNA was dramatically enhanced (Fig. 3.4 A and B). The truncated GyrA proteins showed the same behavior, further indicating that the different purification protocols do not influence the enzymatic activities (Fig. 3.4 B).

The protein purified by affinity chromatography showed complete substrate relaxation under the applied conditions after 5 min of incubation time with no visible change of product DNA topology after 25 or 80 min (Fig. 3.4 A). Incubation with relaxed plasmid DNA in the presence of 2 mM ATP did not yield supercoiled, but even further relaxed plasmid (Fig. 3.4 B), indicating the complete loss of DNA supercoiling activity in the CTD deletion mutants.

These results are in agreement with previous findings for *E. coli* gyrase [53], showing that the deletion of the GyrA CTDs converts gyrase to a conventional type II topoisomerase.
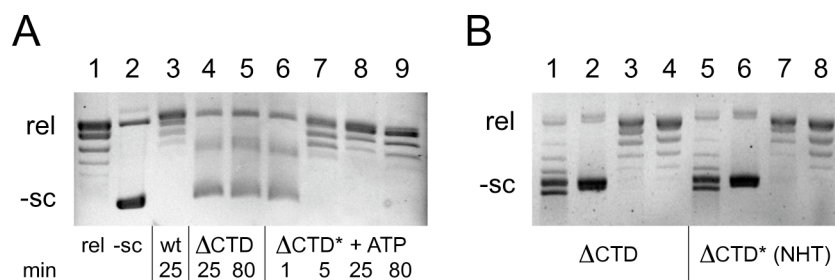
**Fig. 3.4:** DNA relaxation by GyrA CTD-deletion mutants. Reactions were performed using 200 nM GyrA proteins, 800 nM GyrB, and 15 nM plasmid substrates and gyrase activity buffer (section 2.12.1). 2 mM ATP were added as indicated. Incubation times specified below.
**A:** Plasmid DNA relaxation by GyrA*_ΔCTD NHT. 1 and 2: Relaxed and neg. supercoiled plasmid controls (pUC18). 3: Product of relaxation reaction by GyrA wt. 4 and 5: Relaxation by GyrA*_ΔCTD NHT after 25 and 80 min of incubation. 6 – 9: Relaxation by GyrA*_ΔCTD NHT after 1, 5, 25, and 80 min of incubation in the presence of 2 mM ATP.
**B:** Plasmid DNA relaxation by GyrA*_ΔCTD (lanes 1 – 4) and GyrA*_ΔCTD NHT (lanes 5 – 8). 1 and 5: Relaxation after 30 min of incubation. 2 and 6: Relaxation after 5 min incubation. 3 and 7: Relaxation after 5 min of incubation in the presence of 2 mM ATP. 4 and 8: Product of truncated GyrA proteins acting on relaxed plasmid in the presence of 2 mM ATP (2 min incubation).
In contrast to GyrA wt, GyrA*_ΔCTD-catalyzed plasmid DNA relaxation is ATP-dependent. The truncated protein is therefore deficient in plasmid DNA supercoiling. GyrA*_ΔCTD proteins from different preparations exhibit the same relaxation activities.

### 3.1.6  DNA affinity of GyrA

GyrA binds DNA at the DNA gate and the CTDs [90, 91]. In fluorescence anisotropy titrations DNA affinity for the wild-type GyrA and the CTD deletion mutant GyrA*_ΔCTD NHT (hereafter denominated GyrA_ΔCTD) were determined in the absence of GyrB. The 60bp DNA used as a substrate containing one binding site (bs) for *B. subtilis* gyrase [33] was annealed from complementary strands, i.e. Gyr_60bp_1bs_for and fluorescently labeled Gyr_60bp_1bs_rev_A546. The anisotropy signal of Alexa546 linked to the 60bp DNA varied from 0.055 to 0.075 between different experiments (Fig. 3.5 A).

The substrate DNA was titrated with GyrA up to a concentration of 10 μM, causing an increase of the anisotropy to approx. 0.2. The data were analyzed according to a 1 : 1 binding model and yielded a $K_d$ of 2.3 ± 0.2 μM for the DNA enzyme complex. The maximal anisotropy was calculated as 0.225, indicating a 84 % saturation of the 60bp DNA at 10 μM enzyme concentration (Fig. 3.5 A).

Titration of the substrate with GyrA_ΔCTD showed a much lower anisotropy increase than with GyrA wt. Enzyme was added up to a final concentration of 20 μM. The calculated $K_d$ was 73 ± 64 μM. However, the curvature of the fit was not well defined due to incomplete saturation of the substrate, resulting in a standard error in the range of the $K_d$ and a very

unlikely calculated maximal anisotropy of 0.39 (which is very high compared to the one for the DNA-GyrA wt complex). Fixing the maximal anisotropy to 0.225 as for GyrA wt leads to a lower calculated $K_d$ of $43 \pm 2$ µM (Fig. 3.5 A).

The deletion of the C-terminal domains leads to an approx. 20- to 50-fold decrease of affinity for the 60bp DNA. This clearly shows a high DNA affinity for the CTDs. Due to the lack of prominent DNA binding sites other than the DNA gate and on the CTDs, suggesting that the CTDs constitute the main DNA-binding site in GyrA.

### 3.1.7   DNA affinity of GyrB

The DNA affinity of GyrB was determined using the 60bp DNA. 10 nM DNA was titrated with *B. subtilis* wild-type GyrB to reach a final concentration of 20 µM. The anisotropy of the dye increased from a starting value of 0.070 up to approx. 0.20, showing a sigmoidal behavior (Fig. 3.5 B). The data could be described with the Hill equation and the following parameters: $K_d$ was calculated as $17.1 \pm 6.6$ µM and the anisotropy under saturating conditions as 0.21 approx. The Hill coefficient was determined as $1.99 \pm 0.28$, clearly indicating positive cooperative binding of more than one GyrB subunit to one molecule of DNA.
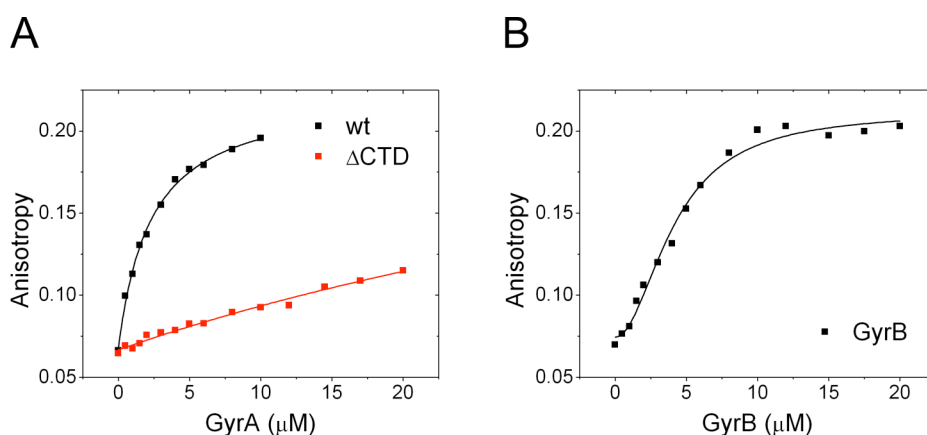


**Fig. 3.5:** Anisotropy titrations with linear double stranded 60bp DNA containing one gyrase binding site (annealed from Gyr_60bp_1bs_for and Gyr_60bp_1bs_rev_A546) and GyrA, GyrA_ΔCTD and GyrB.
**A:** Titrations with GyrA wt (black) and GyrA_ΔCTD (red) yield $K_d$ values of $2.3 \pm 0.2$ and $43 \pm 2$ µM, respectively. The latter is poorly defined due to non-sufficient saturation of the DNA substrate.
**B:** Titration with GyrB wt. The fit employing the Hill equation yields a $K_d$ value of $17.1 \pm 6.6$ µM and a Hill coefficient of $1.99 \pm 0.28$ indicating cooperative binding of at least two GyrB molecules to the 60bp DNA.

### 3.1.8 The presence of GyrB increases GyrA affinity for DNA

Next, the influence of GyrB on the GyrA affinity for DNA was determined. GyrA wt and GyrA_ΔCTD were titrated with 60bp DNA to a final concentration of 10 nM in the presence of 4 μM GyrB. This concentration of GyrB was by far not enough to saturate the DNA substrate in the absence of GyrA as the $K_d$ is approx. 17 μM (Fig. 3.5B), but should saturate the GyrA$_2$-60bp complex (personal communication by A. Gubaev). Most importantly, using 4 μM of GyrB guaranteed for a medium initial anisotropy value and thus for a significant signal change upon addition of GyrA. As the anisotropy in this concentration range is very sensitive to small changes in concentration of GyrB, the start value ranged from 0.9 to 1.2 in different experiments.

Measured $K_d$ values for GyrA wt and GyrA_ΔCTD for the 60bp DNA in the presence of GyrB were 63 ± 5 nM and 299 ± 20 nM, respectively. This finding marks a 5-fold decrease of affinity for the substrate upon deletion of the CTD, which provided evidence of the high DNA affinity of the CTDs as already shown with titrations in the absence of GyrB (Fig. 3.6 A and B).

The affinity constants also showed a sharp increase of affinity of 35-fold for GyrA wt and 15- to 25-fold for GyrA_ΔCTD due to the presence of GyrB (Fig. 3.6 A and B). As GyrA and GyrB mainly interact at the DNA gate, embracing the gate DNA segment, the increase in affinity of GyrA for DNA could be attributed to this interface.

The calculated maximum anisotropies were 0.27 and 0.30 for wt GyrA and ΔCTD in complex with GyrB and 60bp DNA, respectively (Fig. 3.6 A and B), which is significantly higher than 0.225 for the GyrA wt-60bp complex (Fig. 3.5 A).
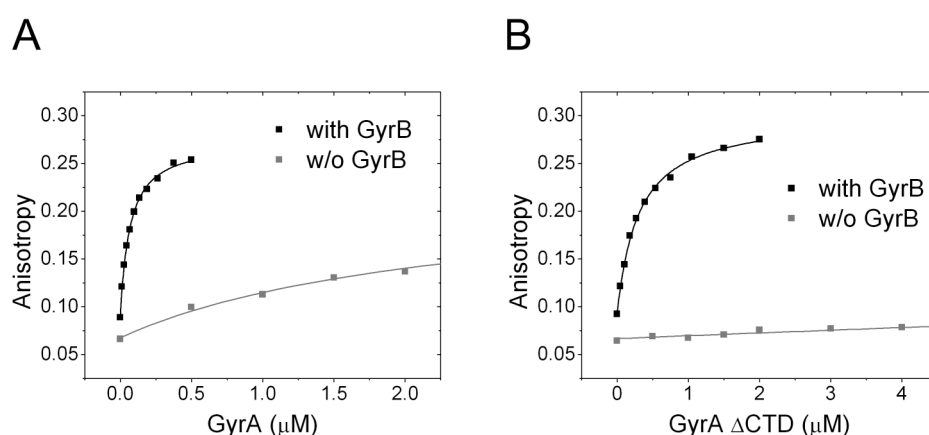


**Fig. 3.6:** Anisotropy titrations of 60bp DNA substrate with GyrA and GyrA_ΔCTD in the presence of 4 μM GyrB.
**A:** Titration with GyrA (black). The $K_d$ value is 63 ± 5 nM in the presence of GyrB, which marks a 35-fold increase in affinity over GyrA in the absence of GyrB (grey).
**B:** Titration with GyrA_ΔCTD (black). The measured $K_d$ is 299 ± 20 nM, which is approx. 25-fold lower than in the absence of GyrB (grey).

### 3.1.9    DNA affinity of GyrA decreases strongly with DNA substrate length

From the 60bp substrate DNA two shorter DNAs of 48 and 37 base-pair length were derived, both containing the preferred binding site in the center of the sequence [92] and an A546 label at the same position (Fig. 3.7). The affinities of GyrA wt and GyrA_ΔCTD for the DNA fragments were measured in fluorescence anisotropy titrations, using 10 nM DNA and 4 μM GyrB. The anisotropy value in the absence of GyrA was 0.085 − 0.095 for both DNAs (Fig. 3.8 A and B).
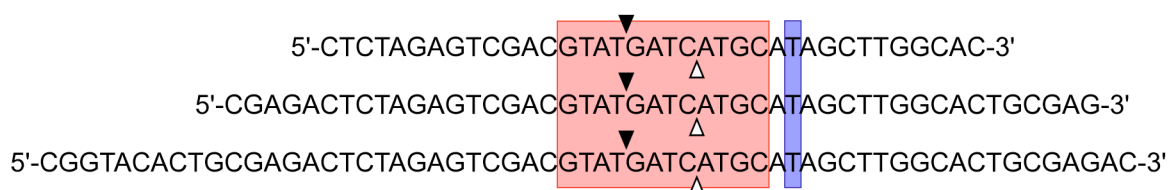


**Fig. 3.7:** DNA substrates used in anisotropy titrations. From top to bottom: nucleotide sequences of Gyr_37bp_1bs_rev, Gyr_48bp_1bs_rev, and Gyr_60bp_1bs_rev DNAs. Sequences of the complementary strands are listed in section 2.3.3. The preferred gyrase binding site is highlighted in red. Cleavage sites on the depicted and complementary strands are marked with black and white arrows, respectively. The thymines highlighted in blue carry the A546 lable.

Titrations with wt GyrA yielded $K_d$ values of 189 ± 13 nM and 654 ± 88 nM for 48bp and 37bp substrates, respectively. Compared to the affinity of 63 nM for the 60bp DNA, the one for the shorter substrates drops approx. 3- and 10-fold, indicating a non-proportional correlation between GyrA affinity and substrate length (Fig. 3.8 A).

The same experiments were performed with GyrA_ΔCTD yielding $K_d$ values for the 48bp and 37bp substrates of 378 ± 27 nM and 462 ± 46 nM, respectively. This corresponds to a 1.3- and 1.5-fold decrease in affinity compared to $K_d$ values of 299 nM measured for the 60bp DNA. These data indicate a linear relation between $K_d$ values and the substrate length (Fig. 3.8 B).

The $K_d$ values for the 60bp and 48bp substrates are 5- and 2-fold lower in wt GyrA than in GyrA_ΔCTD, suggesting that the gain of affinity in the presence of the CTD decreases with DNA chain length. This interpretation is supported by the $K_d$ value for the 37bp DNA which is even 1.4-fold higher in wt GyrA than in GyrA_ΔCTD. The findings suggest that the 60bp and 48bp DNA substrates contact the CTDs, whereas this interaction seems to be lost in case of the 37bp DNA. Thus, the minimal length of a DNA substrate that bridges the DNA-gate and the CTDs should be between 37 and 48 bp.
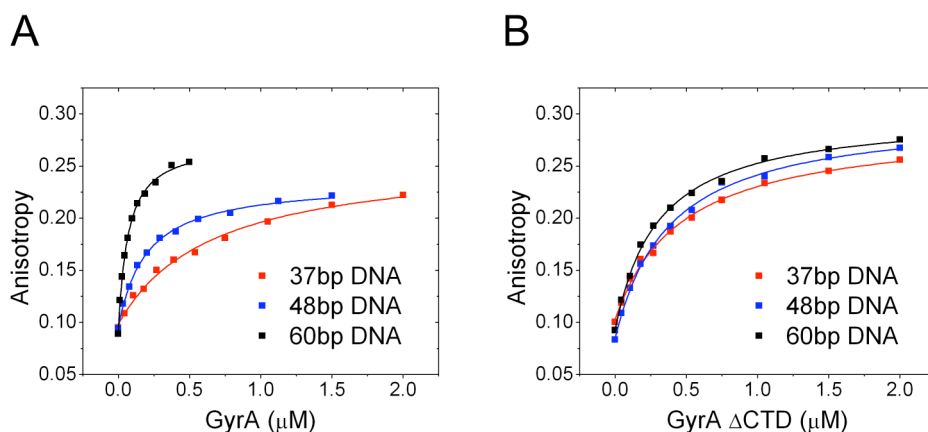
**Fig. 3.8:** Anisotropy titrations of linear double stranded DNAs with GyrA wt and GyrA_ΔCTD in the presence of 4 µM GyrB.
**A:** Titrations of linear double-stranded DNAs with GyrA wt. $K_d$ values are 63 ± 5 nM (60bp), 189 ± 13 nM (48bp) and 654 ± 88 nM (37bp).
**B:** Titrations of linear double stranded DNAs with GyrA_ΔCTD. $K_d$ values are 299 ± 20 nM (60bp), 378 ± 27 nM (48bp) and 462 ± 46 nM (37bp).

### 3.1.10  Construction of GyrA for single molecule experiments

It was shown that the C-terminal domain of GyrA is indispensable for the DNA supercoiling activity of gyrase from *E. coli* [53] and *B. subtilis* (section 3.1.5). The CTD was proposed to undergo conformational changes when binding and releasing DNA during the supercoiling cycle. In order to elucidate potential movement we performed single-molecule FRET measurements, for which two GyrA systems were constructed: A set of homo-dimeric GyrA mutants for fluorescent labeling at one position in both CTDs, and hetero-dimeric GyrA with one subunit bearing two labeling sites, one on the GyrA body (the so-called cleavage and religation domain) and another on the CTD.

### 3.1.11  Homo-dimeric constructs with dyes on both CTDs

*B. subtilis* GyrA CTD was modeled using the structure of the *E. coli* GyrA CTD (PDB entry: 1ZI0, chain B [50]) employing the SWISS-MODEL structure homology-modeling server [93]. Four presumably solvent exposed and non-conserved amino-acid residues as judged from alignments of homologous protein sequences were selected for the mutation to cysteine residues: K570 and K594 on opposite faces of blade 2 close to the amino terminus, and D695 and E726 on blades 4 and 5 respectively, both located on the distant end of the β-pinwheel fold (Fig. 3.9A).
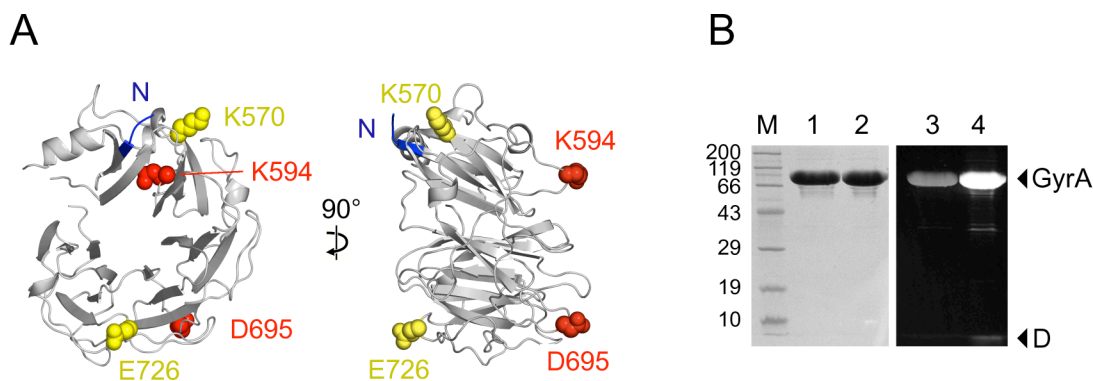
**Fig. 3.9:** Sites for cysteine introduction on GyrA CTD
**A:** Front (left) and side (right) views of a structural model of *B. subtilis* GyrA CTD in cartoon representation. The CTD exhibits a β-pinwheel fold with a pseudo 6-fold symmetry, consisting of 6 sectors (blades) of antiparallel β-sheet structure [50]. N (blue): Amino terminus and the attachment point to the N-terminal domain of GyrA. Residues depicted as yellow (K570, E726) and red spheres (K594, D695) were selected for individual mutation to Cys.
**B:** SDS-polyacrylamide gel of GyrA*_D695C labeled with A488 (1, 3) or A546 (2, 4) in fluorescence view (right) and after coommassie staining (left). Non-reacted dye is annotated D. The protein size marker is denominated M, and corresponding MW are indicated in kDa. Labeling efficiencies were 87 and 92 % for A488 and A546, respectively.

Production, fluorescent labeling, and activity of single Cys FRET mutants

All of the four GyrA Cys mutants lacked the only native cysteine located in the GyrA body [33]. The proteins were produced and purified as described (section 2.10.2). The mutants GyrA*_K594C and E726C had been produced ahead of this work [36]. Mutants K570C and D695C were purified to similar yields (11 – 13 mg/l bacterial culture) and purity (very low protein and nucleic acid contamination) as described for the wild-type.

For single-molecule experiments the proteins were statistically labeled with fluorescent dyes as described in section 2.16.1, using a 3- and 4-fold excess of Alexa488 (A488) and Alexa546 (A 546) maleimide dyes over protein, respectively. The total labeling degree (i.e. the sum of the individual labeling degrees of the dyes) for each of the Cys mutants was up to 100% with respect to available Cys residues, demonstrating good solvent accessibility of the selected positions (e.g. labeling of GyrA*_D695C with either A488 or A546: Fig. 3.9B)

It is of utmost importance that proteins modified for single-molecule experiments retain enzymatic activity. Ahead of this work GyrA*_K594C and _E726C mutants were shown to possess wild-type like supercoiling activity even when labeled with Alexa488 and Alexa546 dyes [36]. Also the newly constructed mutants GyrA*_K570C and _D695C exhibited unchanged DNA supercoiling and relaxation activities, suggesting that neither the mutation of above mentioned residues to cysteine nor the chemical modification altered the enzymatic behavior (Fig. 3.10 A – C).
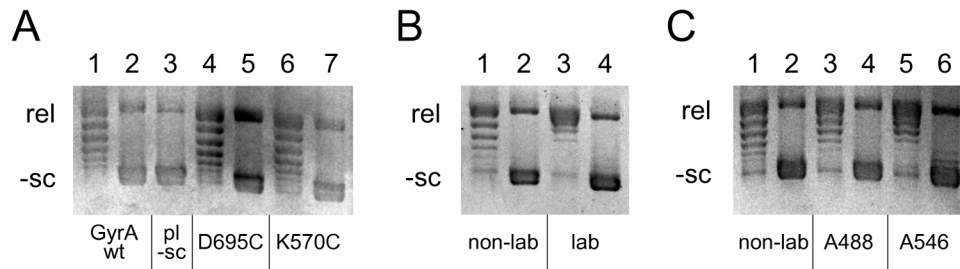
**Fig. 3.10:** DNA relaxation and ATP-dependent supercoiling activity of GyrA single Cys mutants using 200 nM GyrA, 800 nM GyrB, and 15 nM pUC18. Supercoiling reactions used relaxation reactions as starting points and were supplied with 2 mM ATP. Incubation times were 30 and 2 min for the relaxation and supercoiling reactions, respectively. Reactions were performed in gyrase activity buffer (section 2.12.1).
**A:** Plasmid DNA relaxation and supercoiling activity of non-labeled GyrA mutants K570C and D695C compared to wild-type GyrA. 1 and 2: Relaxation and supercoiling by GyrA wt. 3: Supercoiled pUC18 plasmid. 4 and 5: Relaxation and supercoiling by GyrA*_D695C. 6 and 7: Relaxation and supercoiling by GyrA*_K570C. Both mutant proteins exhibited wild-type like relaxation and supercoiling activities.
**B:** Plasmid DNA relaxation and supercoiling activity tests of non-labeled and double labeled GyrA*_K570C. 1 and 2: Relaxation and supercoiling by the non-labeled mutant. 3 and 4: Relaxation and supercoiling by the mutant labeled with A488 and A546 (total labeling degree: 75 %). The double labeled protein showed a slightly increased relaxation but similar supercoiling activity compared to the non-labeled enzyme.
**C:** Plasmid DNA relaxation and supercoiling activity tests of non-labeled and labeled GyrA*_D695C. 1 and 2: Relaxation and supercoiling by the non-labeled mutant. 3 and 4: Relaxation and supercoiling by the mutant labeled with A488 (labeling degree: 95 %). 5 and 6: Relaxation and supercoiling by the mutant labeled with A546 (labeling degree: 100 %). Labeled proteins exhibited the same activities as the non-labeled enzyme.

### 3.1.12 Hetero-dimeric GyrA FRET constructs

Parallel to the construction of single-cysteine mutants, the formation of hetero-dimeric GyrA constructs was attempted: The main objective was to create a FRET mutant composed of one wild-type subunit and one mutant subunit with two labeling sites, one each on the GyrA body and on the CTD. Such a construct has several advantages over the homo-dimeric GyrA FRET mutants: (I) It would allow to observe conformational changes of an individual CTD with respect to the GyrA body. (II) At the same time the degrees of freedom between the domains labeled with fluorescent dyes would be reduced. (III) Very importantly, the number of possible arrangements of the two dyes would be increased: Given the dimensions of the GyrA body dimer of roughly 9 nm in diameter, the distance between the CTDs should be at least in the same range, limiting the applicability of FRET measurements with homo-dimeric constructs. In a hetero-dimeric construct the inter-dye distance could be adjusted to values within the sensitive range of FRET signals (i.e. 3 to 8 nm).

GyrA subunit separation under denaturating conditions

One possibility to construct GyrA hetero-dimers would be the separation and subsequent reconstitution of different GyrA homo-dimers. The chaotropic denaturant GuHCl was used to explore subunit separation by denaturation. GyrA mutants labeled with donor (Alexa488) and acceptor dyes (TMR) at the DNA gate (T140C) or at the C-gate (T408C), both known for small inter-dye distance and FRET efficiencies higher than 0.8 [33], were incubated with varying concentrations of GuHCl. The separation of the dimer interfaces was monitored in ensemble FRET experiments, calculating a apparent FRET efficiency from fluorescence spectra corrected for buffer contributions as described in section 2.17. In the absence of GuHCl, both double-labeled GyrA mutants showed strong acceptor fluorescence emission upon excitation of the donor dye, showing efficient energy transfer between donor and acceptor dyes as expected (Fig. 3.10 A).

GyrA*_T140C exhibited a total loss (as judged from the spectra) of acceptor signal with concomitant increase in donor fluorescence intensity in a GuHCl concentration range between 0.5 and 1.75 M, indicating a structural rearrangement of the DNA-gate with a melting point at approx. 1.25 M GuHCl (visual inspection). At higher GuHCl concentration no further change in fluorescence intensities could be detected apart from a continuous red-shift of fluorescence maxima (from 516 to 521 nm and from 571 to 577 nm for donor and acceptor, respectively) (Fig. 3.11 C).

Incubation of GyrA*_T408C with up to 5 M GuHCl did not strongly influence donor and acceptor fluorescence intensities, apart from shifting the fluorescence maxima to slightly higher wavelengths. This finding indicates that the dimer interface of the C-gate is not disrupted even at high denaturant concentration (3.10 B). This is in contrast to the data for the DNA-gate, indicating much stronger dimer stability at the C-gate.

The two experiments clearly demonstrated that separation of the GyrA dimer at low concentrations of GuHCl is not possible; thus subunit exchange cannot be achieved by this method.
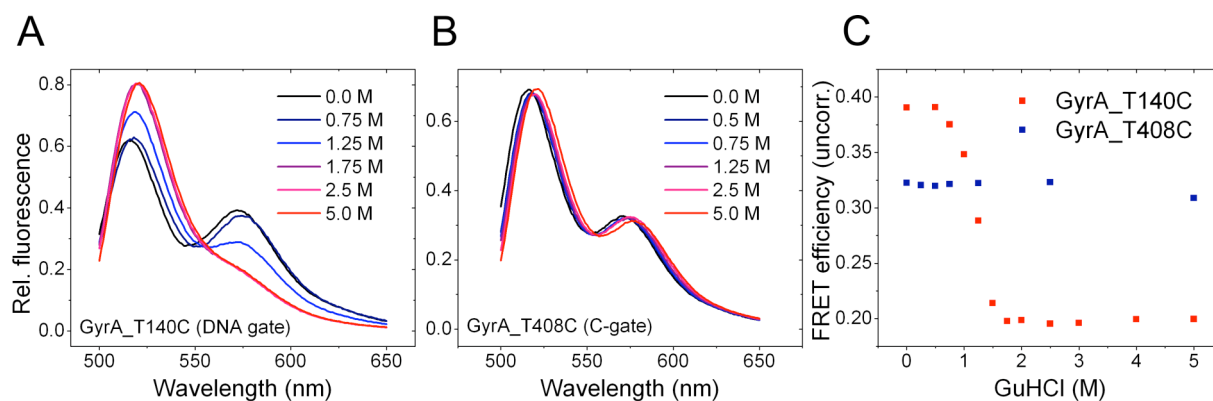
**Fig. 3.11:** Disruption of intersubunit contacts in GyrA mutants in the presence of GuHCl.
**A and B:** Fluorescence emission spectra of GyrA*_T140C and _T408C labeled with A488 and TMR in the presence of different concentrations of GuHCl (0 – 5 M). Spectra are normalized with an apparent FRET efficiency (eq. 2.14). Donor and acceptor fluorescence exhibit a slight red-shift of approx. 5 nm with increasing GuHCl concentration.
**A:** For GyrA*_T140C a sharp decrease of the acceptor flurescence (574 nm) and a concomitant increase of the donor signal (approx. 519 nm) was observed in the range of 0.75 to 1.75 M GuHCl. Labeling efficiencies were 35 and 58 % for A488 and TMR, respectively.
**B:** Normalized fluorescence spectra of GyrA*_T408C labeled with A488 and TMR remain constant across the tested GuHCl concentration range. Labeling efficiencies were 26 and 44 % for A488 and TMR, respectively.
**C:** Apparent FRET efficiencies calculated from fluorescence emission spectra were plotted against the GuHCl concentration for both mutants. GyrA*_T140C (red) exhibited two distinct crude FRET efficiencies (initial: 0.38; final: 0.2) with a transition at approx. 1.25 M GuHCl. The apparent FRET efficiency in GyrA*_T408C (blue) remained constant around a value of 0.32 in the tested GuHCl concentration range.

Co-production of two GyrA proteins

As the separation of the GyrA dimer by denaturation with GuHCl could not be achieved (see section above) the formation of hetero-dimeric GyrA was performed by co-production in *E. coli*. Two plasmids encoding different versions of GyrA and conferring different antibiotic resistance were co-transformed into *E. coli* expression strains. Initial transformation of cloning vectors pET-27b(+)_*gyrA*_mut and pETDuet-1_His$_6$-TEV-*gyrA** resulted in cell proliferation stop, probably following concomitant loss of one plasmid and the antibiotic resistance due to identical replication origins of the two plasmids. However, co-transformation of the vectors pACYCDuet and pET-27b(+) encoding His$_6$-TEV-GyrA*_ΔCTD and full-length GyrA*_ T140C_K594C, respectively, resulted in stable protein co-production (Fig. 3.12 A).

Numerous double cysteine GyrA mutants were co-produced with His$_6$-tagged wild-type GyrA and purified as described in section 2.10.2. The single or double tagged GyrA dimers were separated from host protein and non-tagged homo-dimeric GyrA by adsorption to a Ni$^{2+}$-NTA column (Fig. 3.12 B). The amount of GyrA protein found in the flow-through was high for all

co-expression products, but varied significantly between single purifications, probably depending on the production ratio and differences in solubility of the tagged and non-tagged proteins. The fully purified proteins were of similar purity as the GyrA* NHT purified by IMAC (section 3.1.2) with only low protein or DNA contaminations detectable. The yields were generally lower, ranging from 3 to 6 mg/l bacterial culture for most co-expressed and co-purified GyrA proteins. An exception was GyrA* / GyrA*_N314C_K594C which yielded only 0.5 mg/l culture due to a low expression level and slight solubility problems.

The production and purification of hetero-dimeric GyrA proteins was performed with the help of **Ines Hertel** (group Klostermeier, Biozentrum, University of Basel).
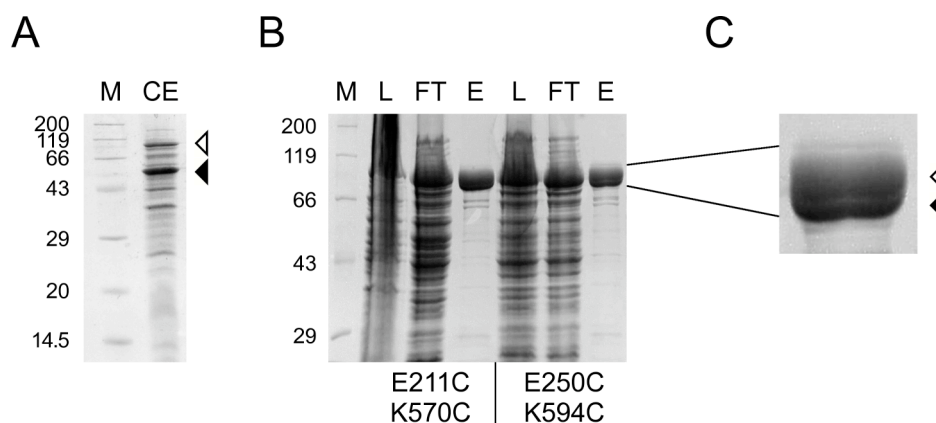


**Fig. 3.12:** Co-expression and co-purification of two GyrA proteins.
**A:** SDS polyacrylamide gel of co-expressed $His_6$-TEV-GyrA*_$\Delta$CTD (◄) and GyrA*_T140C_K594C (◁) from *E. coli* BL21(DE3) cells (CE). Cloning vectors used were pACYCDuet-1 and pET-27b(+) for the CTD-deletion mutant and the full-length enzyme respectively. M: Protein standard with corresponding MW indicated in kDa.
**B:** SDS polyacrylamide gel of early purification steps of co-expressed $His_6$-TEV-GyrA* / GyrA* double Cys mutants E211C_K570C and E250C_K594C. L: Crude cell extracts as loaded to the first $Ni^{2+}$-NTA column. FT and E: Flow-throughs and elutions from the $Ni^{2+}$-NTA column (at 20 and 500 mM imdazol, respectively). A large fraction of GyrA protein was not adsorbed to the resin indicating the lack of $His_6$-tags in the protein complex.
**C:** Magnified view of GyrA bands of E250C_K594C constructs eluted from the $Ni^{2+}$-NTA column (lane E). GyrA, which eluted at high imidazol concentrations, consisted of two different species with a small but visible difference in MW as expected for co-expressed tagged and non-tagged GyrA proteins. This is a strong indication that a large fraction of purified GyrA is indeed hetero-dimeric.

Cysteine positions in double mutants

In order to detect conformational change between the GyrA body and the CTD, double cysteine mutants with one Cys on the CTD and one on the body domain were constructed. Positions on the CTD were equivalent to those described in section 3.1.11. Cysteine mutations on the body were introduced at the DNA gate (T140C), C-gate (N399C, T408C), and on the tower domain (E211C, E250C, T299C, N314C). *B. subtilis* GyrA body was modeled using *E.*

*coli* GyrA body as a template (PDB entry 2Y3P [94]), and mutagenesis sites were chosen on the basis of this homology model. The locations of mutated residues are depicted in Fig. 3.13A.
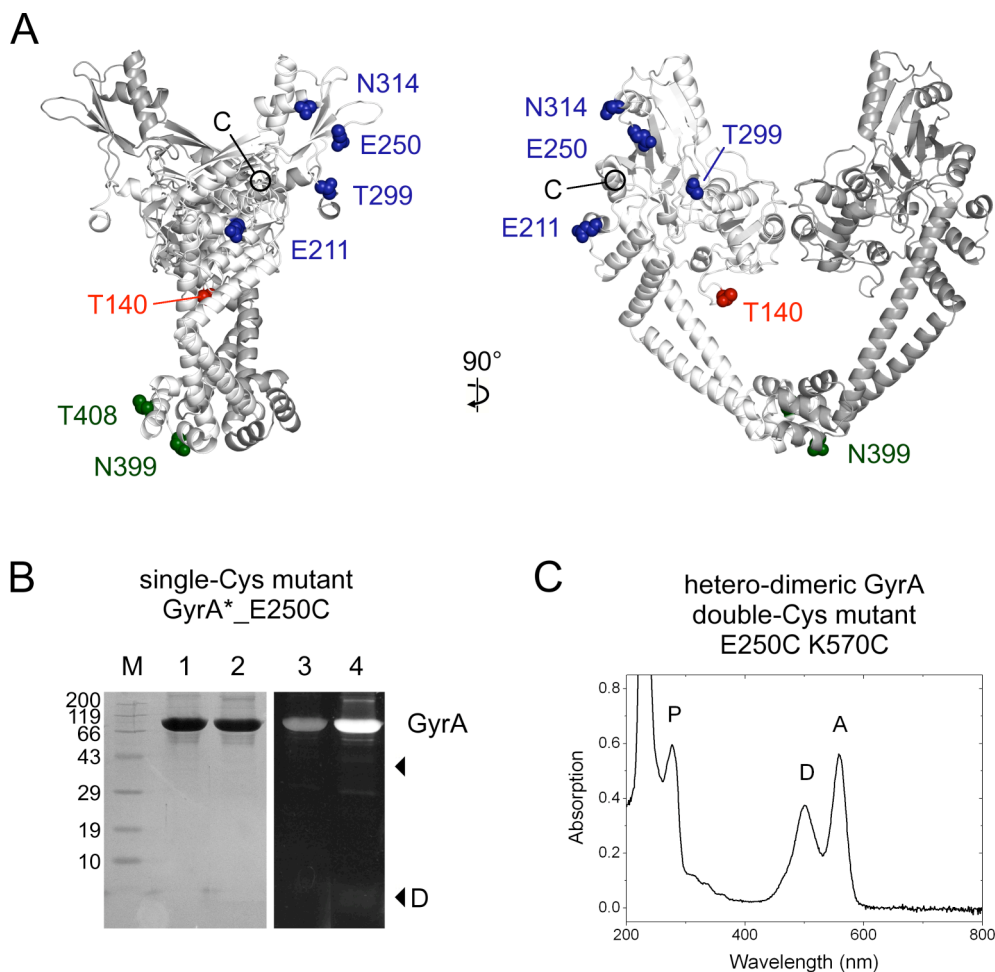


**Fig. 3.13:** Sites for cysteine introduction on the GyrA body; fluorescent labeling of homo-dimeric single-cysteine mutant E250C and hetero-dimeric GyrA containing one double-cysteine mutant subunit (E250C_K570C).
**A:** Side (left) and front view (right) of a structural model of *B. subtilis* GyrA body in cartoon representation (using *E. coli* GyrA as a template: PDB entry 2Y3P [94]). C (black): Carboxy terminus of GyrA and the attachment point of the linker peptide to the CTD. Residues depicted as spheres were selected for mutation to cysteine: T140 at the DNA gate (red); E211, E250, T299, and N314 in the tower domain (blue); N399 and T408 at the C-gate (green).
**B:** SDS-polyacrylamide gel of GyrA*_E250C labeled with A488 (1, 3) and A546 (2, 4) in fluorescence view (right) and after coommassie staining (left). No non-reacted dye is visible (D). The protein size marker is denominated M, and corresponding MW are indicated in kDa. Labeling efficiencies were 85 and 97 % for A488 and A546, respectively.
**C:** Absorption spectrum of hetero-dimeric GyrA* / GyrA*_E250C_K570C labeled with A488 and A546. Contributions of the protein, A488 and A546 are denominated P, D, and A. Labeling degrees were calculated from absorption maxima at 280, 493 and 555 nm as described (section 2.16.3). Values were approx. 35 and 55 % for A488 and A546, respectively, relative to available cysteines (assuming pure hetero-dimeric protein without contaminations by homo-dimeric GyrA wt).

<u>Fluorescent labeling of hetero-dimeric GyrA</u>

Single cysteine mutants GyrA*_T140C, _E211C and E250C were labeled under conditions described in section 2.16.1. Modification degrees were 85 to 100 % for all positions using dyes Alexa488 and Alexa546, indicating good solvent accessibility for the introduced cysteine residues and a sufficiently high accuracy of the structural model of the GyrA body (e.g. labeling of GyrA*_E250C: Fig. 3.13 B). The mutants GyrA*_T140C, _N399C and _T408C were labeled to similar degrees as shown in experiments performed ahead of this work [33, 36].

With the knowledge that individually introduced cysteines could be fully labeled several co-produced GyrA* / GyrA*_double Cys mutants were fluorescently labeled using the same dyes and procedure as for the homo-dimeric single Cys mutants (sections 2.16.1 and 3.1.11). For all the proteins both labeling with one or two dyes resulted in labeling degrees of 80 – 100% with respect to the concentration of GyrA monomers (e.g. absorption spectrum of GyrA* / GyrA*_E250C_K570C: Fig. 3.13 C). This was also the case for double Cys mutants T299C_K594C and N314C_K570C which had not been tested in single Cys mutants, suggesting full solvent accessibility for the positions T299C and N314C.

Hetero-dimeric  GyrA contains two cysteine residues (located both on the same subunit while the other is cysteine-free). Assuming pure hetero-dimeric protein (without contaminations by homo-dimeric GyrA wt) the concentration of subunits should be equal to the one for available cysteine residues. Thus, labeling degrees of close to 100 % (total dye concentration relative to total GyrA concentration) indicated that most of the GyrA dimers actually consisted of two different monomers (Fig. 3.13 C).


<u>Activity of hetero-dimeric GyrA proteins</u>

GyrA*_T140C, _E211C, _N399C, and _T408C were shown to retain wild-type like DNA relaxation and supercoiling activity in their purified and fluorescently labeled states [33, 36]. Hence, it was assumed that hetero-dimeric protein containing a GyrA subunit with combined Cys mutations would also exhibit unaltered activity. This hypothesis was validated in DNA supercoiling assays by gyrase containing the hetero-dimeric GyrA proteins most often used in single molecule experiments (sections 3.1.16, 17). Of all the proteins tested only GyrA* / GyrA*_E211C_K594C showed a slightly reduced activity. Generally labeling of hetero-dimeric GyrA did not result in loss of activity (Fig. 3.14 A and B).
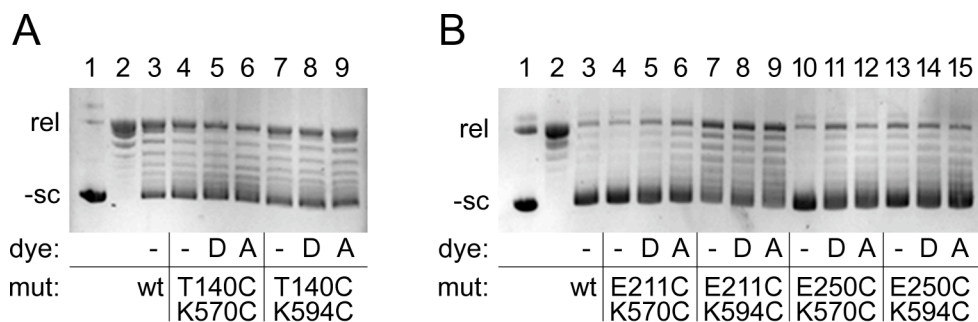
**Fig. 3.14:** DNA supercoiling by non-labeled and fluorescently labeled GyrA dimers containing one GyrA* and one GyrA* Cys double mutant subunit (GyrA$_2$*_double mutant). Reactions were performed using 50 nM GyrA, 800 nM GyrB, 50 nM pUC18 –sc, and 2 mM ATP, in gyrase activity buffer (section 2.12.1). Incubation time was 2 min. Lanes marked D and A contain protein labeled with donor (A488) or acceptor dye (A546), respectively.
**A:** 1 and 2: Negatively supercoiled and relaxed pUC18 plasmid. 3: Plasmid supercoiled by wild-type gyrase. 4 – 6: Supercoiling by gyrase containing GyrA$_2$*_T140C_K570C. 7 – 9: Supercoiling by gyrase containing GyrA$_2$*_T140C_K594C.
**B:** 1 and 2: Negatively supercoiled and relaxed pUC18 plasmid. 3: Plasmid supercoiled by wild-type gyrase. 4 – 6: Supercoiling by gyrase containing GyrA$_2$*_E211C_K570C. 7 – 9: Supercoiling by gyrase containing GyrA$_2$*_E211C_K594C. 10 – 12: Supercoiling by gyrase containing GyrA$_2$*_E250C_K570C. 13 – 15: Supercoiling by GyrA$_2$*_E250C_K594C.

### 3.1.13 Correction parameters for single-molecule measurements

To correctly interpret a FRET efficiency of a donor- and acceptor-labeled molecule and to subsequently extract distance information, the fluorescence signal has to be corrected for photophysical properties of the dyes and contributions of the measurement conditions (e.g. the single-molecule confocal microscope).

The correction parameters α, β, γ and δ for single-cysteine GyrA mutants K570C, K594C, D695C and E726C were determined for the non-complexed GyrA, while parameters for the hetero-dimeric GyrA constructs with two different labeling sites were determined in the absence and presence of GyrB and DNA and for combinations of labeling positions on the GyrA body (T140C, E211C, E250C) and on the CTD (K570C and K594C). Measurements and calculations were done as described (section 2.18.2), and values for correction parameters are listed in tables 3.1 – 3.3. Parameter α correcting for detection of donor fluorescence in the acceptor channel did not deviate more than 10 % between different FRET pairs, with an average value of 0. 35, indicating low change of donor fluorescence signal due to different environment. Parameters β and γ, correcting for acceptor cross-detection and difference in quantum yield and detection efficiencies of donor and acceptor fluorescence, respectively, exhibited higher differences between FRET pairs, suggesting increased acceptor fluorescence intensity changes depending on the attachment site of the dye in GyrA (Tables 3.1 – 3.3). The

parameter δ also showed values of 0.09 to 0.17 with an average of approx. 0.12, indicating significant direct excitation of the acceptor dye (approx. 10 - 17 % of the excitation of the donor dye); variation of approx. 50 % indicate that the local environment of the dyes influence absorption significantly. The correction parameters α', β' and γ' were calculated from the parameters α, β, γ and δ as described (section 2.18.2).

The average correction parameters α', β' and γ' determined from data recorded at 37°C in the absence of DNA and GyrB were calculated as 0.67, 0.0104 and 3.08, respectively (Table 3.2). They were used to correct single-molecule data recorded at 37°C involving labeled GyrA mutants for which site-specific correction parameters had not been determined.

**Table 3.1:** Photophysical correction parameters and Förster distances for homo-dimeric single cysteine GyrA mutants labeled at two equivalent positions, acquired at 25°C for labeled GyrA in the absence of ligands. α, β, γ, and δ denominate correction parameters, α', β' and γ' the ones corrected with δ. $R_0$ is the Förster distance, calculated with the donor fluorescence quantum yield $\Phi_D$ and the overlap integral $J(\lambda)$. The orientation factor $\kappa^2$ and the refractive index n were set to listed values.

| Mutant | K570C | K594C | D695C | E726C |
|---|---|---|---|---|
| α | 0.33 | 0.32 | 0.32 | 0.33 |
| β | 0.0067 | 0.0077 | 0.0073 | 0.0127 |
| γ | 2.5 | 3.11 | 2.85 | 2.33 |
| δ | 0.12 | 0.1 | 0.09 | 0.09 |
| **α'** | **0.63** | **0.63** | **0.58** | **0.54** |
| **β'** | **0.0067** | **0.0077** | **0.0073** | **0.0127** |
| **γ'** | **2.79** | **3.41** | **3.1** | **2.53** |
| $\Phi_D$ | 0.366 | 0.373 | 0.427 | 0.606 |
| $J(\lambda)$ ($*10^{15}$) | 3.32 | 2.62 | 3.26 | 2.70 |
| $\kappa^2$ | 0.667 | | | |
| n | 1.33 | | | |
| **$R_0$ (nm)** | **5.32** | **5.13** | **5.45** | **5.59** |

| Donor / Acceptor | T140C / K570C | K570C / T140C | T140C / K594C | K594C / T140C | E211C / K570C | K570C / E211C | E211C / K594C | K594C / E211C | E250C / K570C | K570C / E250C | E250C / K594C | K594C / E250C | average |
|---|---|---|---|---|---|---|---|---|---|---|---|---|---|
| $\alpha$ | 0.35 | 0.34 | 0.35 | 0.34 | 0.33 | 0.34 | 0.33 | 0.34 | 0.36 | 0.35 | 0.36 | 0.36 | 0.35 |
| $\beta$ | 0.0076 | 0.0015 | 0.0089 | 0.0149 | 0.0076 | 0.0126 | 0.0089 | 0.0126 | 0.0042 | 0.0122 | 0.0078 | 0.0122 | 0.0092 |
| $\gamma$ | 4.25 | 2.40 | 3.68 | 3.12 | 2.84 | 2.55 | 2.46 | 3.10 | 1.94 | 2.14 | 1.70 | 2.94 | 2.76 |
| $\delta$ | 0.10 | 0.15 | 0.11 | 0.12 | 0.10 | 0.14 | 0.11 | 0.12 | 0.11 | 0.15 | 0.12 | 0.12 | 0.12 |
| **$\alpha'$** | **0.77** | **0.70** | **0.75** | **0.71** | **0.61** | **0.69** | **0.60** | **0.71** | **0.57** | **0.67** | **0.56** | **0.71** | **0.67** |
| **$\beta'$** | **0.0076** | **0.0149** | **0.0089** | **0.0149** | **0.0076** | **0.0126** | **0.0089** | **0.0126** | **0.0042** | **0.0122** | **0.0078** | **0.0122** | **0.0104** |
| **$\gamma'$** | **4.66** | **2.75** | **4.07** | **3.48** | **3.12** | **2.89** | **2.72** | **3.46** | **2.15** | **2.45** | **1.90** | **3.28** | **3.08** |
| $\Phi_D$ | 0.48 | 0.37 | 0.48 | 0.41 | 0.45 | 0.37 | 0.45 | 0.41 | 0.58 | 0.37 | 0.58 | 0.41 | 0.45 |
| $J(\lambda)$ $(*10^{15})$ | 3.18 | 3.43 | 3.32 | 3.29 | 3.21 | 3.36 | 3.35 | 3.22 | 3.20 | 3.47 | 3.33 | 3.33 | 3.31 |
| $\kappa^2$ | 0.667 | | | | | | | | | | | | |
| n | 1.33 | | | | | | | | | | | | |
| **$R_0$ (nm)** | **5.53** | **5.37** | **5.56** | **5.42** | **5.49** | **5.35** | **5.52** | **5.40** | **5.71** | **5.38** | **5.75** | **5.43** | **5.49** |

| Donor / Acceptor | T140C / K570C | K570C / T140C | T140C / K594C | K594C / T140C | E211C / K570C | K570C / E211C | E211C / K594C | K594C / E211C | E250C / K570C | K570C / E250C | E250C / K594C | K594C / E250C |
|---|---|---|---|---|---|---|---|---|---|---|---|---|
| $\alpha$ | 0.37 | 0.36 | 0.37 | 0.36 | 0.34 | 0.36 | 0.34 | 0.36 | 0.39 | 0.38 | 0.39 | 0.37 |
| $\beta$ | 0.0177 | 0.0184 | 0.0184 | 0.0184 | 0.0177 | 0.0178 | 0.0184 | 0.0178 | 0.0109 | 0.0115 | 0.0111 | 0.0115 |
| $\gamma$ | 4.76 | 2.83 | 4.10 | 3.20 | 4.25 | 3.29 | 3.64 | 3.77 | 3.09 | 3.24 | 2.68 | 3.80 |
| $\delta$ | 0.11 | 0.15 | 0.12 | 0.13 | 0.10 | 0.14 | 0.11 | 0.12 | 0.12 | 0.14 | 0.13 | 0.12 |
| **$\alpha'$** | **0.89** | **0.78** | **0.85** | **0.77** | **0.76** | **0.81** | **0.73** | **0.81** | **0.76** | **0.83** | **0.74** | **0.82** |
| **$\beta'$** | **0.0177** | **0.0184** | **0.0184** | **0.0184** | **0.0177** | **0.0178** | **0.0184** | **0.0178** | **0.0109** | **0.0115** | **0.0111** | **0.0115** |
| **$\gamma'$** | **5.24** | **3.23** | **4.55** | **3.59** | **4.64** | **3.72** | **4.01** | **4.19** | **3.45** | **3.67** | **3.02** | **4.23** |
| $\Phi_D$ | 0.48 | 0.51 | 0.48 | 0.40 | 0.56 | 0.51 | 0.56 | 0.40 | 0.56 | 0.51 | 0.56 | 0.40 |
| $J(\lambda)$ $(*10^{15})$ | 3.31 | 3.47 | 3.50 | 3.44 | 3.33 | 3.22 | 3.52 | 3.20 | 3.34 | 3.37 | 3.53 | 3.34 |
| $\kappa^2$ | 0.667 | | | | | | | | | | | |
| n | 1.33 | | | | | | | | | | | |
| **$R_0$ (nm)** | **5.57** | **5.66** | **5.62** | **5.44** | **5.72** | **5.60** | **5.77** | **5.37** | **5.72** | **5.64** | **5.77** | **5.41** |

**Tables 3.2 (top) and 3.3 (bottom):** Photophysical correction parameters and Förster distances for hetero-dimeric GyrA proteins labeled at two non-equivalent positions (double cysteine mutant) for the correction of single-molecule FRET data obtained at 37°C in the absence (Tab. 3.2) and in the presence (Tab. 3.3) of DNA and GyrB. $\alpha$, $\beta$, $\gamma$, and $\delta$ denominate correction parameters, $\alpha'$, $\beta'$ and $\gamma'$ the ones corrected with $\delta$. $R_0$ is the Förster distance, calculated with the donor fluorescence quantum yield $\Phi_D$ and the overlap integral $J(\lambda)$. The orientation factor $\kappa^2$ and the refractive index n were set to listed values.

### 3.1.14 Determination of Förster distances for GyrA constructs

Distance information for a given pair of fluorescent dyes can be calculated from corresponding FRET efficiencies according to eq. 2.24., employing the Förster distance for this specific dye pair. Förster distances were determined as described (section 2.18.3) for the following dye arrangements: For single-cysteine GyrA mutants K570C, K594C, D695C and E726C in the non-complexed state; and for hetero-dimeric constructs with two fluorescent labels, one on the GyrA body (T140C, E211C, or E250C) and one on the CTD (K570C or K594C) (Tables 3.1 – 3.3).

The donor quantum yield and the overlap integral of donor fluorescence emission and acceptor absorption were determined, but the orientation factor $\kappa^2$ and the refraction index of the medium between the dyes in a given FRET system were assumed as 2/3 and 1.33, respectively [86, 87]. The quantum yields of A488 coupled to GyrA mutants were determined from absorption data and fluorescence emission spectra as described (section 2.18.3). Corresponding fluorescence measurements were performed at 25°C or 37°C for the correction of measurements involving homo-dimeric single cysteine mutant proteins and hetero-dimeric mutants with non-equivalent labeling positions (double cysteine mutants), respectively.

Quantum yields for A488 attached to different location showed values between 0.37 and 0.61 with an average of 0.44 for measurements at 37°C (Tables 3.2 – 3.3). The overlap integral $J(\lambda)$ was calculated as described (section 2.18.3). $J(\lambda)$ values ranged from 2.62 to $3.52 * 10^{15}$, scattering not more than 10% for the hetero-dimeric proteins (Tables 3.2 – 3.3). The resulting Förster distances $R_0$ for the dye pair used (A488, A546) were close to the values of approx. 5.5 nm determined before [33, 84], the lowest and highest being 5.13 and 5.57 nm, respectively.

The average Förster distance determined from data recorded at 37°C in the absence of DNA and GyrB was calculated as 5.49 nm (Table 3.2). It was used to derive FRET distances from measurements involving GyrA mutants for which $R_0$ had not been determined.

### 3.1.15 Determination of the CTD position with smFRET data from labeled single-cysteine GyrA mutants

To characterize the position of the C-terminal domains of GyrA, the FRET efficiency of protein with two fluorescence labels, one on each CTD, was measured on a single-molecule confocal microscope. GyrA*_K570C, _K594C, _D695C, and E726C single cysteine mutants were labeled with fluorescent dyes (Alexa488 and Alexa546) as described (section 2.16.1).

The temperature of the microscope objective was not controlled; therefore the incubation temperature was estimated as 25°C. FRET efficiencies were calculated from fluorescence bursts of diffusing particles and corrected for photophysical properties of the dyes attached to the protein using correction parameters listed in table 3.1.

FRET efficiency histograms of the labeled GyrA mutants K570C and K594C yielded unimodal distributions with maxima between 0.2 and 0.3 (Fig. 3.15). While the distribution for K594C was very narrow, the one for K570C was less well defined. Distance histograms were calculated from FRET efficiencies using the Förster distances determined before (section 3.1.14). For both mutants the distance distribution were well defined and could be approximated with a Gaussian, yielding mean inter-dye distances of 5.8 and 6.1 nm for mutants K570C and K594C, respectively (Fig. 3.15). The GyrA mutants D695C and E726C exhibited very low FRET efficiencies with distribution maxima of close to 0 and shoulders ranging up to 0.4 (Fig. 3.15), indicating a larger distance between labeling sites than observed for positions 570 and 594. For the mutant E726C a minor high-FRET population was observed. The corresponding distance histograms showed well defined distributions with maxima at approx. 7.5 nm and small shoulders at lower distances that could be correlated to the high FRET-efficiency population. The distance histogram for mutant D695C exhibited a similar behavior; thus, both histograms were described with a double Gaussian (Fig. 3.15).

Each of the four mutants exhibited one major FRET-efficiency distribution, indicating a well-defined position of both CTDs in a symmetrical arrangement. With the presented data set it was not possible to locate the domains with respect to the GyrA body. Nevertheless the position close to the connection points of GyrA body and CTDs could be excluded given a distance of approx. 90 nm (Fig. 3.13 A: C-terminus of GyrA body).
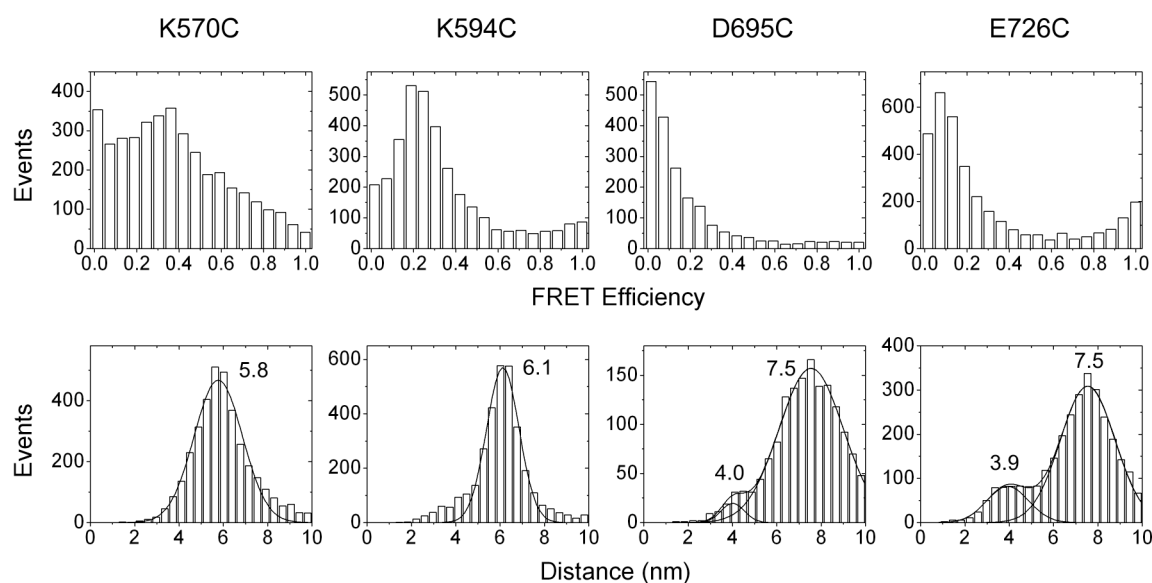


**Fig. 3.15:** Description see following page.

**Fig. 3.15:** SmFRET histograms (top) and corresponding distance histograms (bottom) for GyrA homo-dimers labeled at equivalent sites on the CTDs. FRET efficiency histograms for ligand-free GyrA mutants K570C and K594C exhibited FRET efficiency maxima at 0.3 and 0.2, respectively, which converted to inter-dye distances of 5.8 and 6.1 nm as determined from Gaussian fits of the distance histograms. FRET histograms for mutants D695C and E726C showed maxima at approx. 0 and 0.1 FRET efficiency, respectively, with a small high-FRET peak visible for the latter. Corresponding distance histograms exhibited bi-modal behavior and were thus fitted with a double Gaussian, yielding major and minor maxima at 7.5 and 4.0 nm for D695C as well as 7.5 and 4.0 nm for E726C. The major FRET efficiency populations corresponded to the major distance distribution, indicating a larger distance between distant CTD ends than for the N-terminal ends.

FRET efficiency data were corrected with parameters determined for corresponding homo-dimeric GyrA protein consisting of single cysteine mutant subunits. Distances were calculated using corresponding Förster parameters.

### 3.1.16 Localization of the GyrA CTDs with smFRET measurements of hetero-dimeric GyrA

As the CTDs could not be localized by means of smFRET data from single-cysteine mutants, hetero-dimeric GyrA with a wt and a mutant subunit with two labeling positions were used for single-molecule measurements. This allowed to measure FRET between a label on the GyrA body and one the CTD, avoiding high inter-dye distances.

SmFRET experiments for the localization of GyrA CTD were performed with the hetero-dimeric constructs GyrA* / GyrA*_T140C_K570C, _T140C_K594C, _E211C_K570C, _ E211C_K594C, _E250C_K570C, and _ E250C_K594C. These mutants exhibited labeling efficiencies of close to 100 % for the dyes A488 and A546 and showed wild-type-like activity (section 3.1.12; Fig. 3.14). Correction parameters and Förster distances had been determined for these proteins (tables 3.2 and 3.3). Corrections were done using parameters for both possible dye arrangements (A488 on GyrA body and A546 on the CTD and *vice versa*).

Experiments with all mutants yielded well-defined and uni-modal FRET efficiency distributions, indicating one defined conformation of the labeled CTD (Fig. 3.16 – 3.17). For proteins labeled at position 140 and 570 or 594 medium FRET efficiencies with values between 0.3 and 0.5 were determined (Fig. 3.16). FRET efficiencies involving positions 211 and 250 in the tower domain (GyrA body) were generally higher, ranging from 0.7 to 0.9 (Fig. 3.17). Differences between histograms corrected for different dye arrangements were generally lower than 0.1 FRET efficiency.

Distance histograms were determined from the corresponding FRET efficiencies using the Förster distances listed in table 3.2, and mean inter-dye distances calculated by a Gaussian fit. Distances between the reference points on the CTD and on the tower domain were 5.3 to 6.3 nm, while they were generally lower for GyrA labeled on the tower domain and the CTD (4.1 to 5.1 nm). This indicated that the N-terminal region of the CTD, represented by labeled

positions 570 and 594, is located closer to the tower domain than to the DNA-gate. The distance distributions for the hetero-dimeric constructs were more narrow than the ones for homo-dimeric (single-cysteine) proteins (Fig. 3.15). This finding reports on the degree of conformational freedom of the fluorescently labeled domains relative to each other: In the hetero-dimeric constructs, we observe potential flexibility between two connected domains (GyrA body and CTD), while in homo-dimeric constructs the two labeled domains are only indirectly linked (via the GyrA body) and possess a higher degree of conformational freedom relative to each other.

This data suggests a position of the N-terminal part of the CTD (represented by residues 570 and 594) in proximity to the DNA-gate and the tower domain.
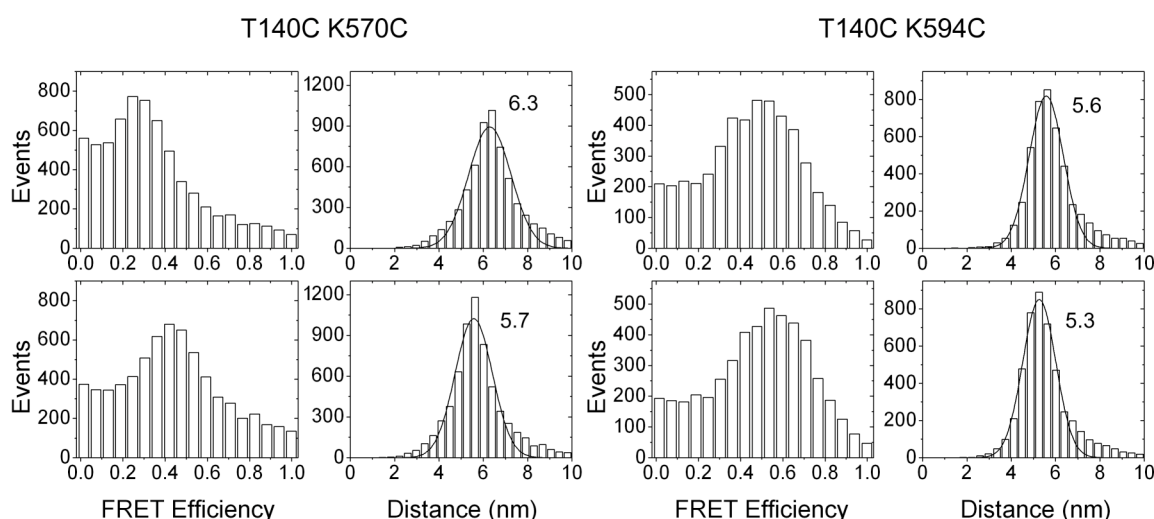


**Fig. 3.16:** SmFRET efficiency and distance histograms for ligand-free GyrA as observed using hetero-dimeric GyrA constructs bearing one double-cysteine mutant subunit. Labeling sites were at the DNA-gate (T140C) and on the CTD (K570C or K594C). Left: FRET efficiencies for mutant T140C_K570C were uni-modal, with maxima between 0.2 and 0.4, depending on the correction-parameter set applied; Gaussian fits of corresponding distance histograms yielded inter-dye distances of 5.7 to 6.3 nm. Right: FRET histograms for mutant T140C_K594C were also uni-modal, with better defined maxima at 0.5 and 0.6 and corresponding inter-dye distances of 5.6 to 5.3 nm.
Histograms were corrected with photophysical parameters and Förster distances for the corresponding mutants, acquired in the absence of ligands, with donor and acceptor dyes attached to GyrA body and the CTD (top row) and *vice versa* (bottom row).
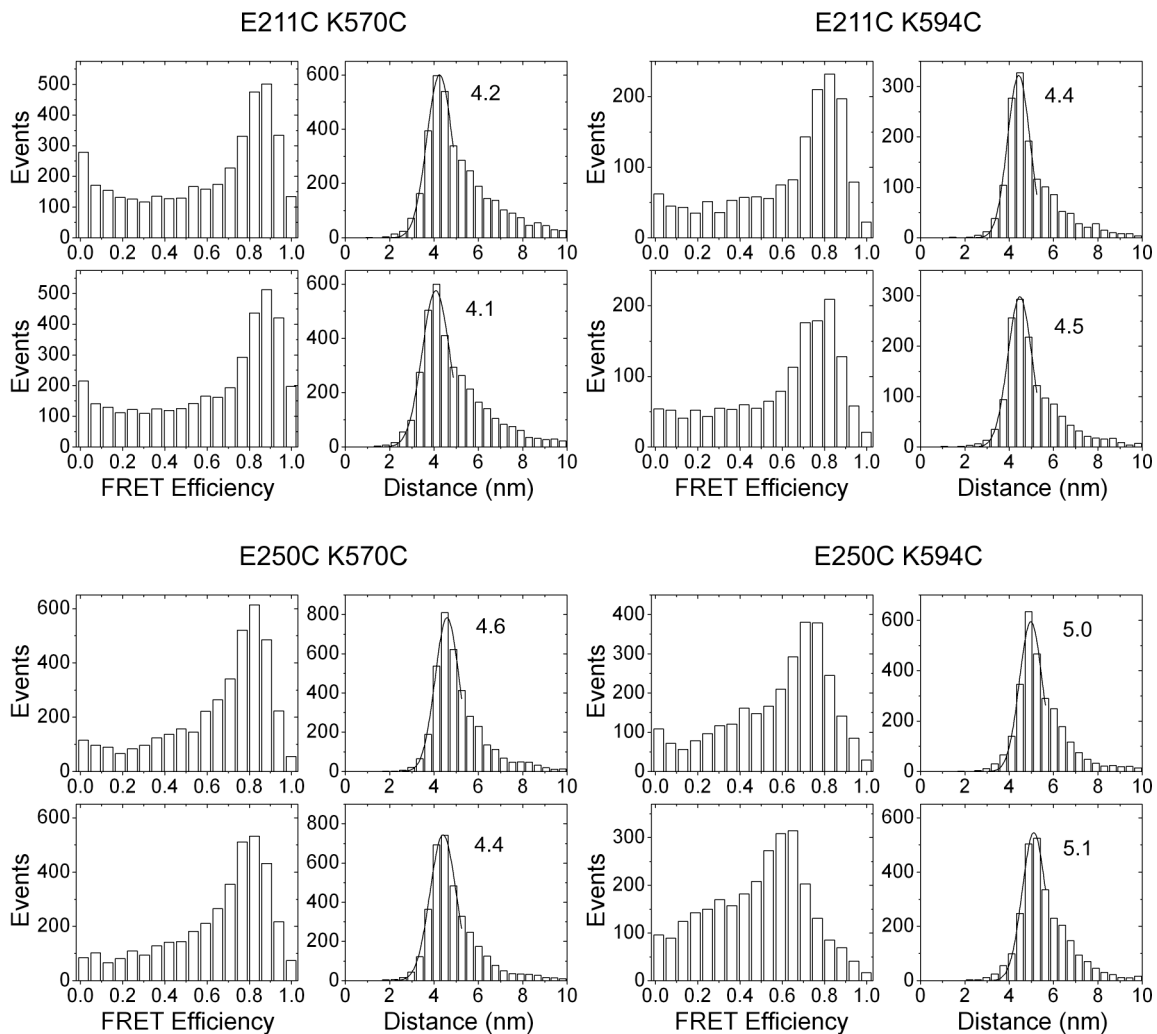
**Fig. 3.17:** SmFRET efficiency and distance histograms for ligand-free GyrA in hetero-dimeric GyrA constructs labeled in the tower domain (E211C or E250C) and on the CTD (K570C or K594C) of one subunit. Sections left (top to bottom): FRET efficiency and distance histograms for mutants E211C_K570C and E250C_K570C, exhibiting uni-modal distributions with FRET efficiency maxima between 0.8 and 0.9. Corresponding inter-dye distances were calculated by Gaussian fitting of the distance histograms, yielding values of 4.2 and 4.1 nm for the first and 4.6 and 4.4 nm for the second mutant, depending on corrections applied. Sections right (top to bottom): FRET efficiency and distance histograms for mutants E211C_K594C and E250C_K594C. FRET-efficiency distributions were uni-modal with maxima at approx. 0.8 and between 0.6 and 0.75 for the two mutants, respectively. Corresponding inter-dye distances were 4.4 and 4.5 nm in E211C_K594C and 5.0 and 5.1 nm in E250C_K594C, depending on the corrections applied. For all mutants distance distributions were asymmetrically with a larger shoulder towards higher distances.

Histograms were corrected with photophysical parameters and Förster distances for the corresponding mutants, acquired in the absence of ligands, with donor and acceptor dyes attached to GyrA body and the CTD (section top rows) and *vice versa* (section bottom rows).

Two additional positions in the GyrA tower domain were considered for the localization of the CTD: T299 close to the DNA-gate and N314 at the periphery of the tower (Fig. 3.13 A). GyrA hetero-dimers containing either a T299C_K570C or a N314C_K594C double-Cys mutant subunit were labeled with A488 and A546 and subjected to single-molecule FRET measurements. Histograms were corrected using averaged photophysical parameters (Tab. 3.2).

Both mutants exhibited a high FRET efficiency, suggesting a small distance (i.e. 3 – 5 nm) between the dyes and confirming the results of GyrA proteins combining mutations E211C or E250C with K570C or K594C (Fig. 3.18).
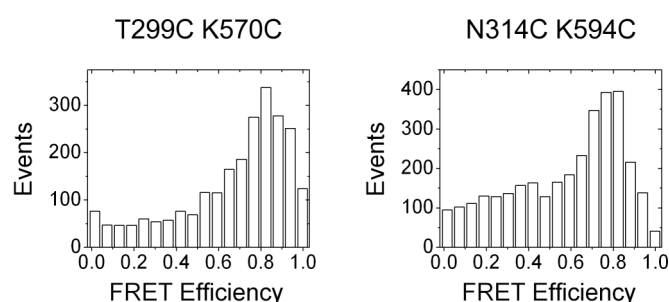


**Fig. 3.18:** SmFRET histograms for additional hetero-dimeric GyrA constructs labeled in the tower domain (T299C or N314C) and on the CTD (K570C or K594C) of one subunit. FRET efficiencies were approx. 0.8 for mutants T299C_K570C (left) and N314C_K594C.
Due to the lack of site-specific correction parameters, histograms were corrected with averaged photophysical parameters with values 0.67, 0.0104 and 3.08 for $\alpha'$, $\beta'$ and $\gamma'$, respectively.

### 3.1.17 Localization of the GyrA CTDs in the gyrase-DNA complex

It has been proposed that the CTDs adopt a different conformations in ligand-free GyrA and gyrase bound to DNA [57]. To address this problem, single-molecule measurements with GyrA in the presence of saturating concentrations of GyrB (8 μM) and neg. supercoiled pUC18 (15 nM) were performed. The same double-labeled GyrA hetero-dimers were used as for the localization of the CTDs in the absence of ligands (section 3.1.16).

FRET efficiencies and the corresponding inter-dye distances were determined using the correction parameters for GyrA in the presence of GyrB and DNA (Table 3.3). For all six arrangements of fluorescent labels, little difference was found between FRET efficiency and distance histograms calculated with two different sets of correction parameters and Förster distances (Fig. 3.19). This indicated that the arrangement of the dyes (donor on the GyrA body, acceptor on the CTD, and *vice versa*) did not significantly influence the detected FRET efficiencies and the corresponding distances. FRET efficiency histograms showed a reduction in burst number compared to measurements without plasmid DNA for the same measurement

time. This might have been due to the higher diffusion time of the labeled protein bound to the DNA causing a higher photon count per burst but a reduction of the number of labeled protein detected.

FRET efficiencies for the T140C_K570C and T140C_K594C mutants were close to 0 (Fig. 3.19), indicating an increase of the inter-dye distance in the gyrase-DNA complex compared to GyrA (Fig. 3.10). The distance histograms of T140C_K594C yielded mean inter-dye distances of 8.1 and 7.5 nm. The T140C_K570C mutant showed a minor high FRET population ($E_{FRET}$ of $> 0.8$); a double Gaussian fit of the corresponding distance histograms resulted in distances of 7.5 and 7.9 nm for the major and 4.1 and 4.4 nm for the minor populations, respectively (Fig. 3.19).

Proteins with one label in the tower domain (E211C, E250C) and on the CTD each (K570C, K594C) generally exhibited higher FRET efficiencies than proteins carrying FRET pairs involving position T140C (Fig. 3.19). Mutants E211C_K594C and E250C_K570C showed uni-modal FRET efficiency distributions at a value of approx. 0.5 and 0.7, respectively. The corresponding distances distribution were fitted with a single Gaussian, yielding mean inter-dye distances of 5.5 to 5.9 and 5.1 nm, respectively. FRET efficiencies of mutants E211C_K570C, E250C_K594C exhibited bimodal behavior. Therefore the corresponding distance distributions were fitted with a double Gaussian. The distributions for the higher distances were of broader width and larger area, signifying the main population; mean distances were 6.0 to 6.4 nm. The minor distributions showed 2.7-, 1.3- and 3.2-fold smaller integral and lower mean distances of 4.3, 4.5 and 4.8 nm for mutants T140C_K570C, E211C_K570C and E250C_K594C, respectively (Fig. 3.19). The meaning of the bi-modal behavior of the distance distributions could not be elucidated but will be discussed in section 4.1.3.

Taken together, for all dye arrangements an increase in FRET efficiency could be observed upon formation of the gyrase-DNA complex, indicating higher inter-dye distances and thus a higher distance between the CTD and the GyrA body than in ligand-free GyrA. In a next step, distance information from six different dye arrangements was used for the localization of the CTD with respect to the GyrA body. For this purpose, the maxima of distributions with the higher integral were considered (Table 3.5).
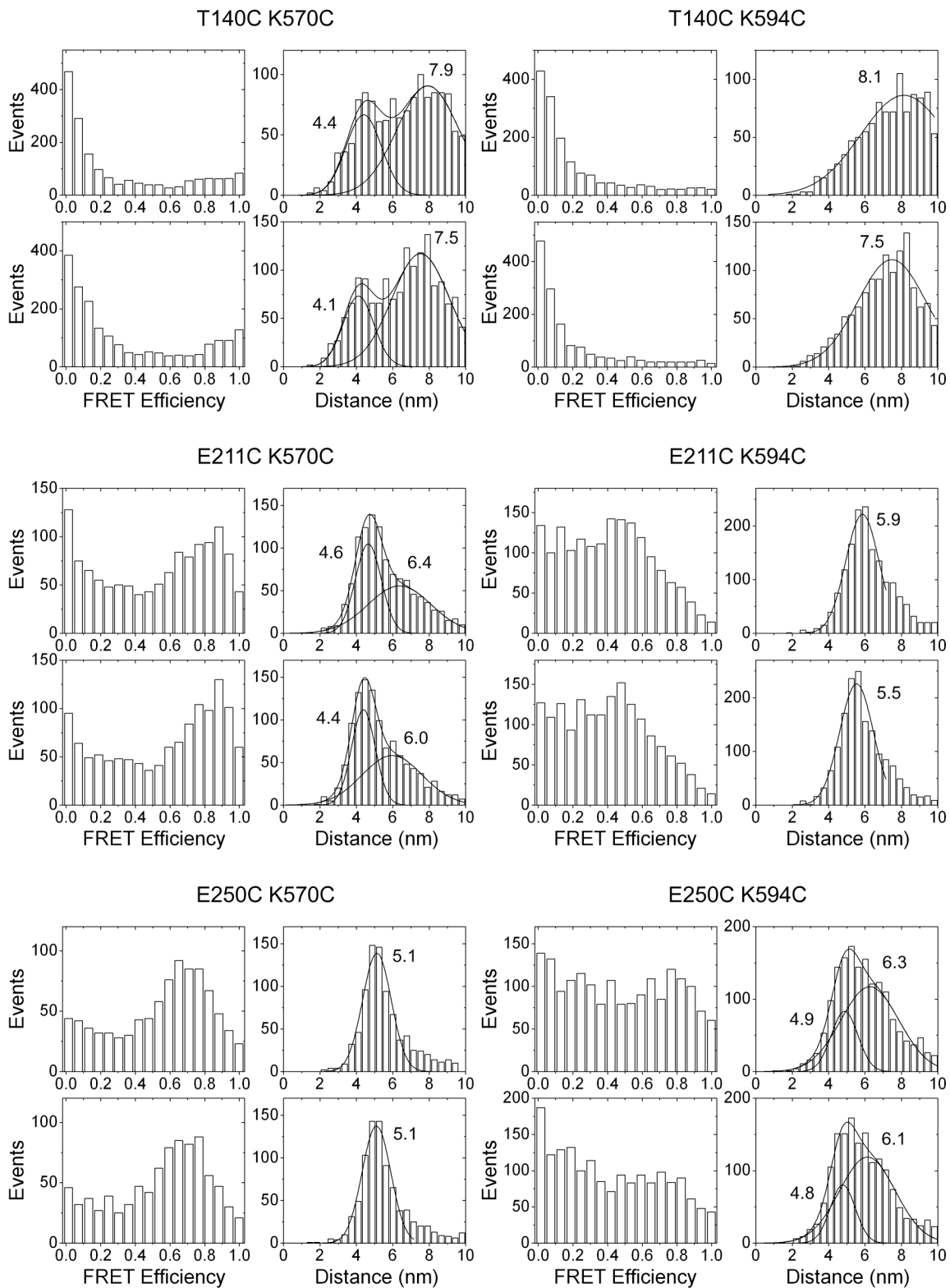
**Fig. 3.19:** SmFRET efficiency and distance histograms for gyrase in the presence of neg. supercoiled plasmid, using hetero-dimeric GyrA constructs labeled on the GyrA body (T140C, E211C or E250C) and on the CTD (K570C or K594C) of one subunit. Double mutants are denominated in the section heads. FRET efficiency histograms for mutants T140C_K570C, E211C_K570C and E250C_K594C exhibited two populations; thus corresponding distance histograms were fitted with double Gaussians. Distributions with maxima at higher distances exhibited the larger integrals and were considered to be the main distributions. Minor distributions exhibited maxima at between 4.1 and 4.9 nm.
Continued on following page.

Double mutants labeled at the DNA-gate (T140C) generally showed very low FRET efficiencies (approx. 0) and higher inter-dye distances (7.5 – 8.1 nm) than mutants labeled in the tower domain (E211C, E250C) with inter-dye distances (maxima of major distributions) between 5.1 and 6.4 nm. Calculated values are listed in table 3.5.

Histograms were corrected with photophysical parameters and Förster distances for the corresponding mutants, acquired in the presence of DNA and GyrB, with donor and acceptor dyes attached to GyrA body and the CTD (section top rows) and *vice versa* (section bottom rows).

### 3.1.18 Quantification of the conformational change in the CTDs upon formation of the gyrase-DNA complex

A study employing small-angle X-ray diffraction elucidated a first full-length structure of GyrA in complex with GyrB and a linear DNA fragment of 140bp length [58]. The position determined for the CTD was close to the C-gate, below the proposed exit site of the T-DNA segment [95]. The present study localized the CTD in ligand-free GyrA and gyrase in complex with neg. supercoiled plasmid DNA by means of single-molecule FRET data described above. FRET data from a pair of labeling positions were corrected for either dye arrangement, yielding two inter-dye distances per FRET pair: This averaged distance was used for triangulation (Tables 3.4 and 3.5). The distance between positions on the GyrA body (T140C, E211C, and E250C) and on the CTD (K570C and K594C) increased for all FRET pairs from the free to the complexed GyrA, indicating a movement of the CTD.

**Table 3.4:** Calculated inter-dye distances in ligand-free GyrA, corrected for dye arrangements with donor on the GyrA body and acceptor on the CTD (top row) and *vice versa* (middle row). Averaged distances used for triangulations of CTD positions are listed in the bottom row. Distances are given in nm.

| GyrA body mutation | T140C | | E211C | | E250C | |
|---|---|---|---|---|---|---|
| GyrA CTD mutation | K570C | K594C | K570C | K594C | K570C | K594C |
| D: body ; A: CTD | 6.29 | 5.58 | 4.25 | 4.43 | 4.59 | 4.97 |
| A: CTD; D: body | 5.57 | 5.26 | 4.08 | 4.48 | 4.41 | 5.11 |
| **Average distance** | **5.93** | **5.42** | **4.16** | **4.45** | **4.50** | **5.04** |

**Table 3.5:** Calculated inter-dye distances for gyrase in complex with neg. supercoiled plasmid, corrected for dye arrangements with donor on the GyrA body and acceptor on the CTD (top row) and *vice versa* (middle row). Averaged distances used for triangulations of CTD positions are listed in the bottom row. Distances are given in nm.

| GyrA body mutation | T140C | | E211C | | E250C | |
|---|---|---|---|---|---|---|
| **GyrA CTD mutation** | **K570C** | **K594C** | **K570C** | **K594C** | **K570C** | **K594C** |
| D: body ; A: CTD | 7.93 | 8.14 | 6.38 | 5.85 | 5.13 | 6.26 |
| A: CTD; D: body | 7.53 | 7.47 | 5.97 | 5.53 | 5.10 | 6.13 |
| **Average distance** | **7.73** | **7.81** | **6.17** | **5.69** | **5.11** | **6.19** |

The position of mutated residues K570C and K594C on the CTD were triangulated using average inter-dye distances. Due to the lack of information about the position of the fluorescent labels relative to the protein, the center of the dyes were assumed to collocate with the thiols of the labeled cysteine residues. Triangulation was done manually, with adjusted distances not deviating more than 0.05 nm with respect to calculated values.

Structural models including the calculated positions of amino acid residues K570C and K594C are depicted in figure 3.20, both for the situations in ligand-free GyrA and in gyrase bound to DNA. Distance changes between the two situations were approx. 2.6 and 2.5 nm for K570C and K594C, respectively. The distance between these two positions as measured from the model were 1.2 and 2.8 nm in the ligand-free GyrA and in gyrase bound to DNA, respectively. These data clearly document for the first time a conformational change of the GyrA CTDs when GyrA binds to GyrB and DNA, supporting previous suggestions [57].
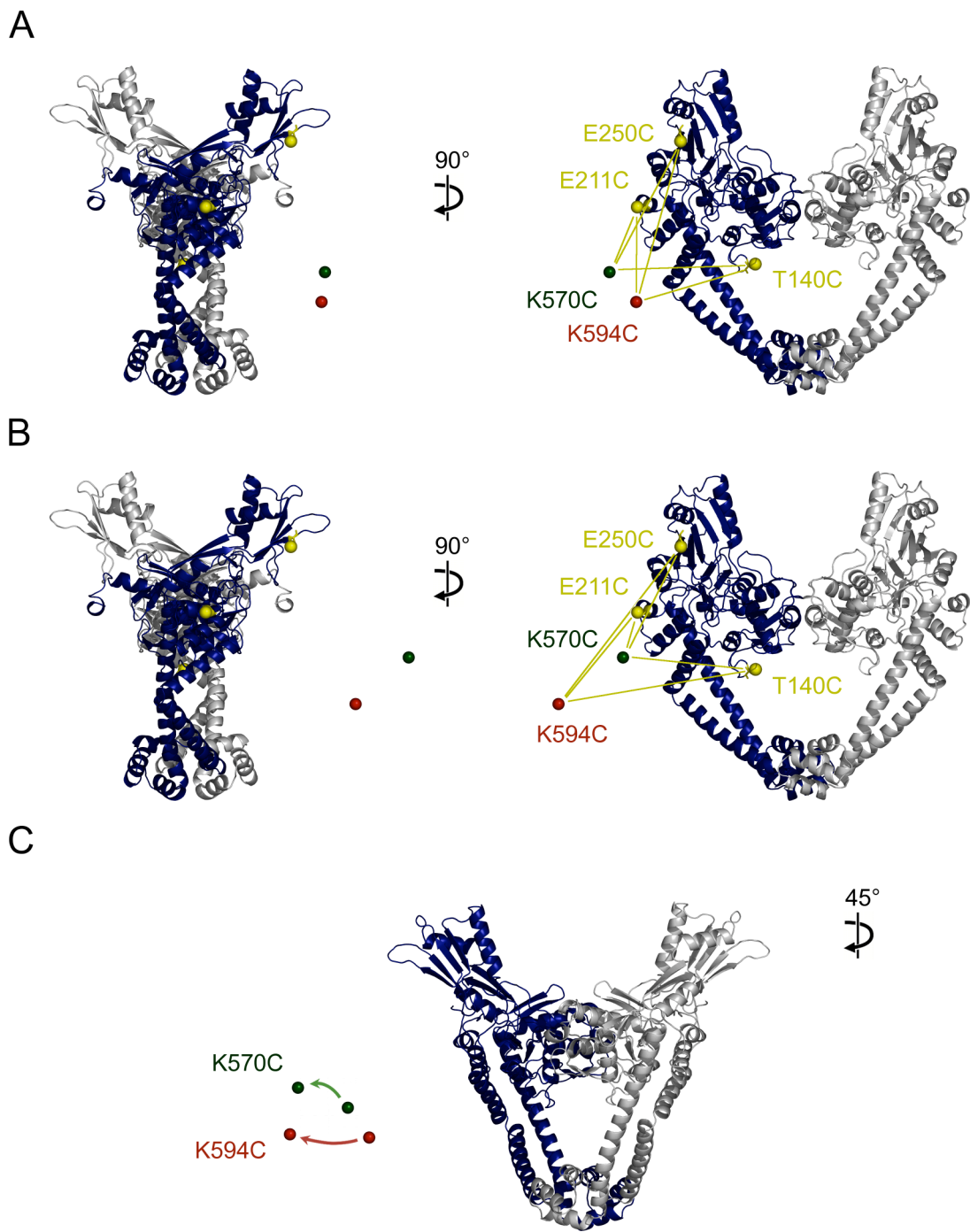
**Fig. 3.20:** Homology models of the dimeric GyrA body from *B. subtilis* with calculate positions of mutated residues K570C and K594C located on the CTD. Residues on the GyrA body used for triangulation are depicted in yellow, CTD residue position are depicted in green (K570C) and red spheres (K594C).
**A:** Side (left) and front (right) view of GyrA body with CTD positions triangulated for the situation in ligand-free GyrA, using averaged inter-dye distances for each FRET pair.
**B:** Side (left) and front (right) view of GyrA body with CTD positions in the gyrase-DNA complex, using averaged inter-dye distances.
**C:** 45°-rotated view of GyrA with CTD positions indicated for situations in free GyrA (arrow starts) and in the gyrase-DNA complex (arrow ends). Both positions move away from the body domain upon complex formation, indicating a movement of the CTD from a rather contracted to an extended conformation.

### 3.1.19 Domain localization from other FRET pairs

The previous sections documented the localization of the upper region of the GyrA CTD with respect to the DNA-gate and tower regions of the enzyme body, both in the free GyrA dimer and in the complex of GyrA, GyrB and DNA. Additional FRET mutants were used to determine the CTD position with respect to the C-gate and to localize the lower part of the CTD. None of the cysteine mutations mentioned in this section affected the supercoiling activity of gyrase. Correction parameters and Förster distances were not determined for these labeling positions; instead FRET efficiencies were corrected using averaged parameters (Table 3.2). Distances between labels were not determined.

The FRET histogram of a hetero-dimeric GyrA with one subunit labeled at the C-gate (N399C) and on blade 2 of the CTD (K594C) shows a FRET efficiencies of approx. 0.1 for the ligand-free protein (Fig. 3.21A), indicating an inter-dye distance of approx. 8 nm, which corresponds well with the distance of 7.8 nm calculated for the FRET model. Upon addition of GyrB and DNA (for this measurement relaxed pUC18 was used), the FRET efficiency maximum dropped to approx. 0 with the shape of the main distribution remaining similar, suggesting an increase of the inter-dye distance, which is in agreement with the model (approx. 10 nm).

The lower part of the CTD was tracked by combined labeling of positions 695 or 726 on the CTD and the DNA- (T140C) and C-gate (T408C). The FRET efficiency of T408C_D695C and T408C_E726C were close to 0 with considerable shoulders towards higher values, indicating a high mean distance of more than 8 nm with potentially high local fluctuations (Fig. 3.21A – 3.21B). For mutant T408C_D695C in complex with GyrB and DNA, the FRET efficiency remained high, thus change of the inter-dye distance be detected.

A GyrA mutant carrying labels on positions T140 (DNA-gate) and C695 (CTD) did not show a well-defined FRET-efficiency distribution (Fig. 3.21A). In the presence of GyrB and supercoiled pUC18 DNA, the distribution slightly shifted to higher FRET-efficiency values, but remained broad. Due to the non-linear scaling of FRET efficiency and corresponding inter-dye distance (Eq. 2.24), the latter was expected to be distributed around medium values, i.e. around the Förster distance (approx. 5.5 nm for this dye pair), both in the absence and presence of ligands. Experiments were reproducible, and the broad distributions should be trusted. These results and the ones obtained for the mutant T408C_D695C (see above) suggest a position of the CTD lateral to the GyrA body, closer to the DNA-gate than the C-gate. They also indicated that the distant part of the CTD is more flexible with respect to GyrA body than the upper part linked to the body.

The main FRET efficiencies for the single-cysteine mutants K594C, D695C, E726C were close to 0 in the presence of GyrB and neg. supercoiled plasmid (Fig. 3. 21C and 3.22). For mutants K594C and E726C this marked a decrease in FRET efficiency of 0.2 and 0.1 compared to the ones in ligand-free GyrA (Fig. 3.15), respectively, indicating an increase of the inter-dye distance between labels on both CTDs. The width of the FRET efficiency distributions both in GyrA and in the gyrase-DNA complex, exhibiting shoulders up to medium FRET values, suggested fluctuation of the inter-dye distance and thus increased local flexibility of the distant end of the CTDs.
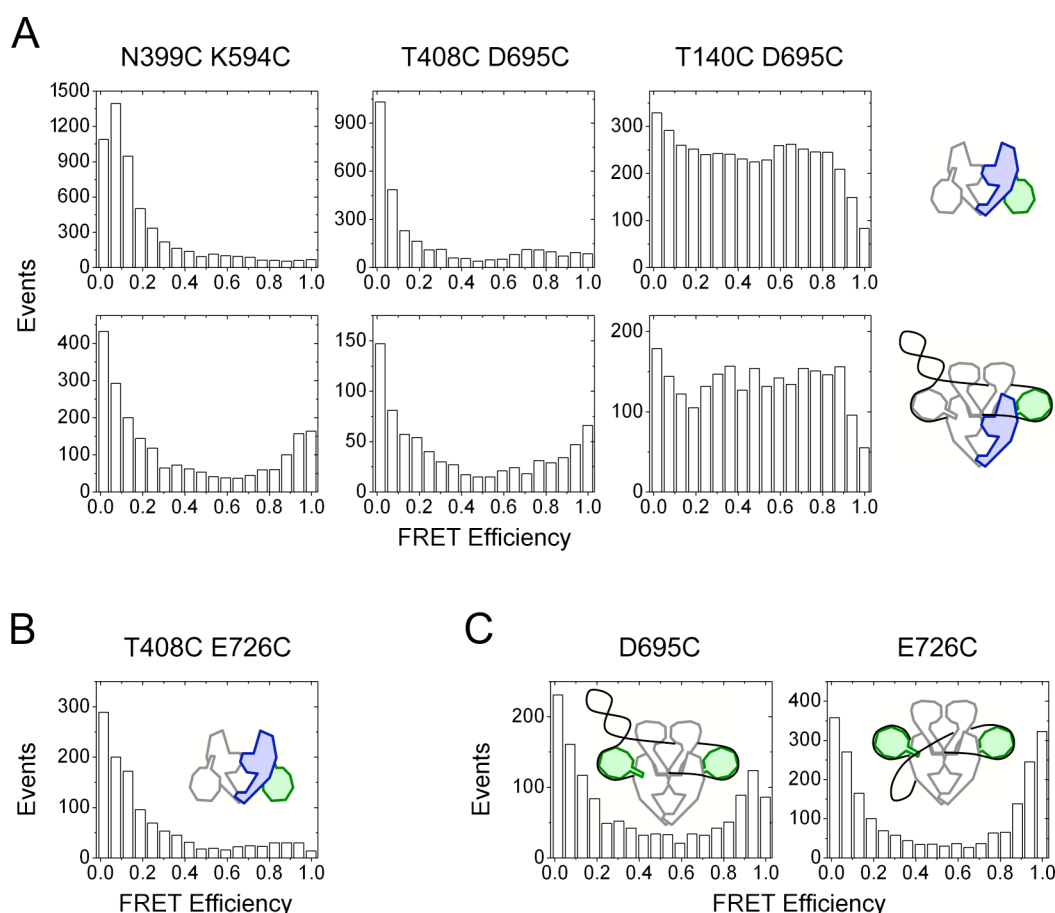


**Fig. 3.21:** SmFRET efficiency histograms for different FRET constructs, in free GyrA and gyrase bound to neg. supercoiled DNA.
**A:** FRET efficiency histograms for hetero-dimeric GyrA proteins with one double-cysteine mutant subunit (from left to right): N399C_K594C, T408C_D695C, and T140C_D695C. Top: for ligand-free GyrA; bottom: for the gyrase-DNA complex. FRET efficiencies were very low for the first two constructs labeled on the C-gate and the N-terminal or the distant end of the CTD, respectively, with a small decrease in FRET efficiency upon complex formation for the first and a small increase for the second. The third construct labeled at the DNA-gate and on the distant end of the CTD exhibited a very broad FRET efficiency distribution, indicating high local flexibility of the lower CTD. The distribution was shifted to slightly higher values in the gyrase-DNA complex. The first two mutants showed high-FRET populations in the gyrase-DNA complex.
Continued on following page.

**B:** SmFRET histogram for a hetero-dimeric GyrA construct labeled at positions 408 (C-gate) and 726 (distant CTD end), exhibiting a value close to 0, indicating a large inter-dye distance.

**C:** FRET efficiency distributions of single-cysteine mutants D695C and E726C (both labeled on equivalent positions at the distant ends of each CTD) in the gyrase-DNA complex. FRET efficiencies were close to 0, with high-FRET populations of different intensities for both mutants.

FRET data for hetero-dimeric GyrA proteins were corrected with averaged photophysical parameters (0.67, 0.0104 and 3.08 for $\alpha$', $\beta$' and $\gamma$', respectively). SmFRET histograms for homo-dimeric proteins were corrected with parameters obtained for corresponding mutants in the absence of ligands.

### 3.1.20 CTD conformations during complex assembly

As demonstrated in the previous sections, the CTD is located laterally with respect to the GyrA-body dimer and describes a movement to a more extended conformation when gyrase is complexed with supercoiled DNA. In order to understand the conformational changes during the assembly of the complex, single-molecule measurements in the presence of individual ligands were performed with hetero-dimeric GyrA constructs containing either a T140C_K594C or a T140C_K570C subunit, and with the homo-dimeric single-cysteine mutant K594C. Experiments with the latter protein were performed at room temperature and should be compared to all other measurements only qualitatively (performed at 37°C).

Complexation of GyrA by different ligands was monitored qualitatively by following changes in the autocorrelation of the donor fluorescence signal (Fig. 3.23A): Fluorescently labeled GyrA and its complex with GyrB exhibited dwell times of approx. 1 ms (corresponding to the inflection point of the autocorrelation curve). Addition of plasmid DNA to GyrA in the absence or presence of GyrB resulted in a 10-fold increase in diffusion time; this indicated a drastic increase in molecular weight of the complex bearing the labeled species, consistent with the expected binding of the plasmid. Nucleotide addition to GyrA in complex with GyrB and plasmid DNA resulted in a slightly flattened autocorrelation curve, but not in a change of diffusion time, indicating that the gyrase-DNA complex remains intact.

### 3.1.21 Effect of GyrB on the GyrA CTD position

Having documented the conformational change of the GyrA CTDs from free GyrA to the gyrase-DNA complex, contributions of the individual complexation partners needed to be determined. First, the influence of GyrB binding on the conformation of the GyrA CTD was tested.

GyrB binds weakly to the GyrA dimer; a $K_d$ was not published so far. Addition of 8 µM GyrB induced a shift to lower FRET efficiencies in the following three observation systems: In the

homo-dimeric mutant (K594C) the distribution maximum decreased from 0.2 to 0.1, while the peak width increased. In the hetero-dimeric proteins the FRET efficiency decreased from 0.5 to 0.2 for the T140C_K594C mutant and from 0.3 to almost 0 for T140C_K570C. In T140C_K594C increasing the GyrB concentration to 20 µM did not result in a change of FRET efficiency or distribution shape, indicating saturation of both binding sites for GyrB at the DNA-gate using 8 µM GyrB (Fig. 3.22B).

The combination of data from different mutants suggests that the change in FRET efficiencies was not caused by changes in the photophysical behavior of the labels, since the shifts were observed with substitution of all individual labeling positions. Thus, the change in energy transfer should originate from a conformational change in the CTDs. This finding was surprising, as there had not been any report of an interaction between GyrB and the CTDs. However, from this data alone the cause for the conformational change in the CTDs could not be explained.

### 3.1.22  Complexation of DNA by GyrA induces conformational freedom to the CTDs

Next, the influence of DNA on the CTD conformation in the absence of GyrB was tested, using 20 nM supercoiled pUC18 plasmid. Less events per time were detected than in measurements with GyrA and gyrase due to slower diffusion time.

FRET efficiency distributions of hetero-dimeric constructs T140C_K594C and T140C_K570C as well as of homo-dimeric mutant K594C were clearly different from the ones in the free GyrA dimer and in the presence of DNA and GyrB, indicating a conformational change in the CTDs upon subsequent additions of DNA and GyrB (Fig. 3.22C). All histograms showed broadened distributions compared to GyrA, indicating increased flexibility of the CTDs or conformational heterogeneity. For mutant T140C_K594C, the FRET efficiency exhibited bimodal behavior, with the high-FRET shoulder at a value of 0.6, corresponding to the distribution for free GyrA, and the low-FRET side closer to the FRET value for GyrA in complex with GyrB and supercoiled plasmid DNA. Thermodynamic population of the DNA-free state could be excluded, as increasing the DNA concentration by 5-fold to 100 nM did not influence the FRET distributions, i.e. the population of the two states. Kinetic characterization of the system was not possible, as the interconversion of the two states was a rare (i.e. not statistically relevant) event as judged from analysis of FRET traces of individual events.

These results show that addition of neg. supercoiled plasmid to GyrA causes conformational flexibility in the CTDs. it is also clear, that presence of DNA alone is not sufficient to introduce the extended CTD conformation.
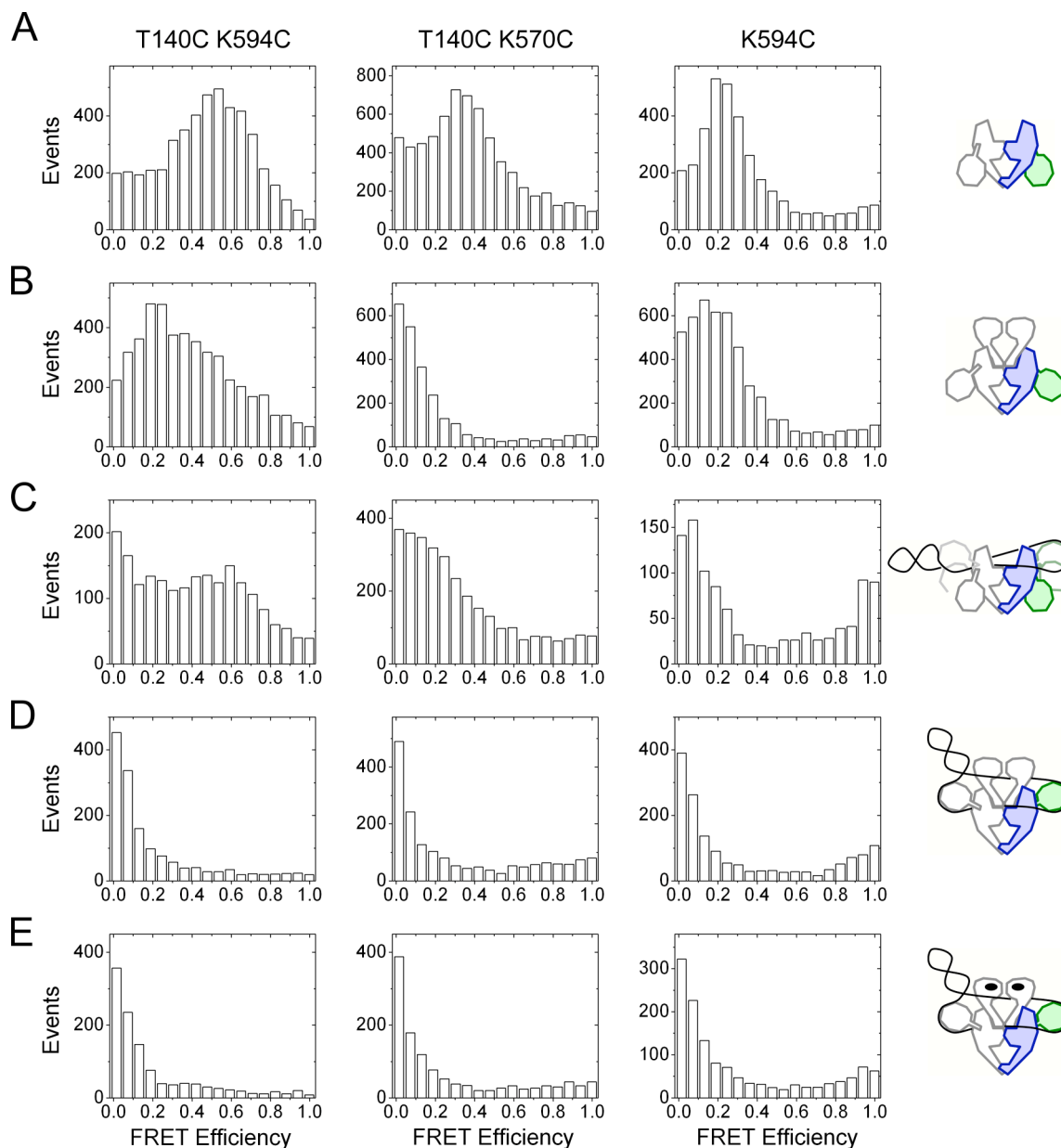


**Fig. 3.22:** SmFRET histograms of the gyrase-DNA complex formation for GyrA mutants with different dye attachment sites (from left to right): Hetero-dimeric GyrA double cysteine mutants T140C_K594C and T140C_K570C, homo-dimeric single cysteine mutant K594C.
**A:** Histograms for ligand-free GyrA.
**B:** Histograms for GyrA in complex with GyrB (i.e. gyrase).
**C:** Histograms for GyrA in complex with neg. supercoiled plasmid.
**D:** Gyrase in complex with neg. supercoiled plasmid.
**E:** Histograms for complex D with ADPNP added.
Continued on following page.

All three mutants exhibited FRET efficiencies between 0.2 and 0.5 for free GyrA. Formation of gyrase (upon addition of GyrB) reduced the FRET efficiency for all constructs. Addition of neg. supercoiled plasmid to GyrA resulted in a broadening of the FRET efficiency distributions (in the case of T140C_K594C to bi-modality with contributions of FRET 0.6 and approx. 0), indicating conformational flexibility in the CTDs. The gyrase-DNA complex showed FRET efficiencies of 0 in all mutants, corresponding to the extended conformation established above (Fig. 3.19, 20). Addition of ADPNP, a non-hydrolysable ATP-analogue, did not result in further FRET efficiency changes.

FRET data for double cysteine mutants T140C_K570C and T140C_K594C were corrected with averaged photophysical parameters for corresponding mutants acquired in the absence (A; C) and presence (B; D; E) of DNA and GyrB. FRET efficiencies for the single cysteine mutant K594C were corrected with parameters acquired in the absence of ligands.

Cartoons represent the GyrA dimer with one subunit in blue (GyrA body) and green (CTD) and the other in grey. GyrB subunits, neg. supercoiled DNA and ADPNP are shown in white, by a black line and black ellipses.

### 3.1.23 Addition of ADPNP to the gyrase-DNA complex does not induce further conformational changes

The addition of ADPNP to a GyrA_GyrB fusion construct has been shown to induce dimerization of the nucleotide domains of GyrB (N-gate) and a pre-closure in the presence of plasmid DNA [42]. Here, we tested the influence of a partially closed N-gate on the conformation of the GyrA CTDs.

Addition of 2 mM ADPNP to GyrA and GyrB in complex with supercoiled plasmid DNA resulted in FRET efficiency distribution similar to the gyrase-DNA complex, indicating no major conformational change of the CTDs (Fig. 3.22D – E). For both hetero-dimeric GyrA FRET systems and the homo-dimeric GyrA mutant the FRET efficiencies remained close to 0 as it was the case in the absence of nucleotide. A rapid change in FRET efficiency due to a conformational change connected to potential strand passage was not observed in traces of single-molecule events.

This data suggests that partial closure of the ATPase gate does not influence the CTD conformation. A potential movement of the CTDs upon strand passage might be to fast to be detected in single-molecule studies using a confocal microscope.

### 3.1.24 GyrA-ligand complex formation does not depend on the order of ligand addition

For the GyrA-GyrB fusion protein it had been shown that dimerization of the nucleotide-binding domains, i.e. the closure of the N-gate, impedes binding of a DNA to the DNA-gate [42]. To simulate this situation in the gyrase hetero-tetramer supercoiled plasmid was added

to gyrase pre-saturated with ADPNP. The FRET system used was a hetero-dimeric GyrA mutant with one subunit labeled at positions 140 (DNA-gate) and 570 (CTD).

In gyrase saturated with ADPNP the FRET efficiency dropped to approx. 0.1 (Fig. 3.23B), compared to the value of approx. 0.35 for GyrA (Fig. 3.22A). The shape of the distribution is similar to the one in GyrA bound to GyrB (Fig. 3.22B). Addition of DNA reduced the FRET efficiency to 0, indicating binding of the DNA and concomitant movement of the CTDs. This finding was supported by the increase of the diffusion time (as judged from the autocorrelation data (Fig. 3.23B) and the decrease of the number of burst within similar exposure time, which was both due to the increase in MW of upon binding of plasmid to the gyrase.

As the sequence of ligand addition did not influence the conformation of the CTDs, the resulting complex should not depend on the order of ligand addition. This finding indicated that gyrase is a dynamic complex. Even the potential stabilization of gyrase with the non-hydrolysable nucleotide ADPNP did not inhibit the formation of the gyrase-DNA complex.
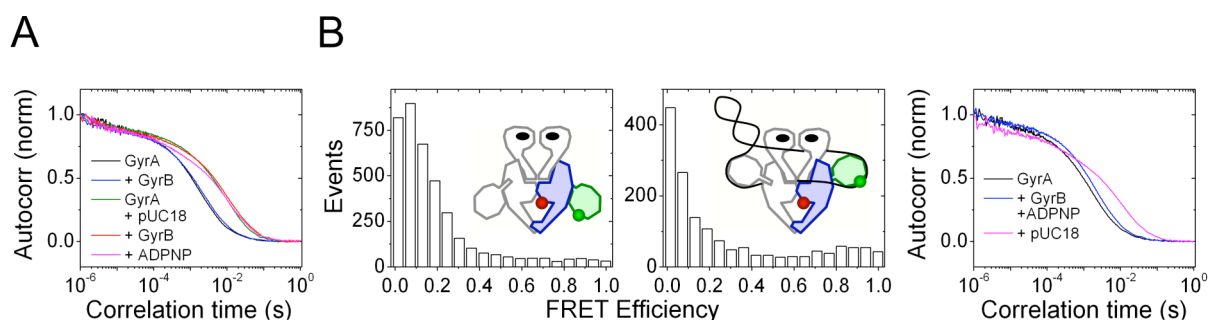


**Fig. 3.23:** Autocorrelation curves and reverse order smFRET measurements for gyrase-DNA complex assembly, using GyrA mutant T140C_K570C.
**A:** Autocorrelation curve for the donor fluorescence signal from measurements involving GyrA (black), gyrase (blue), GyrA in complex with neg. supercoiled plasmid (green), with GyrB (red) and ADPNP added (pink). GyrA and gyrase exhibited a similar diffusion time (corresponding to the inflection point at approx. $10^{-3}$ s), while all complexes with DNA showed a 10-fold higher diffusion time (approx. $10^{-2}$ s).
**B:** (from left to right): SmFRET histograms for gyrase in the presence of ADPNP; with neg. supercoiled plasmid added; autocorrelation curves of the donor fluorescence signal for both measurements (blue and pink, respectively), compared to the one for ligand-free GyrA. The FRET efficiency for gyrase in the presence of ADPNP showed a peak at approx. 0.1, similar to the one for gyrase in the absence of nucleotide (Fig. 3.22B); the FRET efficiency was further reduced by the addition of plasmid. Plasmid complex formation was monitored with FCS, exhibiting a higher diffusion time than gyrase in the presence of ADPNP. FRET data were corrected with averaged photophysical parameters determined for the mutant T140C_K570C in the absence (B: left) and presence of DNA and GyrB (B: middle).
Cartoons represent the GyrA dimer with one subunit in blue (GyrA body) and green (CTD) and the other in grey. GyrB subunits, neg. supercoiled DNA and ADPNP are shown in white, by a black line and black ellipses. Red and green dots represent the fluorescent dyes.

### 3.1.25 Relaxed and pos. supercoiled DNA induce similar conformational changes

Single molecule data shown so far were obtained using neg. supercoiled plasmid DNA, which is the product of the supercoiling reaction by gyrase [96]. The influence of the reaction substrate, i.e. relaxed plasmid DNA, on the CTD conformation should be also elucidated.

The FRET histogram for hetero-dimeric GyrA bearing the mutant subunit T140C_K594C supplied with 20 nM relaxed pUC18 exhibited a broad bi- or tri-modal distribution. Both the maxima at 0.65 and 0 FRET efficiencies were similar to the ones found in the histogram for GyrA in complex with neg. supercoiled plasmid (Fig. 3.24A; compared to Fig. 3.22C). A third small maximum is observed at 0.3, which could be due to insufficient data statistics. Due to high fluorescent background originating from low DNA quality and concentration, the number of events recorded was approx. 3-fold lower than in measurements of similar duration involving supercoiled plasmid.

The addition of 8 μM GyrB resulted in a sharp decrease in FRET efficiency close to 0, with a shoulder towards higher values, as seen for gyrase bound to neg. supercoiled plasmid. The distance histograms for data calculated with the averaged set of site-specific correction parameters and Förster distance exhibited a bimodal distribution (Fig. 3.24B), similar to histograms of experiments involving GyrA in complex with neg. supercoiled plasmid DNA. Integrals for the two maxima were not determined due to the low number of detected events. The peak corresponding to the low-FRET species showed an averaged inter-dye distance of approx. 8.0 nm, which was in agreement with the results for GyrA bound to neg. supercoiled plasmid DNA. The second distribution probably corresponded to the medium FRET efficiency shoulder, the origin of which could not be explained so far.

Addition of ADPNP to gyrase in complex with relaxed plasmid did not influence the FRET-efficiency distribution, with the maximum remaining close to 0 (Fig. 3.24C).

The results suggest that binding of GyrA to relaxed and neg. supercoiled plasmid DNA of the same nucleotide sequence, i.e. educt and product of the supercoiling reaction, induce similar conformational change in the CTD; this indicates no or a very low dependence on the topology of the DNA ligand.
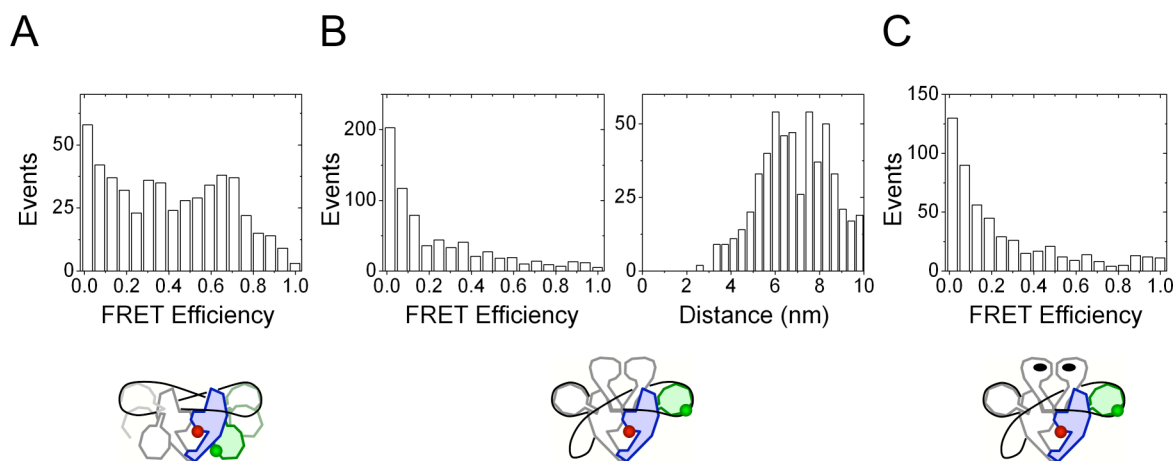
**Fig. 3.24:** SmFRET and distance histograms for complexes of relaxed plasmid DNA with the GyrA mutant T140C_K594C.
**A:** GyrA in the presence of relaxed DNA.
**B:** FRET and corresponding distance histograms of gyrase in the presence of relaxed DNA.
**C:** B with ADPNP added.
GyrA in complex with relaxed DNA exhibits a bi-modal FRET-efficiency distribution. The higher-FRET species disappeared completely upon addition of GyrB, indicating the CTDs swinging away from the GyrA body; addition of ADPNP did not further influence the histogram. All histograms resemble closely the ones for complexes with neg. supercoiled plasmid (Fig. 3.22C – E). FRET data were corrected with averaged photophysical parameters for mutant T140C_K594C acquired in the absence (A) and presence of DNA and GyrB (B, C).
Cartoons represent the GyrA dimer with one subunit in blue (GyrA body) and green (CTD) and the other in grey. GyrB subunits, relaxed DNA and ADPNP are shown in white, by a black line and black ellipses. Red and green dots represent the fluorescent dyes.

### 3.1.26 Linear DNA ligands induce CTD movement depending on DNA length

The previous sections documented the conformational change of GyrA CTD into an extended position in gyrase bound to plasmid of different topology (relaxed or neg. supercoiled). By employing non-modified DNA fragments of 37 to 110 base-pairs (bp) in length we wanted to elucidate whether the CTD movement could likewise be induced by linear oligonucleotides. Measurements were performed in the presence of GyrB, with concentrations of 2 μM for the 37bp or 48bp DNAs and 500 nM for the 60bp, 90bp or 110bp DNAs. This ensured that more than 75 and 90% of the protein molecules were saturated with 37bp DNA and DNAs of ≥48bp length, respectively (section 3.1.9).

For hetero-dimeric GyrA labeled at amino-acids 140 (DNA-gate) and 594 (CTD) complexes with DNA ligands of ≥48bp length the FRET efficiency dropped from 0.5 for the ligand-free protein (Fig. 3.22A) to close to 0 (Fig. 3.25B). This value corresponds to the one found for gyrase in complex with plasmid, indicating that linear DNAs of ≥48bp were sufficient to

promote CTD movement to an extended conformation. At least for the shorter DNAs of 48 and 60 bp in length this finding was surprising as the number of contacts between the DNA molecule and the CTD should be reduced compared to the ones in complexes with longer DNAs.

In contrast to results involving longer DNA ligands, the FRET efficiency distribution for the complex of gyrase and a 37bp DNA fragment yielded a maximum at approx. 0.4. (Fig. 3.25A). This finding is indicative for a conformation different from the ones found in ligand-free GyrA, in gyrase and in gyrase complexed with plasmid or longer linear DNA, characterized by FRET efficiencies of approx. 0.5, 0.25 and close to 0, respectively (Fig. 3.22A – C; Fig. 3.25B). The FRET efficiency value for the gyrase-37bp DNA complex indicated a CTD position between those found in GyrA and gyrase. Due to the high fluorescence background of the 37bp DNA stock solution and the concomitant increase in fluorescence noise, the burst number was reduced compared to experiments with 48bp DNA of the same concentration and the same exposure time. Measurements with different batches of 37bp DNA could not increase the quality of the data, but the FRET efficiency distribution was reproducible.
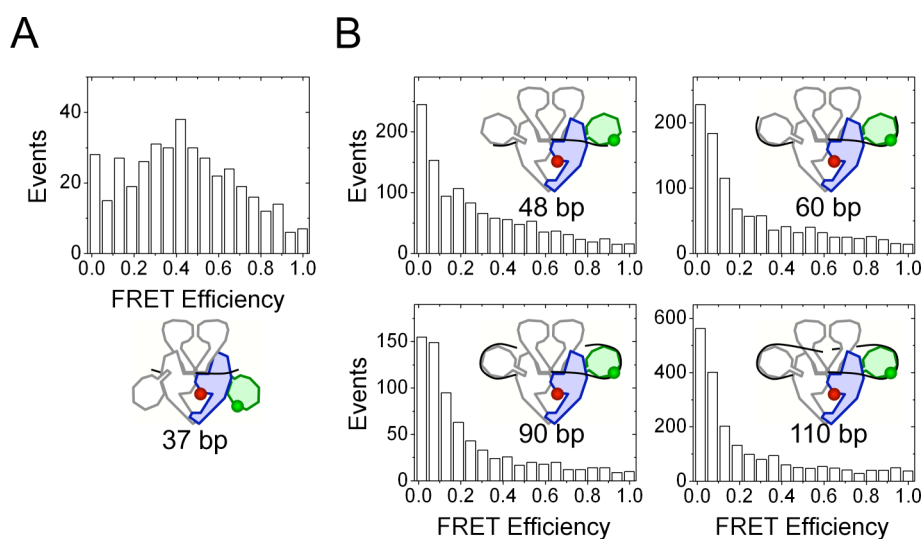


**Fig. 3.25:** SmFRET histograms for gyrase in complex with linear DNA ligands of different length, using the GyrA double mutant T140C_K594C.
**A:** Gyrase in complex with 37bp DNA. The FRET efficiency maximum was at 0.4, indicating a CTD position between those in GyrA and the one in gyrase.
**B:** Gyrase in complex with 48bp (top left), 60bp (top right), 90bp (bottom left), and 110bp DNAs (bottom right). For all complexes with DNA of 48bp and more, the FRET efficiency was approx. 0, indicating that the CTDs adopted the extended conformation.
FRET data were corrected with averaged photophysical parameters for mutant T140C_K594C acquired in the presence of DNA and GyrB.
Cartoons represent the GyrA dimer with one subunit in blue (GyrA body) and green (CTD) and the other in grey. GyrB subunits and linear DNAs are shown in white and by a black lines. Red and green dots represent the fluorescent dyes.

### 3.1.27 Conformational change of the CTDs in the cleavage-deficient mutant Y123F

DNA bound to the DNA gate of gyrase adopts a distorted conformation; the degree of distortion depends on DNA cleavage by the catalytic Tyr residues located at the GyrA dimerization interface [33]. As the CTDs bind the DNA which protrudes from the DNA-gate, it is reasonable to assume that distortion of the DNA might influence the CTD position. Thus, we tested whether the degree of distortion influences the CTD affinity for DNA and the CTD conformational upon complex formation by using the DNA-cleavage deficient GyrA mutant Y123F.

*B. subtilis* GyrA_Y123F had been purified ahead of this work and shown to be deficient in DNA cleavage, plasmid DNA relaxation and supercoiling [33]. The DNA affinity of the mutant was determined in fluorescence anisotropy titrations using a 60bp DNA internally labeled with A546 (Fig. 3.7). Experiments were performed under the same conditions as described for GyrA wt (sections 2.15.1 and 3.1.6). The measured $K_d$ value for GyrA_Y123F was $1.5 \pm 0.1$ µM. In the presence of 4 µM GyrB the $K_d$ decreased to $13 \pm 1$ nM, indicating a 100-fold increase in affinity in the presence of GyrB (Fig. 3.26A – B). The same effect was observed for GyrA wt and ΔCTD (section 3.1.8). The $K_d$ values measured for GyrA_Y123F were approx. 1.5 and 4 times smaller in the absence and the presence of GyrB, respectively, than the ones determined for the wild-type protein, indicating a higher DNA affinity with prevented DNA cleavage.

To test the influence of DNA-cleavage deficiency on CTD conformations, a hetero-dimeric GyrA*_Y123F FRET construct was produced, of which only one subunit carried the mutations T140C and K594C (GyrA*_Y123F / GyrA*_Y123F_T140C_K594C; abbreviated GyrA**_Y123F). The protein was expressed and purified as described (sections 2.10.2) yielding 8.5 mg of protein with purity similar to other hetero-dimeric GyrA constructs. Single-molecule FRET experiments were performed as described (sections 2.18).

The FRET efficiency distribution for ligand-free GyrA**_Y123F was uni-modal with a maximum between 0.5 and 0.6 (Fig. 3.26A). The shape of the distribution was very similar to wild-type like GyrA, indicating a similar CTD conformation. Addition of neg. supercoiled plasmid induced conformational flexibility to the domains, judged by the very broad FRET efficiency distribution. Again, no difference could be detected between wild-type and cleavage-deficient mutant (Fig. 3.26A and 3.22C).

Addition of GyrB to GyrA**_Y123F and DNA was accompanied by a strong drop in FRET efficiency to less than 0.1, indicative of the formation of the gyrase-DNA complex and induction of the extended conformation of the CTDs (Fig. 3.26A). As expected from previous experiments, addition of ADPNP did not further influence the FRET efficiency distribution.

Also, using a linear 60bp DNA instead of plasmid resulted in a similarly low FRET efficiency of approx. 0.1 (Fig. 3.26D). These results indicate that the CTDs adopt a similarly extended conformation in GyrA**_Y123F for all experiments involving DNA and GyrB. Compared to the GyrA mutant T140C_K594C the FRET efficiency distributions showed peaks at slightly higher values (Fig. 3.26A, compared to Fig. 3.22D – E, Fig. 3.25B); this could be an indication of a slightly different position of the CTDs in the complex of cleavage-deficient gyrase with DNA, following depopulation of the covalent DNA-tyrosyl intermediate state. Nevertheless, no major conformational differences could be detected between CTD conformations in wild-type like GyrA and the cleavage-deficient mutant.
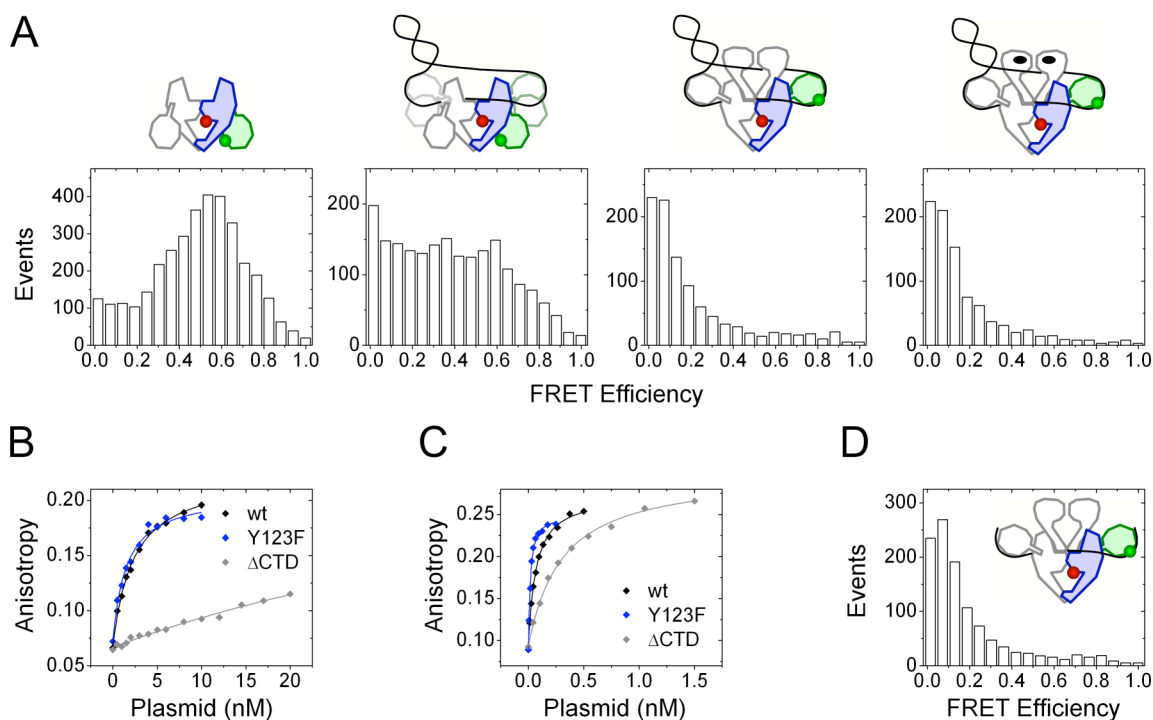


**Fig. 3.26:** SmFRET histograms and fluorescence anisotropy titrations for the cleavage-deficient GyrA mutant Y123F, with one subunit labeled at position 140 and 594.
**A (from left to right):** Histograms for measurements in the absence of ligands; in the presence of neg. supercoiled plasmid; gyrase in the presence of neg. supercoiled plasmid; with ADPNP added.
**B:** Titrations of 60bp DNA with GyrA wt (black), GyrA_Y123F (blue), and GyrA_ΔCTD (grey) with $K_d$ values of $2.3 \pm 0.2$ and $1.5 \pm 0.1$ µM for the first two, respectively.
**C:** Titrations of 60bp DNA in the presence of 4 µM GyrB, using GyrA wt (black), GyrA_Y123F (blue), and GyrA_ΔCTD (grey) with $K_d$ values of $63 \pm 5$ , $13 \pm 1$ and $299 \pm 20$ nM, respectively.
**D:** SmFRET histogram for gyrase in the presence of 60bp DNA.
FRET data were corrected with averaged photophysical parameters for mutant T140C_K594C acquired in the absence (A: 1, 2) and presence (A: 3, 4; D) of DNA and GyrB.
Cartoons represent the cleavage-deficient GyrA dimer with one subunit in blue (GyrA body) and green (CTD) and the other in grey. GyrB subunits, supercoiled or linear DNA and ADPNP are shown in white, by a black line and black ellipses. Red and green dots represent the fluorescent dyes.

### 3.1.28 The GyrA-box is required for the supercoiling activity

One of the most conserved amino-acid sequences in the GyrA CTD is the GyrA-box, a highly positively charged hepta-peptide located on a loop in blade 1, that closes the gap to blade 6. In *E. coli* GyrA, alterations of the GyrA-box including the change of the sequence to alanines and the deletion resulted in complete DNA supercoiling deficiency, but did not show a strong influence on nucleotide-independent DNA relaxation [55]. In order to elucidate the mechanism behind these observations, several *B. subtilis* GyrA mutants were produced and tested for their DNA supercoiling and relaxation activities, DNA affinities, and their conformational behavior with respect to the CTDs.

Judged from amino-acid sequence alignments for different species, the GyrA-box in *B. subtilis* GyrA comprises residues 527 − 533 with the amino-acid sequence QKRGGKG, featuring three positively charged residues (Fig. 3.27A). GyrA constructs lacking the A-box (GyrA_ΔAbox) or having it exchanged to alanines (GyrA_AboxA) were produced and purified as described (section 2.10.2). Yields were approx. 25 mg of pure protein per liter bacterial culture, marking a two-fold increase compared to Gyr wt and single cysteine mutants (section 3.1.1). As expected, GyrA_ΔAbox exhibited wild-type like nucleotide-independent plasmid-relaxation activity, but no detectable supercoiling activity (Fig. 3.27B). Both activities were similar for GyrA_AboxA, but were only tested ones in comparison with GyrA_ΔAbox (Fig. 3.27C).
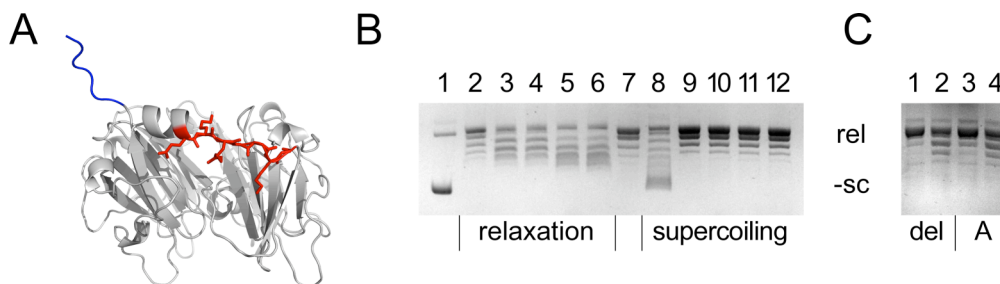


**Fig. 3.27:** Deletion or substitution of the GyrA-box.
**A:** Cartoon representation of a homology model of *B. subtilis* GyrA CTD, based on the template of *X. campestris* GyrA CTD (PDB entry: 3L6V, chain A [38]). The GyrA-box is depicted in red sticks; the N-terminus in blue.
**B and C:** Plasmid relaxation and supercoiling reactions. Incubation times were 30 and 2 min for nucleotide-independent plasmid relaxation and ATP-dependent plasmid supercoiling reactions, respectively. Buffer used was gyrase activity buffer (section 2.12.1).
**B:** Plasmid relaxation (lanes 2 − 6) and supercoiling (lanes 8 − 12) by GyrA wt (2, 8), GyrA_ΔAbox (3, 9), non-labeled GyrA**_ΔAbox (4, 10), GyrA**_ΔAbox fully labeled with A488 (5, 11) and A546 (6, 12). Substrates for the relaxation and supercoiling reaction were neg. supercoiled (1) and relaxed pUC18 plasmid (7), respectively. Nucleotide-independent DNA relaxation reactions were performed with 200 nM GyrA proteins, 800 nM GyrB, and 15 nM relaxed plasmid. ATP-dependent supercoiling reactions were performed using 50 nM GyrA proteins, 800 nM GyrB, 50 nM relaxed plasmid, and 2 mM ATP.
Continued on following page.

**C:** Relaxation (1, 3) and supercoiling reactions (2, 4) by GyrA_ΔAbox (del) and GyrA_AboxA (A). Plasmid substrates were identical with the ones in B. Concentrations used were 200, 800, and 15 nM GyrA proteins, GyrB, and plasmid, respectively. Supercoiling reactions were supplied with 2 mM ATP.

Under these conditions, plasmid relaxation was complete after 30 min for both GyrA-box mutants. However, no supercoiling activity could be detected.


### 3.1.29 Effect of the GyrA-box on DNA binding

Proteins interacting with nucleic acids often mediate contact with highly positively charged patches by forming salt bridges to the negatively charged phosphate backbone. The GyrA CTD exhibits this kind of positively charged regions at the periphery of the domain, stretching two thirds of the outer edge, which is supposed to bind DNA [49]. The GyrA-box being one of them [38], GyrA_ΔAbox was tested for changes in DNA affinity compared to GyrA wt.

GyrA_ΔAbox was titrated to an internally fluorescently labeled 60bp DNA (Fig. 3.7), using 10 nM DNA and up to 10 μM of protein. The measured $K_d$ was $1.9 \pm 0.2$ μM, which was very similar to the value measured for wild-type GyrA (2.3 μM), but much lower than the one for the CTD-deletion mutant (Fig. 3.28A). In order to test the affinity of plasmid DNA to GyrA proteins, displacement titrations were performed using the labeled 60bp DNA and non-modified neg. supercoiled pUC18 plasmid as described (section 2.15.1). Titrations of 1 GyrA wt and GyrA_ΔAbox bound to 60bp DNA with neg. supercoiled plasmid resulted in partial displacement of the 60bp DNA, as the 60bp DNA the starting anisotropy was 0.090 to 0.094, and the anisotropy for the free DNA was not reached even at high plasmid concentrations (0.075 compared to the expected value of approx. 0.070) (Fig. 3.28B). No $K_d$ values for the plasmid DNA were obtained, as the data could not be described quantitatively. Judged from visual inspection of the anisotropy plots, plasmid-DNA affinity for GyrA wt and ΔAbox did not significantly differ.

Titration of 60bp DNA with GyrA_ΔAbox in the presence of 4 μM GyrB yielded a $K_d$ value of $50 \pm 2$ nM. The DNA affinity was very similar (Fig. 3.28C), but the calculated maximal anisotropy differed between experiments with GyrA wt and ΔAbox (approx. 0.27 and 0.30, respectively). The reason for this difference is not known, but it should neither be due to differences in concentration of the present molecules nor due to a different binding mode (in presence of GyrB, DNAs bind to the DNA-gate region of GyrA; Fig. 3.6, 3.8). Again, displacement titrations were performed, adding neg. supercoiled plasmid to 10 nM 60bp DNA and 250 nM GyrA in the presence of 4 μM GyrB. Anisotropy starting values of GyrA wt or ΔAbox complexes reflected the difference in end values obtained from titrations of the 60bp DNA in the presence of GyrB. Addition of plasmid up to 10 nM resulted in reduction of the anisotropy signal to 0.14 for both GyrA complexes, indicating only partial release of linear

DNA fragment, which was expected to have an anisotropy of approx. 0.070 in its non-complexed form (Fig. 3.28D). Due to the complexity of the system consisting of four complex-forming species (GyrA dimer, GyrB, 60bp DNA, plasmid), even more possible complexes and potential enzymatic activity (nucleotide-independent plasmid relaxation) the displacement titrations were not analyzed quantitatively. Interpretation of the data was very difficult due to the difference in starting anisotropies for the complexes with GyrA wt and ΔAbox (see above). Still, as judged from the high similarity in plot curvature and end point values, the DNA binding properties of complexes with GyrA wt and ΔAbox are unlikely to differ substantially.

The results obtained from fluorescence anisotropy gave evidence that affinities of GyrA wt and ΔAbox for DNA were similar, both on addition of a linear 60bp DNA fragment or of circular DNA (neg. supercoiled plasmid); this finding suggested that the difference in enzymatic activity was not due to altered DNA affinity. As the deletion of the GyrA-box did not result in a change of DNA affinity, the GyrA-box did not seem to be involved in DNA binding.
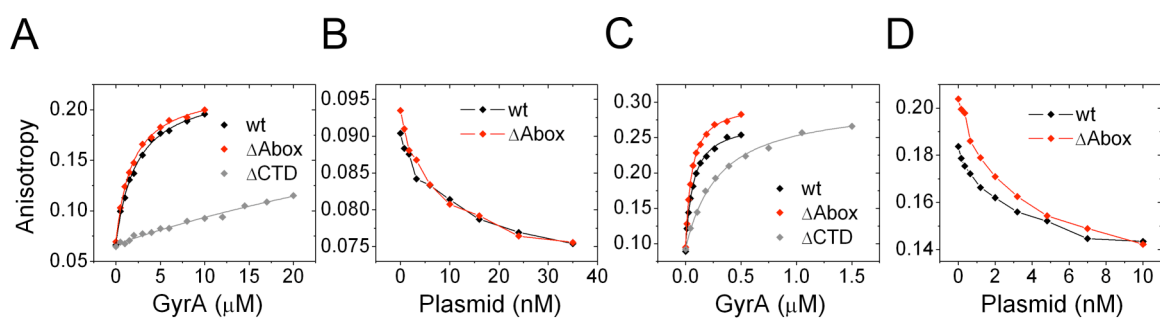


**Fig. 3.28:** Fluorescence anisotropy titrations with GyrA_ΔAbox.
**A:** Titration of the fluorescently labeled 60bp DNA with GyrA wt (black), GyrA_ΔAbox (red), and GyrA_ΔCTD (grey). $K_d$ values were $2.3 \pm 0.2$ and $1.9 \pm 0.2$ μM for the first two proteins, respectively.
**B:** Displacement titrations with neg. supercoiled plasmid DNA. Proteins used were GyrA wt (black) and GyrA_ΔAbox (red).
**C:** Titrations of a 60bp DNA with GyrA wt (black), GyrA_ΔAbox (red), and GyrA_ΔCTD (grey) in the presence of 4 μM GyrB. $K_d$ values were $63 \pm 5$ , $50 \pm 2$ and $299 \pm 20$ nM, respectively.
**D:** Displacement titrations with neg. supercoiled plasmid DNA in the presence of GyrB. Proteins used were GyrA wt (black) and GyrA_ΔAbox (red).

### 3.1.30 SmFRET with a ΔAbox mutant

It was shown that the conformational change of the GyrA CTDs is connected to complex formation of the domain with DNA (sections 3.1.6 and 3.1.22). Although the affinity for DNA was not changed upon deletion of the GyrA-box and differences in conformational changes between the mutant and the wild-type enzyme could not be expected, single-molecule FRET measurements were performed to follow the conformational changes in the mutant.

A hetero-dimeric FRET construct was produced lacking both GyrA-box regions. The well-characterized positions 140 at the DNA-gate and 594 on the CTD were chosen as labeling sites. GyrA*_ΔAbox / GyrA*_ΔAbox_T140C_K594C (abbreviated GyrA**_ΔAbox) was expressed and produced as described (sections 2.10.2) to similar yields (3.5 mg of protein per liter of bacterial culture) and purity as the other hetero-dimeric proteins. DNA-relaxation and supercoiling activities for the non-modified and labeled GyrA**_ΔAbox were similar to the ones for GyrA_ΔAbox (Fig. 3.27B). Single-molecule experiments were performed as described (section 2.18).

The FRET efficiency distribution for the ligand-free enzyme showed one maximum between 0.5 and 0.6 (Fig. 3.29A). It did not differ from the one for the wild-type like FRET mutant (Fig. 3.22A), indicating the same conformation for the ΔAbox mutant. Surprisingly, addition of neg. supercoiled plasmid DNA did not result in broadening of the FRET efficiency distribution: In contrast to the wild-type like GyrA the FRET efficiency remained uni-modal with the same maximum as for the ligand-free GyrA**_ΔAbox (Fig. 3.29A, compared to Fig. 3.22C), despite similar affinities for plasmid DNA. This effect was not due to a lack of complex formation, as the autocorrelation curve clearly shows a shift to higher diffusion time compared to the free protein, confirming DNA binding under those conditions (Fig. 3.22B). The result was reproduced three times, thus excluding an experimental error.
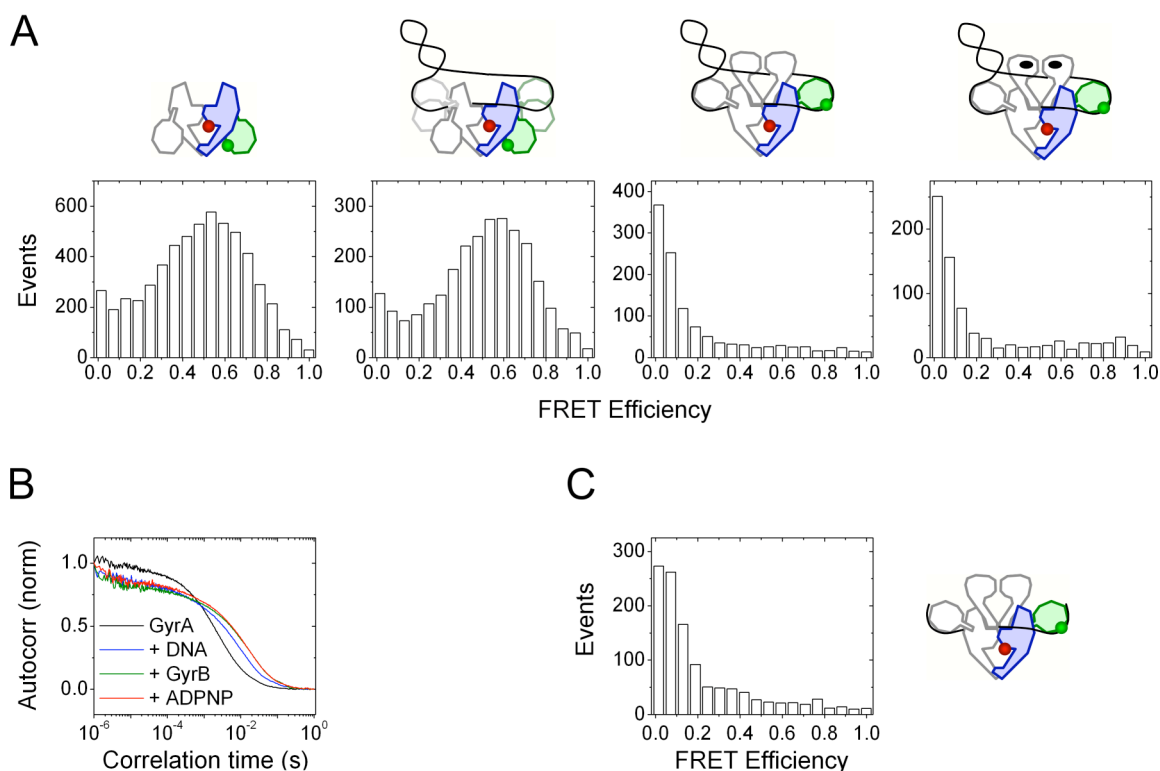
**Fig. 3.29:** SmFRET histograms for the GyrA**_ΔAbox mutant.
**A** (from left to right): In the absence of ligands; in the presence of neg. supercoiled plasmid; gyrase in the presence of neg. supercoiled plasmid; with ADPNP added.
**B:** Autocorrelation curves for the donor signal of smFRET measurements with GyrA (black) and its complexes with neg. supercoiled plasmid (blue), GyrB (green), and ADPNP (red) (correspond to measurements for histograms in A). Addition of DNA increases the diffusion time, as does further addition of GyrB. The diffusion time is not further influenced by the addition of ADPNP.
**C:** SmFRET histogram for gyrase in complex with 60bp DNA.
FRET data were corrected with averaged photophysical parameters for mutant T140C_K594C acquired in the absence (A: 1, 2) and presence (A: 3, 4; C) of DNA and GyrB.
Cartoons represent the GyrA_ΔAbox dimer with one subunit in blue (GyrA body) and green (CTD) and the other in grey. GyrB subunits, supercoiled or linear DNA and ADPNP are shown in white, by a black line and black ellipses. Red and green dots represent the fluorescent dyes.

Addition of GyrB to GyrA**_ΔAbox and plasmid DNA resulted in a strong decrease in FRET efficiency to approx. 0 (Fig. 3.29A). The histogram was similar in shape and position as for the wild-type like FRET mutant, suggesting that the CTDs adopted the extended conformation (Fig. 3.22D). Also similarly, the addition of ADPNP did not show a major influence on the distribution. For both situations, the diffusion time was slightly longer than for GyrA in complex with DNA (Fig. 3.29B), suggesting a change of complex mass or shape, which was not observed for the wild-type like FRET mutant. The low-FRET state was also observed for gyrase_ΔAbox in the presence of the 60bp DNA (Fig. 3.29C).

The cause of supercoiling deficiency in gyrase lacking the GyrA-box could not be elucidated by the presented smFRET and fluorescence anisotropy data. No significant change in behavior could be detected between GyrA wt and ΔAbox, apart from a slightly altered CTD conformation for the GyrA**_ΔAbox-DNA complex, indicating that the loss of DNA supercoiling activity in gyrase lacking the GyrA-box is not connected to DNA binding or conformational change in the CTDs.

## 3.2 Part II: Topoisomerase VI from *M. mazei*

### 3.2.1 Co-expression and co-purification of *M. mazei* topoisomerase VI A and B

Biochemical and biophysical data for the archaeal topoisomerase VI (TopoVI) is scarce. In order to characterize the DNA relaxation and ATP hydrolysis activities and the conformational behavior of *M. mazei* TopoVI, the two subunits A and B were co-expressed and co-purified using a bi-cistronic expression vector derived from a pET system (kind gift from James Berger, University of California, Berkeley, CA); the construct had been purified before [61]. Here we present a slightly modified purification protocol.

TopoVI A and B were co-expressed in *E. coli* BL21(DE3) Rosetta cells, with the B subunit being produced as an N-terminal $His_6$-tag fusion protein cleavable with TEV protease ($His_6$-TEV-B, abbreviated $His_6$-TopoVI-B). Over-expression of TopoVI yielded approx. 50 % of the total protein with subunits A and $His_6$-TEV-B visible on a polyacrylamide gel at apparent molecular weight of 40 and 70 kDa, respectively (Fig. 3.30A), corresponding well with the calculated MWs of 42.1 and 71.1 kDa for the A subunit and the $His_6$-TEV-B fusion protein, respectively. TopoVI-A exhibited a higher expression level than the B subunit.

After cell disruption, a large fraction of TopoVI proteins were found to be insoluble (Fig. 3.30B). The crude extract containing soluble proteins was passed over a $Ni^{2+}$-NTA column; the TopoVI A + $His_6$-TEV-B complex was adsorbed to the resin via the $His_6$-tagged B subunits, indicating a stable subunit association. The co-purified TopoVI complex was incubated with TEV protease for the enzymatic removal of the $His_6$-tag from the B subunits, giving rise to processed B subunits with a calculated MW of 69.0 kDa (hereafter denominated B). The cleaved protein was separated from non-cleaved by a second IMAC step, where the former was found in the flow-through (Fig. 3.30B). The eluted TopoVI was applied to an SP sepharose column: The complex was not adsorbed to the resin and found in the flow-through, in contrast to non-complexed B subunits and a major protein contamination with an apparent MW of approx. 55 kDa, reported to be a fragment of TopoVI-B [61]. In an anion-exchange chromatography step using a Q sepharose column the protein was separated from co-precipitated nucleic acids in an NaCl gradient. The fraction containing TopoVI A and B showed only minor protein contaminations (Fig. 3.30C). The last purification step consisted of a SEC run, where the major fraction of TopoVI complex eluted in a peak at approx. 54 ml retention volume, corresponding to a calculated MW of approx. 295 kDa (Fig. 3.30D), which roughly corresponds to the theoretical MW of approx. 222 kDa for the hetero-tetrameric complex. The purified TopoVI was virtually free of foreign protein and nucleic acid contaminations, as judged by polyacrylamide gel and UV absorption (Fig. 3.30C and E). The

$A_{280nm} / A_{260nm}$ ratio was 2.0. Protein yields were between 2 and 3.5 mg per liter of bacterial culture.
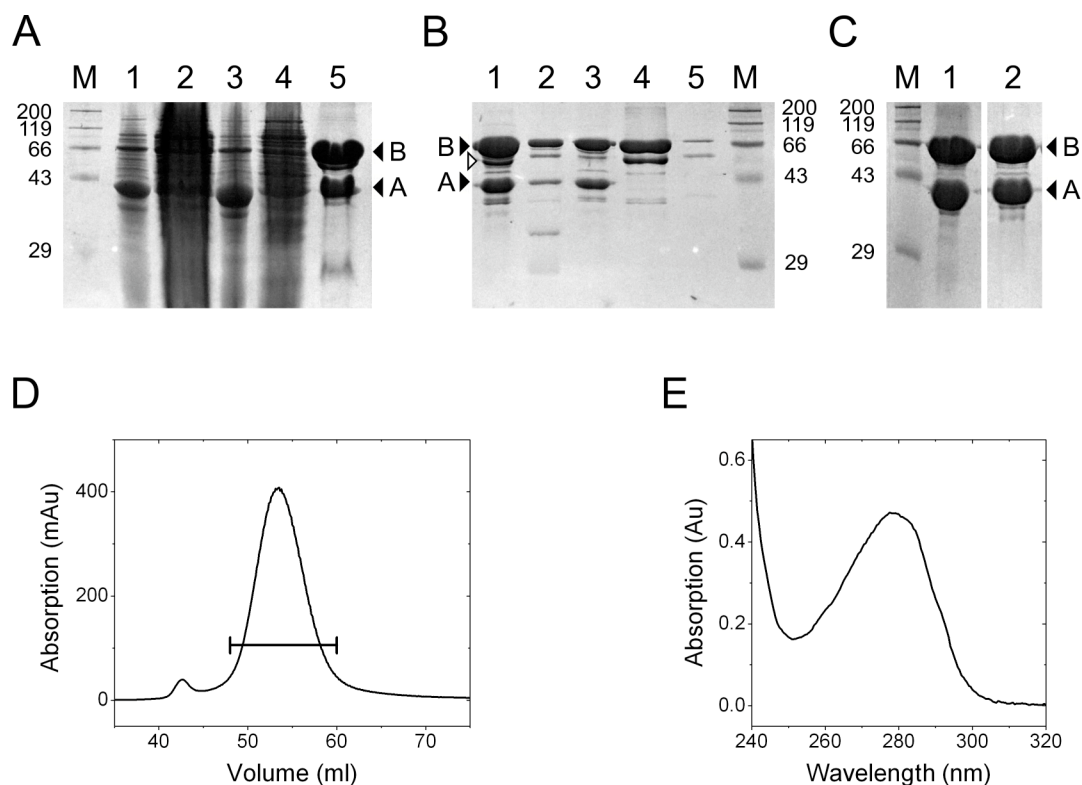


**Fig. 3.30:** Co-production and co-purification of wild-type topoisomerase VI subunits A and B from *M. mazei*.
**A – C:** SDS polyacrylamide gels of different purification stages with protein marker (M) and corresponding MW indicated in kDa. Samples were taken at different purification steps of TopoVI A+B; the subunits are annotated with letters A and B, respectively.
**A:** Lane 1: Co-expression from *E. coli* BL21(DE3) Rosetta cells. Subunits A and His$_6$-TEV-B show MWs of approx. 40 and 70 kDa, respectively. Lanes 2 and 3: Soluble and insoluble fraction of crude extract, respectively. Lanes 4 and 5: Flow-through and elution from the first Ni$^{2+}$-NTA column: The TopoVI A + His$_6$-TEV-B complex was pulled down via the N-terminally His$_6$-tagged B-subunits.
**B:** Lanes 1 and 2: Flow-through and elution from the second Ni$^{2+}$-NTA column: TopoVI A+B without His$_6$-tag (cleaved with TEV protease) was not adsorbed to the nickel resin. Lanes 3 and 4: Flow-through and elution from an SP sepharose cation-exchange column: Separation of the TopoVI complex (not adsorbed: lane 3) and free full-length B subunits and a major contamination with a MW of approx. 55 kDa. 5: Flow-through from a Q sepharose anion-exchange column: The TopoVI complex did not bind to the column resin.
**C:** Lane 1: Elution from a Q sepharose column by increasing concentration of NaCl. Pooled fractions containing purified TopoVI complex. Lane 2: Pooled fractions containing protein as eluted from a Sephadex S200 size-exclusion column.
**D:** Elution chromatogram of the SEC step for TopoVI A+B, monitored by the UV absorption at 280 nm. Fractions from main peak containing TopoVI A+B were pooled and concentrated (horizontal bar).
**E:** UV absorption spectrum of co-purified TopoVI A+B in storage buffer at approx. 5 μM monomer concentrations. The absorption maximum was at 278 nm; the $A_{280nm} / A_{260nm}$ ratio was 2.0.

### 3.2.2 Optimization of TopoVI activity buffer conditions

*M. mazei* TopoVI was shown to possess ATP-dependent DNA relaxation activity [61]. Buffer conditions for the assay were optimized in relaxation reactions containing 1 μM of TopoVI (monomeric concentrations for subunits A and B), 15 nM neg. supercoiled pUC18 and 1 mM ATP using varying concentrations of buffer components (Fig. 3.31A – D). Incubation times and temperatures were chosen as described (section 2.12.2). In absence of ATP, no plasmid relaxation was visible.

For initial experiments the pH was set to 6.5 as reported [61] using MOPS instead of Bis-Tris-Propane (BTP) as a buffering agent. Concentrations of components were 20 mM MOPS, 100 mM potassium glutamate (Kglu), 10 mM $MgCl_2$, and 1 mM DTT.

Screening for the optimal concentration of MOPS (20, 50, and 100 mM) resulted in best relaxation with 50 mM buffering agent concentration and almost equal relaxation extend at 20 mM (Fig. 3.31A). A parallel screen of the salts consisting of monovalent cations and anions was performed in presence of 100 mM NaCl, KCl or Kglu. TopoVI showed highest activity in buffer containing Kglu. The use of KCl resulted in a slightly reduced activity, indicating a slightly inhibitory effect of $Cl^-$ anions. Plasmid relaxation activity was completely abolished in the reaction performed using NaCl, suggesting a very strong inhibitory effect on the enzymatic activity of TopoVI by the $Na^+$ cations (Fig. 3.31A). Kglu was chosen as the primary salt for the activity buffer.

The of Kglu on plasmid relaxation activity was tested in a concentration range between 0 and 300 mM, using a slightly unfavorable MOPS concentration of 20 mM. The extent of plasmid relaxation was maximal in the reaction containing 150 mM Kglu. The relaxation activity was slightly reduced between 100 and 200 mM of Kglu, but almost completely abolished in the absence of salt or at 300 mM (Fig. 3.31B).

DNA cleavage and religation by TopoVI as well as ATP hydrolysis strictly depend on $MgCl_2$ [59, 62]. The relaxation activity was tested as a function of $MgCl_2$ concentration in a range between 0 and 100 mM. The enzymatic activity was maximal in 10 mM of $MgCl_2$; no relaxation was visible for concentrations of 0, 2 and 100 mM (Fig. 3.31C).

Plasmid relaxation by *M. mazei* TopoVI documented in literature was performed using Bis-Tris propane (BTP) as a buffering agent [61]. The compound was tested at concentrations between 0 and 70 mM. Relaxation occurred in a concentration range of 0 to 50 mM, but was most efficient at 40 mM BTP. The reaction containing 70 mM BTP showed no product formation (Fig. 3.31D). Compared to the MOPS buffer system, BTP resulted in higher TopoVI DNA relaxation activity.

Thus, optimized buffer conditions were 40 mM BTP (pH 6.5), 150 mM Kglu and 20 mM MgCl$_2$, with higher concentrations of buffer components compared to the ones mentioned before (20 mM BTP (pH 6.5), 100 mM Kglu and 10 mM MgCl$_2$) [61].
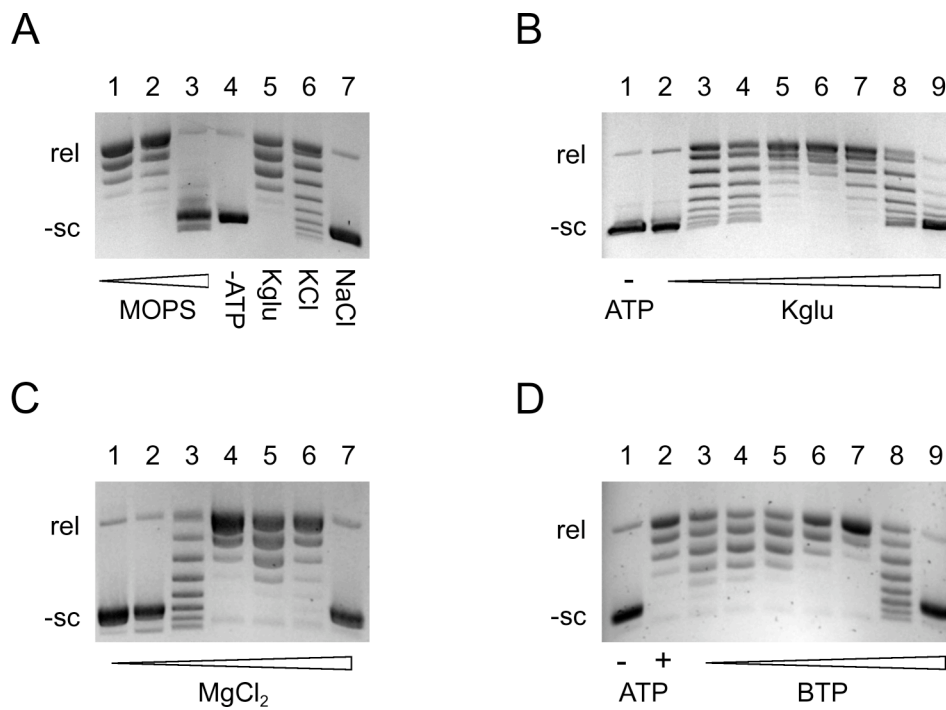


**Fig. 3.31:** Optimization of buffer components and concentrations for activity measurements. Depicted are agarose gels of plasmid relaxation products by TopoVI. Concentrations of TopoVI, substrate plasmid and ATP were 1 μM, 15nM and 1 mM, respectively. Bands corresponding to neg. supercoiled and relaxed pUC18 plasmid are denominated –sc and rel, respectively.
**A:** Screening of different concentration of the buffering agent MOPS and different salts of monovalent cations and anions. Lanes 1, 2, 3: 20, 50, 100 mM of MOPS. Lane 4: Incubation of TopoVI and supercoiled plasmid in absence of ATP, using a buffer containing 20 mM MOPS and 100 mM Kglu. Lanes 5, 6, 7: Relaxation in buffers containing 100 mM Kglu, KCl, or NaCl.
**B:** Screening of different concentrations of Kglu, using 20 mM of MOPS pH 6.5 and 10 mM MgCl$_2$. Lane 1: Reaction in absence of ATP, using 100 mM of Kglu: No relaxation is visible. Lanes 2 – 9: Relaxation in presence of 0, 50, 80, 100, 150, 200, 250, and 300 mM of Kglu.
**C:** Screening of different concentrations of MgCl$_2$, using 20 mM of MOPS pH 6.5 and 150 mM Kglu. Lanes 1 – 7: Relaxation in presence of 0, 2, 5, 10, 20, 50, and 100 mM of MgCl$_2$.
**D:** Screening of different concentrations of buffer agent BTP; the pH was adjusted to 6.5. Concentrations for Kglu and MgCl$_2$ used were 150 and 10 mM, respectively. Lanes 1 and 2: Control reactions performed using 20 mM MOPS, pH 6.5, in the absence and the presence of ATP. Lanes 3 – 9: Relaxation in buffers containing 0, 10, 20, 30, 40, 50, and 70 mM BTP.

### 3.2.3 TopoVI from *M. mazei* is an ATP-dependent DNA relaxase

Having optimized the buffer conditions for the DNA relaxation activity of TopoVI, the enzymatic activity could be quantified. A DNA relaxation assay was performed in presence of 1 mM ATP using 15 nM neg. supercoiled plasmid DNA substrate and varying concentrations of TopoVI enzyme.

No relaxation activity was visible in absence of TopoVI. While at 20 nM a distribution of relaxed and supercoiled plasmid topoisomers was visible, at 50 to 100 nM enzyme concentration the substrate was fully relaxed indicating that maximal relaxation activity was reached at 50 nM (Fig. 3.32A). Reactions performed at higher enzyme concentrations (i.e. 200 – 1000 nM) resulted in partially relaxed plasmid, suggesting that the relaxation activity depends on the enzyme : plasmid ratio. The calculated optimal ratio would be between 3 and 7 (50 - 100 nM enzyme : 15 nM plasmid). The control reaction performed in absence of ATP at 1 µM enzyme concentration clearly showed no plasmid relaxation, which gives evidence that the reaction is ATP-dependent. The control also shows that no ATP-independent topoisomerase contaminant was co-purified with TopoVI. This result confirmed previous findings for TopoVI from *S. shibatae* and *M. mazei* [25, 61].

The relaxation activity of TopoVI was further tested in presence of different nucleotides, using ATP, ADP, and the structural ATP analog ADPNP. Reactions were incubated for 30 or 60 min. At 50 nM concentration of the enzyme, the plasmid substrate was fully relaxed in presence of ATP. As expected, no relaxation was visible for reactions performed in the presence of ADP or ADPNP, demonstrating that DNA relaxation by TopoVI depends on ATP hydrolysis (Fig. 3.32B). The reaction performed in presence of ATP was completed after 30 min.
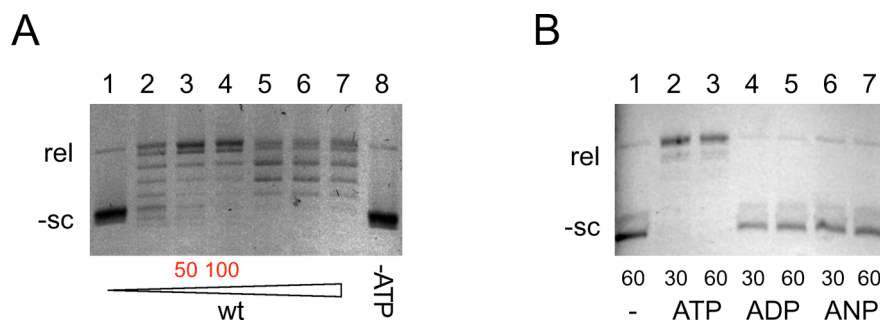


**Fig. 3.32:** Plasmid DNA relaxation activity by *M. mazei* TopoVI. Plasmid and nucleotide concentrations were 15 nM and 1 mM, respectively. Bands corresponding to neg. supercoiled and relaxed pUC18 plasmid are denominated –sc and rel, respectively. Reactions were performed in TopoVI activity buffer (section. 3.2.2).
**A:** Relaxation using different TopoVI concentrations. Lanes 1 – 7: 0, 20, 50, 100, 200, 500, 1000 nM TopoVI, respectively. Lane 8: Reaction in absence of ATP. Reactions showing the highest TopoVI activities are denominated with corresponding TopoVI concentrations (lanes 3 and 4).
**B:** Incubation of supercoiled plasmid with 50 nM TopoVI and different nucleotides. Incubation times were 30 or 60 min (as indicated). Reactions were performed in absence of nucleotide (lane 1), in presence of ATP (lanes 2, 3), ADP (lanes 4, 5), or ADPNP (lanes 6, 7; abbrev: ANP).

### 3.2.4 DNA relaxation by TopoVI is inhibited in presence of NaCl

In section 3.2.2 it was demonstrated, that the relaxation activity of TopoVI is abolished in presence of 100 mM NaCl; responsible for this loss of activity is mainly the presence of $Na^+$ cations. For different experiments TopoVI was diluted from storage conditions resulting in a systematic contamination with NaCl due to the storage buffer conditions (300 mM NaCl); thus it was of great importance to determine the inhibitory concentration of $Na^+$.

DNA relaxation was performed under optimized buffer conditions using 50 nM of TopoVI, 15 nM of neg. supercoiled plasmid DNA and 1 mM of ATP in presence of varying concentrations (0 – 200 mM) of NaCl. At salt concentrations below 10 mM the relaxation activity was not affected, whereas addition of 20 mM of NaCl already resulted in the presence of supercoiled and partially relaxed plasmid. At salt concentrations of 50 mM and above the relaxation activity of TopoVI was completely inhibited (Fig. 3.33A).

These results suggest that a maximal NaCl concentration of approx. 10 to 15 mM is tolerated by TopoVI. The concentrations of NaCl in all experiments described hereafter were lower than 15 mM.
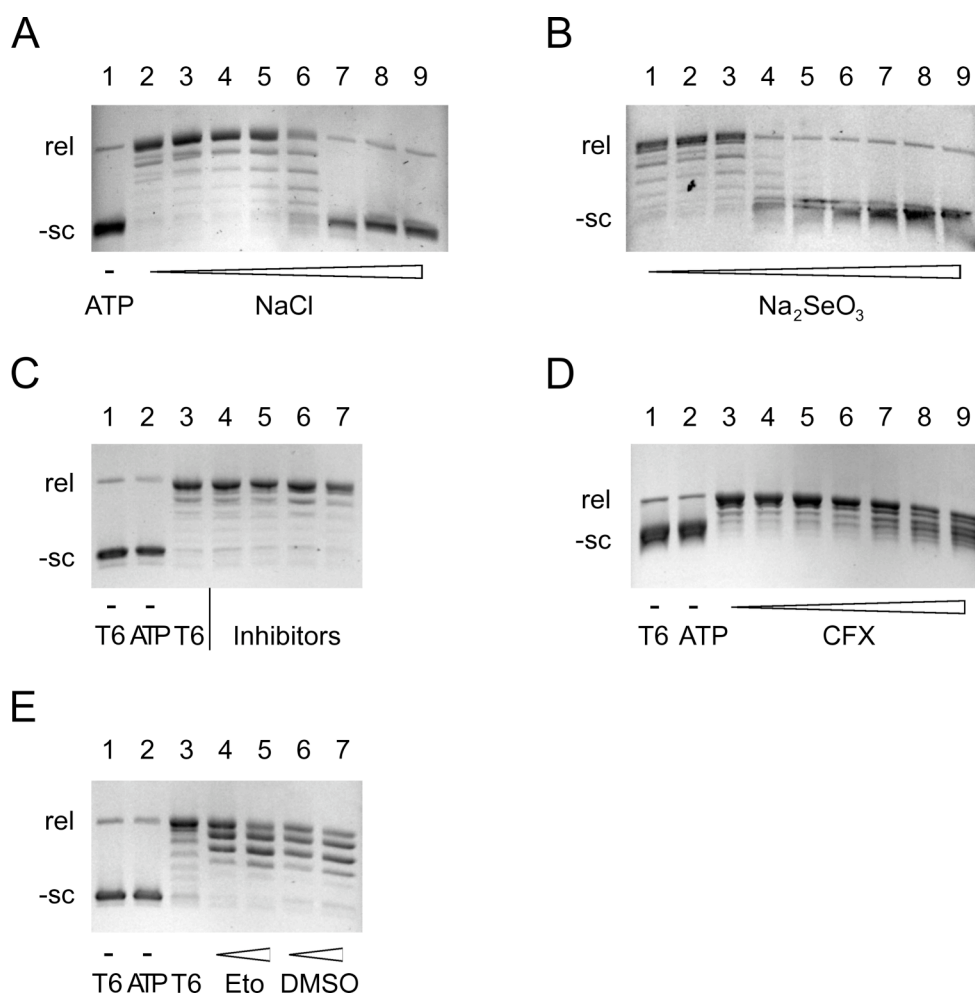


**Fig. 3.33:** For legend see following page.

**Fig. 3.33:** Inhibition of TopoVI DNA relaxation activity by salts and specific topoisomerase poisons. Concentrations of TopoVI, neg. supercoiled plasmid and ATP were 50 nM, 15 nM and 1 mM, respectively. Bands corresponding to neg. supercoiled and relaxed pUC18 plasmid are denominated – sc and rel, respectively. Reactions were performed in TopoVI activity buffer (section. 3.2.2).
**A:** Relaxation reactions by TopoVI in absence of ATP (lane1) and presence of 0, 2, 5, 10, 20, 50, 100, and 200 mM NaCl (lanes 2 – 9).
**B:** Relaxation reactions by TopoVI in presence of 0, 100, 150, 200, 250, 300, 350, 400, and 500 μM of $Na_2SO_3$ (lanes 1 – 9).
**C:** Relaxation reactions in absence of TopoVI (lane 1), in absence of ATP (lane 2), in presence of TopoVI and ATP (lane 3), and with 50 μM of topoisomerase inhibitors added (lanes 4 – 7): oxolinic acid, ciprofloxacin, nalidixic acid, and sparfloxacin.
**D:** Relaxation reactions in absence of TopoVI (lane 1), in absence of ATP (lane 2), in presence of TopoVI and ATP (lane 3), and with varying concentrations of ciprofloxacin added (lanes 4 – 9): 50, 100, 150, 250, 300, and 350 μM, respectively.
**E:** Relaxation reactions in absence of TopoVI (lane 1), in absence of ATP (lane 2), in presence of TopoVI and ATP (3), with 100 and 200 μM of etoposide (lanes 4 and 5) or 2.1 and 4.2 % (v/v) DMSO added (lanes 6 and 7), respectively.

### 3.2.5   Screening potential DNA cleavage and religation inhibitors

Only one specific inhibitor of TopoVI is known today: The drug radicicol completely inhibits DNA relaxation by *S. shibatae* TopoVI at concentrations higher than 125 μM [97], occupying the ATP binding site of the B subunits [98]. With a view to experiments addressing the DNA cleavage and religation site of *M. mazei* TopoVI, located on subunit A, several compounds known for their inhibitory effect in type IIA topoisomerases were tested on TopoVI.

Inorganic selenite was shown to induce complexation of DNA and human topoisomerases I and II in vitro [99]. $Na_2SO_3$ was added to DNA relaxation reactions up to 500 μM. Above a concentration of approx. 250 μM, TopoVI was completely inhibited (Fig. 3.33B). The corresponding concentration of $Na^+$ cations was around 500 μM, which is not in the inhibitory range. Thus selenite acts as an inhibitor to TopoVI.

Compounds tested next belong to the class of quinolones which are potent antibacterial drugs targeting the Gyrase-DNA complex [100]. Oxolinic acid, ciprofloxacin (CFX), nalidixic acid and sparfloxacin were added to DNA relaxation reactions in concentrations of 50 μM. No inhibitory effect could be observed for either of them (Fig. 3.33C). CFX was tested in a concentration-dependent manner up to 350 μM. The DNA relaxation activity of TopoVI was slightly lowered at concentrations above 250 μM, but complete inhibition was not achieved (Fig. 3.33D).

The last compound to be tested was etoposide, a topoisomerase II poison, and used as a chemotherapeutic agent [101]. It also was shown to inhibit *S. shibatae* TopoVI (personal communication by D. Gadelle, Group Forterre, Paris). Etoposide, dissolved in DMSO was

added to the relaxation reaction at concentrations of 100 and 200 µM, exhibiting a slight inhibitory effect. However, this effect was due to DMSO, as shown in control reactions (Fig. 3.33E).

Compounds found to inhibit *M. mazei* TopoVI were the salt $Na_2SO_3$ and the fluoroquinolone drug CFX, with inhibition observable at concentrations above 250 µM for either of them. Both drugs need to be tested in DNA cleavage reactions (section 3.2.8).

### 3.2.6  A fluorescently labeled 50bp DNA to monitor DNA-gate dynamics in TopoVI

One of the main objectives of this work was to monitor gate dynamics in TopoVI. One way to do so is to detect conformational changes and cleavage events in a DNA bound to the DNA-gate. A fluorescently double-labeled 50bp DNA (abbrev. 50bp FRET DNA) was devised to serve as ligand for TopoVI in smFRET studies. It contained a putative binding site for *S. shibatae* TopoVI [59]. Different non-labeled and single-dye labeled versions of the 50bp DNA bearing the same nucleotide sequence were used for binding and cleavage studies.

### 3.2.7  Binding of the 50bp DNA to TopoVI wt and Y106F

In order to characterize the influence of the fluorescent dyes on binding of the 50bp FRET DNA to TopoVI, single-dye labeled 50bp DNAs (50bp-A488, 50bp-A546) were titrated with TopoVI and compared to a 50bp DNA of the same sequence end-labeled with fluorescein (50bp-Fluor). Binding was monitored by fluorescence anisotropy.

Anisotropy signals of the non-complexed DNAs were in a range between 0.05 (A488) and 0.082 (A546), differing slightly due to the differences in mobility and attachment points of the dyes. The anisotropy signal increased for all three DNAs upon addition of protein, indicating complex formation. A 1:1-binding model was fitted to the data yielding $K_d$ values of 3.2 ± 0.6, 1.9 ± 0.1 and 0.36 ± 0.03 µM for 50bp-Fluor, -A488 and –A546, respectively (Fig. 3.34C). Anisotropy values for saturating conditions were calculated as 0.133, 0.179 and 0.335, respectively. The large differences in binding affinity (up to 6.5-fold) and end anisotropies among the three DNAs suggested a considerable influence of the identity and position of the fluorescent labels on the binding behavior towards TopoVI.

In the course of the validation of the 50bp DNA as a model substrate, the influence of the Y106F mutation in the TopoVI-A subunit on DNA binding was tested. The protein was deficient in DNA-cleavage activity, as indicated by the lack of plasmid relaxation (Fig. 3.34B) and sequence comparison with homologues proteins. Titration of 50bp-A546 with

TopoVI Y106F yielded a $K_d$ value of 4.1 ± 0.2 μM, marking an approx. 10-fold decrease in affinity compared to the wt protein. A possible explanation for this result is the potential lack of formation of a covalent tyrosyl-DNA intermediate.

Titration of the double-labeled 50bp DNA with TopoVI Y106F showed a $K_d$ value of 1.4 ± 0.1 μM. The increase in affinity for TopoVI was due to the presence of a second dye, suggesting an additive effect of the two labels on the binding. This finding questions the validation of the 50bp DNA for FRET experiments.

### 3.2.8   Cleavage of the 50bp DNA by TopoVI

After showing the formation of the DNA-protein complex it was important to test whether wt TopoVI was able to cleave the substrate, and if this would be at the expected position of the preferred cleavage site. For this purpose a 50bp DNA was annealed from a non-modified and a $^{32}$P-labeled strand incubated with TopoVI in absence or presence of 2 mM nucleotide (ATP or ADPNP) and 500 μM inhibitors (ciprofloxacin or inorganic selenite) to induce the formation of a DNA-protein complex, i.e. DNA cleavage (section 2.13). DNA products were separated by gelelectrophoresis and visualized by a phosphorimager. Despite the high sensitivity of the method, cleaved DNA product was observed in none of the reactions (Fig. 3.34A). This finding was somewhat surprising, as from differences in DNA affinity between wt TopoVI and the cleavage-deficient mutant one would expect the population of the covalent DNA-protein intermediate: It was not clear, if DNA cleavage did not occur or if the cleavage complex could not be trapped by the method used.

### 3.2.9   SmFRET experiments with the double-labeled 50bp DNA

It could be demonstrated that the fluorescent labels alter the binding properties of the 50bp DNA towards TopoVI. In addition no cleavage product could be detected. Nevertheless, the double-labeled 50bp DNA was used in smFRET measurements to detect potential conformational changes in the DNA upon binding to TopoVI and different nucleotides. Concentrations for the DNA, protein and nucleotides were 40 pM, 2.5 μM and 1 mM, respectively. Experiments were performed at room temperature. FRET efficiencies were corrected using parameters determined with single-dye labeled 50bp DNA, in the absence and the presence of TopoVI. Correction parameteres for ligand-free and TopoVI-bound DNA were determined as described (section 2.18.2); values for α', β', and γ' were (A) 0.53, 0.014, 2.00 and (B) 0.64, 0.11, 3.41 in absence and presence of TopoVI, respectively. SmFRET

measurements of ligand-free DNA were corrected with parameter set A, while all measurements involving TopoVI were corrected with parameter set B.

FRET histograms of the free DNA showed a narrow distribution with a maximum at approx. 0.6 (Fig. 3.34D). Upon addition of wt TopoVI the FRET efficiency distribution shifted to a mean value of 0.4 and adopted a broader shape, suggesting a conformational change of the DNA or a change of the environment of the dyes. Addition of ADPNP or ATP to the DNA-protein complex (which might result in a conformational rearrangement of the ATPase-gate) did not further influence the position of the FRET efficiency distribution, suggesting no rearrangement of the complex in the region of the DNA-gate (Fig. 3.34D, F). Judged from anisotropy titration data, the fluorescent labels alter the binding of the 50bp DNA to TopoVI and might therefore be restricted in motion; thus it is possible that the change in FRET efficiency is due to physical contact of one or both dyes with the protein.

The single-molecule experiments were also performed with the cleavage-deficient TopoVI Y106F mutant. Addition of the protein to the labeled 50bp DNA resulted in a shift of the FRET efficiency very similar to the one induced by the wt protein. The FRET efficiency distribution also remained constant upon addition of ADPNP (Fig. 3.34E). Thus, no difference in FRET efficiency of the DNA bound to wt and mutant TopoVI could be detected, indicating similar DNA conformations and complex formation for both proteins.

In DNA cleavage experiments with TopoVI, no cleaved DNA products were observed. It is not clear whether the cleavage complex was formed. As a result, the lack of difference in DNA conformation in the complex with wt TopoVI and the cleavage-deficient mutant could be either because cleavage in the wt enzyme did not occur or because the conformation of the DNA does not change upon cleavage by TopoVI.

From the presented results it is not clear if the 50bp DNA can be used as G-segment for TopoVI: No cleavage product could be detected, and the fluorescent labels attached to the DNA influenced the affinity for the enzyme. Due to this uncertainty, this project was not further developed.
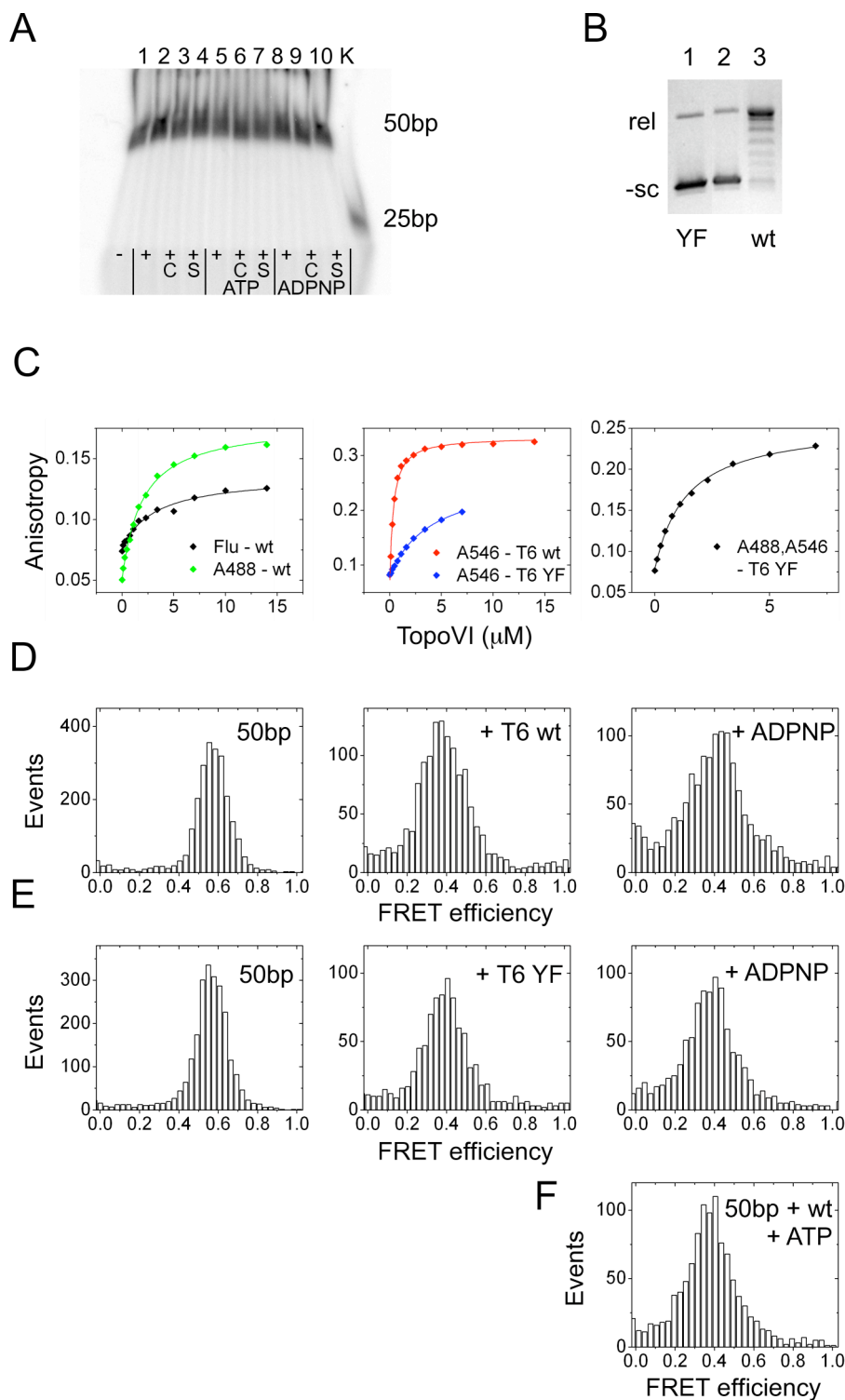
**Fig. 3.34:** A 50bp DNA ligand for TopoVI: Binding, cleavage, and smFRET experiments.
**A:** DNA cleavage assay using a $^{32}$P-labeled 50bp DNA. 1, K: Labeled control DNAs of 50 and 25 bp in length. Reactions denominated with + were incubated with TopoVI wt. Reactions 2 – 4 were performed in absence of nucleotide; reactions 5 – 7 in presence of ATP; and reactions 8 – 10 in presence of ADPNP. Inhibitors ciprofloxacin (C) and sodium selenite (S) were added to reactions 3, 6, 9 and 4, 7, 10, respectively. In neither of the reactions was a cleavage product observed.
**B:** DNA relaxation assay with the cleavage-deficient mutant TopoVI Y106F (YF). Relaxation reactions by TopoVI Y106F in the presence of ATP (lane 1) and by TopoVI wt in the absence (lane 2) and the presence of ATP (lane 3).
Continued on following page.

**C:** Fluorescence anisotropy titrations of 50bp DNA. Left: Titration of the DNA labeled at one end with fluorescein (black) or internally labeled with A488 (green) with TopoVI wt. $K_d$ values were $3.2 \pm 0.6$ and $1.9 \pm 0.1$ µM, respectively. Middle: Titrations of the DNA labeled internally with A546 with TopoVI wt (red) and Y106F (blue; abbrev: YF). Measured $K_d$ values were $0.36 \pm 0.03$ and $4.1 \pm 0.2$ µM, respectively. Right: Titration of the double labeled 50bp DNA (FRET construct) with TopoVI Y106F, yielding a $K_d$ value of $1.4 \pm 0.1$ µM. Bands corresponding to neg. supercoiled and relaxed pUC18 plasmid are denominated –sc and rel, respectively.
**D − F:** SmFRET histograms for the double-labeled 50bp DNA, corrected with parameters listed in section 3.2.9.
**D** (left to right): Histograms for free DNA, DNA bound to TopoVI wt, and with ADPNP added.
**E** (left to right): Histograms for free DNA, DNA bound to cleavage-deficient mutant TopoVI Y106F, and with ADPNP added.
**F:** Histogram for the 50bp DNA in complex with TopoVI wt in presence of ATP. FRET efficiencies for free DNA were corrected with parameters determined from single-fluorophore labeled DNA; all other FRET efficiencies were corrected with parameters determined in presence of TopoVI wt.


### 3.2.10  Mutation of solvent-accessible cysteine residues in TopoVI

Observation of conformational changes in TopoVI via a fluorescently labeled DNA was not successful, as described above. Another possibility was to couple fluorescent dyes to the protein surface, making use of the specific modification of thiols (present in side-chains of cysteine residues) by maleimide groups. Site-specific labeling of proteins requires the removal of solvent-accessible cysteines and the introduction of cysteines in the desired positions.

*M. mazei* TopoVI contains one and six cysteine residues in subunits A and B, respectively (Fig. 3.35A). In order to determine the residues which are accessible to the solvent, the protein was fluorescently labeled with Alexa546-$C_5$-maleimide, using 30 µM protein and a ten-fold excess of fluorescent dye (300 µM). The reaction was incubated at 25°C for 2 h, the protein separated from non-reacted dye by SEC and subsequently analyzed on an SDS-polyacrylamide gel. The labeling degree was calculated as described (section 2.16.3), yielding a value of 140 % (120 – 160 % in repeated experiments) of dye with respect to available A and B subunits. Fluorescent labeling was restricted to the B subunit, while the A protein was not modified (Fig. 3.35C). As judged from the X-ray structure of the TopoVI holoenzyme [61], cysteine residues C267, C278, C316 (all located in the ATPase domain) and C550 (on the C-terminal domain of TopoVI-B) were considered potentially solvent-accessible.

The number of cysteine residues in the TopoVI-B subunit was reduced in a step-wise fashion, and each mutant was fluorescently labeled to test for remaining solvent-accessible thiols. The mutants were purified after the protocol developed for the wt protein (section 2.10.3). C550 was the first to be exchanged to alanine, reducing the labeling efficiency of TopoVI-B with A546 to approx. 110 % (Fig. 3.35C). Next proteins tested for fluorescence labeling were the double mutants C267S_C550A and C278A_C550A. Both proteins were purified by IMAC

using His SpinTrap microcolumns and labeled with A546, using micromolar protein concentrations and 50 dye concentrations in the low micromolar range and 50 μM of fluorescent dye. The wild-type protein showed a labeling degree of approx. 120 %, while the labeling efficiencies of the mutants were reduced to 75 and 110 % for the protein preparations, assuming pure TopoVI mutants. These values indicate C267 to be solvent-accessible, while C278 was barely labeled with A546 (Fig. 3.35D). The modification of C267 was confirmed by mass spectrometry of tryptic fragments of labeled wild-type protein (Lab of Bernhard Schmidt, University of Göttingen, Germany). C316 was exchanged next: The labeled triple cysteine mutant C267S_C316S_C550A (SSA) showed a further reduced labeling degree of 24 % compared to the one of 110 % of the wild-type under labeling conditions described above (Fig. 3.35E). Considering that a contaminating protein present in the preparation of TopoVI SSA was labeled to a much higher degree than the mutant B subunit, the labeling efficiency for the remaining cysteine residues was considered low enough to further reduce it using a modified labeling procedure. TopoVI SSA was used as a basis to introduce cysteine residues for labeling and subsequent smFRET experiments.
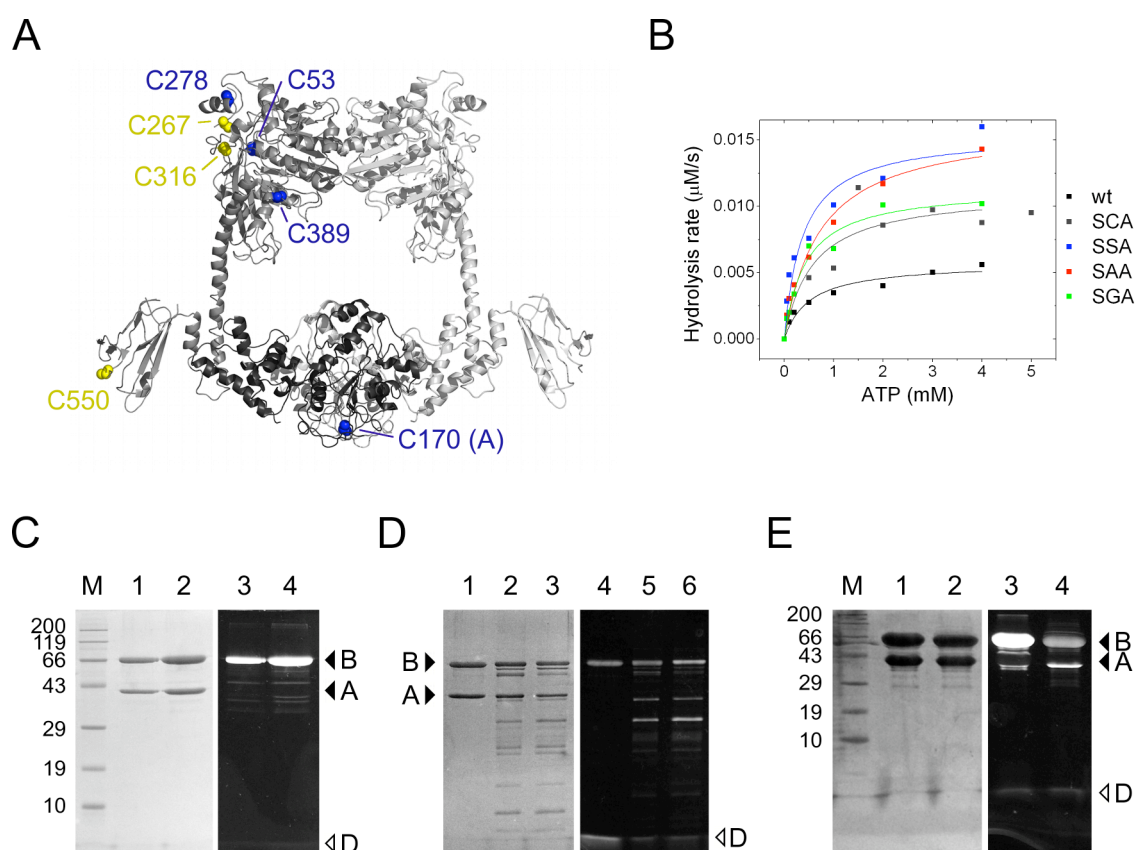


**Fig. 3.35:** Determination and removal of solvent-accessible cysteine residues and influence of mutations on the ATPase activity.

**A:** X-ray structure of the *M. mazei* TopoVI hetero-tetrameric holoenzyme with cysteine residues depicted in sphere representation. Cysteines represented in yellow and blue spheres were found to be solvent-accessible or less accessible in labeling experiments, respectively.

**B:** Steady-state ATP hydrolysis assays with TopoVI wt (black), double mutant C267S C550A (green; SCA) and triple mutants C267S C316S C550A (blue; SSA), C267S C316A C550A (blue; SAA) and C267S C316G C550A (blue; SGA), using 4 μM and varying concentrations of ATP. Values for $K_M$ and $k_{cat}$ are given in section 3.2.11.

**C – E:** SDS-polyacrylamide gels of TopoVI proteins labeled with A546 in fluorescence view (right) and after coommassie staining (left). The protein size marker is denominated M, and corresponding MW are indicated in kDa. TopoVI subunits are annotated with letters A and B, respectively. Non-reacted dye is annotated with D.

**C:** Fluorescently labeled TopoVI wt (lanes 1, 3) and C550A (lanes 2, 4).

**D:** Fluorescently labeled TopoVI wt (lanes 1, 4) with mutants C267S C550A (lanes 2, 5) and C278A C550A (lanes 3, 6).

**E:** Fluorescently labeled TopoVI wt (lanes 1, 3) and mutant C267S C316S C550A (lanes 2, 4).

### 3.2.11  ATP hydrolysis and DNA relaxation assays with TopoVI mutants

As the modification of an enzyme by mutagenesis often leads to a change in the catalytic properties, the TopoVI mutants C267S_C550A (SCA) and C267S_C316S_C550A (SSA) were tested for potential activity loss.

First, the ATPase activity of the wild-type protein was determined under steady-state conditions and monitored spectrophotometrically, using 4 μM of enzyme and varying concentrations of ATP. ATP hydrolysis rates could be described according to the Michaelis-Menten formalism, yielding values for $K_M$ and $k_{cat}$ of $0.50 \pm 0.14$ mM and $(1.4 \pm 0.1) \cdot 10^{-3}$ per second (Fig. 3.35B). The plasmid relaxation activity was determined before: The maximal relaxation was observed at a protein concentration of $50 - 100$ nM (Fig. 3.32A). The test was performed in presence of 15 nM neg. supercoiled pUC18 plasmid and 1 mM ATP.

The ATPase and DNA relaxation activities of TopoVI mutants SCA and SSA were determined under the same conditions as for the wt protein. While the $K_M$ values remained similar (difference in the range of the error), the turn-over number $k_{cat}$ was increased to $(2.8 \pm 0.4)$ and $(3.9 \pm 0.4) \cdot 10^{-3}$ per second for mutants SCA and SSA (Fig. 3.35B). The DNA relaxation activity of SCA remained unchanged compared to the wt, showing maximal plasmid relaxation at a protein concentration of approx. 100 nM (Fig. 3.36A). In SSA however, maximal relaxation was achieved only between 500 and 1000 nM of enzyme, indicating a change in the enzymatic behavior by the mutation of C316 to serine (Fig. 3.36B).

In order to reduce the loss in plasmid relaxation activity for the C316 mutant, the residue was exchanged to alanine and glycine. The triple mutants C267S_C316A_C550A (SAA) and C267S_C316G_C550A (SGA) exhibited wild-type like $K_M$ values, but higher turn-over numbers of $(4.1 \pm 0.3)$ and $(2.9 \pm 0.2) \cdot 10^{-3}$ per second. Plasmid relaxations activities were

similar to the one for SSA, namely at enzyme concentrations of approx. 500 nM (Fig. 3.35B and Fig. 3.36C, D).

It is evident, that the exchange of C316 to S, A or G only moderately affects the ATP turnover number (2 – 3-fold increase), but results in an approx. 5- to 10-fold decrease of plasmid relaxation activity compared to wt. This finding suggests that mutation of C316 partially uncouples DNA relaxation and ATP hydrolysis. Still, the TopoVI mutant SSA was used as a basis for the introduction of cysteines for smFRET measurements: The plasmid relaxation activity might be reduced, but at least the protein retains ATP-dependent topoisomerase activity.



**Fig. 3.36:** Plasmid DNA relaxation activity by *M. mazei* TopoVI mutants. Plasmid and nucleotide concentrations were 15 nM and 1 mM, respectively. Bands corresponding to neg. supercoiled and relaxed pUC18 plasmid are denominated –sc and rel, respectively. Protein concentrations resulting in maximal plasmid relaxation are mentioned (red). Reactions were performed in TopoVI activity buffer (section 3.2.2).
**A:** Plasmid relaxation by TopoVI SCA. Lanes 1 – 9: 0, 0.02, 0.05, 0.1, 0.2, 0.5, 1.0, 2.0, and 5.0 μM.
**B:** Plasmid relaxation by TopoVI SSA. Lanes 1 – 9: 0, 0.05, 0.1, 0.2, 0.5, 1.0, 2.0, 5.0 and 10.0 μM.
**C:** Plasmid relaxation by TopoVI SAA. Lane 1: Relaxation by 50 nM TopoVI wt as a control. 2 – 9: 0.02, 0.05, 0.1, 0.2, 0.5, 1.0, 2.0, and 5.0 μM.
**D:** Plasmid relaxation by TopoVI SGA. Lane 1: Relaxation by 50 nM TopoVI wt as a control. 2 – 9: 0.02, 0.05, 0.1, 0.2, 0.5, 1.0, 2.0, and 5.0 μM.

### 3.2.12 Construction and validation of FRET mutants

The TopoVI triple mutant C267S_C316S_C550A (SSA) was hardly labeled under extreme reaction conditions, i.e. using high dye concentrations of 300 μM and long incubation times of 2 h. Several mutants for labeling of positions in the upper (R87C, D159C, E164C) and lower ATPase-gate (P408C) were constructed by introducing cysteine residues to the SSA triple mutant (Fig. 3.37A). Production and purification of these mutants were performed as for the wild-type, resulting in protein of similar purity (as judged from SDS polyacrylamid gels and UV absorption), but with lower yields of 3 – 5 mg per liter bacterial culture.

Labeling of the FRET mutants was performed using 30 μM protein and 24 and 36 μM of A488 and A546, respectively, and reducing the incubation time to 10 min. Initial labeling reactions were performed in parallel on FRET mutants and TopoVI SSA to monitor the labeling of residual native cysteines. Total labeling degrees were 60 – 100 % (relative to introduced cysteine residues) for the FRET mutants, but maximally 5 % for the SSA mutant (Fig. 3.37B).

The enzymatic activities of the FRET mutants were determined in plasmid relaxation assays. The mutants R87C, E164C and P408C reached exhibited maximal relaxation activity at concentrations of approx. 500 μM, i.e. at the same concentration as the SSA mutant, indicating no loss of activity due to exchange of certain residues to cysteine (Fig. 3.37D, E and G). The mutant D159C showed maximal plasmid relaxation at an enzyme concentration of 5 μM, marking a 10-fold reduction in activity compared to the SSA mutant (Fig. 3.37C); this was probably due to the proximity of the mutation site to the dimerization interface of the ATPase-gate (Fig. 3.37A). Only for the FRET mutant E164C, the relaxation activity was tested using the labeled enzyme. Maximal plasmid relaxation was exhibited at approx. 1 μM protein concentration, indicating a small loss of activity due to fluorescent labeling (Fig. 3.37F).

All of the four above-mentioned TopoVI SSA FRET mutants were shown to retain the relaxation activity of the SSA mutant (with the exception of the mutant D159C) and could be fluorescently labeled in a site-specific manner. Thus single molecule measurements could be performed with all mutants.
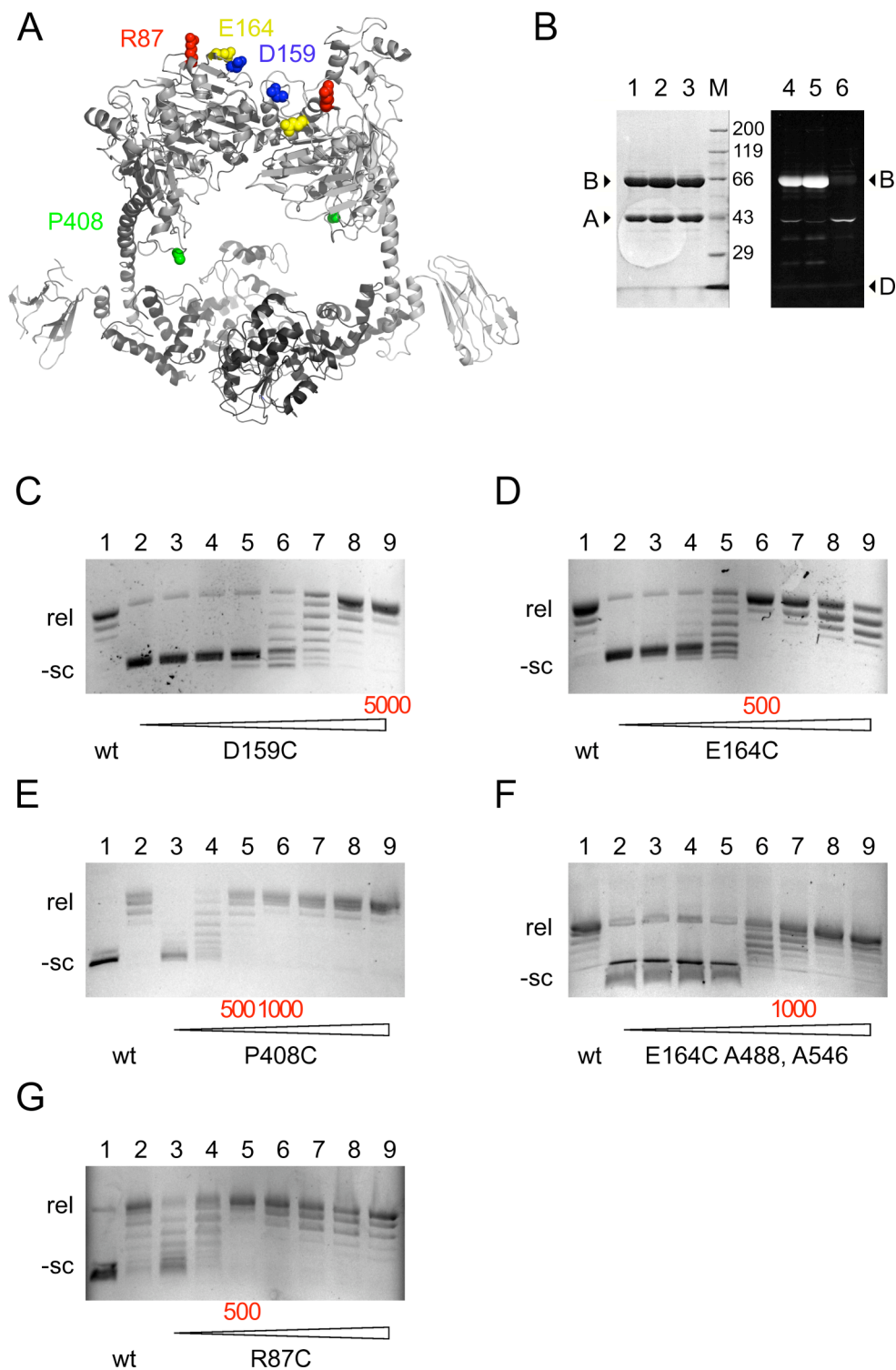
**Fig. 3.37:** Labeling positions and validation of TopoVI FRET mutants.

**A:** X-ray structure of the *M. mazei* TopoVI hetero-tetrameric holoenzyme, with cysteines introduced for site-specific labeling depicted in spheres. Exchanged residues in the upper ATPase-gate region are colored in red (R87C), blue (D159C) and yellow (E164C), while the one in the transducer region is depicted in green (P408C).

**B:** Fluorescence view (right) and coomassie staining (left) of an SDS-polyacrylamide gel of TopoVI mutants double-labeled with A488 and A546. The protein standard is denominated M, and corresponding MW are indicated in kDa. Proteins depicted are TopoVI FRET mutants E164C (1) and D159C (2) together with TopoVI SSA triple mutant (3). TopoVI subunits are denominated with A and B. No free dye was observed (D).

Continued on following page.

115

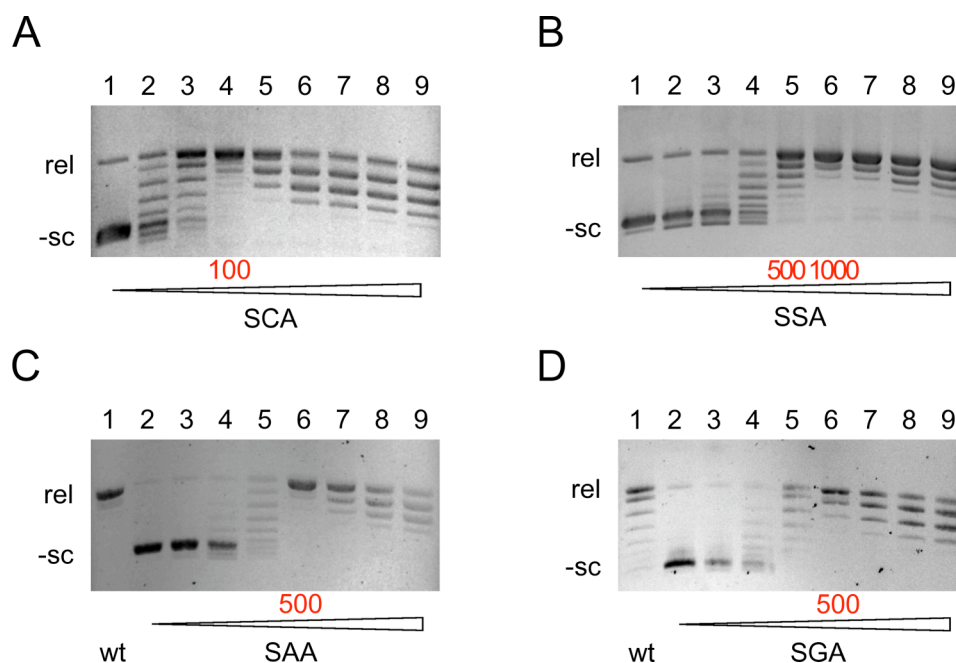**C – G:** Plasmid DNA relaxation activity by TopoVI FRET mutants. Plasmid and nucleotide concentrations were 15 nM and 1 mM, respectively. Bands corresponding to neg. supercoiled and relaxed pUC18 plasmid are denominated –sc and rel, respectively. Protein concentrations resulting in maximal plasmid relaxation are mentioned (red). Reactions were performed in TopoVI activity buffer (section 3.2.2).
**C, D and F:** Plasmid relaxation by FRET mutants D159C, E164C and double labeled E164C, respectively. Lane 1: Relaxation by 50 nM TopoVI wt as a control. Lanes 2 – 9:  Relaxation with TopoVI mutants at concentrations of 0.02, 0.05, 0.1, 0.2, 0.5, 1.0, 2.0, and 5.0 μM.
**E, G:** Plasmid relaxation by FRET mutants P408C and R87C, respectively. Lane 1 and 2: Reactions in absence and presence of 50 nM TopoVI wt as a control. Lanes 3 – 9:  Relaxation with TopoVI mutants at concentrations of 0.1, 0.2, 0.5, 1.0, 2.0, 5.0, and 10.0 μM.


### 3.2.13  Conformational changes in the ATPase-gate of TopoVI revealed by smFRET

TopoVI FRET mutants R87C, E164C and P408C have been validated for smFRET experiments. Although mutant D159C exhibited a decreased plasmid relaxation activity, it was also considered for smFRET measurements. Experiments were performed at 37°C in activity buffer lacking DTT. FRET efficiencies were corrected with average correction parameters for the dye pair A488 / A546 (Tab. 3.2, section 3.1.13).


### 3.2.14  Nucleotide-induced locking of the ATPase domains

First, experiments were performed with double-labeled TopoVI free from ligands with the concentration of the donor dye fixed to 50 pM. Mutants E164C and D159C showed medium FRET efficiencies and broad distributions, indicating high flexibility of the inter-dye distance (Fig. 3.38A, B). This finding was supported by the data from mutant R87C, which showed a FRET efficiency distributed between 0.1 and 0.9 with two small maxima at 0.3 and 0.9 FRET efficiency (Fig. 3.38B). These results suggest significant conformational freedom of the ATPase domains in the ligand-free state.

Addition of 4 mM ADPNP to mutant E164C did not shift the FRET peak, but resulted in a narrowed FRET efficiency distribution compared to the free enzyme, indicating the restriction of the inter-dye distance and thus of the ATPase domains. For mutant R87C, population of a high-FRET state with a maximum of approx. 0.85 was observed in presence of 4 mM ADPNP, suggesting a decrease of the inter-dye distance well below the Förster distance of 5.5 nm (Fig. 3.38C). As ADPNP was proposed to promote dimerization in the ATPase domains [62], this state should reflect the closed gate. Addition of 4 mM ATP to mutant E164C did not yield a defined FRET efficiency distribution, but the mean efficiency seemed to remain unchanged compared to the free enzyme (Fig. 3.38D). A reason for this behavior could be ATP-hydrolysis dependent opening and closing of the domain.

In contrast to FRET from labels located in the upper ATPase-gate region, the FRET efficiency for dyes coupled to the mutant P408C showed a narrow distribution with a defined maximum at approx. 0.1, indicating a rather fixed inter-dye distance of more than 7 nm (Fig. 3.38B). No change in FRET efficiency was observed upon addition of up to 10 mM ADPNP or ATP to the enzyme, suggesting a constant distance between the lower ATPase regions even upon potential dimerization of the upper ATPase domains (Fig. 3.38C, D).

### 3.2.15 Opening of the ATPase gate in presence of supercoiled plasmid

Data presented in the previous section suggest dynamic opening and closing of the ATPase domains in absence of nucleotides. We wanted to know whether this conformational flexibility was influenced by binding of a large DNA, in this case neg. supercoiled pUC18 plasmid. Plasmid DNA was added in concentrations between 30 and 40 nM. Interestingly, the mutant E164C exhibited a strong FRET efficiency shift from medium values in the ligand-free state to almost 0 for the protein-DNA complex. A similar effect, albeit less pronounced, was observed for the R87C mutant: The FRET efficiency was still distributed between values of 0 and 0.95, but with a clear shift toward lower FRET efficiencies. These results indicate an opening of the ATPase-gate upon binding of supercoiled plasmid, but also considerable conformational freedom in the ATPase domains, similar to the one seen in ligand-free enzyme.

In mutant P408C, addition of 50 nM DNA resulted in broadening of the histogram and a slight shift of the peak to 0.2 FRET efficiency. Also a small high-FRET population was observed. Both could be due to steric hindrance of the DNA with the fluorescent labels, as the latter should face the central cavity that is thought to be occupied by the bound DNA.

In mutant D159C addition of 50 nM plasmid DNA resulted in a shift of the FRET efficiency to approx. 0.7, suggestive of a decrease of the inter-dye distance. This result disagrees with the findings for mutants E164C and R87C, but could be due to the altered enzymatic activity of mutant D159C.
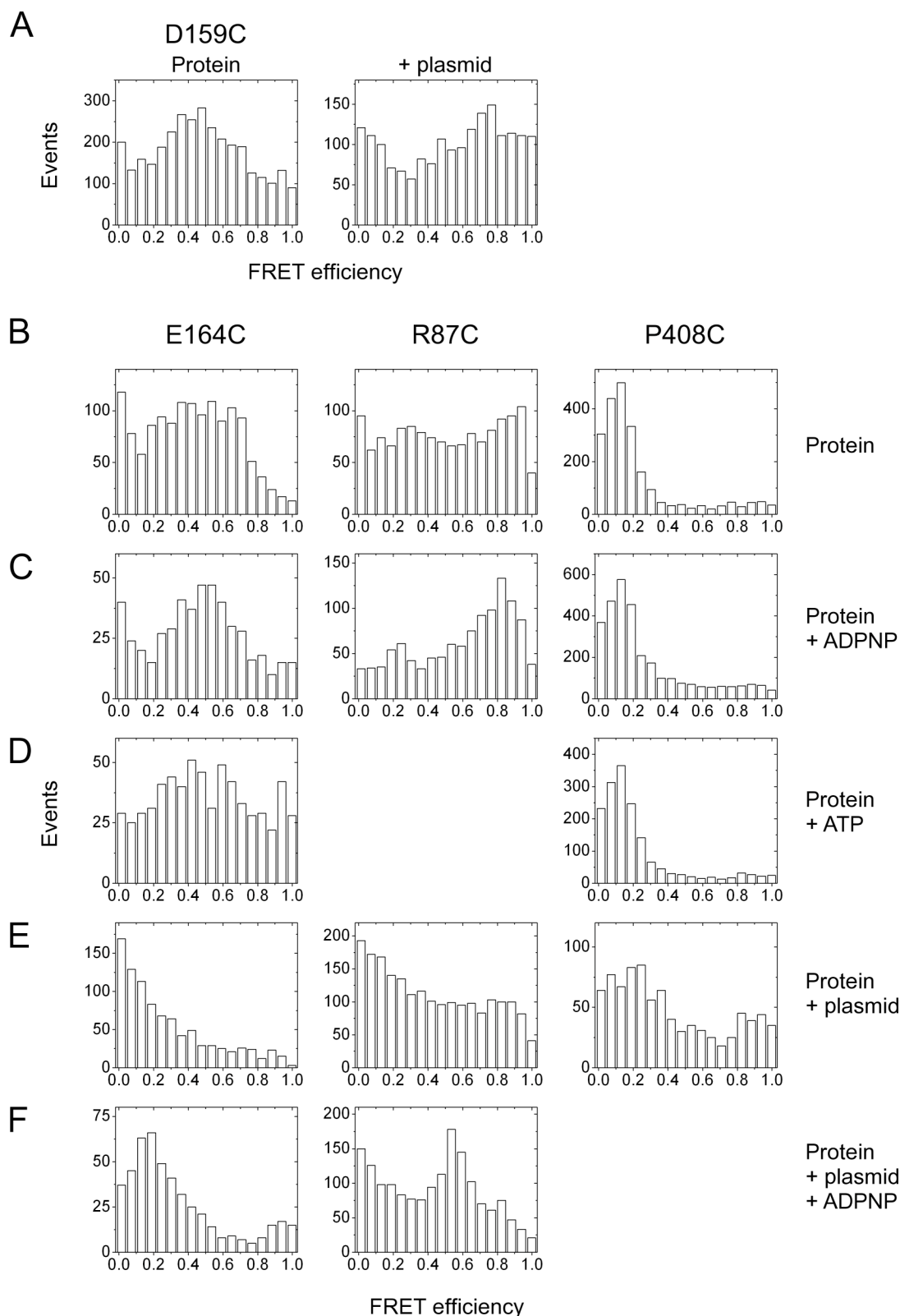
**Fig. 3.38:** SmFRET histograms for TopoVI mutants labeled in the ATPase gate region and their complexes with neg. supercoiled DNA and the nucleotides ADPNP and ATP.
**A:** Histograms for TopoVI D159C in the ligand-free state (left) and bound to DNA (right).
**B – F:** FRET efficiency histograms of complex formation for TopoVI mutants fluorescently labeled at different positions in the ATPase domains (left to right): Mutants E164C and R87C with labeling sites in the upper region of the ATPase domains, and P408C labeled in the lower ATPase domains.
**B:** Histograms for the ligand-free TopoVI proteins; **C and D:** Histograms for TopoVI in presence of ADPNP or ATP; **E:** Histograms for TopoVI in complex with neg. supercoiled plasmid; **F:** Histograms for the protein-DNA complex in presence of ADPNP.

### 3.2.16 ADPNP induces a fixed ATPase gate conformation in presence of plasmid DNA

Addition of ADPNP to the protein-plasmid complex lead to well-defined FRET efficiency peaks both in the E164C and R87C mutants. Maxima were found at values of approx. 0.2 and 0.6, respectively, which were clearly different from the ones found for the protein in presence of ADPNP, but without DNA, indicating a locked but open conformation of the ATPase domains. In case of E164C the low-FRET distribution for the complex in absence of nucleotide completely disappeared, while for R87C the low-FRET state was still populated. This could be due to the different ADPNP concentrations used (10 and 4 mM, respectively).

The fixed conformation of the ATPase gate in the tripartite complex of TopoVI with supercoiled plasmid and ADPNP was independent of the order of addition (DNA first, ADPNP second, or *vice versa*), indicating only transient closure of the ATPase gate by ADPNP to allow binding of the plasmid to TopoVI.

# 4. Discussion

## 4.1 Part I: Conformational changes in the C-terminal domain of GyrA from *B. subtilis*

### 4.1.1 The C-terminal domain of *B. subtilis* GyrA confers supercoiling activity

One major goal of this work was to monitor conformational changes in the C-terminal domain of GyrA and characterize the influence of the CTD on the DNA-binding properties of GyrA. Full-length GyrA from *B. subtilis* and a truncated version lacking the C-terminal domain (GyrA_ΔCTD) were expressed as N-terminal His$_6$-tag fusion constructs cleavable by TEV protease and purified by immobilized-metal affinity chromatography. This purification strategy was recently reported for GyrA from *A. aeolicus* and previously attempted but not achieved for the full-length *B. subtilis* enzyme [102, 103]. Gyrase from *B. subtilis*, constituted from the subunits GyrA and GyrB, exhibits nucleotide-independent DNA relaxation as well as ATP-dependent DNA supercoiling activity, similar to its counterpart from *E. coli* [18, 36, 104]. Deletion of the CTD of *B. subtilis* GyrA abolishes the DNA supercoiling activity and strongly reduces the nucleotide-independent DNA relaxation activity. However, GyrA_ΔCTD exhibits an ATP-dependent DNA relaxation activity which is approx. 5 times faster than the relaxation activity of the full-length enzyme, showing a comparable final topoisomer distribution (sections 3.1.3 and 3.1.5). These findings give evidence that the GyrA CTD is indispensable for the supercoiling activity gyrase in *B. subtilis*. The behavior is also found in *E. coli* gyrase: Deletion of the GyrA CTD results in the above-mentioned activity change. Additionally, it strongly enhances decatenase activity in an ATP-dependent manner, indicating a similar enzymatic activity for GyrA_ΔCTD as found in topoisomerase II and IV [105, 106].

### 4.1.2 Fluorescently labeled GyrA constructs to monitor conformational changes in the CTDs

Type IIA topoisomerases transport a double-stranded DNA through a transiently cleaved second DNA duplex bound to a region termed DNA-gate, thereby exhibiting tightly controlled sequential opening and closing of three gates. Conformational changes in the ATPase-gate and the DNA-gate of gyrase and TopoII have been monitored by smFRET techniques [33, 42, 43] and were proposed also for the C-gate of gyrase and topoisomerase II [44, 95]. Apart from gate dynamics typical for all type IIA topoisomerases, gyrase was

proposed to exhibit movements of the GyrA CTDs in response to DNA binding, resulting in the delivery of the T-segment for transport through the transiently cleaved G-segment [57, 107]. To monitor potential conformational changes in the GyrA CTD two approaches were used: (1) *B. subtilis* GyrA with a single cysteine mutation in the C-terminal domain was expressed and produced as described before [46]. The mutants can be readily labeled with fluorescent dyes and exhibits wild-type like DNA supercoiling and relaxation activity both in their non-modified and labeled states, validating them for smFRET studies (section 3.1.11). As GyrA is a constitutive dimer [108], the isolated protein complex contains two equivalent free thiols symmetrically arranged in the CTDs. One limitation is the large distance between the CTDs (illustrated by the distance of the attachment points of the CTDs on the GyrA body of $\geq$ 9 nm) almost beyond the dynamic range of fluorescence resonance energy transfer, making the reliable determination of inter-dye distances difficult. Indeed, FRET efficiencies for labeled single-cysteine mutants in the free GyrA dimer are 0.3 and 0.2 for GyrA mutants K570C and K594C, respectively, and even close to 0 for D695C and E726C (Fig. 3.15). A second disadvantage of the symmetrical GyrA FRET constructs is the simultaneous observation of the movements of two CTDs. It is not possible to assign potential shifts in FRET efficiency and corresponding conformational changes to one domain, and FRET efficiency histograms could exhibit increased complexity due asymmetric behavior of the complex.

(2) To avoid the drawbacks of the GyrA with equivalent labeling sites, asymmetric GyrA dimers were developed. Two different versions of GyrA were co-expressed in *E. coli*, randomly assembling to homo-dimeric complexes of either species or to hetero-dimeric complexes containing one GyrA subunit of each version. Wild-type like GyrA was expressed as an N-terminal His$_6$-tag fusion protein, while the other GyrA version was non-tagged, but contained two cysteines, one on the GyrA body and one on the CTD. By means of Ni$^{2+}$-affinity chromatography homo-dimeric wild-type like and hetero-dimeric proteins were separated from homo-dimeric non-tagged proteins. SmFRET measurements of labeled hetero-dimeric GyrA resulted in unimodal well-defined FRET efficiency distributions, giving evidence that homo-dimeric protein consisting from mutant subunits is efficiently removed. Fluorescent labeling of the co-expression product shows nominal labeling degrees of approx. 100 % (i.e. approx. 2 dye molecules per GyrA dimer), indicating a low fraction of homo-dimeric wt GyrA.

GyrA hetero-dimeric proteins containing mutant subunits T140C_K570C, T140C_K594C, E211C_K570C, E211C_K594C, E250C_K570C, and E250C_K594C were validated for smFRET experiments. All of them exhibit wild-type like DNA supercoiling and relaxation

activities both in their non-modified and labeled states. In principle the test does not give evidence that the mutant subunit confers wild-type like activity, as the wild-type CTD might compensate for a potential loss of function of the modified, mutant partner CTD (e.g. loss of wrapping, sterical clashes between the DNA and the fluorophores). However, all homo-dimeric single-cysteine mutants show unaltered DNA supercoiling and relaxation activities, thus validating the use of the hetero-dimeric GyrA proteins for smFRET experiments.

### 4.1.3   Localization of the GyrA CTDs by molecular triangulation

To localize the GyrA CTDs relative to the cleavage-religation domain („GyrA body") different GyrA constructs were fluorescently labeled with A488 and A546 dyes and the inter-dye distances calculated from single molecule FRET data, a procedure performed previously in a localization study with YxiN helicase [66]. By triangulation of distances between three reference points on the GyrA body and two on the CTD it was possible to localize the N-terminal part of the CTD in the ligand-free state and in the DNA-gyrase complex.

In the free GyrA dimer positions 570 and 594 on the second sector (blade) of the CTD are located close to the extended α-helices linking the C-gate to the G-segment-binding part of the enzyme, consisting of the cleavage-reunion domain and the tower domain (Fig. 3.20A) [108]. Uni-modal FRET efficiency distributions indicate a well-defined position of the CTDs. Positioning of the residue 695 on the CTD could give a hint to where the lower part (blades 4 and 5) of the CTD could reside: As estimated from smFRET data the inter-dye distances from labeling positions 140_695 (DNA-gate_CTD) and 408_695 (C-gate_CTD) are approx. 5.5 and more 7.5 nm, respectively (Fig. 3.21A); the distance between positions 594 (as determined by triangulation) and 695 on the CTD should be around 3 nm (after [50]), placing residue 695 lateral of the DNA-gate (Fig. 4.1A). Our model localizes the CTD in a similar position as a model derived from SAXS data [57] (Fig. 4.1C).

In gyrase bound to plasmid, the N-terminal part of the CTDs is located further away from all reference points on GyrA body used for triangulation: Distance changes of the reference points 570 and 594 upon formation of the gyrase-DNA complex are calculated as 2.6 and 2.5 nm, respectively (Fig. 3.20B, Fig. 4.1B). This finding indicates a ligand-induced conformational change of the CTD to a more extended position with respect to the GyrA body compared to non-complexed GyrA. Additional evidence for a movement of the CTDs is given by the reduction in FRET efficiency between labels attached to the C-gate (N399C) and the CTD (K594C) (Fig. 3.21A) and between two labels attached to the both CTDs in position 594

(Fig. 3.22A, D), indicating distance increase between the C-gate and the CTDs as well as between the two CTDs upon formation of the gyrase-DNA complex. A number of FRET efficiency distributions from measurements of GyrA in complex with GyrB and plasmid DNA exhibit bi-modal behavior, which could be interpreted in a sense that the CTDs can occupy two different positions; however, this effect is not systematically observed for all GyrA constructs, indicating that the CTDs rather adopt one defined conformation. The cause for bi-modal FRET efficiency distributions is not known.

FRET histograms for mutants T140C_D695C and T408C_D695C do not exhibit a large change (Fig. 3.21A), indicating only minor movement of blade 4 of the CTD (represented by residue 695) relative to the GyrA body, placing it in position similar to the one in ligand-free GyrA (Fig. 4.1). This model places the CTD such that the loops from blades 1, 4, 5, and 6 are facing away from the GyrA body (Fig. 4.1D). This part of the circular rim of the CTD is proposed to bind DNA due to its negative charge, thus introducing a sharp turn into the double helix [49]. The model derived from our smFRET data seems to fit the suggested path of the DNA: The G-segment extending from the binding site at the DNA-gate is wrapped around the CTD in a turn of approx. 180° and delivered as a T-segment to the upper cavity, spanned by the ATPase- and the DNA-gate of gyrase.

The conformational change of the GyrA CTDs upon formation of the gyrase-DNA complex was proposed previously [43, 49, 57], but has not been observed so far in gyrase. The CTD was suggested to adopt a conformation extended along the axis connecting the tower domains, resulting in the lower part of the CTD facing away from GyrA body. However, smFRET data from the mutant T140C_D695C argue against such a conformation, suggesting a position of the lower CTD region within a distance of 4 – 6 nm from the DNA-gate.

A recent structural model of gyrase in complex with a 140bp DNA, based on SAXS data, places the CTDs close to the C-gate, away from the catalytic core [58]. Our smFRET data clearly argue against such a conformation, placing both the upper and the lower part of the CTDs in (1) proximity of the DNA-gate and (2) at a distance of more than 7 nm from the C-gate.
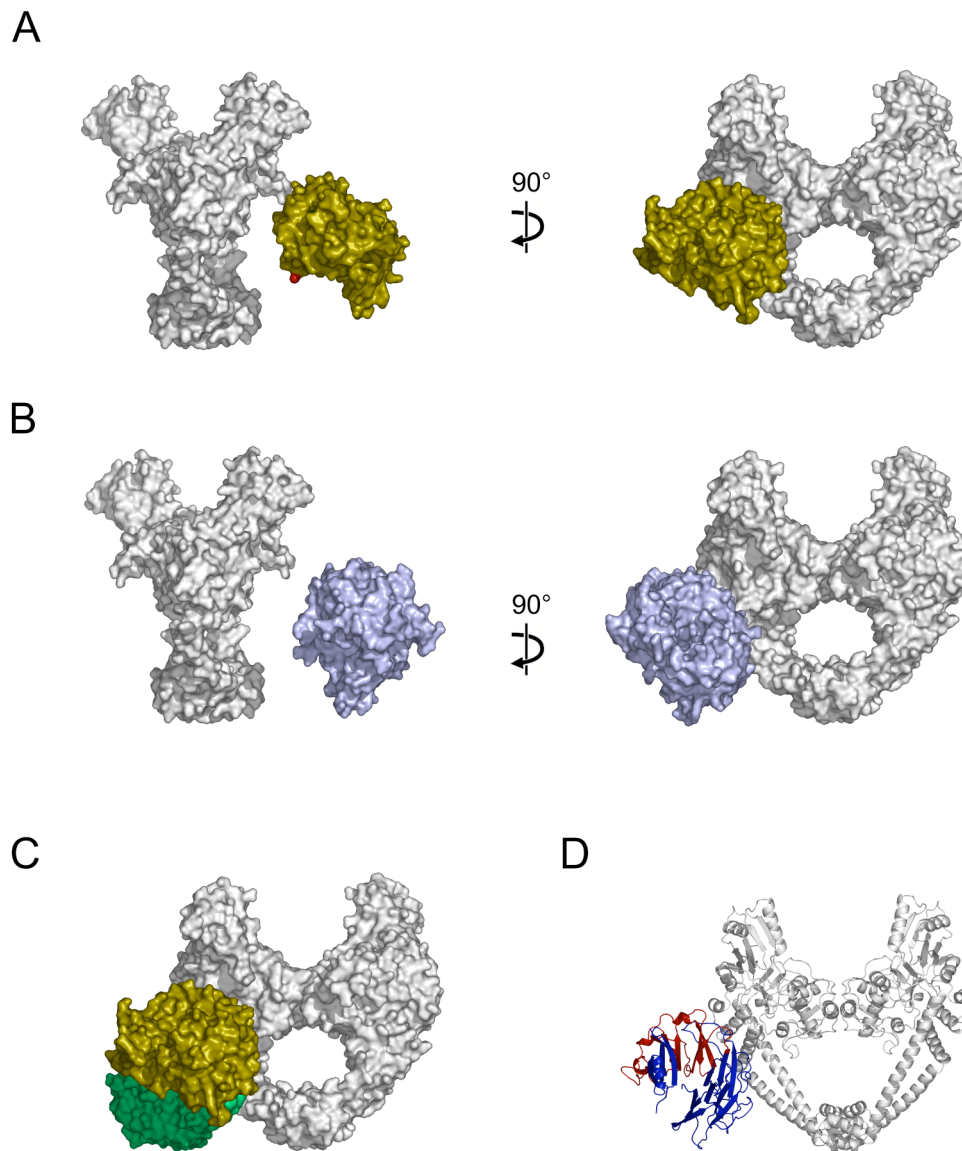
**Fig. 4.1:** Localization of the GyrA CTD (in color) relative to GyrA core (grey). Presented *B. subtilis* GyrA core and CTD structures are homology models of structures of individual subunits of *E. coli* GyrA (PDB entries: 2Y3P and 1ZI0 [50, 94]).

**A and B:** Side (left) and front views (right) with CTD positions placed relative to GyrA according to smFRET data. In the uncomplexed GyrA, the CTD adopts a contracted conformation lateral to the catalytic core domain (**A**). In the gyrase-DNA complex (GyrB and DNA not shown) it swings away from the GyrA core domain to a slightly extended conformation (**B**).

**C:** Structural alignments of models for full-length GyrA, derived from smFRET (yellow CTD) and SAXS data of *E. coli* GyrA (green CTD) [57]; GyrA cores are aligned. The proposed CTD conformations are in good agreement, as both models place the domain lateral to GyrA core. However, the FRET-model shows a slight rotation of the CTD relative to the SAXS model.

**D:** Cartoon representation of full-length GyrA as in gyrase-DNA complex (equivalent to B, right). CTD blades 2 and 3 (red) face the GyrA core domain, while 1, 6, 5, and 4 (blue) are positioned to wrap DNA. This CTD position is supported by structural data: This region is highly negatively charge and was therefore suggested to constitute the main DNA interaction site on the CTD [49].

### 4.1.4 Potential errors in the determination of spatial arrangements of GyrA subunits by smFRET

The accuracy of positioning the mutated amino acid residues K570C and K594C by means of measuring energy transfer between fluorescent labels attached to the thiols is limited by factors of structural and photophysical nature of the fluorescent dyes:

(1) In FRET measurements we determined several inter-dye distances. For the localization of labeled residues, the position of the dye and its attachments point on the thiol were assumed to colocalize (in reality the fluorophore is thought to tumble in proximity of its attachment point). This simplification results in localization error that should be in the range of the linker length of the fluorescent dye (approx. 1 nm). However, the change in FRET efficiency observed for all the mutants involved in triangulation of positions 570 and 594 on the CTD is trustworthy, as the labeling positions on the protein were chosen such that the position of the dyes relative to the attachment sites on the protein should be the same in the ligand-free GyrA and the in the gyrase-DNA complex. Thus FRET efficiency changes should just depend on the relative orientation of the GyrA core and C-terminal domains.

(2) Following statistical double-labeling (i.e. labeling with two different dyes at the same time), hetero-dimeric GyrA constructs containing two different labeling sites are assumed to exhibit statistical labeling distributions of the two cysteines. Out of technical reasons, labeling with two dye molecules of the same species results either in a FRET efficiency below 0 (for protein labeled with donor only) or in a peak of FRET 1 (for protein labeled with acceptor only) that is often not detected. The relevant protein species labeled with one donor and one acceptor dye each exhibit two different dye arrangements. SmFRET data are corrected for photophysical properties of either one or the other dye arrangement, resulting in slightly different histograms, corresponding to two different apparent inter-dye distances (Fig. 3.16, 3.17, 3.19). The two values indicate a possible distance range, within which the real mean distance of the dyes should fall. In the ligand-free state and the gyrase-DNA complex, differences in inter-dye distances calculated for either dye arrangement do not exceed 0.4 nm, with the exception of the mutant T140C_K570C in free GyrA and T140C_K594C in the gyrase-DNA complex of 0.7 nm each. This variation can be taken as a systematic error in the determined inter-dye distances, resulting in a decreased positioning accuracy. As the distance variations are small (less than 10 %), the qualitative description of the CTD movement should be trustworthy.

(3) The Förster distance used to calculate the inter-dye distance from the corresponding FRET efficiency is a function of the orientation factor $\kappa$ and the diffraction index $n$ (among other parameters: eq. 2.25), describing the local flexibility of the transition dipoles of the

fluorescent dyes and the diffraction index of the medium between them, respectively. They were not determined, but set to idealized values: (a) $\kappa^2$ could be determined in anisotropy decay measurements, but was set to 2/3, assuming complete motional freedom and thus random orientation of the dyes [86]. Theoretically, $\kappa^2$ can adopt values between 0 and 4 (corresponding to perpendicular and parallel arrangement of the dipoles), but the assumption of rotational averaging of the dipole alignments is reasonable as already rotational flexibility of one dye should minimize the error in the Förster distance to less than 10 % [109]. (b) The refractive index of the medium between the fluorescent dyes was approximated to with the one for water (n = 1.33), not taking into account the potential presence of peptide structure between the dyes [87]; however, as a large fraction of the transition dipole field should occupy an aqueous environment, this simplification should be reasonable.

The uncertainty of the dye position relative to the protein, statistical labeling of non-equal cysteine positions and difficulties in the determination of the Förster distance for a given dye pair affect the accuracy of the absolute positioning of the domain, but not the conclusion that the GyrA CTDs adopt an extended conformation upon binding of plasmid DNA and GyrB to GyrA.


### 4.1.5   Assembly of the gyrase-DNA complex

In the previous sections the conformational change of the CTDs from a rather contracted state in the ligand-free protein to an extended state in the gyrase-DNA complex has been discussed. The effect of DNA or GyrB binding to GyrA on the conformation of the CTD was addressed in anisotropy experiments and smFRET measurements.

As demonstrated in DNA anisotropy titrations of full-length GyrA and GyrA_ΔCTD to a linear 60bp DNA clearly show the contribution of the CTDs to DNA binding (Fig. 3.5A): While binding of the DNA to the GyrA body is only weak, the DNA-GyrA complex is drastically stabilized in the full-length GyrA, indicated by the 20- to 35-fold increase in affinity. This finding agrees with previous observations [91]. However, from these experiments it is not clear whether the DNA almost exclusively binds to one CTD or complexes simultaneously several binding sites, i.e. one CTD and the DNA gate, or both CTDs and the DNA gate. Binding of two DNAs to the individual CTDs in one GyrA dimer could be possible, but is rather unlikely due to the concentration ratio DNA : GyrA of up to 1000. The findings indicate that the CTDs are the main DNA binding sites in GyrA.

The effect of DNA binding to GyrA on the CTD conformation was determined using neg. supercoiled plasmid. Three different GyrA constructs showed a broadening of the FRET

efficiency distributions upon formation of the GyrA-DNA complex, indicating a conformational change of the CTDs (Fig. 3.22C). Saturating conditions were confirmed, as 5-fold increase of the DNA concentration did not result in a change of the FRET efficiency distribution for mutant T140C_K594C. The broadening of the distribution is an indication for conformational dynamics: T140C_K594C shows a bimodal FRET efficiency distribution with maxima similar to the ones found in non-complexed GyrA and in the gyrase-DNA complex, clearly indicative of some CTDs adopting an extended conformation. Together with the anisotropy results, this finding suggests that the conformational change is due to simultaneous binding of the DNA to the CTD and core domain of GyrA. As the DNA-affinity of the GyrA core is small, this bridging interaction might be transient, causing the CTDs to swing back in the contracted conformation. From these data it is not clear, if the observed heterogeneity CTD conformation is due to asymmetric behavior of the two CTDs in one complex, or if it is caused by conformational change in all CTDs.

However, it is clear from these results that DNA binding to GyrA induces conformational change in the CTDs, but is not sufficient for the completely extended conformation found in the gyrase-DNA complex. This finding again indicates that GyrB is necessary to induce a stable extended CTD conformation.

The formation of the gyrase complex in absence of DNA has not been extensively studied so far. Our smFRET data of GyrB binding to labeled GyrA (Fig. 3.22B) indicate a partial release of the CTDs resulting in a slightly less contracted conformation than in GyrA, but clearly different from the one in the gyrase-DNA complex (Fig. 3.22A, C). There has been no report of direct physical interaction between the GyrA CTDs and GyrB, leaving only speculation what the cause for the conformational change might be. (1) Structural rearrangement of GyrA in the DNA gate leading indirectly to higher distances between the fluorescent labels cannot be excluded, but is not very probable: Gate opening has not been observed under physiological conditions [33], indicating that the open state is barely populated. In addition, X-ray structures of the GyrA-body dimer in the absence and presence of GyrB-TOPRIM domain do not show structural rearrangement in GyrA, indicating a very rigid and stable fold [28, 108]. (2) More likely seems a non-specific interaction between the GyrA CTDs and GyrB bound to GyrA. GyrB subunits bind to GyrA DNA-gate region via the TOPRIM domains, which occupy the sides of the heart-shaped GyrA dimer. In our model of ligand-free GyrA (Fig. 4.1A), the CTDs are located at some distance of the GyrA body. However, considering the significant conformational flexibility of the lower part of the CTDs with respect to the GyrA core and potential inaccuracies in domain localization, the structural space of the CTDs might overlap with the location of the TOPRIM domains on GyrB and result in sterical clash

between the CTD and GyrB upon complex formation. As a result, GyrB would displace the GyrA-CTD by pushing them into a slightly extended conformation.

Formation of the gyrase-DNA complex from the individual components is thermodynamically favored, as shown by the 35-fold affinity increase of GyrA to the 60bp DNA in the presence GyrB compared to the DNA only. A similar effect is observed for GyrA_ΔCTD (25-fold affinity increase), giving two important hints: (1) In gyrase, the 60bp DNA clearly binds to the DNA-gate and stabilizes the gyrase complex. (2) The 60bp DNA simultaneously contacts the GyrA CTDs. A longer circular DNA should thus also contact both CTDs. This hypothesis is supported by measured FRET efficiencies of close to 0 for all three constructs mentioned above (Fig. 3.22D). For some hetero-dimeric constructs (e.g. for mutant T140C_K570C: Fig. 3.19), bi-modal distance distributions were observed, which could indicate conformational heterogeneity of the CTDs and possible asymmetric behavior of the two CTDs in one gyrase-DNA complex, as mentioned in section 4.1.3. As the effect is not systematically observed, it is save to state that both CTDs in the gyrase-DNA complex adopt an extended conformation. The highly dynamic (and potentially asymmetric) state of the CTDs observed for the GyrA-DNA complex is mostly abolished in the presence of GyrB.

### 4.1.6 Influence of the conformation, topology and length of DNA substrates on the CTD conformation

Gyrase is a DNA manipulating enzyme, introducing neg. superhelicity to (circular) DNA in an ATP-dependent manner. Before the actual supercoiling reaction, characterized by the DNA strand passage, the CTD binds and wraps DNA extending from the DNA-gate [110], thereby undergoing a conformational change to present the T-segment to the cavity between the ATPase- and the DNA-gate. SmFRET experiments elucidate the links between movement of the CTDs and events up- and down-stream in the supercoiling cycle.

The DNA bound to the DNA-gate of gyrase (G-segment) exhibits different levels of distortion, depending on cleavage of the DNA double strand and the formation of the covalent tyrosyl-DNA intermediate [33]. The cleavage-deficient mutant Y123F clearly shows movement of the CTDs to an extended conformation upon binding of plasmid DNA and GyrB, supported by the observation of simultaneous binding of the DNA to the DNA-gate and the CTDs (Fig. 3.26A, C). However, conformational differences in the DNA extending from the DNA gate should result in a different direction of the DNA relative to the enzyme, which in turn should influence the position of the CTD upon gyrase-DNA complex formation. Indeed, the FRET efficiency maximum for the cleavage-deficient GyrA mutant (Y123F) in

complex with GyrB and supercoiled plasmid exhibits a slight, but reproducible shift of approx. 0.05 compared to wt GyrA, indicating a small conformational difference of the CTDs in the absence of DNA cleavage and distortion.

In a further step, the influence of the topology of a plasmid substrate on the CTD position was tested. The CTD conformations are the same for all complexes of GyrA with negatively supercoiled and relaxed plasmid (Fig. 3.22, in comparison with Fig. 3.2). The CTDs have been proposed not to bind to supercoiled DNA and to remain in the contracted conformation, potentially resulting in a CTD- and thus wrapping-independent DNA relaxation mode [57]. Our data argues against this model as neg. supercoiled DNA induces a similar extended conformation of the CTDs as relaxed DNA. However, smFRET measurements addressing the ATPase-gate dynamics in gyrase showed that DNA wrapping and presentation of the T-segment to the enzymatic core by the CTD is less efficient for neg. supercoiled than for relaxed DNA [42]. This raises the question, if the conformational change observed for the CTDs is due to wrapping of the DNA around the domain or mere simultaneous contact of the DNA to the DNA-gate and the CTDs.

In order to understand the link between CTD movement and events like DNA wrapping and T-segment presentation, linear double-stranded DNAs were used as substrates for gyrase. In presence of GyrB a DNA of 37 bp length binds to the DNA-gate without contacting the CTDs. In contrast a 48bp DNA is long enough to simultaneously offer binding sites to the DNA-gate and the CTDs (Fig. 3.8). This finding is supported by data from hydroxyl-radical footprinting using a 147bp DNA that clearly show protection of a central 40bp region by GyrA, which is supposed to be excluded from the solvent [107]. Moreover, binding of a 37bp DNA to gyrase does not influence the conformation of the CTD, indicating that the FRET efficiency shift is caused by binding of GyrB only (Fig. 3.25). This finding indicates, that (1) GyrB is not responsible for the extended conformation of the CTDs, but only for the stabilization of the gyrase-DNA complex; (2) simultaneous contact of DNA to the DNA-gate and the CTDs is necessary to induce the extended conformation of the CTDs.

Surprisingly, in the presence of GyrB the 48bp DNA induces the CTDs to adopt the extended conformation, indicating that only a very small DNA-CTD interface is necessary to induce CTD movement. SmFRET studies of the ATPase-gate have shown, that linear DNAs of 110 bp and longer completely wrap around the CTDs and possibly present a T-segment to the GyrB cavity, whereas shorter DNAs do not serve as T-DNAs. Apparently the movement of the CTD does not require extensive wrapping of the DNA and is independent of potential T-segment presentation.

Taken together, in the gyrase-DNA complex the CTDs adopt an extended conformation independent of the conformation or the topology of the double-strand bound to the DNA-gate, the DNA length, the extent of wrapping and potential T-segment presentation. Thus, the role of the CTDs can be reduced to binding of DNA and facilitating the geometry of an arbitrary DNA substrate in order to present a T-segment.

### 4.1.7  The role of the CTDs during strand passage

A very important point in understanding the supercoiling activity of gyrase would be the observation of strand passage. Binding of ATP to type II topoisomerases induces dimerization of the ATP-domains, while the hydrolysis and phosphate release of the first and the second nucleotide is supposed to induce strand passage and resetting of the enzyme for another supercoiling cycle, respectively [45, 47]. Somewhat contradictory, binding of the non-hydrolysable ATP analog ADPNP to gyrase has been found to allow one strand transfer step; as phosphate release cannot take place, the enzyme should be stalled with a closed ATPase-gate [111]. Binding of ADPNP to the gyrase-DNA complex results in a loss of DNA wrapping, which was taken as an indication for a loss of interaction between DNA and CTD [48]. A potential release of the CTDs should result in a contracted conformation similar to the one in the complex of gyrase with the 37bp DNA. However, addition of ADPNP to the gyrase-plasmid complex does not result in a FRET-efficiency change: In all tested mutants (Fig. 3.22E), using supercoiled or relaxed plasmid DNA, the CTDs remain in the extended conformation. Two explanations could be given for the fact, that no release of the CTDs is observed: (1) Conformational change of the CTDs connected to strand transfer is not detected, because gate opening and connected to this CTD movement is a transient and very rare event. (2) Or the CTDs do not follow the passage of the T-segment towards the C-gate of the GyrA body, remaining in the extended conformation during strand passage.

Not surprisingly, the CTDs in the cleavage-deficient gyrase bound to DNA do not move in presence of ADPNP, proving that the extended conformation of the CTDs is not affected by ATPase-gate movements upon nucleotide binding. However, CTD movement at later stages of the supercoiling cycle cannot be excluded as discussed above.

### 4.1.8 Deletion of the GyrA-box abolishes the supercoiling activity by gyrase despite only minor changes in the DNA-binding of the CTDs and its conformations

The GyrA CTD contains a highly conserved and positively charged heptapeptide sequence known as the GyrA-box. The region is part of a peripheral loop bridging the gap between the first and the sixth blade of the β-pinwheel fold, probably stabilizing a spiral assembly of the blades [38]. Deletion or substitution of the GyrA-box in *B. subtilis* gyrase results in a completely changed enzymatic profile unique among type II topoisomerases: The mutants exhibit wild-type like nucleotide-independent DNA relaxation activity, but no residual ATP-dependent DNA supercoiling [55]. Binding of a 60bp DNA and neg. supercoiled plasmid to the A-box deletion mutant in absence of GyrB do not show a significant difference to wild-type GyrA. However, in contrast to wt GyrA no conformational change of the CTDs is observed upon binding of neg. supercoiled plasmid to GyrA, indicating that no bridging interaction of the DNA between DNA-gate and CTD takes place in the A-box-deletion mutant. A possible explanation would be that the GyrA-box introduces a kink into DNA to contact both GyrA core and CTD, as proposed before [112]. Considering the small difference in DNA affinity compared to the wt protein, we can conclude that, in the absence of GyrB, GyrA binds to DNA mainly via the CTDs, and that the GyrA-box might be involved in DNA-bridging interactions to the DNA-gate.

In presence of GyrB, however, the binding to linear or circular DNA and the resulting CTD conformation are the same for GyrA wt and the A-box deletion mutant. This finding argues against the hypothesis, that the primary function of the GyrA-box might be the complexation of DNA. A possible function, as already proposed, could be the stabilization of the spiral β-pinwheel fold and guidance of the DNA to serve as a T-segment [38], indicated by the loss of inducing positive supercoils into DNA upon deletion of the GyrA-box.

### 4.1.9 The role of the GyrA CTDs in DNA supercoiling catalyzed by gyrase

The present work contributes to the understanding of the events during the ATP-dependent DNA supercoiling cycle in gyrase, a unique bacterial type II topoisomerase. Formation of the active enzyme complex is initiated either by binding of the GyrA dimer to the DNA, with the CTDs being the main interaction sites, and the subsequent binding of two GyrB subunits to form a high-affinity complex; or by binding of GyrB to GyrA and later simultaneous binding of a DNA to the DNA-gate and the CTDs. The conformation of the GyrA-CTDs is influenced by both DNA and GyrB. While bridging of the GyrA body domains and CTD by the DNA is the main driving force for the movement of the CTDs to an extended conformation, GyrB

only slightly displaces the CTDs in the gyrase and mainly stabilizes the complex with DNA (Fig. 4.2; A).

A small contact of the DNA to the CTD of only several nucleotides length initiates the conformational change of the CTDs, which, as a result, wrap the DNA around their periphery in a turn of 180° and deliver the extending strand, i.e. the T-segment, to the cavity formed by the two GyrB-ATPase domains. Upon nucleotide binding, GyrB dimerizes, thereby closing the ATPase-gate over the T-segment and stabilizing the hetero-tetrameric protein complex. The G-DNA bound to the DNA-gate exhibits different states of distortion, being cleaved and re-ligated by the active site tyrosines located on GyrA; DNA cleavage and distortion results in small changes in the extended conformations of the CTDs. Simultaneous closure of the ATPase-gate and DNA cleavage will eventually lead to sequential opening of the DNA- and the C-gate and concomitant transport of the T-segment through the gap of the cleaved G-DNA segment, followed by the hydrolysis of ATP, which resets the enzyme for another supercoiling cycle [42]. The transport was shown to be a very rare event [33], as gate openings are hardly ever observed. The role of the CTD in strand passage is not clear, but could be addressed by measuring FRET from an immobilized protein as a function of time, e.g. using TIRF microscopy. The proposed conformations of the CTDs during the catalytic cycle are depicted in Fig. 4.2 (S).
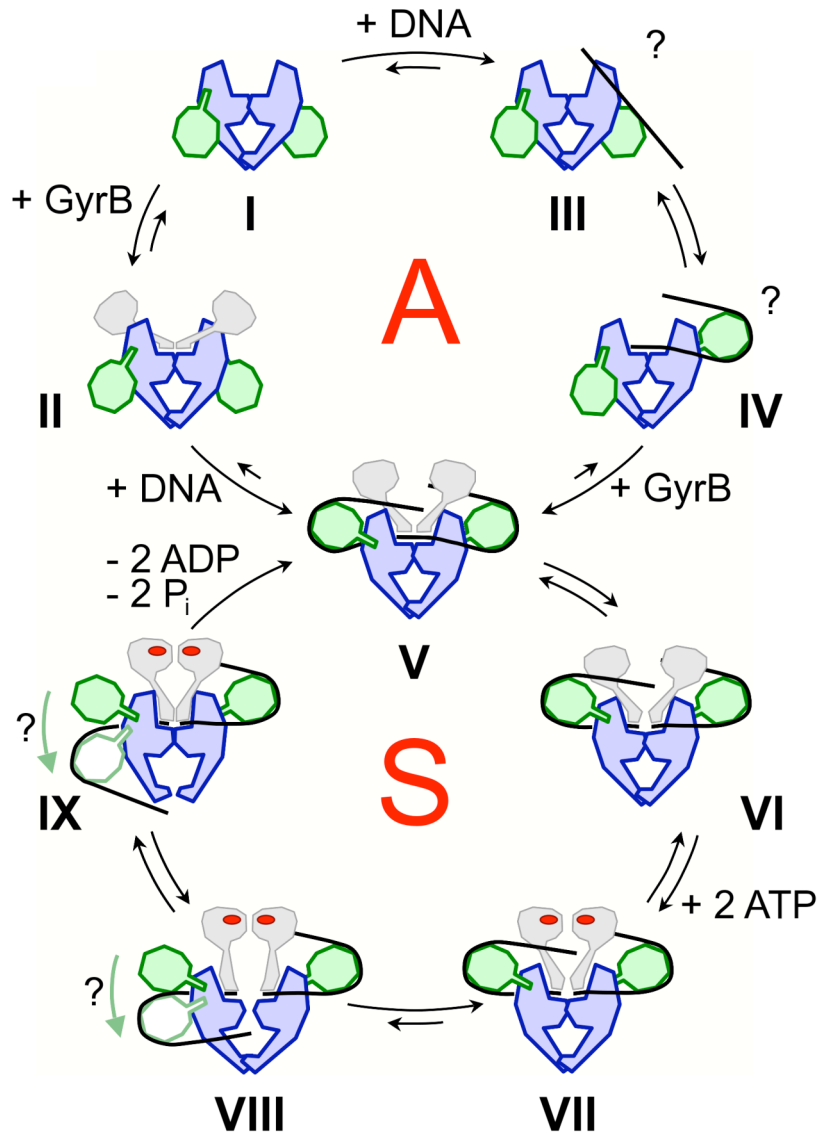
**Fig. 4.2:** Model of the CTD movements during the assembly of DNA with gyrase complex (top: A with states I – V) and the supercoiling reaction cycle (bottom: S with states V – IX). GyrA body, GyrA CTDs, and GyrB are shown in blue, green, and grey, respectively; DNA is depicted as a black line, and nucleotide is shown in red. CTD movements are exaggerated for increased clarity.

I: CTDs are located close to the GyrA body in the free enzyme. II: Upon binding of GyrB, they slightly move away from the core. III: Presumably, initial binding of DNA to GyrA takes place on the CTDs. IV: Contacts of the DNA with the DNA-gate induces the extended CTD conformation; this state should be in equilibrium with (III). V: The active enzyme complex with an extended conformation of the CTDs is formed in presence of both DNA and GyrB.

V, VI: The active enzyme complex can cleave DNA (VI); VI exhibits a slightly more extended CTD conformation than V. VII: Nucleotide binding induces ATPase-gate closure, but does not cause a significant change of the CTD conformation. VIII, IX: hypothetical CTD movements upon transfer of the T-DNA segment through the open DNA-gate (VIII) and C-gate (IX). The CTD bound to the T-segment may guide or follow the transfer movement and transiently swing towards the C-gate, predicting asymmetry with respect to the position of the two CTDs in gyrase. However, no asymmetric conformation is detected in experiments involving nucleotide. The supercoiling cycle is completed by hydrolysis of ATP and release of ADP and phosphate (V).

**4.1.10 Outlook**

For the first time the conformational changes in the GyrA CTDs have been monitored. Several conformational states during gyrase-DNA complex assembly and supercoiling have been identified. The GyrA-DNA complex shows bi-modal behavior, caused either by (1) conformational flexibility of the CTDs or (2) asymmetric behavior of the two CTDs in one GyrA-DNA complex. In smFRET measurements with a non-symmetrical GyrA dimer with one CTD only it should be possible to exclude either of these possibilities: the first should result in a similar conformational behavior as found in GyrA with both CTDs, while the second should lead to increased level of extended CTD conformation.

In fact, an asymmetric GyrA dimer containing just one CTD should exhibit a distinct activity profile, being an ATP-dependent supercoiling enzyme on one side and an ATP-dependent DNA relaxase on the other. Which activity would be prominent could be elucidated in supercoiling assays.

A very important step towards the understanding the supercoiling mechanism of gyrase is connected to the observation of T-DNA strand passage: So far we have not detected a conformational change in the CTDs which could be attributed to strand transfer. A TIRF instrument in combination with immobilization of GyrA directly or via a DNA could extend the observation time of one GyrA molecule, allowing to observe a potential movement of the CTDs when the attached T-segment is guided towards the GyrA C-gate. The immobilization of GyrA could be achieved indirectly by linking DNA to a surface and binding of fluorescently labeled GyrA to the DNA. Monitoring the conformational dynamics of the CTD in gyrase bound to immobilized plasmid of different topology could provide insight in the kinetics of strand passage and the dependence of CTD movements on substrate topology.

For the present study a hetero-dimeric expression / purification system for GyrA with different subunits was developed. The method could be extended to GyrB-GyrA fusion proteins (compare to [42]): Hetero-dimeric fusion constructs could give evidence about the symmetry of certain conformational changes or enzymatic activities during the supercoiling reaction, e.g. conformational changes connected to ATP-hydrolysis, T-segment delivery (monitored with a fusion enzyme lacking one CTD), and intra-subunit conformational dynamics (as shown in the present work by monitoring FRET between the GyrA body and CTD).

In the present study attempts have been made to characterize the molecular properties of the highly conserved GyrA-box which confer supercoiling activity to gyrase. However, the GyrA-box deletion mutant (ΔAbox) exhibited wild-type like DNA affinity and CTD movements; thus no hint to explain the change in activity was obtained. Possible differences between wt

and ΔAbox might be found in internal conformations of the CTD [55] or in DNA wrapping and T-segment presentation. Potential opening of a cleft between blades 1 and 6 of the CTD which are connected by a loop containing the GyrA-box might lead to a different conformation or increased internal flexibility of the domain in the ΔAbox mutant; this could be tested using an isolated fluorescently double-labeled CTD. Alterations in T-segment presentation might be detected by monitoring the conformational change of the ATPase-gate, using a GyrB-GyrA fusion construct [42]: The wild-type like construct exhibits a half-closed ATPase-gate in the presence of a 140bp DNA or relaxed plasmid and ADPNP, indicative of the presence of a T-segment in the upper cavity of the enzymatic core. Potential deficiency of T-segment presentation in the ΔAbox mutant might result in a fully closed ATPase-gate in the presence of the same substrates.

## 4.2 Part II: Conformational changes in topoisomerase VI from *M. mazei*

Topoisomerase VI (abbrev. TopoVI) is a type IIB topoisomerases. In an ATP-dependent mechanism, it relaxes supercoiled DNA and decatenates circular daughter chromosomes prior to cell division by transient cleavage of a double-stranded DNA and transport of a second DNA duplex through the gap before resealing it. In the present work the gate conformations in TopoVI from *M. mazei* were addressed by measuring FRET in a double fluorescently labeled 50bp DNA, which acts as a ligand of TopoVI, and in fluorescently labeled TopoVI. An important part of this work was the validation of a mutant protein which could not be labeled at native cysteine residues to serve as a basis for the introduction of cysteine residues.

### 4.2.1 Formation of the TopoVI-DNA complex: Validation of a 50bp DNA ligand as a binding and cleavage substrate

In order to characterize DNA binding to TopoVI and to monitor conformational changes in the double helix following binding and cleavage, a 50bp DNA containing a preferred binding site for TopoVI from *S. shibatae* was used to serve as a G-DNA segment [59], similar to experiments performed with gyrase and TopoII [33, 43]. The 50bp DNA binds TopoVI with a $K_d$ value of 3.2 μM (Fig. 3.34C), indicating an at least 15-fold higher affinity of the DNA-gate than the one found for a 60bp DNA in GyrA lacking the CTDs (43 μM, Fig. 3.5A). This is not surprising as in TopoVI the DNA-gate is the main DNA-binding site, while GyrA comprises several DNA-binding sites, namely the DNA-gate and the CTDs. However, compared to the GyrA-GyrB complex the DNA affinity of TopoVI has to be judged as rather weak: In presence of GyrB a 48bp DNA exhibits $K_d$ values of 378 and 189 nM for GyrA ΔCTD and wt, corresponding to a 8.5- and 17-fold higher DNA affinity than found for TopoVI.

The DNA devised for smFRET measurements contained two internal fluorescent labels (A488 and A546) with one dye attached to each of the strands. While the presence of the A488 dye did not strongly influence the affinity of the 50bp DNA for TopoVI, the presence of A546 resulted in a almost 10-fold affinity increase, posing limits to the suitability of the double-labeled DNA as a ligand for TopoVI.

A radioactively labeled version of the 50bp DNA was used in a cleavage assay. Despite the high sensitivity of the method no cleaved product could be detected in reactions performed in the absence and presence of nucleotides and / or inhibitory compounds like ciprofloxacin and inorganic selenite. The cause for this finding is debatable: The preferred binding site for *S. shibatae* TopoVI might not be preferentially cleaved by the *M. mazei* enzyme or the cleavage complex not trapped by the method used. A problem arising from the lack of cleavage product formation is that no information about the position of the DNA on the DNA-gate is provided; from the length of potential products the approximate location on the DNA-gate could have been deduced. As a result potential conformational change of the DNA monitored by smFRET could not be interpreted sufficiently well. In an extreme case DNA cleavage and gate opening might not be tracked due to an unfavorable dye arrangement away from the central cleavage site.

Nevertheless, smFRET measurements were performed using the fluorescently double-labeled DNA. The non-complexed DNA shows a medium FRET efficiency of approx. 0.6. Binding of the DNA to TopoVI results in a decrease of the FRET efficiency to approx. 0.4 (Fig. 3.34). The cause could be a distortion of the DNA upon association with the enzyme, manifested by a change of the inter-dye distance, but could also be due to a change in the Förster distance of the two dyes when attached to the DNA or a different arrangement of the dyes relative to each other.

Interestingly, the cleavage-deficient mutant TopoVI-A_Y106F exhibited a 10-fold lower DNA-affinity than the wild-type protein, suggesting the formation of the covalently linked protein-DNA intermediate upon DNA binding for the wt, which would contribute to a lower $K_d$. The DNA conformation in the complex seems to be independent of DNA cleavage, as suggested by the unchanged FRET efficiency for the 50bp DNA in complex with cleavage-deficient TopoVI. These findings are in strong contrast to the interactions found in the gyrase-DNA complex: DNA binding is stronger for a cleavage-deficient gyrase mutant, indicating fundamental differences between the DNA-gates of type IIA and IIB topoisomerases. Also the DNA is mildly and severely distorted upon binding to the DNA-gate and phosphate-backbone cleavage, respectively, indicating that cleavage-induced distortion of the DNA accounts for the lower affinity for the enzyme [113].

The ATPase-gate of TopoVI is supposed to adopt a closed conformation in the presence of ADPNP (Fig. 3.38 and [62]). Addition of ADPNP to the different DNA-protein complexes did not show any influence on the conformation of the DNA bound to the DNA-gate of TopoVI. This might be an indication that the conformation of the DNA-protein complex is not changed upon closure of the ATPase-gate, at least in the absence of a T-DNA segment.

### 4.2.2 Changes in the enzymatic activity of TopoVI caused by the step-wise removal of solvent-accessible cysteine residues

Conformational changes in the ATPase-gate of *M. mazei* TopoVI were addressed by smFRET measurements, using fluorescently labeled protein with one dye introduced to a cysteine residue in each of the ATPase domains. In order to avoid labeling of native cysteines, three residues in the B subunits which could be modified with Alexa 546 (C267, C316, and C550) were exchanged in a step-wise process. The four remaining cysteines in TopoVI were barely labeled by Alexa 488 and 546 (Fig. 3.37B).

While exchange of C267 and C550 to serine and alanine, respectively, did not influence the ATP-dependent relaxation activity of TopoVI, mutation of C316 to either Ser, Ala or Gly marked an activity decrease of 5 to 10-fold (Fig. 3.36). Moreover, the substitutions resulted in a two- to three-fold increase of the ATP hydrolysis activity (Fig. 3.35B). These findings strongly indicate that mutation of C316 causes partial uncoupling of DNA relaxation and ATP hydrolysis. Given the location of C316 in the ATP-binding pocket between the ATPase- and transducer-domain, this explanation seems plausible. The triple-cysteine mutant TopoVI_(B)C267S_C316S_C550A (TopoVI_SSA) was chosen as a basis for the introduction of cysteine residues for fluorescent labeling. Despite showing partial un-coupling, it still exhibits the characteristic DNA relaxation activity of the wt TopoVI and should therefore be suitable for studies of conformational dynamics.

### 4.2.3 Conformational dynamics in the ATPase-gate of TopoVI: Implications for the DNA relaxation cycle

To monitor conformational changes in the ATPase-gate of TopoVI, four amino-acid residues located either on the ATPase domain (R87, D159, E164) or on a loop on the transducer domain (P408) were selected for individual mutation to cysteine (Fig. 3.37A). Mutants were constructed on the basis of TopoVI_SSA. All proteins exhibit the same DNA relaxation activity as the SSA mutant, with the exception of the mutant D159C, which showed 10-fold reduced activity compared to SSA at the same enzyme concentrations. Although the residue is not conserved among TopoVI proteins of different organisms, the loss in activity could be caused by a potential disturbance of the putative dimerization interface of the ATPase domains upon the exchange of D159.

SmFRET measurements with fluorescently labeled TopoVI mutants report on the conformational states of the ATPase-gate: Broad FRET efficiency distributions are observed

for the mutants labeled in the upper ATPase domain, indicating considerable conformational flexibility of the domains in the absence of nucleotide or DNA. In contrast, the FRET efficiency for the P408C mutant is well defined, suggesting low flexibility of the transducer domain (Fig. 3.8B). Upon binding of ADPNP, the ATPase domains are fixed in a well-defined conformation, indicated by the narrow FRET efficiency distributions seen for mutants E164C and R87C. The latter protein exhibits high-FRET, suggesting dimerization of the two ATPase domains (Fig. 3.8C). Nucleotide-induced dimerization of the ATPase domains has been proposed for TopoVI [62, 65] and was demonstrated for other proteins of the GHKL family (e.g. GyrB, Hsp90) [42, 114].

In contrast to the ADPNP-induced closure of the ATPase-gate, binding of neg. supercoiled plasmid to TopoVI results in an increased distance between the domains, indicated by the clear FRET efficiency shift to almost 0 for the mutants E164C and R87C (Fig. 3.8E). Still the distributions are broad, suggesting a high flexibility of the ATPase domains. This behavior has been proposed on the basis of high-resolution crystal structures from the ATPase domains of *S. shibatae* TopoVI [65]: The central cavity of TopoVI has the size to just accommodate two DNA duplexes, with the G-DNA segment bound to the DNA gate and the T-segment residing in the residual space between the DNA-gate and the ATPase-gate [61]. Due to its DNA double-strand crossings this is the case for neg. supercoiled plasmid, a native substrate of TopoVI [25]. In gyrase, the presence of a T-segment induces a pre-closed state of the ATPase-gate[42]; the difference in conformational behavior between topoisomerase VI and gyrase must lie in the domains linking the ATPase- and DNA-gate: While for the first one the structural organization of the connecting region is known, the architecture of full-length GyrB and the orientation of the GHKL domain relative to the DNA-gate is still a matter of speculation.

What happens in the ATPase-gate of TopoVI in presence of both ADPNP and plasmid DNA? Data for mutants E164C and R87C show narrow FRET efficiency distributions, indicating a well-defined conformation. The values are lower than in the absence of DNA, suggesting a higher inter-dye distance than for the dimerized ATPase domains: The ATPase gate seems to be stabilized in a half-open conformation, a state which has not been proposed for TopoVI: The presence of DNA (presumably of a T-segment) in the central cavity inhibits ADPNP-induced dimerization, while the ATPase domains could be fixed relative to the transducer domains in response to ADPNP binding. This was observed in crystal structures of a fragment of the TopoVI-B subunit with ADPNP present in the nucleotide-binding pockets: A conserved lysine in the transducer domain contacts the γ-phosphate of the nucleotide, thereby causing the rotation of the ATPase domain relative to the transducer domain [62]. At this stage of the

reaction cycle (prior to strand passage), TopoVI and gyrase seem to share similarities again: As in TopoVI, the fully closed state for the ATPase-gate of gyrase is barely populated in the presence of a T-DNA segment and ADPNP, indicating that the gate of both enzymes struggle with physical strain induced by DNA [42].

However, TopoVI as well as gyrase might overcome this half-open state for transient dimerization of the ATPase domains: In order to stabilize the DNA-enzyme complex during opening of the DNA-gate and passage of the T-segment, the ATPase-gate needs to close. Dimerization of the ATPase-gate in presence of two DNAs (G- and T-segment) in the cavity might be a short-lived event due to the physical strain such a state might impose on the enzyme and should result in passing the T-segment through the DNA-gate, which is proposed to be mediated by the hydrolysis of one of the two bound ATP molecules [45]. In both enzymes ATPase-gate closure in presence of G- and T-segment has not been observed, indicating that strand passage is a very rapid process.

### 4.2.4  Outlook

The data presented in this work document conformational changes in the ATPase domains of *M. mazei* TopoVI. Four conformational states can be observed: Dynamic states for the ligand-free enzyme and in complex with neg. supercoiled plasmid, with the latter exhibiting a higher distance between the domains; and fixed states in presence of ADPNP (probably representing a closed ATPase-gate) and ADPNP and neg. supercoiled plasmid (half-open).

It is not clear if the well-defined ATPase-gate conformation in presence of ADPNP corresponds to domain dimerization and thus to a closed gate. Determination of photophysical correction parameters and the Förster distance for the different TopoVI mutants will allow the calculation of inter-dye distances, which can be compared to structural models and might either support or argue against the hypothesis of gate closure.

Binding of neg. supercoiled DNA to TopoVI induces spreading of the ATPase-gate: From the data presented it is not clear, if this is due to the presence of a G-DNA or a T-segment. SmFRET measurements using linear DNA or relaxed plasmid, both of which should not serve as a T-segment, might solve this question. According to docking model of a TopoVI-A dimer or the holoenzyme and a G-DNA, the latter should not be in physical contact with the domains forming the ATPase-gate (GHKL, transducer) [61, 63]. Hence, we propose that the

conformation of the ATPase-gate is not influenced by the G-DNA segment, and that the T-segment induces spreading of the ATPase domains and locking of the ATPase domains in half-open state in the absence and presence of ADPNP, respectively.

So far only wild-type like TopoVI has been used for smFRET measurements. In order to link the conformational changes of the ATPase-gate to catalytic steps, active-site mutants deficient in DNA strand cleavage and ATP hydrolysis should be used. Mutants with alterations of the invariant lysine in the transducer domain or in the N-terminal lid could give evidence about their role in the dimerization of the ATPase domains.

Presumably all of the conformational states of the ATPase-gate described so far (see above) represent stages before the transport of a T-segment. ATPase-gate closure in presence of neg. supercoiled plasmid seems to be a reasonable conformational intermediate during the relaxation cycle (section 4.2.3). By increasing the observation time of a single complex, it might be possible to observe interconversion of different states under relaxation conditions using ATP and to detect short-lived states such as closure of the ATPase-gate in the plasmid-bound complex. This should be achieved by single-molecule experiments using TIRF microscopy and immobilized fluorescently labeled TopoVI proteins. A similar experiment has been performed for topoisomerase II, where DNA-gate dynamics were detected [43]. The immobilization of TopoVI could be achieved by biotinylation of the enzyme and direct coupling to a streptavidin-coated surface [115]. However, immobilization via DNA seems to be more reasonable as this can be done using synthetic DNA molecules and avoids further modification of the protein.

We have presented smFRET data reporting on conformational changes in the ATPase-gate, but not in the DNA-gate. Potential conformational changes in the DNA-gate should be detectable using proteins labeled in the TopoVI-A subunits. Gate opening should be a very short-lived event and has been proposed to happen only in presence of G- and T-DNAs as well as nucleotide [61, 63]. SmFRET measurements on a TIRF microscope as proposed above should provide evidence of DNA-gate dynamics, linking them to events like T-segment capture and ATPase-gate closure.

# 5. List of abbreviations

Amino acids are abbreviated in their common three or single letter codes.

| | |
|---|---|
| A488 | Alexa Fluor 488 |
| A546 | Alexa Fluor 546 |
| AboxA | GyrA-box substituted with an alanine heptapeptide |
| ADP | adenosine 5'-diphosphate |
| ADPNP | adenosine 5'-(beta,gamma-imido)triphosphate |
| ATP | adenosine 5'-triphosphate |
| *B. subtilis* | *Bacillus subtilis* |
| *B. burgdorferi* | *Borellia burgdorferi* |
| bp | base-pairs |
| CFX | ciprofloxacin |
| CTD | C-terminal domain |
| ΔAbox | GyrA-box deletion mutant |
| ΔCTD | CTD deletion mutant |
| DTT | 1,4-dithiothreitol |
| *E. coli* | *Escherichia coli* |
| EDTA | Ethylenediaminetetraacetic acid |
| FRET | Förster resonance energy transfer |
| G-DNA / G-segment | gate-DNA segment |
| GyrA* | GyrA_C350L (Cys-free mutant) |
| GyrA* NHT | $His_6$-TEV-GyrA* with $His_6$-tag cleaved with TEV protease |
| GyrA**_Y123F | Hetero-dimeric FRET mutant GyrA*_Y123F / GyrA*_Y123F_T140C_K594C |
| GyrA**_ΔAbox | Hetero-dimeric FRET mutant GyrA*_ΔAbox / GyrA*_ΔAbox_T140C_K594C |
| $His_6$-GyrA* | GyrA* with N-terminal $His_6$-tag |
| $His_6$(-tag) | Hexa-histidine tag |
| $His_6$-TEV-GyrA* | GyrA* with N-terminal $His_6$-tag cleavable with TEV protease |
| $His_6$-TEV-TopoVI-B | TopoVI-B with N-terminal $His_6$-tag cleavable with TEV protease |
| IEX | ion exchange |
| IMAC | immobilized metal affinity chromatography |
| $K_d$ | dissociation constant |
| *M. mazei* | *Methanosarcina mazei* |
| MW | molecular weight |
| NADH | nicotinamide adenine dinucleotide |

| | |
|---|---|
| OD | optical density |
| ORF | open reading frame |
| PCR | poly-chain reaction |
| PEP | phosphoenolpyruvate |
| *S. shibatae* | *Sulfolobus shibatae* |
| SDS | sodium dodecylsulfate |
| SEC | size-exclusion chromatography |
| sm | single molecule |
| TCEP | tris(2-carboxyethyl)phosphine |
| T-DNA / T-segment | transfer-DNA segment |
| TEV | Tobacco edge virus |
| TIRF | total internal reflection fluorescence |
| TMR | Tetramethyl rhodamine |
| TopoVI | topoisomerase VI |
| TopoVI_SSA | Topoisomerase triple-mutant (B)C267S_C316S_C550A |
| TopoVI-A | topoisomerase subunit A |
| TopoVI-B | topoisomerase subunit B |
| TOPRIM | topoisomerase-primase fold |
| Tris | tris(hydroxymethyl)aminomethane |
| WHD | winged-helix domain |
| wt | wild-type |
| *X. campestris* | *Xanthomonas campestris* |

# 6. List of references

1.  Wang, J.C., *Cellular roles of DNA topoisomerases: a molecular perspective.* Nat Rev Mol Cell Biol, 2002. **3**(6): p. 430-40.
2.  Wu, H.Y., et al., *Transcription generates positively and negatively supercoiled domains in the template.* Cell, 1988. **53**(3): p. 433-40.
3.  Baxter, J., et al., *Positive supercoiling of mitotic DNA drives decatenation by topoisomerase II in eukaryotes.* Science, 2011. **331**(6022): p. 1328-32.
4.  Zechiedrich, E.L. and N.R. Cozzarelli, *Roles of topoisomerase IV and DNA gyrase in DNA unlinking during replication in Escherichia coli.* Genes Dev, 1995. **9**(22): p. 2859-69.
5.  Liu, L.F. and J.C. Wang, *Interaction between DNA and Escherichia coli DNA topoisomerase I. Formation of complexes between the protein and superhelical and nonsuperhelical duplex DNAs.* J Biol Chem, 1979. **254**(21): p. 11082-8.
6.  Morrison, A. and N.R. Cozzarelli, *Site-specific cleavage of DNA by E. coli DNA gyrase.* Cell, 1979. **17**(1): p. 175-84.
7.  Wang, J.C., *Interaction between DNA and an Escherichia coli protein omega.* J Mol Biol, 1971. **55**(3): p. 523-33.
8.  Slesarev, A.I., et al., *DNA topoisomerase V is a relative of eukaryotic topoisomerase I from a hyperthermophilic prokaryote.* Nature, 1993. **364**(6439): p. 735-7.
9.  Dekker, N.H., et al., *The mechanism of type IA topoisomerases.* Proceedings of the National Academy of Sciences of the United States of America, 2002. **99**(19): p. 12126-31.
10. Stivers, J.T., T.K. Harris, and A.S. Mildvan, *Vaccinia DNA topoisomerase I: evidence supporting a free rotation mechanism for DNA supercoil relaxation.* Biochemistry, 1997. **36**(17): p. 5212-22.
11. Koster, D.A., et al., *Friction and torque govern the relaxation of DNA supercoils by eukaryotic topoisomerase IB.* Nature, 2005. **434**(7033): p. 671-4.
12. Taneja, B., et al., *Topoisomerase V relaxes supercoiled DNA by a constrained swiveling mechanism.* Proceedings of the National Academy of Sciences of the United States of America, 2007. **104**(37): p. 14670-5.
13. Das, B.B., et al., *Reconstitution and functional characterization of the unusual bi-subunit type I DNA topoisomerase from Leishmania donovani.* FEBS Lett, 2004. **565**(1-3): p. 81-8.
14. Champoux, J.J., *DNA is linked to the rat liver DNA nicking-closing enzyme by a phosphodiester bond to tyrosine.* J Biol Chem, 1981. **256**(10): p. 4805-9.
15. Kikuchi, A. and K. Asai, *Reverse gyrase--a topoisomerase which introduces positive superhelical turns into DNA.* Nature, 1984. **309**(5970): p. 677-81.
16. del Toro Duany, Y., et al., *The reverse gyrase helicase-like domain is a nucleotide-dependent switch that is attenuated by the topoisomerase domain.* Nucleic Acids Res, 2008. **36**(18): p. 5882-95.
17. Brown, P.O., C.L. Peebles, and N.R. Cozzarelli, *A topoisomerase from Escherichia coli related to DNA gyrase.* Proceedings of the National Academy of Sciences of the United States of America, 1979. **76**(12): p. 6110-4.
18. Gellert, M., et al., *DNA gyrase: an enzyme that introduces superhelical turns into DNA.* Proc Natl Acad Sci U S A, 1976. **73**(11): p. 3872-6.
19. Gadelle, D., et al., *Phylogenomics of type II DNA topoisomerases.* Bioessays, 2003. **25**(3): p. 232-42.
20. Bergerat, A., et al., *An atypical topoisomerase II from Archaea with implications for meiotic recombination.* Nature, 1997. **386**(6623): p. 414-7.

21. Hartung, F. and H. Puchta, *Molecular characterization of homologues of both subunits A (SPO11) and B of the archaebacterial topoisomerase 6 in plants.* Gene, 2001. **271**(1): p. 81-6.

22. Malik, S.B., et al., *Protist homologs of the meiotic Spo11 gene and topoisomerase VI reveal an evolutionary history of gene duplication and lineage-specific loss.* Mol Biol Evol, 2007. **24**(12): p. 2827-41.

23. Zechiedrich, E.L., et al., *Roles of topoisomerases in maintaining steady-state DNA supercoiling in Escherichia coli.* J Biol Chem, 2000. **275**(11): p. 8103-13.

24. Forterre, P., A. Bergerat, and P. Lopez-Garcia, *The unique DNA topology and DNA topoisomerases of hyperthermophilic archaea.* FEMS Microbiol Rev, 1996. **18**(2-3): p. 237-48.

25. Buhler, C., et al., *Reconstitution of DNA topoisomerase VI of the thermophilic archaeon Sulfolobus shibatae from subunits separately overexpressed in Escherichia coli.* Nucleic Acids Res, 1998. **26**(22): p. 5157-62.

26. Levine, C., H. Hiasa, and K.J. Marians, *DNA gyrase and topoisomerase IV: biochemical activities, physiological roles during chromosome replication, and drug sensitivities.* Biochim Biophys Acta, 1998. **1400**(1-3): p. 29-43.

27. Chatterji, M., et al., *The additional 165 amino acids in the B protein of Escherichia coli DNA gyrase have an important role in DNA binding.* J Biol Chem, 2000. **275**(30): p. 22888-94.

28. Schoeffler, A.J., A.P. May, and J.M. Berger, *A domain insertion in Escherichia coli GyrB adopts a novel fold that plays a critical role in gyrase function.* Nucleic Acids Res, 2010. **38**(21): p. 7830-44.

29. Berger, J.M., et al., *Structure and mechanism of DNA topoisomerase II.* Nature, 1996. **379**(6562): p. 225-32.

30. Wigley, D.B., et al., *Crystal structure of an N-terminal fragment of the DNA gyrase B protein.* Nature, 1991. **351**(6328): p. 624-9.

31. Laponogov, I., et al., *Structural insight into the quinolone-DNA cleavage complex of type IIA topoisomerases.* Nat Struct Mol Biol, 2009. **16**(6): p. 667-9.

32. Dong, K.C. and J.M. Berger, *Structural basis for gate-DNA recognition and bending by type IIA topoisomerases.* Nature, 2007. **450**(7173): p. 1201-5.

33. Gubaev, A., M. Hilbert, and D. Klostermeier, *The DNA-gate of Bacillus subtilis gyrase is predominantly in the closed conformation during the DNA supercoiling reaction.* Proc Natl Acad Sci U S A, 2009. **106**(32): p. 13278-83.

34. Hardin, A.H., et al., *Direct measurement of DNA bending by type IIA topoisomerases: implications for non-equilibrium topology simplification.* Nucleic Acids Res, 2011.

35. Dutta, R. and M. Inouye, *GHKL, an emergent ATPase/kinase superfamily.* Trends Biochem Sci, 2000. **25**(1): p. 24-8.

36. Gottler, T., *Untersuchung der katalytischen Funktion der Gyrase aus Bacillus subtilis mit Einzelmolekül-Fluoreszenzspektroskopie.* Dissertation, Universität Basel, 2008.

37. Brino, L., et al., *Dimerization of Escherichia coli DNA-gyrase B provides a structural mechanism for activating the ATPase catalytic center.* J Biol Chem, 2000. **275**(13): p. 9468-75.

38. Hsieh, T.J., et al., *Twisting of the DNA-binding surface by a beta-strand-bearing proline modulates DNA gyrase activity.* Nucleic Acids Res, 2010. **38**(12): p. 4173-81.

39. Kampranis, S.C., A.D. Bates, and A. Maxwell, *A model for the mechanism of strand passage by DNA gyrase.* Proceedings of the National Academy of Sciences of the United States of America, 1999. **96**(15): p. 8414-9.

40. Harkins, T.T. and J.E. Lindsley, *Pre-steady-state analysis of ATP hydrolysis by Saccharomyces cerevisiae DNA topoisomerase II. 1. A DNA-dependent burst in ATP hydrolysis.* Biochemistry, 1998. **37**(20): p. 7292-8.

41. Harkins, T.T., T.J. Lewis, and J.E. Lindsley, *Pre-steady-state analysis of ATP hydrolysis by Saccharomyces cerevisiae DNA topoisomerase II. 2. Kinetic mechanism for the sequential hydrolysis of two ATP.* Biochemistry, 1998. **37**(20): p. 7299-312.

42. Gubaev, A. and D. Klostermeier, submitted, 2011.

43. Smiley, R.D., et al., *Single-molecule measurements of the opening and closing of the DNA gate by eukaryotic topoisomerase II.* Proc Natl Acad Sci U S A, 2007. **104**(12): p. 4840-5.

44. Williams, N.L. and A. Maxwell, *Probing the two-gate mechanism of DNA gyrase using cysteine cross-linking.* Biochemistry, 1999. **38**(41): p. 13502-11.

45. Skouboe, C., et al., *A human topoisomerase II alpha heterodimer with only one ATP binding site can go through successive catalytic cycles.* J Biol Chem, 2003. **278**(8): p. 5768-74.

46. Gottler, T. and D. Klostermeier, *Dissection of the nucleotide cycle of B. subtilis DNA gyrase and its modulation by DNA.* J Mol Biol, 2007. **367**(5): p. 1392-404.

47. Baird, C.L., et al., *Topoisomerase II drives DNA transport by hydrolyzing one ATP.* Proceedings of the National Academy of Sciences of the United States of America, 1999. **96**(24): p. 13685-90.

48. Heddle, J.G., et al., *Nucleotide binding to DNA gyrase causes loss of DNA wrap.* J Mol Biol, 2004. **337**(3): p. 597-610.

49. Corbett, K.D., R.K. Shultzaberger, and J.M. Berger, *The C-terminal domain of DNA gyrase A adopts a DNA-bending beta-pinwheel fold.* Proc Natl Acad Sci U S A, 2004. **101**(19): p. 7293-8.

50. Ruthenburg, A.J., et al., *A superhelical spiral in the Escherichia coli DNA gyrase A C-terminal domain imparts unidirectional supercoiling bias.* J Biol Chem, 2005. **280**(28): p. 26177-84.

51. Corbett, K.D., et al., *The structural basis for substrate specificity in DNA topoisomerase IV.* J Mol Biol, 2005. **351**(3): p. 545-61.

52. Mirski, S.E., et al., *Bipartite nuclear localization signals in the C terminus of human topoisomerase II alpha.* Exp Cell Res, 1997. **237**(2): p. 452-5.

53. Kampranis, S.C. and A. Maxwell, *Conversion of DNA gyrase into a conventional type II topoisomerase.* Proceedings of the National Academy of Sciences of the United States of America, 1996. **93**(25): p. 14416-21.

54. Kirchhausen, T., J.C. Wang, and S.C. Harrison, *DNA gyrase and its complexes with DNA: direct observation by electron microscopy.* Cell, 1985. **41**(3): p. 933-43.

55. Kramlinger, V.M. and H. Hiasa, *The "GyrA-box" is required for the ability of DNA gyrase to wrap DNA and catalyze the supercoiling reaction.* J Biol Chem, 2006. **281**(6): p. 3738-42.

56. Huang, Y.Y., et al., *The key DNA-binding residues in the C-terminal domain of Mycobacterium tuberculosis DNA gyrase A subunit (GyrA).* Nucleic Acids Res, 2006. **34**(19): p. 5650-9.

57. Costenaro, L., et al., *Small-angle X-ray scattering reveals the solution structure of the full-length DNA gyrase a subunit.* Structure, 2005. **13**(2): p. 287-96.

58. Baker, N.M., et al., *Solution structures of DNA-bound gyrase.* Nucleic Acids Res, 2011. **39**(2): p. 755-66.

59. Buhler, C., et al., *DNA topoisomerase VI generates ATP-dependent double-strand breaks with two-nucleotide overhangs.* J Biol Chem, 2001. **276**(40): p. 37215-22.

60. Bergerat, A., D. Gadelle, and P. Forterre, *Purification of a DNA topoisomerase II from the hyperthermophilic archaeon Sulfolobus shibatae. A thermostable enzyme with both bacterial and eucaryal features.* J Biol Chem, 1994. **269**(44): p. 27663-9.

61. Corbett, K.D., P. Benedetti, and J.M. Berger, *Holoenzyme assembly and ATP-mediated conformational dynamics of topoisomerase VI.* Nat Struct Mol Biol, 2007. **14**(7): p. 611-9.

62.    Corbett, K.D. and J.M. Berger, *Structure of the topoisomerase VI-B subunit: implications for type II topoisomerase mechanism and evolution.* Embo J, 2003. **22**(1): p. 151-63.

63.    Nichols, M.D., et al., *Structure and function of an archaeal topoisomerase VI subunit with homology to the meiotic recombination factor Spo11.* EMBO J, 1999. **18**(21): p. 6177-88.

64.    Graille, M., et al., *Crystal structure of an intact type II DNA topoisomerase: insights into DNA transfer mechanisms.* Structure, 2008. **16**(3): p. 360-70.

65.    Corbett, K.D. and J.M. Berger, *Structural dissection of ATP turnover in the prototypical GHL ATPase TopoVI.* Structure, 2005. **13**(6): p. 873-82.

66.    Karow, A.R. and D. Klostermeier, *A structural model for the DEAD box helicase YxiN in solution: localization of the RNA binding domain.* J Mol Biol, 2010. **402**(4): p. 629-37.

67.    van den Berg, S., et al., *Improved solubility of TEV protease by directed evolution.* J Biotechnol, 2006. **121**(3): p. 291-8.

68.    Marinus, M.G. and N.R. Morris, *Isolation of deoxyribonucleic acid methylase mutants of Escherichia coli K-12.* J Bacteriol, 1973. **114**(3): p. 1143-50.

69.    Bertani, G., *Studies on lysogenesis. I. The mode of phage liberation by lysogenic Escherichia coli.* J Bacteriol, 1951. **62**(3): p. 293-300.

70.    Studier, F.W., *Protein production by auto-induction in high density shaking cultures.* Protein Expr Purif, 2005. **41**(1): p. 207-34.

71.    Laemmli, U.K., *Cleavage of structural proteins during the assembly of the head of bacteriophage T4.* Nature, 1970. **227**(5259): p. 680-5.

72.    Gasteiger, E., et al., *Protein Identification and Analysis Tools on the ExPASy Server.* The Proteomics Protocols Handbook, Humana Press, 2005: p. 571-607

73.    Cantor, C.R., M.M. Warshaw, and H. Shapiro, *Oligonucleotide interactions. 3. Circular dichroism studies of the conformation of deoxyoligonucleotides.* Biopolymers, 1970. **9**(9): p. 1059-77.

74.    Bergmeyer, H.U., *New values for the molar extinction coefficients of NADH and NADPH for the use in routine laboratories (author's transl).* Z Klin Chem Klin Biochem, 1975. **13**(11): p. 507-8.

75.    Theissen, B., *Konformationsänderungen im katalytischen Zyklus der RNA-Helikase YxiN - Fluoreszenz-Resonanz-Energie-Transfer in einzelnen Molekülen.* Dissertation, Universität Bayreuth, 2006.

76.    Mullis, K., et al., *Specific enzymatic amplification of DNA in vitro: the polymerase chain reaction.* Cold Spring Harb Symp Quant Biol, 1986. **51 Pt 1**: p. 263-73.

77.    Papworth, C., et al., *QuikChange site-directed mutagenesis.* . Strategies, 1996. **9**: p. 3-4.

78.    Sanger, F., S. Nicklen, and A.R. Coulson, *DNA sequencing with chain-terminating inhibitors.* Proc Natl Acad Sci U S A, 1977. **74**(12): p. 5463-7.

79.    Adam, H., *Adenosin-5'Disphosphat und Adenosin-5'Monophosphat.* Methoden der enzymatischen Analyse, 1962: p. 573-577.

80.    Greenstein, J.P., *Sulfhydryl groups of proteins.* JBC, 1938. **125**: p. 501-513.

81.    Hassiepen, U., et al., *Analysis of protein self-association at constant concentration by fluorescence-energy transfer.* Eur J Biochem, 1998. **255**(3): p. 580-7.

82.    Spreitler, F., *Einzelmolekül-FRET an Biomolekülen.* Diplomarbeit, Universität Bayreuth, 2006.

83.    Kinjo, M. and R. Rigler, *Ultrasensitive hybridization analysis using fluorescence correlation spectroscopy.* Nucleic Acids Res, 1995. **23**(10): p. 1795-9.

84.    Theissen, B., et al., *Cooperative binding of ATP and RNA induces a closed conformation in a DEAD box RNA helicase.* Proc Natl Acad Sci U S A, 2008. **105**(2): p. 548-53.

85.	Förster, T., *Zwischenmolekulare Energiewanderung und Fluoreszenz*. Annalen der Physik, 1948. **2**.

86.	Stryer, L., *Fluorescence energy transfer as a spectroscopic ruler*. Annu Rev Biochem, 1978. **47**: p. 819-46.

87.	Steinberg, I.Z., *Long-range nonradiative transfer of electronic excitation energy in proteins and polypeptides*. Annu Rev Biochem, 1971. **40**: p. 83-114.

88.	Parker, C.A. and W.T. Rees, *Correction of fluorescence spectra and measurement of fluorescence quantum efficiency*. Analyst, 1960. **85**: p. 587-600.

89.	Magde, D., R. Wong, and P.G. Seybold, *Fluorescence quantum yields and their relation to lifetimes of rhodamine 6G and fluorescein in nine solvents: improved absolute standards for quantum yields*. Photochem Photobiol, 2002. **75**(4): p. 327-34.

90.	Moore, C.L., et al., *Gyrase . DNA complexes visualized as looped structures by electron microscopy*. J Biol Chem, 1983. **258**(7): p. 4612-7.

91.	Reece, R.J. and A. Maxwell, *The C-terminal domain of the Escherichia coli DNA gyrase A subunit is a DNA-binding protein*. Nucleic Acids Res, 1991. **19**(7): p. 1399-405.

92.	Bashkirov, V.I. and D.J. Zvingila, *Sequence specificity of Bacillus subtilis DNA gyrase in vivo*. Genetica, 1991. **85**(1): p. 3-12.

93.	Arnold, K., et al., *The SWISS-MODEL Workspace: A web-based environment for protein structure homology modelling*. Bioinformatics, 2006. **22**: p. 195-201.

94.	Edwards, M.J., et al., *A crystal structure of the bifunctional antibiotic simocyclinone D8, bound to DNA gyrase*. Science, 2009. **326**(5958): p. 1415-8.

95.	Roca, J., et al., *DNA transport by a type II topoisomerase: direct evidence for a two-gate mechanism*. Proceedings of the National Academy of Sciences of the United States of America, 1996. **93**(9): p. 4057-62.

96.	Gellert, M., et al., *DNA gyrase: an enzyme that introduces superhelical turns into DNA*. Proceedings of the National Academy of Sciences of the United States of America, 1976. **73**(11): p. 3872-6.

97.	Gadelle, D., et al., *Inhibition of archaeal growth and DNA topoisomerase VI activities by the Hsp90 inhibitor radicicol*. Nucleic Acids Res, 2005. **33**(7): p. 2310-7.

98.	Corbett, K.D. and J.M. Berger, *Structural basis for topoisomerase VI inhibition by the anti-Hsp90 drug radicicol*. Nucleic acids research, 2006. **34**(15): p. 4269-77.

99.	Zhou, N., et al., *DNA damage-mediated apoptosis induced by selenium compounds*. J Biol Chem, 2003. **278**(32): p. 29532-7.

100.	Pommier, Y., et al., *DNA topoisomerases and their poisoning by anticancer and antibacterial drugs*. Chem Biol, 2010. **17**(5): p. 421-33.

101.	Sinha, B.K., et al., *DNA strand breaks produced by etoposide (VP-16,213) in sensitive and resistant human breast tumor cells: implications for the mechanism of action*. Cancer Res, 1988. **48**(18): p. 5096-100.

102.	Barnes, M.H., W.A. LaMarr, and K.A. Foster, *DNA gyrase and DNA topoisomerase of Bacillus subtilis: expression and characterization of recombinant enzymes encoded by the gyrA, gyrB and parC, parE genes*. Protein Expr Purif, 2003. **29**(2): p. 259-64.

103.	Tretter, E.M., J.C. Lerman, and J.M. Berger, *A naturally chimeric type IIA topoisomerase in Aquifex aeolicus highlights an evolutionary path for the emergence of functional paralogs*. Proceedings of the National Academy of Sciences of the United States of America, 2010. **107**(51): p. 22055-9.

104.	Higgins, N.P., et al., *Purification of subunits of Escherichia coli DNA gyrase and reconstitution of enzymatic activity*. Proc Natl Acad Sci U S A, 1978. **75**(4): p. 1773-7.

105.	Kampranis, S.C. and A. Maxwell, *Conversion of DNA gyrase into a conventional type II topoisomerase*. Proc Natl Acad Sci U S A, 1996. **93**(25): p. 14416-21.

106.    Liu, L.F., C.C. Liu, and B.M. Alberts, *Type II DNA topoisomerases: enzymes that can unknot a topologically knotted DNA molecule via a reversible double-strand break.* Cell, 1980. **19**(3): p. 697-707.

107.    Orphanides, G. and A. Maxwell, *Evidence for a conformational change in the DNA gyrase-DNA complex from hydroxyl radical footprinting.* Nucleic Acids Res, 1994. **22**(9): p. 1567-75.

108.    Morais Cabral, J.H., et al., *Crystal structure of the breakage-reunion domain of DNA gyrase.* Nature, 1997. **388**(6645): p. 903-6.

109.    Schwille, P., J. Korlach, and W.W. Webb, *Fluorescence correlation spectroscopy with single-molecule sensitivity on cell and model membranes.* Cytometry, 1999. **36**(3): p. 176-82.

110.    Kirkegaard, K. and J.C. Wang, *Mapping the topography of DNA wrapped around gyrase by nucleolytic and chemical probing of complexes of unique DNA sequences.* Cell, 1981. **23**(3): p. 721-9.

111.    Sugino, A., et al., *Energy coupling in DNA gyrase and the mechanism of action of novobiocin.* Proceedings of the National Academy of Sciences of the United States of America, 1978. **75**(10): p. 4838-42.

112.    Oram, M., et al., *Dissection of the bacteriophage Mu strong gyrase site (SGS): significance of the SGS right arm in Mu biology and DNA gyrase mechanism.* J Bacteriol, 2006. **188**(2): p. 619-32.

113.    Gubaev, A., M. Hilbert, and D. Klostermeier, *The DNA-gate of Bacillus subtilis gyrase is predominantly in the closed conformation during the DNA supercoiling reaction.* Proceedings of the National Academy of Sciences of the United States of America, 2009. **106**(32): p. 13278-83.

114.    Kampranis, S.C. and A. Maxwell, *Conformational changes in DNA gyrase revealed by limited proteolysis.* J Biol Chem, 1998. **273**(35): p. 22606-14.

115.    Lesaicherre, M., et al., *Intein-Mediated Biotinylation of Proteins and Its Application in a Protein Microarray.* Journal of the American Chemical Society, 2002. **124**: p. 8768-8769.

# 7. Acknowledgments

Many people made this period very instructive and enjoyable for me. My sincere thanks go to

**Dagmar** for offering me to work on the projects presented here. She gave me the chance to be part of a really fine research group, to develop as a person and as a researcher. Thanks for fair discussion of my work, for taking time even if she did not have a lot to spend. Under Dagmar's supervision I could progress in my own speed and according to my own ideas, which made working in her lab a very satisfying experience.

**the many Klostermeier lab-mates** (in chaotical order); the ones from lab 677: **Ines, Bruno, Stef, Lenz, Regula, Tobi, Fabian, Miriam, Martin and Bettina**; and the ones from „the other lab": **Agneyo, Anne, Manuel, Yoa, Airat, Alexandra, Andreas, Diana and Jacqueline**. I expected to meet colleagues, but found friends instead! Thanks a lot for constant scientific advice and discussion, for many enjoyable lunch and coffee breaks, evening beers and game nights. **Special thanks** go to **Ines Hertel**: Without her support in the production of so many GyrA constructs, my work would have progressed much slower. Thanks so much for the reliable collaboration, the good benchside neighborship, and the many encouraging words in recent coffee breaks; **Airat Gubaev**: for sharing the precious gyrase project with me and for his support with initial single-molecule measurements: His expertise was a big help in many experiments; **Agneyo Ganguly and Tobias Heck** for patiently correcting this manuscript; and **Diana Blank and Andreas Schmidt** for their work on *B. subtilis* gyrase constructs produced ahead of this work, but influenced the out-come significantly.

**Corinne, Susanna, Angie**: For perfect administrative support and refreshingly non-scientific laughs!

**Leo Faletti, Bea Lang and Simon Saner**: They managed everything around the labs on their own. Thanks a lot for your reliable service and good mood facing urgent needs!

**the members of the Seelig groups**, espacially to: Cinzia, Caroline, Estefania, Matthias, Therese, André, Rita, Gabi, Christian, and Mike, for good times on floor six.

**Prof. James M. Berger** at UC Berkeley for gifting the topoisomerase VI A+B coexpression construct.

**My parents, Rosmarie and Paul, and my sister Kathrin**: You helped me find my way to where I am now. Thank you so much for giving me care and protection before my PhD time; for Sunday evening dinners, week-ends on the countryside, for phone calls and the many little somethings during the recent years; and for believing in me.

**Luz Maria, my mother-in-law**: During the first years of my PhD I spent many week-ends at your place: You offered me a home. Thank you so much for your interest in what I am working on, and for accepting me as your son!

**Mia**: Thank you for your company, for supporting me in times of doubt, for our life balanced between individual freedom and strong connection. Thank you for diving into molecules with me, and for bringing me back to real life again. This work is our work – *gracias*!

# 8.  Curriculum vitae

## Martin Andreas Lanz

**Personal:**

| | |
|---|---|
| Born: | June 12th, 1980, in Bern, Switzerland |
| E-mail: | martinlanz@gmx.de |

**Academic track record:**

| | |
|---|---|
| 04/2007 – 06/2011 | PhD studies in Biophysics, University of Basel, Switzerland |
| | PhD thesis in the group of Prof. Dagmar Klostermeier, Biophysical Chemistry / Single-molecule FRET studies of Biomolecules |
| | ‚Conformational change in the C-terminal domain of B. subtilis gyrase and in the ATPase-gate of M. mazei topoisomerase VI' |
| 10/2004 | Diploma (Master of Science) in Biochemistry from the University of Berne, Switzerland |
| 07/2003 – 07/2004 | Diploma thesis in the group of Prof. Ulrich Baumann, Structural Biology / X-ray Crystallography of Proteases. |
| | ‚Die AAA-Protease FtsH und ihre regulatorischen Faktoren HflK und HflC' |
| 10/2000 – 10/2004 | Undergraduate studies in Biochemistry, University of Berne, Switzerland |
| 08/1996 – 06/2000 | Gymnasium Köniz, Switzerland |

**Publication:**

Lanz, M.A. and Klostermeier, D.: *Guiding strand passage: DNA-induced movement of the gyrase C-terminal domains defines an early step in the supercoiling cycle.* Nucleic Acids Res., **2011**.